Universidade Federal do Rio Grande do Sul
Instituto de Pesquisas Hidráulicas
Programa de Pós-graduação em Recursos Hídricos e Saneamento Ambiental

Tese de Doutorado

Surface water and energy fluxes in South America: An integrated approach based on remote sensing and flux measurements

Adriana Aparecida Moreira

Orientador
Prof. Dr. Anderson Ruhoff (IPH/UFRGS)

Porto Alegre, RS – Brasil

Março de 2022

ADRIANA APARECIDA MOREIRA

Surface water and energy fluxes in South America: An integrated approach based on remote sensing and flux measurements

Tese apresentada ao Programa de Pós-graduação em Recursos Hídricos e Saneamento Ambiental da Universidade Federal do Rio Grande do Sul, como requisito parcial à obtenção do grau de doutora.

Orientador: Prof. Dr. Anderson Ruhoff

Porto Alegre, RS – Brasil

Março de 2022

CIP - Catalogação na Publicação

Moreira, Adriana
Surface water and energy fluxes in South America: An integrated approach based on remote sensing and flux measurements / Adriana Moreira. -- 2022.
171 f.
Orientador: Anderson Ruhoff.

Tese (Doutorado) -- Universidade Federal do Rio Grande do Sul, Instituto de Pesquisas Hidráulicas, Programa de Pós-Graduação em Recursos Hídricos e Saneamento Ambiental, Porto Alegre, BR-RS, 2022.

1. evapotranspiração. 2. sensoriamento remoto. 3. eddy covariance. 4. uso e cobertura do solo. I. Ruhoff, Anderson, orient. II. Título.

Elaborada pelo Sistema de Geração Automática de Ficha Catalográfica da UFRGS com os dados fornecidos pelo(a) autor(a).

ADRIANA APARECIDA MOREIRA

Surface water and energy fluxes in South America: An integrated approach based on remote sensing and flux measurements

Tese apresentada ao Programa de Pós-graduação em Recursos Hídricos e Saneamento Ambiental da Universidade Federal do Rio Grande do Sul, como requisito parcial à obtenção do grau de doutora.

Aprovado em: Porto Alegre, 25 de março de 2022.

Prof. Dr. Anderson Ruhoff (IPH/UFRGS)
Orientador

Prof. Dra. Denise Cybis Fontana (PPGSR/UFRGS)
Examinadora

Prof. Dr. Marcelo Sacardi Biudes (UFMT)
Examinador

Prof. Dr. Rodrigo Cauduro Dias de Paiva
(IPH/UFRGS)
Examinador

À minha mãe (*in memoriam*)

AGRADECIMENTOS

Ao final desta trajetória é muito gratificante pensar em todo o caminho percorrido, e perceber como esse trabalho foi construído com apoio e incentivo de muitas pessoas.

Não poderia iniciar esses agradecimentos sem primeiro mencionar a minha família. Mesmo sem entender os motivos de eu estar sempre estudando, eles sempre foram muito compreensivos, principalmente com a minha ausência. Em especial à minha mãe (*in memoriam*), que acreditava mais em mim mais do que qualquer pessoa.

Ao meu grande incentivador, Dairan Severo. Muito obrigada pelo apoio e por me inicializar no mundo da programação.

Aos meus amigos e colegas do IPH, especialmente à Alice Fassoni, que foi essencial para que eu iniciasse o doutorado e permanecesse nele. Muito obrigada! Também gostaria de agradecer ao pessoal da sala de Hidrologia, que me acolheu e com quem eu puder ter trocas muito valiosas. Em especial à Dani Adamatti, Regina Cadore e Fran Vanelli.

Agradeço ao meu orientador, Anderson Ruhoff, por aceitar com bastante entusiasmo conduzir a minha tese de doutorado, pelas valiosas contribuições e por sempre estar presente e me incentivando.

Por fim, gostaria de agradecer aos professores do IPH por todo o aprendizado proporcionado. Ao Conselho Nacional de Desenvolvimento Científico. E as redes de monitoramento de fluxo, LBA, Ameriflux, Fluxnet, Sulflux, ONDACDCB e PELD, pela disponibilidade de dados, sem os quais este trabalho não seria possível.

RESUMO

A América do Sul é um continente abundante em água, abrigando as maiores bacias hidrográficas e a maior floresta tropical do mundo, a floresta Amazônica. A Amazônia desempenha um papel crucial no fornecimento de umidade para outras regiões do continente por meio da evapotranspiração (ET). A ET é um indicador crucial do funcionamento do ecossistema terrestre, interligando os ciclos da água, energia e carbono. Devido ao grande desafio de obtenção de informações de ET por medições *in situ*, o uso de dados de sensoriamento remoto tem se mostrado uma grande alternativa para obter estimativas desta variável. Com base em dados medidos e estimados por sensoriamento remoto foi conduzido um estudo que visou analisar a dinâmica, os padrões e os controles dos fluxos de água e energia na América do Sul, buscando responder a três questões principais: *i*) os dados de sensoriamento remoto podem fornecer informações precisas sobre o balanço hídrico?; *ii*) como os fatores que controlam a ET variam em diferentes biomas e condições de uso e cobertura do solo (LULC)?; e *iii*) os modelos de sensoriamento remoto conseguem representar com acurácia os padrões de ET e das suas componentes em diferentes condições de LULC? Para responder a primeira pergunta realizou-se uma análise de balanço hídrico, na qual foi avaliada as incertezas das estimativas de precipitação e ET usando medições *in situ*, e uma análise do quanto essas incertezas podem ser afetadas devido ao efeito de escala das bacias analisadas. Os resultados mostraram que devido às incertezas relacionadas com cada uma das componentes estimadas por sensoriamento remoto ainda não é possível alcançar o fechamento do balanço hídrico. No entanto, a abordagem demonstrou ser uma grande alternativa para avaliar a dinâmica dos fluxos de água, de pequenas a grandes bacias, especialmente naquelas onde a medição *in situ* ainda é escassa. Para buscar responder a segunda pergunta analisou-se a influência dos fatores bióticos e abióticos no controle dos processos de ET, por meio da análise das condutâncias de superfície e aerodinâmica e do fator de desacoplamento em 20 locais de monitoramento de fluxo na América do Sul. Por meio desta análise verificou-se diferentes padrões dos fluxos de calor latente (LE) e sensível (H), além de diferentes graus de importância dos controles bióticos e abióticos sobre o processo de ET e de acordo com as diferentes condições de LULC. Por fim, com base em 11 locais de monitoramento de fluxo e quatro modelos de ET (MOD16, GLEAM, PML e SSEBOP), analisou-se a acurácia destas estimativas na bacia amazônica, e a representação dos fluxos de ET em áreas de floresta, pastagem e soja, na bacia do Tapajós. Os resultados mostraram que a obtenção de estimativas acuradas de ET ainda é um grande desafio na bacia Amazônica, principalmente em locais úmidos e sazonalmente inundados. Discrepâncias significativas entre os modelos e entre as medições foram encontradas, sendo estas discrepâncias ainda mais expressivas quando se analisou as componentes individuais de ET. No entanto, os resultados deste estudo demonstraram que apesar de cada modelo não apresentar um desempenho significativo em todas as condições climáticas e de vegetação, estes apresentam em conjunto, uma grande oportunidade para melhorar a acurácia das estimativas de ET, propiciando um aprimoramento na compreensão dos impactos nos fluxos de água e energia devido a atividades antrópicas. Deste modo, estes resultados enfatizam os potenciais e limitações das variáveis hidrológicos obtidas por sensoriamento remoto, especialmente para a ET, e como as mudanças LULC podem modificar este fluxo na América do Sul.

Palavras-chave: evapotranspiração, sensoriamento remoto, *eddy covariance*, uso e cobertura do solo.

ABSTRACT

South America is a water-abundant continent, home to the world's largest river basins and rainforest, which plays a crucial role in providing moisture to other regions of the continent through evapotranspiration (ET). ET is a crucial indicator of the earth's ecosystem functioning, linking the water, energy, and carbon cycles. Due to the great challenge of obtaining ET information based on *in situ* measurements, remote sensing data has become a great opportunity to obtain ET estimations. Based on measurements and estimations based on remote sensing data, this study aimed to evaluate the dynamics, patterns and controls of water and energy fluxes in South America, seeking to answer three main questions: *i*) can remote sensing data provide accurate information on the water balance?; *ii*) how do the factors controlling ET vary across different biomes and land use and land cover (LULC) conditions? and *iii*) can remote sensing models represent accurately ET patterns and its components under different LULC conditions? To answer the first question, we performed a water balance analysis, evaluating the uncertainties of precipitation and ET estimations using *in situ* measurements, and conducting an analysis to understand how much these uncertainties can be affected due to the basin's scales. The results showed that due to the uncertainties related to each of the variable from remote sensing it is not yet possible to achieve the water balance closing. However, the approach proved to be a great alternative to evaluate the dynamics of water fluxes from small to large basins, especially in those where *in situ* measurement is still scarce. To seek to answer the second question, we evaluated the influence of biotic and abiotic factors on ET control processes, based on surface and aerodynamic conductances and the decoupling factor, at 20 flux measurement sites in South America. Through this analysis, different patterns of latent (LE) and sensible (H) heat fluxes were verified, and different degrees of importance of biotic and abiotic controls on the ET process according to different LULC conditions. Finally, based on 11 flux measurement sites and four ET models (MOD16, GLEAM, PML and SSEBOP), we assessed the accuracy of ET estimates in the Amazon basin, and the representation of ET fluxes in forest, pasture, and soybean areas, in the Tapajós basin. The results showed that obtaining accurate ET estimates is still a major challenge in the Amazon basin, especially in humid and seasonally flooded sites. Significant discrepancies between the models and between measurements were found, and these discrepancies were even more significant when evaluated the individual ET components. However, even though each model did not perform significantly under all climatic and vegetation conditions, they present together a great opportunity to improve the accuracy of ET estimates, leading to an improved understanding of the impacts on water and energy fluxes due to human activities. Thus, these results demonstrate the potential and limitations of hydrological components obtained by remote sensing, especially for ET, and how LULC changes may modify this flux in South America.

Keywords: evapotranspiration, remote sensing, eddy covariance, land use and land cover.

SUMMARY

CHAPTER 1 12
1.1 Introduction 12
1.2 Objectives 14
1.3 Thesis scope 15
CHAPTER 2 Theoretical revision 16
2.1 South America hydrology overview 16
2.2 Evapotranspiration measurements 21
2.3 Evapotranspiration models 27
2.4 Uncertainties of evapotranspiration remote sensing models 36
2.5 Evapotranspiration drivers and controls 38
CHAPTER 3 Assessment of terrestrial water balance using remote sensing data in South America 41
3.1 Introduction 41
3.2 Dataset descriptions and methodological analysis 44
3.2.1 Study area 44
3.2.2 Remote sensing dataset descriptions 46
3.2.2.1 Precipitation 46
3.2.2.2 Evapotranspiration 46
3.2.2.3 Terrestrial water storage 47
3.2.3 Surface observations 48
3.2.3.1 River discharge measurements 48
3.2.3.2 Precipitation measurements 48
3.2.3.3 Evapotranspiration measurements 48
3.2.4 Assessment of accuracy of the precipitation and evapotranspiration estimations 50
3.2.5 Water balance and uncertainty analysis 51
3.3 Results and discussion 53
3.3.1 Uncertainties in precipitation and ET estimations 53
3.3.1.1 Uncertainties in Precipitation 53
3.3.1.2 Uncertainties in Evapotranspiration 55
3.3.1.3 Uncertainties in the terrestrial water balance 57
3.3.2 Assessment of water balance dynamics 64
3.4 Conclusions 69

CHAPTER 4 What controls evapotranspiration in South America? An assessment of multiple climate and land cover conditions 71
4.1 Introduction 71
4.2 Datasets and analysis method 73
4.2.1 Evapotranspiration measurement sites 73
4.2.2 Data filtering and quality control 75
4.2.3 Energy balance closure 76
4.2.4 Evapotranspiration control analysis 77
4.3 Results 78
4.3.1 Patterns of energy fluxes 78
4.3.2 Patterns of aerodynamic conductance 80
4.3.3 Patterns of surface conductance 82
4.3.4 Patterns of the Jarvis and McNaughton decoupling factor 84
4.4 Discussion 89
4.4.1 How do energy fluxes range over multiple biomes and LULC conditions across South America? 89
4.4.2 How different are ET drivers over multiple biomes and LULC conditions? 90
4.5 Conclusions 92
CHAPTER 5 How the remote sensing models represent evapotranspiration at different land use and land cover conditions? 94
5.1 Introduction 94
5.2 Data 97
5.2.1 Basin-Forest Amazon system 97
5.2.2 Evapotranspiration models 99
5.2.3 Amazon evapotranspiration measurement sites 100
5.2.4 Land use and land cover data 101
5.3 Methods 101
5.3.1 Data filtering and quality control of evapotranspiration measurements 101
5.3.2 Assessing remote sensing evapotranspiration models 101
5.3.3 Evapotranspiration at different land use and land cover conditions 102
5.3.4 Statistical analysis 102
5.4 Results 102

5.4.1 Patterns and accuracy of the remote sensing ET models over measurements sites in the Amazon 102
5.4.1.1 Forested sites in equatorial region 104
5.4.1.2 Cropland/Pasture site in equatorial region 105
5.4.1.3 Tropical semideciduous forest sites in southern region 106
5.4.1.4 Pasture in southwestern Amazon 107
5.4.1.5 Seasonally flooded site 107
5.4.2 Patterns of evapotranspiration at forest, pasture, and soybean areas in the Tapajós basin 108
5.4.3 Patterns of evapotranspiration components (transpiration, soil evaporation and loss interception) at forest, pasture, and soybean areas in the Tapajós basin 110
5.5 Discussion 113
5.5.1 How accuracy the remote sensing models estimate and ET pattern in the Amazon basin? 113
5.5.2 How is the evapotranspiration flux and its components patterns at different LULC in Tapajós basin? 117
5.6 Conclusions 119
CHAPTER 6 121
6.1 Final conclusions 121
6.2 Future perspectives 122
References 123
Supplementary Information S3 159
Supplementary Information S5 168

CHAPTER 1

1.1 Introduction

South America's landscape has been transformed in recent years, mainly due to anthropogenic activities, such as the expansion of agricultural areas. Recent information about the land use and land cover (LULC) from MapBiomas project (MapBiomas 2021) showed that in Brazil, from 1985 to 2020, there was a loss of forest cover about 74 million hectares, that is equivalent to a reduction of 12.8%, while agricultural areas increased 44.6% in the same period.

The LULC transformation has shown significant rates of deforestation across all biomes in South America, including the Amazon Forest, the largest tropical forest in the world (Cohen et al. 2007), that lost about 44.50 million hectares of forested areas between 1985-2020 (MapBiomas, 2021) in Brazilian territory. Deforestation and anthropogenic expansion areas (such as pasture and agriculture areas) are even more pronounced in the transition area between Cerrado and Amazon biomes, in the south and eastern regions (known as the arc of deforestation).

Several studies have linked changes in LULC with impacts on water availability, mainly over the Amazon (but not limited to this biome), affecting rainfall regime (Wongchuig et al. 2021), surface temperature (Loarie et al. 2011), occurrence of extreme events (such as droughts) (Marengo 2014; Marengo et al. 2016; Nobre et al. 2016), changes in dry season length (Costa and Pires 2010), in moisture recycling (Baker and Spracklen 2019; Dias et al. 2015; Khand et al. 2017; Laipelt et al. 2020; de Oliveira et al. 2020; Panday et al. 2015; von Randow et al. 2004; Wongchuig et al. 2021), in carbon dioxide (CO_2) concentrations, and occurrence of fires (Aragão et al. 2018).

The impacts observed in the water, energy, and carbon cycles due to landscape modifications can be even further intensified in the face of scenarios projected by global models that indicate increasing land surface temperature and changes in precipitation, evapotranspiration (ET), and discharge, providing increase in flooding and drought events in South America (Brêda et al. 2020; Fisher et al. 2017; Marengo 2014; Sorribas et al. 2016).

Some methodologies have been proposed to monitor droughts (Anderson et al. 2011, 2016), and water resources management world-wide (ANA 2020; Melton et al. 2021), considering ET as a key indicator of the interaction between the surface and the

atmosphere. Variations in ET can influence precipitation, surface water availability and CO_2 storage. For instance, changes in latent heat flux (LE), can impact sensible heat flux (H), altering land surface temperature (Wang and Dickinson 2012; Zhang et al. 2016a). In addition, CO_2 concentrations and water exchange can significantly be affected by impacts on vegetation transpiration and soil evaporation processes (Davidson and Artaxo 2004).

Several initiatives have significantly contributed to improving our knowledge about the processes involving water and energy exchanges, through flux measurement sites (Cabral et al. 2015; Hasler and Avissar 2007; von Randow et al. 2004; Restrepo-Coupe et al. 2013, 2017, 2021b; a; da Rocha et al. 2009; Rubert et al. 2018; Souza et al. 2019; Timm et al. 2014; Zimmer et al. 2016). However, the current flux measurement network does not have a sufficient density to cover all the climate and vegetation heterogeneity that exists in South America. To overcome this spatial coverage challenge, remote sensing, and land surface models (LSMs) have been presented as a great alternative to obtain water and energy fluxes estimates for large scales and long-term periods.

LSMs are based on biophysical and biogeochemical processes, estimating water and energy fluxes at multiple temporal conditions, depending on observed atmospheric data or coupled with climate models to estimations of variables under future climate change scenarios (Getirana et al. 2014; Sörensson and Ruscica 2018).

Furthermore, based on land surface temperature and vegetation information, several remote sensing models, from regional to global scale, have been proposed to estimate ET. Some of them are based on vegetation index and physical equations, such as *Penman-Monteith* (Monteith 1965; Penman 1948) and *Priestley and Tayler* (Priestley and Taylor 1972) (Martens et al. 2017; Miralles et al. 2011a; Mu et al. 2007, 2011; Zhang et al. 2016b, 2019). Other models are based on energy balance, and the simplified surface energy balance (Allen et al. 2007; Bastiaanssen 1995; Senay et al. 2013).

Nevertheless, it is not trivial for these models to represent all physical processes related to water and energy exchange. The accurate estimates are directly related to how much we understand the patterns, drivers and ET controls over multiple conditions. Accurate ET estimation is crucial to improve our understanding of the physical processes that happen in the interaction between surface and atmosphere, across multiple LULC and climate conditions. Many of the processes involving ET and its components (transpiration, soil evaporation, and interception) have not yet been fully evaluated across the heterogeneity of South America. For instance, some early vegetation models have

shown ET limited by water availability in the central Amazon region, while measurement sites have shown that ET in this region is not limited by water availability, but rather by energy availability (Restrepo-Coupe et al. 2013). Estimates of ET from water balance have reinforced these findings, showing that in the Amazon basin, neither rainfall nor radiation alone can explain ET patterns, in this basin the water fluxes are driven by a combination of energy and water availability (Maeda et al. 2017).

The literature has pointed to two important paths for ET-based science: *i*) improving our understanding of ET processes based on measurement sites, and *ii*) improving our understanding of how models represent these processes. These two points are crucial for advancing ET-based science, providing high-quality information for climate change prediction, extreme event monitoring, and water resource management.

Thus, this study aimed to evaluate the integration of several remote sensing products to estimate the water cycle variables, mainly focusing on multiple ET models, and on the extensive South American flux sites network, in order to understand *i*) can remote sensing provide accurate water balance information for multiple basin scales?; *ii*) how do ET controls range across different biomes and land use and land cover (LULC) conditions?; and *iii*) can the remote sensing models represent accurately the patterns of ET and its components at different LULC conditions?

1.2 Objectives

The main purpose of this study is to assess in an integrated approach, water, and energy fluxes, based on remote sensing and flux measurements, evaluating their dynamics, accuracy, patterns, drivers, and controls, at multiple scales and vegetation conditions in South America.

Specifically, this study aims to:

1) Evaluate the remote sensing data to estimate water balance, assessing the accuracy, uncertainties of terrestrial water storage and discharge based on water balance, and the scale effect over the accuracy of the water balance estimations.
2) Assess patterns, drivers, ET controls to investigate how they can be impacted by LULC changes.

3) Evaluate the accuracy of remote sensing models and their ability to represent ET and their component patterns over natural and anthropogenic vegetation types.

1.3 Thesis scope

This thesis is divided into six chapters. The first presents a general introduction, emphasizing the importance of studies on the biosphere-atmosphere interaction in South America. The second chapter presents a theorical revision, focusing on South America hydrology, description of part of the South American measurement sites, revision of the approaches of the main and freely available ET models based on remote sensing, a revision of the accuracy of these models over global and South America sales, as well as, an overview about the patterns, drivers and ET controls in South America. The following chapters (3-5) seek to answer the specific objectives of the thesis, assessing the water balance analysis by remote sensing, the impacts of LULC on ET drivers and controls based on measurements of ET, and the remote sensing model's performance to estimate ET and how these models represent the LULC changes on ET and its components. Finally, chapter 6 brings the final conclusions and perspectives of this study.

CHAPTER 2

Theoretical revision

2.1 South America hydrology overview

South America is a continent abundant in freshwater availability, in forest coverage, and is home of the largest basin in the world, the Amazon basin, covering about 40% of the continent, with an area of approximately 6 million km², and contributing about 15 to 20% of the total freshwater that goes to the ocean (~200,000 m³/s) (Brêda et al. 2020; Fassoni-Andrade et al. 2021; Marengo et al. 2012; Salati et al. 1979; Salati and Vose 1984). South America presents a huge diversity and complexity of hydrologic and climatic systems, covering regions of low and mid latitudes, and a diversity of geographic regions, such as Andes Mountains in the west coast, the Atacama Desert located in northern Chile in addition to the vast regions containing water surfaces, such as Amazon basin (Reboita et al. 2010). **Figure 2.1** presents the major hydrological basins, Rivers, ET, and precipitation mean annual rates in South America.

In the Amazon basin, the precipitation varies across the east-west and north-south gradient, with higher precipitation rates in the north region (~3,000 mm/year), without a defined dry season (Heerspink et al. 2020; Maeda et al. 2017), while lower rates (~1,500 mm/year) and longer dry season (4-5 months) are verified in the south region (Maeda et al. 2017; da Rocha et al. 2009). These variations are mainly related to the intertropical convergence zone (ITCZ), that depending on the period of the year, moves further north or further south in the Amazon region, characterizing periods of less rainfall in mid-July and more rainfall in mid-January (Reboita et al. 2010). However, in the northernmost region of South America, and this includes the northern Amazon basin, is almost always under the ITCZ influence, presenting high precipitation rates, and non-dry season (Villar et al. 2009). Furthermore, through tropical forest in this basin, a significant amount of precipitation is recycled through ET (49-65%) (Maeda et al. 2017), providing humidity to the southern region in South America, especially the La Plata basin (Salati et al. 1979; Satyamurty et al. 2013). As precipitation, ET also presents different magnitudes, patterns, and controls in the Amazon basin. For example, in the Negro basin, in the north region,

ET rates are around 1,600 mm/year[1], in the southern region, at Madeira basin, ET rates are around 1,200 mm/year[1], and considering whole basin (Óbidos station), mean annual ET is about 1,400 mm/year[1]. When we consider the patterns and limiting factors in the wetter basins (*i.e.* central and western Amazon regions), ET presents no defined seasonality and is mostly limited by energy availability (Costa et al. 2010; Hasler and Avissar 2007; Maeda et al. 2017; Restrepo-Coupe et al. 2013; da Rocha et al. 2009). On the other hand, in the southern region, ET decreases over the dry season, and the process is limited by water availability in this period (Costa et al. 2010; Hasler and Avissar 2007; Maeda et al. 2017; da Rocha et al. 2009).

Another important basin in South America is the Orinoco basin, located on the border between Venezuela and Brazil, covering an area of around one million of km² (Stokes et al. 2018). This basin presents a mean annual discharge of about 33 thousand of m³/s (Frappart et al. 2015; Gallay et al. 2019), and a length around 2,140 km from its source at the Cerro Delgado Chalbaud in Sierra Parima to the Orinoco Delta (Gallay et al. 2019). Orinoco basin is characterized by savanna forests, where the precipitation is mainly influenced by ITCZ, with defined dry (November - April) and wet seasons (May - October) (Arias et al. 2020).

La Plata basin is the second largest basin in South America, and the fifth largest basin in the world, in terms of area, covering 3.2 million of km², and five South American countries (Argentina, Bolivia, Brazil, Paraguay and Uruguay) (Chen et al. 2010; Tucci and Clarke 1998). This basin has three main tributaries, Paraguay, Paraná, and Uruguay Rivers, which present different water fluxes conditions and has a great importance in terms of economy, since it is home to the largest hydroelectric power plants, and important agricultural areas, in South America (Berbery and Barros 2002; Chen et al. 2010). The annual precipitation in the La Plata basin decreases from north to south, and from east to west, reaching about 1,800 mm/year in the upper parts of both the Paraguay and Paraná River basins and around 200 mm/year along the western boundary of the basin (Tucci and Clarke 1998).

The Paraguay basin is in one of the most densely populated regions of South America, where agriculture and livestock is an important economic activity (Berbery and Barros 2002). A significant part of Paraguay basin is covered by one of the largest wetland areas in the world, the Pantanal (Hamilton et al. 1996), that has a flat relief and mild slope,

[1] Evapotranspiration data from GLEAM model, considering the period between 2003-2014.

resulting in very slow and large flooded areas, regulating the Paraguay streamflow (Tucci and Clarke 1998). The Paraná River basin is usually divided into three regions, Upper, Middle, and Lower Paraná sub-basins, with most River streamflow coming from the upper and middle parts, with a small contribution from the lower sub-basins (Berbery and Barros 2002). The smallest basin in the La Plata basin is the Uruguay River basin, covering an area of around 365 thousand of km² in parts of Brazil, Uruguay, and Argentina, with a mean flow of around 4,500 m^3/s (Camilloni et al. 2013). This region is under humid subtropical climate conditions, where the precipitation is well distributed throughout the year, associated with the action of subtropical cyclonic vortices, cold frontal systems, and the South Atlantic convergence zone (SACZ) (Filho et al. 2005; Reboita et al. 2010). Precipitation in this region ranges from 1,050 to 1,750 mm/year, with higher rates in southern Brazil on the border with Paraguay (1,750-2,100 mm/year) (Reboita et al. 2010).

In these basins ET presents similar magnitude, ranging from 930 to 1,125 mm/year¹. However, they present different limiting factors. For instance, in Paraná and Paraguay basins ET present lower rates during the dry season due to the limited water availability in this period, in the Uruguay basin, the lower ET is occurs during the winter (coincident with the dry season in the Paraná and Paraguay basins), due to the lesser radiation incidence (Moreira et al. 2019).

Important hydrological basins border with the Amazon and La Plata basins, such as Tocantins–Araguaia and São Francisco. These basins are under Cerrado biome and tropical wet–dry climate. Tocantins-Araguaia basin has a drainage area of 767 thousand of km², entirely within in Brazilian territory (Ho et al. 2015; Pelicice et al. 2021). The Tocantins and Araguaia Rivers are the two main tributaries of this basin. The Tocantins River has 1,960 km of extension, and the Araguaia River presents an extension of 1,670 km, and hosting along the middle of its course the Bananal Island, the largest wetland in the Cerrado biome (Ho et al. 2015; de Oliveira Serrão et al. 2021; Progênio and Blanco 2020; Siqueira et al. 2018). In this region the precipitation presents characteristics dry and wet seasons, with an annual an average of 1,869 mm/year, mainly occurring during the austral summer (December-February), due to the moisture transport from the Atlantic Ocean (Ciemer et al. 2018; Gan et al. 2004; dos Santos et al. 2022). As precipitation, ET presents a defined seasonality pattern, with minimum rates during the dry season and maximum along the wet season, mainly due to the water availability, presenting a mean annual ET around 1,000 mm/year¹.

São Francisco basin also covers large part of Cerrado, in addition to part of Caatinga biome, under tropical and semi-arid climate conditions. This basin drains an area of 622 thousand of km² with an annual mean discharge of 1,961 m^3/s (Almagro et al. 2021; Paredes-Trejo et al. 2021). São Francisco River has a length of 2,696 km, from Serra da Canastra, at Minas Gerais State until reach the Atlantic Ocean near Alagoas and Sergipe States border (Paredes-Trejo et al. 2016, 2021). The annual precipitation varies across different climatic conditions, reaching rates around >1500 mm/year in the lower and middle sub-basins, while in the semi-arid region precipitation rates are less than 700 mm/year, with maximum rates during the summer/autumn and minimum in the winter, comprising the driest Brazilian region (Borges et al. 2020; de Oliveira et al. 2021; Reboita et al. 2010), where prevailing semi-arid conditions, strongly influence of the ITCZ (Filho et al. 2005; Marengo et al. 2016). ET in this basin varies according to the water availability, with higher rates when considering the lower and mid sub-basins (mainly in the tropical climate region and Cerrado biome) (~930 mm/year¹), and lower rates (~756 mm/year¹) when we considering the whole basin (Traipu station), including the semi-arid region (Caatinga biome).

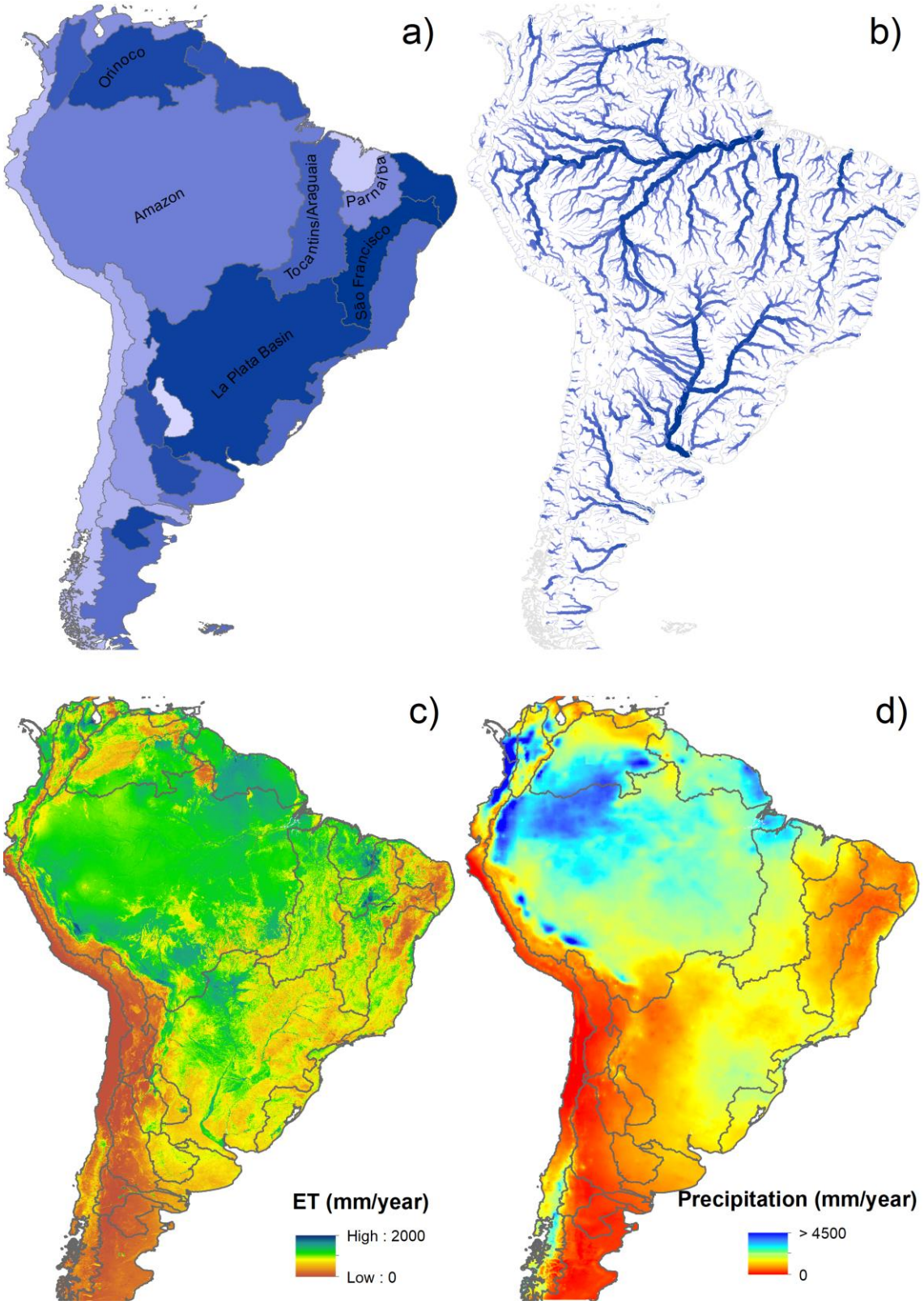

Figure 2.1 South America a) major hydrological basins, b) major Rivers, c) mean annual evapotranspiration (*ET*) based on Operational Simplified Surface Energy Balance model (SSEBOP) (Senay et al. 2013), and d) mean annual precipitation based on Climate

Hazards Group InfraRed Precipitation with Station data (CHIRPS) (Funk et al. 2015). Mean annual ET and precipitation information was obtained from 2003 to 2017. Hydrological information was obtained from Brazilian Water Agency (ANA) (https://www.gov.br/ana/pt-br).

2.2 Evapotranspiration measurements

Through ET measurements crucial information about the patterns, drivers and ET controls, was provided at local scales, covering multiples biomes and LULC conditions in South America (Biudes et al. 2015; Borges et al. 2020; Costa et al. 2010; Diaz et al. 2019; Gonçalves de Gonçalves et al. 2013; de Oliveira et al. 2021; Restrepo-Coupe et al. 2021a; da Rocha et al. 2009; Rubert et al. 2018; Souza et al. 2019). However, due to the cost and maintenance difficulties of the flux towers, there is a low density of coverage in South America, as well as in other regions of the world, that do not cover all vegetation and climate complexity. In South America, multiple initiatives have contributed to advance of ET science through flux networks. Twenty two sites were used in this study covering part of the South America are from: *i*) the Large-Scale Biosphere and Atmosphere Experiment in the Amazon (LBA) program (Davidson and Artaxo 2004; Gonçalves de Gonçalves et al. 2013; Keller et al. 2004; Restrepo-Coupe et al. 2021b; Saleska et al. 2013), *ii*) AmeriFlux (Baldocchi et al. 2001), *iii*) Fluxnet (Pastorello et al. 2020), *iv*) Long-term Ecological Research in Pantanal (PELD) (Biudes et al. 2015), *v*) South Brazilian Network of Surface Fluxes and Climate Change (Sulflux) (Roberti and Acevedo 2012), and *vi*) National Observatory of Water and Carbon Dynamics in the Caatinga Biome (ONDACBC) (Borges et al. 2020; de Oliveira et al. 2021). These programs are intended to measure water flux, energy, and CO_2 measurements, providing studies about the interactions between terrestrial ecosystems and the atmosphere. **Figure 2.2** presents the localization of these measurement sites across South America.

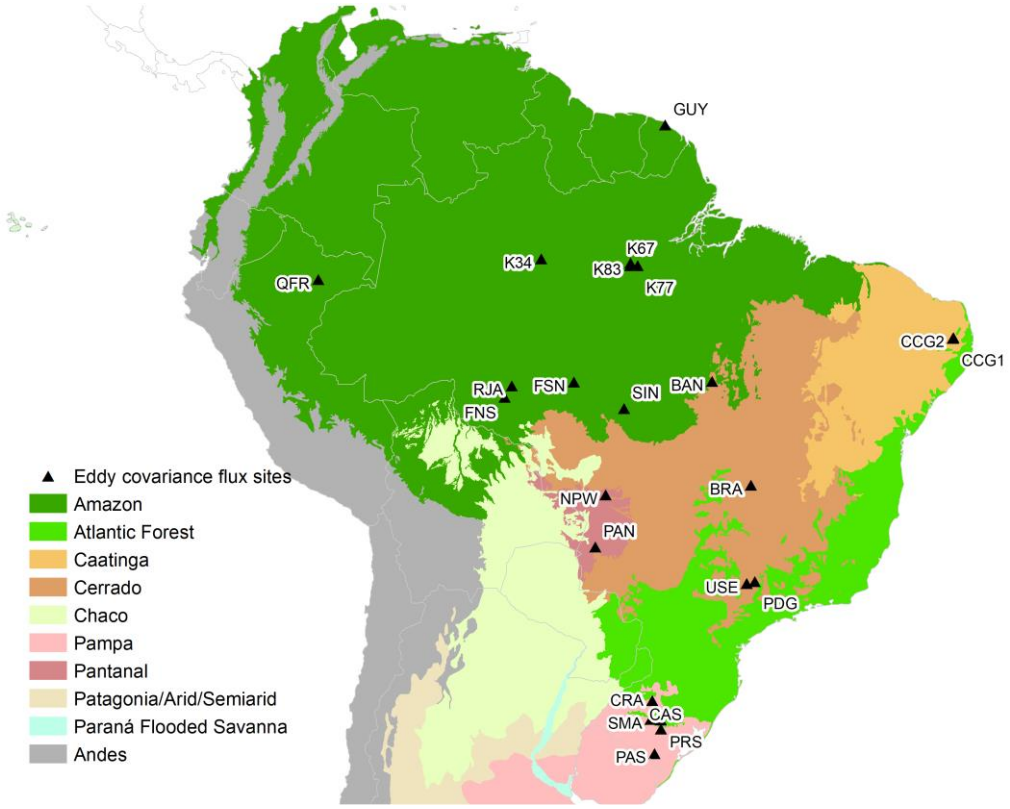

Figure 2.2 Location of the sites in South America. South America biomes were adapted from the Terrestrial Ecoregions of the World (Olson et al. 2001), and modified based on Turchetto-Zolet et al. (2013).

The sites are located in a wide range of climate and biomes, mainly in Brazil. The Amazon biome is covered by ten measurement sites, from west, east, and southwest region. The westernmost site is in Peru, in a tropical peatland area, (Quistococha Forest Reserve - QFR). The region is still few explored in terms of water, energy, and carbon fluxes, representing important biophysical feedback about climate change. Peatlands are important carbon and methane budgets ecosystems, which can be sensitive to disturbances in natural cover land and become a major source of CO_2 (Griffis et al. 2020). The most eastern site is Guyaflux (GUY) in French Guiana, at tropical climatic conditions, mainly driven by the north/south movement of the Inter-Tropical Convergence Zone (ITCZ), and the dry period extending from August to November (Bonal et al. 2008). In the central area, Manaus K34 (K34) is also in a humid tropical climatic zone and has a three-month dry season (July–September) (da Rocha et al. 2009) and has high precipitation rates (~2,400 mm/year). The easternmost sites, Santarém K67 (K67), Santarém K77 (K77), and Santerém K83 (K83) are near the confluence of the

Tapajos and Amazon Rivers and have a four-month dry season (July–October) (da Rocha et al. 2009; Saleska et al. 2003), and the annual precipitation rates is around 1,900 mm/year. K67 and K83 are two forested sites, however, K83 was selectively logged in 2001, removing only 5% of the aboveground biomass, creating a patchwork of intact forest surrounding newly created gaps (Goulden et al. 2004). K77 is a cropland/pasture site, approximately 500 ha field surrounded by tropical forest that was first used as pasture field (~1990) to cattle grazing, and then, a rainfed cropland (rainfed rice and other crops), after December 2001 (Sakai et al. 2004). However, after the harvest, in June 2002, the field was not replanted (Restrepo-Coupe et al. 2013; Sakai et al. 2004).

In Southern Amazon Forest, we have four more sites (FNS, FSN, SIN and RJA), in a transitional region between the Amazon and Cerrado biomes, presenting marked precipitation seasonality and longer dry season. While Reserva Jaru (RJA) and Sinop (SIN) are two tropical semi-deciduous forests, with longer dry season (from 4 to 5 month, generally May to September) (Biudes et al. 2015; von Randow et al. 2004), Fazenda Nossa Senhora (FNS), and Fazenda São Nicolau (FSN) are two pasture sites. FNS was originally cleared in 1977 and consists of perennial grass, and in FSN, the forest was converted to pasture in 1987, where the grass is similar to those dominant pasture grass in FNS (Hasler and Avissar 2007).

At Pantanal biome there are two sites evaluated in this study, Northern Pantanal wetland (NPW) and Fazenda São Bento (PAN). NPW is in a protected area known as Baia das Pedras, located in the northern Pantanal, a region that is seasonally flooded (Dalmagro et al. 2018). Floods typically reach the maximum flooding at March beginning, when become an aquatic ecosystem, with peak flood levels typically not exceeding one meter (Dalmagro et al. 2018, 2019). Whilst PAN is located to the south of the biome, in the municipality of Corumbá-MS, in a typical seasonally flooded area, consisting of grasses and tree elements with a height of 8 to 10 meters (de Oliveira et al. 2006), where the average annual precipitation showed lower values than in the north region, about 1,100 mm and the dry season between the months of April to September.

Cerrado is covered in this study by four sites. The biome is a savanna, which presents a strong precipitation seasonality, where the wet season is usually from October to March, and the dry season, from April to September (Sano et al. 2010). One site is in floodplain area Tocantins-Javaés (BAN), in a native Cerrado area, located 1 km east the Javaés River (Borma et al. 2009). The region has seasonal floods between the months of January and March, when precipitation totals reach 300 mm/month, and last for about three to five

months. The climate is predominantly humid tropical, and the dry season generally lasts five months (May-September) (da Rocha et al. 2009). At native Cerrado there is one more site, Brasília (BRA), characterized by a xeromorphic, open-shrub savanna vegetation with scattered shrubs and tree-like vegetation (defined as Cerrado *Campo Sujo*) (Santos et al. 2003). This site is in the Ecological Reserve of the Brazilian Institute of Geography and Statistics (IBGE), 35 km south of Brasília-DF. The region presents a strong seasonal precipitation pattern, with a dry season from May to September, with practically no precipitation from June to August, and a total annual precipitation of approximately 1,400 mm/year (Santos et al. 2003). Further south in the biome are two other sites, one in a native Cerrado area, Pé-de-Gigante (PDG) (da Rocha et al. 2002), characterized by pristine woodland savanna vegetation, and another is Usina Santa Elisa (USE), a cropland site cultivated with rainfed sugarcane (Cabral et al. 2003). Both are in the state of São Paulo, region with a long dry season, from April to September and total annual precipitation around 1,300 mm.

The driest biome studied here is Caatinga, one of the largest semiarid regions in South America, covering a large area in Northeast Brazil, around 800,000 km² (IBGE 2004). This region experiences a hot and dry climate, presenting average rainfall lower than 1,000 mm/year, markedly seasonal, causing longer dry period, high temperatures (23 to 27 °C), and lower relative humidity, usually below 50% (Menezes et al. 2012; de Oliveira et al. 2012). Droughts are part of the natural climate variability in this region, mainly affecting vulnerable populations, and providing risk of water scarcity and food security, such as the 2012-2015 drought, which had significant impacts on agricultural production in this region (Barbosa et al. 2019; Marengo et al. 2016). And, according to climate change projections, this phenomenon is likely to continue occurring and intensifying in the future (Marengo et al. 2016). This biome was assessed by two sites, with different vegetation structures and densities: (*i*) Caatinga Campina Grande 1 (CCG1), a pristine Caatinga area with dense vegetation, and (*ii*) Caatinga Campina Grande 2 (CCG2), a degraded Caatinga area with sparse vegetation and less than 2 m height (Borges et al. 2020).

It also evaluated sites in a subtropical condition, in Pampa biome, located in eastern side of South America, covering parts of Argentina, Brazil, and Uruguay countries (Modernel et al. 2016; Overbeck et al. 2007). In Brazil, Pampa biome occupies the southern region, a transitional zone between tropical and temperate climates, with hot summers and cool winters and no well-defined dry season (Overbeck et al. 2007). Thus, in this region, the

climate is predominantly humid subtropical, with precipitation of around 1,600 mm/year, distributed throughout the year, with an expressive thermal amplitude, where temperatures are lower during the winter season, around 16 °C, and higher in the warmer months, around 29 °C.

A mosaic of grassland and shrubland composes natural vegetation of this biome, which are used to cattle, and agricultural production, highly influencing the economy and culture of this region (Oliveira et al. 2017; Overbeck et al. 2007).

In this study, Pampa biome was evaluated through five sites, all in Rio Grande do Sul state, Brazil. Two of them are in the natural grassland area, used to graze cattle, Santa Maria (SMA), in the central region, and Pedras Altas (PAS), in the south (Rubert et al. 2018). The other three sites are in croplands areas, where Cachoeira do Sul (CAS) and Paraíso do Sul (PRS) (Souza et al. 2019; Timm et al. 2014; Zimmer et al. 2016), are irrigated rice sites, in the central region, and Cruz Alta (CRA) (Aguiar 2011), in the northwest region, is cultivated with summer and winter crops (mainly soybeans in the summer and wheat in the winter) in a rainfed system. **Table 2.1** summarizes the information on the flux measurement sites to be used in this study, as well as indicating the references for each site, where more information can be found on instrumentation, measurement procedures, and methods for gaps filling and data validation.

Table 2.1 Evapotranspiration measurements sites in South America.

Site	Name	Biome	Lat. (˚)	Lon. (˚)	Land cover	Data availability	Reference
FNS	Fazenda Nossa Senhora	Amazon	-10.76	-62.35	Pasture	Jun 2000–Mar 2004	(von Randow et al. 2004)
FSN	Fazenda São Nicolau	Amazon	-9.85	-58.26	Pasture	Mar 2002–Oct 2003	(Priante-Filho et al. 2004)
GUY	Guyaflux	Amazon	5.28	-52.92	Tropical forest	Jan 2004–Dec 2014	(Bonal et al. 2008)
K34	Manaus – K34	Amazon	-2.60	-60.20	Tropical humid forest	Jan 2000–Sep 2006	(de Araújo et al. 2002)
K67	Santarém – K67	Amazon	-2.85	-54.95	Tropical humid forest	Jun 2002–Jan 2006	(Saleska et al. 2003)
K77	Santarém – K77	Amazon	-3.01	-54.53	Pasture and rainfed cropland (soybeans and rice)	Aug 2000–Nov 2005	(Sakai et al. 2004)
K83	Santarém – K83	Amazon	-3.01	-54.97	Tropical humid forest	Jun 2000–Mar 2004	(Goulden et al. 2004)

QFR	Quistococha Forest Reserve	Amazon	-3.83	-73.31	Tropical peatland	Jan 2018–Dec 2019	(Griffis et al. 2020)
RJA	Reserva Jaru	Amazon	-10.08	-61.93	Tropical semideciduous forest	Jan 2000–Nov 2002	(von Randow et al. 2004)
SIN	Sinop	Amazon	-11.41	-55.32	Tropical forest	May 2005–Oct 2008	(Biudes et al. 2015)
NPW	Northern Pantanal wetland	Pantanal	-16.49	-56.41	Woodland savanna (seasonally flooded)	Dec 2013–Jun 2017	(Dalmagro et al. 2018)
PAN	Fazenda São Bento	Pantanal	-19.56	-57.01	Grassland	Sep 2000–Dec 2002	(de Oliveira et al. 2006)
BAN	Javaés/ Tocantins	Cerrado	-9.82	-50.15	Woodland savanna (seasonally flooded)	Oct 2003–Dec 2006	(Borma et al. 2009)
BRA	Brasília	Cerrado	-15.93	-47.87	Savanna (*campo sujo*)	Jan 2011–Dec/2011	(Santos et al. 2003)
PDG	Reserva Pé de Gigante	Cerrado	-21.61	-47.64	Woodland savanna	Jan 2001–Dec 2006	(da Rocha et al. 2002)
USE	Usina Santa Elisa	Cerrado	-21.72	-48.11	Cropland (rainfed sugarcane)	Jan 2001–Dec 2002	(Cabral et al. 2003)
CCG1	Campina Grande 1	Caatinga	-7.27	-35.97	Dense Caatinga	Jan 2013–Sep/2017	(Borges et al. 2020)
CCG2	Campina Grande 2	Caatinga	-7.25	-35.95	Sparse Caatinga	Mar 2013–Feb/2017	(Borges et al. 2020)
CAS	Cachoeira do Sul	Pampa	-30.27	-53.14	Cropland (irrigated rice)	Oct 2009–Mar/2015	(Souza et al. 2019)
CRA	Cruz Alta	Pampa	-28.60	-53.66	Cropland (rainfed soybean and wheat)	Jan 2009–Sep 2014	(Aguiar 2011)
PAS	Pedras Altas	Pampa	-31.71	-53.53	Natural grassland	Sep 2013–Sep 2016	(Rubert et al. 2018)
PRS	Paraíso do Sul	Pampa	-29.74	-53.14	Cropland (irrigated rice)	Oct 2003–Mar 2004	(Timm et al. 2014; Zimmer et al. 2016)
SMA	Santa Maria	Pampa	-29.72	-53.76	Natural grassland	Jan 2013–Dec 2016	(Rubert et al. 2018)

2.3 Evapotranspiration models

ET is of significant importance to the terrestrial climate system, providing moisture to the atmosphere, and plays a crucial role in linking water, energy, and carbon cycles (Fisher et al. 2017; Jung et al. 2010). Studies have demonstrated that changes in land LULC can alter the water exchange between the surface and the atmosphere, causing impacts over precipitation, surface water availability, and Earth's surface temperature (Baker and Spracklen 2019; Khand et al. 2017; de Oliveira et al. 2020; Vergopolan and Fisher 2016). Since 1980s satellite images have become a valuable source of information to model ET. Currently, there are a variety of models and approaches to estimate ET in multiple spatial and temporal scales. The earliest method to estimate ET at large scale, based on remote sensing was the surface energy balance (Zhang et al. 2016a). This approach allows us to understand how the exchange of radiative, heat and moisture fluxes can affect the biosphere (Bastiaanssen et al. 1998). This approach is described in **Equation 2.1** account net radiation (Rn) as a residual of LE, H and ground (G) heat fluxes.

$$R_n = LE + H + G \tag{2.1}$$

Bastiaanssen (1995) proposed the Surface Energy Balance Algorithm for Land (SEBAL) to overcome most of the problems of the early surface energy balance models, which were suitable for local and micro scales due to their dependence on local calibration and data. This algorithm estimates the spatial variation of surface energy balance parameters empirically, deriving H from remote sensing thermal infrared, and LE as a residual of surface energy balance. H is determined as a function of temperature gradients, based on maximum hot and cold pixels (Bastiaanssen et al. 1998; Zhang et al. 2016a). Therefore, (Allen et al. 2007), based on SEBAL approach, proposed the Mapping ET at high Resolution with Internalized Calibration (METRIC). This model improved the method to select the hot and cold pixels and used an internally calibrated based on ET measurements to reduce computational biases (Allen et al. 2007, 2011).

To overcome the computation challenge due to the selection of hot and cold pixels, to determinate the temperature differential at SEBAL and METRIC models, Senay et al. (2013) developed the Operational Simplified Surface Energy Balance (SSEBOP). The model is based on simplified surface energy balance since it does not solve the energy

balance equation completely. Based on this assumption, the formulation of the model is more approximate of the psychrometric principle (Senay et al. 2013; Senay 2018). In the SSEBOP approach, the psychrometric constant for the air is adapted to a comparable constant for the surface, creating a unique surface psychrometric constant to a region and day-of-year, simplifying the ET estimate, and providing operational applications (Senay 2018). Thus, land surface temperature from satellite images is used to estimate the equivalent dry-bulb (Ts), and the wet-bulb (Tc) surface temperature, which is then used to estimate ET fraction (**Equation 2.2**) (Senay 2018; Senay et al. 2020):

$$ET_f = 1 - \gamma^S(Ts - Tc) \tag{2.2}$$

where ET_f is the ET fraction, γ^S is the surface psychrometric constant based on the aerodynamic properties of a dry-bare surface.

ET is computed based on **Equation 2.3**, as a product of ET_f, ET reference (ET_o), and a k factor, used to scale the grass-reference ET to an alfalfa reference type (Senay et al. 2020).

$$ET = ET_f * k * ET_o \tag{2.3}$$

Recently, (Senay et al. 2020) provided ET estimates from SSEBOP model on a global scale, using land surface temperature data from Moderate Resolution Imaging Spectroradiometer (MODIS) and meteorological data from Daymet/WorldClim and Global Land Data Assimilation System (GLDAS). The data are available at 10 days, monthly and yearly temporary scale and at 1km of spatial resolution.

Another physical approach was also formulated to represent the ET process by Penman (1948) based on two terms: radiation and aerodynamic (Shuttleworth 2012). Since the Penman equation was more related to calculating evaporation from open water, Monteith (1965) added surface resistance terms in the equation. Therefore, the *Penman-Monteith* equation (**Equation 2.4**) (Monteith and Unsworth 1990) becomes more consistent with an estimate ET from vegetated surfaces.

$$\lambda E = \frac{\Delta(R_n - G) + \rho c_p \frac{VPD}{r_a}}{\Delta + \gamma\left(1 + \frac{r_s}{r_a}\right)} \tag{2.4}$$

where VPD is the vapor pressure deficit, Δ is the slope of the vapor pressure curve, λ is the latent heat of evaporation, ρ is air density, C_p is the specific heat capacity of air, γ is the psychrometric constant, and r_a, and r_s, are the aerodynamic and surface resistances.

Widely known and used by the scientific community, the MODIS Global Evapotranspiration project (MOD16) was formulated by Mu et al. (2007, 2011) based on *Penman-Monteith* equation, using the algorithm first proposed by Cleugh et al. (2007). MOD16 calculates the total ET as the sum of water evaporation intercepted by the canopy, canopy transpiration, and soil evaporation, partitioning available energy using fractional cover (Mu et al. 2011). MOD16 estimates ET at the 8-day and monthly time-scales, at a spatial resolution ranging from 500 m to 0.05°, the inputs include remote sensing and global meteorological reanalysis data. The remote sensing inputs are derived from MODIS, and include the land-cover classification, leaf area index (LAI), fraction of photosynthetically active radiation, and albedo. The daily meteorological inputs include shortwave incident radiation, air temperature, and specific humidity from the Global Modeling and Assimilation Office (GMAO) Modern-Era Retrospective Analysis for Research and Applications (MERRA) reanalysis datasets, with have a spatial resolution of 0.5° x 0.6°.

Another model based on *Penman-Monteith* equation is the Penman-Monteith-Leuning Evapotranspiration (PML) (Gan et al. 2018; Zhang et al. 2016b, 2019). This approach was formulated by Leuning et al. (2008) and Zhang et al. (2010) who developed formulations to compute the canopy and soil water loss using a simple biophysical model to calculate surface conductance and LAI. PML approach was improved to include evaporation from precipitation interception by the canopy and coupled ET with gross primary production (GPP) based on canopy conductance model (Gan et al. 2018; Zhang et al. 2016b, 2019). The model uses data from MODIS, including LAI, albedo, and emissivity, in addition to meteorological inputs derived from GLDAS.

To minimize the uncertainties in the aerodynamic and surface resistance estimates related to *Penman-Monteith* approach, it was proposed the *Priestley and Taylor* equation (Priestley and Taylor 1972) that use an empirical parameter to represent the aerodynamic and surface resistances (**Equation 2.5**):

$$\lambda E = \alpha \frac{\Delta(R_n - G)}{\Delta + \gamma} \qquad (2.5)$$

where α is the *Priestley and Taylor* parameter that is usually set as 1.26 to variety of well-watered vegetated, and water surfaces (Fisher et al. 2009).

Based on *Priestley and Taylor* equation Fisher et al. (2008) developed the Priestley-Taylor Jet Propulsion Laboratory model (PT-JPL), aiming to estimate the evaporative flux on a global scale, using of approach eco-physiological constraints to reduce potential ET estimates in actual ET, determined by relative humidity, VPD, and vegetation indexes. Another remote sensing ET model based on this approach is the Global Land Surface Evaporation: The Amsterdam Methodology (GLEAM) (Martens et al. 2017; Miralles et al. 2011a). This model was designed to estimate terrestrial evaporative fluxes, and root-zone soil moisture using maximum observations derived from remote sensing, at a spatial resolution of 0.25° and a daily temporal resolution. GLEAM separates the terrestrial components of ET into canopy transpiration, soil and open water evaporation, interception loss, and sublimation. Each grid cell consists of four different fractions of land cover: bare soil, sparse vegetation, dense vegetation, and open water. The evaporative flux is computed separately for each cover fraction, and then aggregated at the pixel scale. The *Priestley–Taylor* equation is used to calculate the potential ET and then convert this to actual ET, according to the land cover and an evaporative stress factor, the latter estimated from the root zone soil moisture and vegetation water content (Martens et al. 2017; Miralles et al. 2011a, 2014).

The model requires minimal dependence on static fields of variables, proving reliable ET estimates. In contrast to other models, a detailed module is used to estimate interception loss, in addition coupling of the radiation-driven transpiration to the ground bio-physical processes, and estimating soil evaporation separately (Martens et al. 2017; Miralles et al. 2011a).

These remote-sensing models can map ET at an unprecedented spatial and temporal resolution, proving valuable information about variations of water exchange, seasonal patterns, ET processes, and contribute to improve our understanding about the human impact over energy and water cycles at a regional to global scales.

Energy balance models-based present as an advantage to estimate ET at finer spatial resolution, providing valuable information about the impact of anthropogenic activities on energy, water, and carbon cycles. Nevertheless, these models are mainly limited by clear-sky conditions, since they are heavily dependent on land surface temperature

information from remote sensing, which are only reliable for cloud-free conditions (Zhang et al. 2016a). The requirement of clear sky conditions is a challenge to estimate ET for longer time scales, especially when we are working with a finer resolution, such as Landsat, which has a temporal resolution of 16 days, or in tropical regions, where the wet season can be extended for longer time in some regions.

On the other hand, models based on vegetation index can estimate ET at long-term scale and cover the most regions world-wide, providing information about the ET patterns, drivers and limiting factors, from local to global regions. However, these models use some static input data and parametrizations, which can add uncertainties in the estimations. Furthermore, the uncertainties from meteorological reanalysis datasets can also be one reason for errors and for discrepancies observed between different models world-wide (Gomis-Cebolla et al. 2019; Melo et al. 2021; Michel et al. 2016; Miralles et al. 2016; Talsma et al. 2018).

The spatial comparison between the main remote sensing models to estimate ET that are freely available is shown in **Figure 2.3**. It worthy to note the spatial scale differences between them, and the divergencies to inform the ET magnitudes. For instance, MOD16 and SSEBOP show more details over South America than GLEAM and PML. Higher divergencies are observed mainly in the northeast region, central Brazilian region (Cerrado biome), and in the northern Amazon. In chapter 5 we will return to this discussion to bring the main reasons for the disagreement between the remote sensing models to estimate ET. The summary of the advantages, limitations, and main references of the ET models based on remote sensing are presented in **Table 2.2**.

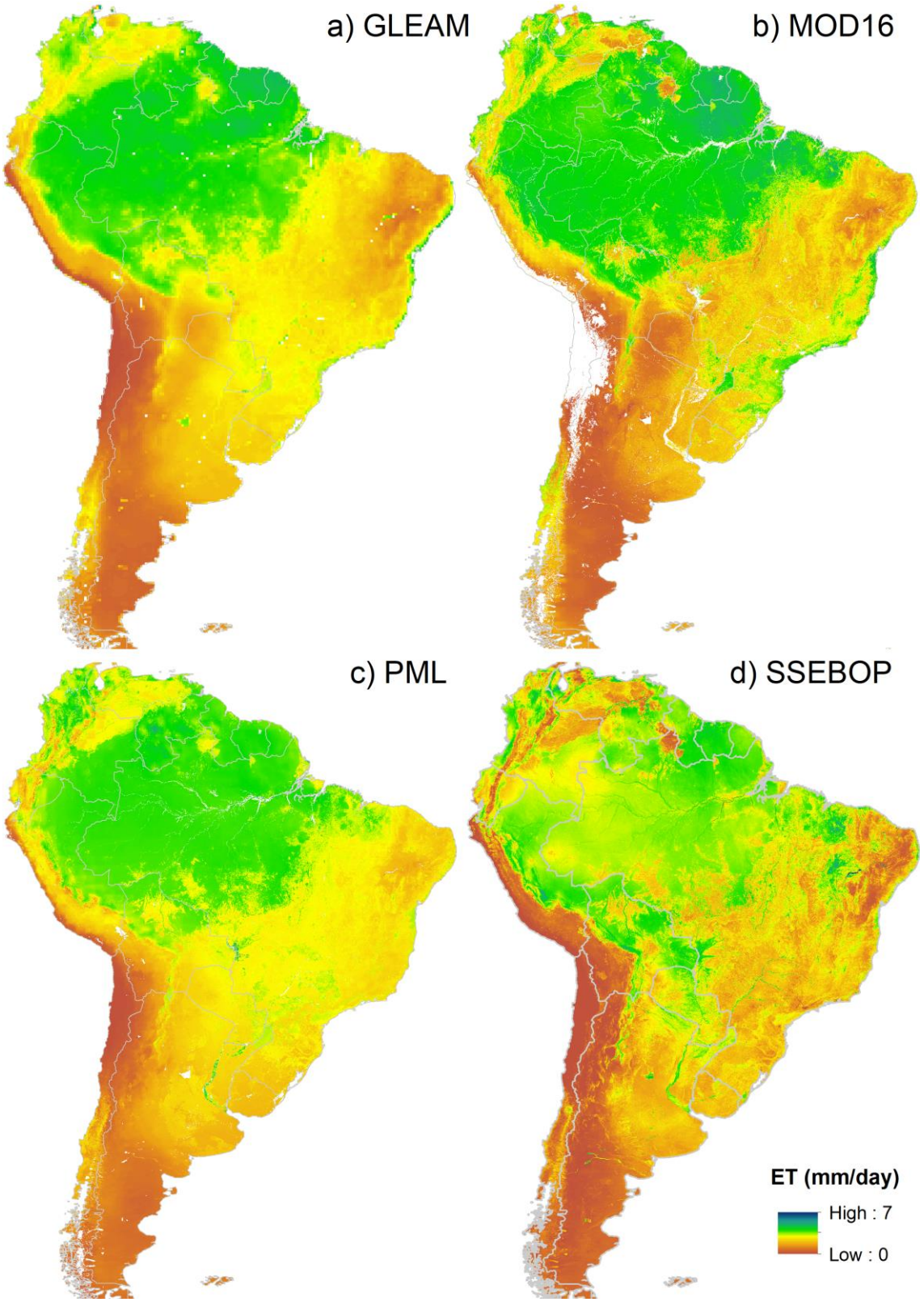

Figure 2.3 Remote sensing models estimating spatial evapotranspiration (ET), on daily average, for 2003-2017 period, covering South America. a) Global Land Evaporation Amsterdam Model (GLEAM) (Martens et al. 2017; Miralles et al. 2011a), b) MODIS Global Evapotranspiration project (MOD16) (Mu et al. 2011), c) Penman-Monteith-

Leuning Evapotranspiration (PML) (Gan et al. 2018; Zhang et al. 2016b, 2019), and d) Operational Simplified Surface Energy Balance (SSEBOP) (Senay et al. 2013).

Table 2.2 Summary of evapotranspiration models evaluated in this study

Model	Methods	Spatial Resolution	Temporal Resolution	Main remote sensing drivers	Advantages	Limitations	References
SEBAL	Surface energy balance	dependent on the satellite spatial resolution	dependent on the satellite temporal resolution	Land surface temperature	High spatial resolution, useful to water management and anthropogenic impacts evaluation, less parametrizations	Require clear-sky condition, dependent of image domain, sensibility of hot and cold pixels selection, do not distinguish between soil evaporation and canopy transpiration	(Bastiaanssen 1995)
METRIC							(Allen et al. 2007)
SSEBOP	Simplify surface energy balance				Global coverage, low complexity to implementation, useful to water management and anthropogenic impacts evaluation, publicly available, long period of data	Do not distinguish between soil evaporation and canopy transpiration, do not solve all energy balance terms	(Senay et al. 2013)
MOD16	Penman-Monteith	500 meters to 0.05 degree	8 days, monthly	Leaf area index, land cover, albedo, emissivity	Global coverage, publicly available, long period of data	Parametrization of surface conductance, use of static input data, requirement of measurement data for calibration	(Mu et al. 2007, 2011)

PML	Penman-Monteith	500 meters	8 days	Leaf area index, fraction of photosynthetically active radiation, land cover, albedo	Global coverage, publicly available, long period of data, couple ET and gross primary production	Simplification of processes, parameterization schemes	(Gan et al. 2018; Zhang et al. 2016b, 2019)
GLEAM	Priestley-Taylor	0.25 degree	daily, monthly, yearly	Vegetation cover fraction, vegetation optical dept, soil moisture, precipitation	Global coverage, publicly available, long period of data, maximizes the use of remote sensing data	Low spatial resolution, overestimate of water stress	(Martens et al. 2017; Miralles et al. 2011a)
PT-JPL		1 degree	monthly	Vegetation indexes	Global coverage, low complexity to implementation	Many ecophysiological, parameterizations, low spatial resolution	(Fisher et al. 2008)

2.4 Uncertainties of evapotranspiration remote sensing models

Considering ET-based science, Fisher et al. (2017) emphasized that despite the significant advances that have been made, more information about ET is still necessary to scientific questions and challenges within Earth System Science can be fully resolved. An important point highlighted was the need for refinements and improvement of ET accuracy, in order to enable better management of water use, as well as provide more accurate predictions of climate changes scenarios.

ET model uncertainties have been evaluated at different spatial scales, at multiple measurement sites and basins world-wide (Elnashar et al. 2021; Khand et al. 2017; Kim et al. 2012; McCabe et al. 2016; Melo et al. 2021; Michel et al. 2016; Miralles et al. 2016; Ruhoff et al. 2013; Senay et al. 2020; Sörensson and Ruscica 2018; Souza et al. 2019; Zhang et al. 2019).

At global scale, Elnashar et al. (2021); McCabe et al. (2016); Michel et al. (2016); Miralles et al. (2016); Senay et al. (2020) and Zhang et al. (2019) conducted analyses evaluating remotely sensed based ET estimates under different approaches against measurement sites and basins across the globe.

Michel et al. (2016) evaluated four models, two of them based *on Priestley and Taylor* approach (GLEAM and PT-JPL[2]), one based on *Penman-Monteith* equation (MOD16), and one based on surface energy balance (Surface Energy Balance System - SEBS). It was demonstrated that PT-JPL and GLEAM provided the best performance, when forced by satellite or measurement sites data, and considering different temporal resolution (sub-daily and daily). On the other hand, MOD16 and SEBS demonstrated a systematic under and overestimation, respectively, across global sites. In addition, the authors inform that all models provide better agreement on wet and moderately wet climate regime, since at dry climate the models demonstrate a tendency to overestimate ET, mainly due to water availability constraining.

Corroborating these findings, McCabe et al. (2016), who also evaluated ET models (PT-JPL, MOD16, GLEAM and SEBS) against 45 globally distributed measurement sites, showed that PT- JPL provided the highest overall statistical performance when compared to the other models, followed by GLEAM. The authors also verified an underestimation tendency in the MOD16 and an overestimation in the SEBS estimations. Furthermore, the

[2] Priestly-Taylor Jet Propulsion Laboratory

study demonstrated that when it is considered ET estimations to all globe, there is a tendency to reduce the performance of all models, mainly due to a response to scale mismatch and issues related to forcing quality. Also evaluating these same models (PT-JPL, MOD16, GLEAM and SEBS), (Miralles et al. 2016) conducted an analysis of 837 globally distributed basins, intercomparing the performance of these models between them, demonstrating that all models showed large dissimilarities over water stress and drought conditions.

Other ET models have been still also evaluated in terms of accuracy. For instance, Zhang et al. (2019), assessed PML model based on 95 measurement sites across the globe. The main results demonstrated that PML presents a high accuracy when compared with the measurements and outperforms most available ET models. Senay et al. (2020), evaluated the performance of the SSEBOP using 12 measurement sites over six continents and verified a reasonable performance of this model in capturing ET seasonality, despite the model demonstrate regional biases.

At South America scale, Ruhoff et al. (2013) assessed MOD16 estimations based on two measurement sites, at Cerrado biome, under natural land cover and agricultural area, and based on basin scale. The results showed variations in the uncertainties of this model as a function of scale, emphasizing that analyses at different spatial and temporal scales are of great importance in the evaluation of ET estimates based on remote sensing.

Also based on a local scale, Souza et al. (2019) evaluated the MOD16 model at irrigated cropland sites in Southern Brazil. The results informed an underestimation of the MOD16 in these sites, corroborating to the previous global studies. However, this study was also demonstrated that ET from MOD16 has a significant divergence with the measurements in terms of the main drivers. For instance, while the measurements showed higher agreement between ET and net radiation, ET from the MOD16 yielded higher correlation with LAI and fraction of photosynthetically active radiation.

Considering large scale of South America, Sörensson and Ruscica (2018) performed an intercomparison between several ET estimations, based on reanalysis, land surface, and remote sensing models, demonstrating that in dry regions the relative uncertainty of annual mean ET is higher than energy-limited regions. Melo et al. (2021) who evaluated a set of remote sensing models using 25 measurement sites over the continent showed that the models seem to be unrelated to land-use, presenting some dependency on biome and climate, since they performed better in wet and moderately wet environments.

These studies reinforced that the different model approaches to estimate ET can imply in divergency between the model estimations. Furthermore, it was demonstrated that model uncertainties can vary with spatial scale and climate conditions and was indicated that there is no single best performing model across all global biome types. In addition, despite the uncertainties of the models, these studies demonstrated that ET estimations reasonably agree with the measurement sites.

2.5 Evapotranspiration drivers and controls

ET is controlled by both physical and biophysical processes, ranging at multiple temporal and spatial scales (Zhang et al. 2016a). Some studies reinforce that we need to improve our understanding of the ET control in space and time to advance ET estimates and improve climate models (Hutyra et al. 2007; Zhang et al. 2016a). Considering that water is not a limiting factor, ET is primarily a function of available radiation to vaporize water. However, other factors can also affect ET, such as (i) wind speed (u), (ii) vapor pressure deficit (VPD), (iii) temperature, (iv) soil moisture (soil water availability), and (v) vegetation conditions (Xu and Levy 2011).

The effects over the ET process are accounted in *Penman-Monteith* equation. Both, net radiation, and surface-atmosphere interactions are considered in this equation, where net radiation accounts for the ability of the surface in capturing incoming radiation (Pereira 2004). The surface-atmosphere interactions, that depends on the aerodynamic characteristics of the surface express the conversion of sensible heat of the surrounding air into latent heat, representing the effect of vegetation over ET (Fredlund et al. 2012; Priante-Filho et al. 2004; Stewart 1989).

In South America, mainly in tropical rainforest, several studies have been assessing the factors that can control ET. One of the first studies was conducted by Hasler and Avissar (2007), who used eight measurement sites to evaluate spatial variability and ET patterns over the Amazon basin. It was shown that ET patterns are consistently controlled by radiation at equatorial sites (2°S–3°S), increasing during the dry season and decreasing over the wet season. On the other hand, in the southern Amazon sites, (9°S to 11°S), no clear seasonality was identified between ET and net radiation. In these sites, over the wet season, it was verified a strong relationship between radiation and ET. However, during

the dry season lower correlation coefficients were found with radiation, while ET seems to be likely correlated with water stress during this period.

da Rocha et al. (2009), and Costa et al. (2010), who also evaluated measurement sites in the Amazon, reinforced the Hasler and Avissar (2007) findings, showing that radiation is the main driver of ET in wet equatorial sites, while in a transition region, between Amazon/Cerrado the importance of biotic response to water stress increases.

Corroborating with these findings, Restrepo-Coupe et al. (2013) demonstrated that photosynthetic activity at sites in central Amazonia is maintained or increased during the dry season, implying that water availability is not a limiting factor, but rather net radiation availability. Furthermore, Maeda et al. (2017) evaluated the seasonal patterns of ET and its relationship with environmental factors, using the water balance approach, in five sub-basins in the Amazon. The results showed that ET patterns differ in time and magnitude, confirming findings based on flux measurement sites, and demonstrating that limiting factors also vary across climatic gradients.

According to Biudes et al. (2015) and to Sanches et al. (2011), in Pantanal, a wetland region, ET pattern is pronounced and largely attributable to seasonal variations in radiation and soil water availability. In addition, despite the importance of these factors, it was also suggested that ET decreasing over the dry season can be more related to decreases in soil evaporation than reduction in tree transpiration, implying that there is a significant resistance to water vapor exchange from stomatal closure as the dry season progresses.

As demonstrated by these studies, the relative importance of water availability and biophysical controls over ET increases from the North-South climatic and biome gradients in South America, mainly over the dry season.

In Cerrado and Caatinga biomes, we can verify more clearly the vegetation control on ET over the year. For instance, in Cerrado (Cabral et al. 2015; Rodrigues et al. 2014; Vourlitis et al. 2002), and Caatinga biomes (Marques et al. 2020), during dry and transition seasons, water exchange is mainly driver by water available, and controlled by vegetation, indicating that biophysical factors have more relative importance on ET than physical limitations, while, for Cerrado biome, in wet season, abiotic factors exert more relative importance.

When we discussed subtropical biomes, such as Pampa in the South of Brazil, we verified that water availability is not a limiting factor for water exchange, and ET is mainly

determined by atmospheric forcing, as net radiation and VPD (Rubert et al. 2018). However, as this biome is usually used to cattle grazing and to cultivation of agricultural crops, it can be differently affected by these anthropic land uses. As related by Diaz et al. (2019), who evaluated measurement site under cropland condition, the ET interannual variability could is not entirely explain by the interannual variability of the atmospheric conditions in this biome, suggesting the biophysical conditions may represent a more significant influence on ET patterns. As commented by Restrepo-Coupe et al. (2013), and von Randow et al. (2012) changes in land cover, such as conversion from forest to pasture in the Amazon, exhibit energy flux patterns consistent with water limitations, while intact forests do not present suffer water stress, and this replacement may affect the regional water and flux cycles. These studies have demonstrated a substantial contribution in advancing our knowledge of how environmental and biological factors can control ET, clarifying the ET controls, as LULC are altered.

CHAPTER 3

Assessment of terrestrial water balance using remote sensing data in South America[3]

3.1 Introduction

Improve the knowledge of the earth's surface and atmosphere interactions is essential for understanding how anthropogenic activities can affect the climate, as well as their potential to impact the water cycle. One of the possibilities for assessing such dynamics is the quantification of water and energy cycles. Estimates of water balance enable us to understand water basins dynamics in relation to the changes they experience, which is crucial in terms of water availability, extreme climatic events, such as droughts and floods, water resources management (Reichert et al. 2017; Sahoo et al. 2011; Sheffield et al. 2009).

Overall, the measurements of hydrological cycle components are not dense enough to cover the large spatial that represent the surface heterogeneity, or to provide an understanding of the water balance dynamics at larger spatial scales. Due to this, particularly in developing countries, large-scale water balance estimation using *in situ* measurements is still a challenge (Gao et al. 2010; Sheffield et al. 2009).

Remote sensing is a promising possibility for achieving water cycle component estimates at different spatial and temporal resolutions, with the potential to provide data for regions with low-density *in situ* measurements around the globe. For example, the number of available rain gauges and measurement fluxes towers are not enough to reflect the surface and atmospheric heterogeneity. Remote sensing has the advantage of being able to provide observations of the earth’s surface and atmosphere, enabling analysis of the scenarios that account for natural variability, LULC or climate changes (Gao et al. 2010). Since the launch of the twin-satellites GRACE the Gravity Recovery and Climate Experiment (GRACE), in 2002, it has been possible to use remote sensing data for water balance estimations. Several studies have assessed the water balance from remote sensing data in basins around the world (Azarderakhsh et al. 2011; Long et al. 2014; Maeda et al.

[3] Published in the Journal of Hydroloy (2019).

2017; Rodell et al. 2004, 2011; Sahoo et al. 2011; Sheffield et al. 2009; Swann and Koven 2017; Zhang et al. 2018)

Sheffield et al. (2009) presented one of the first attempts to apply remote sensing data to water balance estimation, concluding that the water balance closure still could not be purely achieved using remote sensing estimations, mainly due to problems with the overestimation of precipitation and uncertainties in the GRACE terrestrial water storage changes (TWSC) data. Other studies have also been devoted to water balance estimations using remote sensing, but most have acknowledged that uncertainties in the hydrological datasets' are still a challenge for water balance assessment (Azarderakhsh et al. 2011; Gao et al. 2010; Oliveira et al. 2014; Sheffield et al. 2009; Swann and Koven 2017; Zhang et al. 2018). However, they have also agreed that such estimates offer significant information on water cycles and can be useful to monitor extreme events and provide valuable information to water resources management, particularly in regions where water is a limiting resource (Azarderakhsh et al. 2011; Sahoo et al. 2011). Some of these studies have highlighted gaps that demand further examination. One of these is the water balance closure (Gao et al. 2010; Sheffield et al. 2009). Pan et al. (2012), Sahoo et al. (2011), and Zhang et al. (2018) proposed some data assimilation methods from various sources (remote sensing, *in situ* measurements, reanalysis and land surface models) for the purpose of evaluating the water balance closure. A dataset combining water cycle variables from multiple sources, with the Climate Data Record, on a monthly scale, with spatial resolution of 0.5° was developed by Zhang et al. (2018), aimed at providing spatially and temporally consistent water-cycle variables, which can help the scientific community to understand climate variability through water balance estimates.

Understanding the origin of uncertainties in remote sensing products and their spatial variability is another critical issue that deserves further study. Investigation of the errors that can exist in these products is important for achieving future water-cycle observation missions with fewer errors regarding water balance closure (Gao et al. 2010; Penatti et al. 2015; Sahoo et al. 2011).

There is also a need for studies to evaluate remote sensing products in different climatic regions and at different temporal scales, since most studies have evaluated basins in the Northern Hemisphere (Long et al. 2014; Rodell et al. 2004; Senay et al. 2011; Sheffield et al. 2009).

Some basins have been studied in South America, including the Amazon basin (Azarderakhsh et al. 2011; Swann and Koven 2017), in the Cerrado (Brazilian savannah) and Pantanal (Brazilian tropical wetland) (Oliveira et al. 2014; Penatti et al. 2015) biomes. South America is a freshwater-abundant continent, with several large-scale basins, such as the Amazon and the La Plata. The discharge from the Amazon River contributes about 15–20% of the world's total discharge of fresh water to the ocean (Davidson and Artaxo 2004; Salati and Vose 1984), whilst the La Plata basins play an important role in South American agriculture and hydroelectricity production (Chen et al. 2010; Popescu et al. 2012; Tundisi et al. 1998). On the other hand, this region has been affected by hydrological extremes in recent years, such as the occurrence of droughts (2005 and 2010) and floods (2009 and 2012) in the Amazon, and multiyear droughts in northeastern (2012–2015) and southeastern (2014–2015) Brazil, which had significant effects on the water supply (Marengo 2014; Marengo et al. 2016; Nobre et al. 2016).

Future projections by the Intergovernmental Panel on Climate Change suggest more numerous occurrences of extreme hydrological events, which will mainly affect the Amazon and northeastern regions, with a greater frequency, intensity, and duration of dry seasons, and the occurrence of heavy rains in the southern region of Brazil (Fisher et al. 2017; Marengo 2014). In this context, remote sensing estimations of the terrestrial water cycle become important tools for comprehensively understanding the water dynamics in South America.

In this regard, we aimed to evaluate the water balance accuracy through different remote sensing datasets, at multiple basin scales across South America, covering a wide range of biomes and climatic conditions. The following scientific questions helped shape the development of this research: 1) how consistent are precipitation and ET remote sensing estimations over South America?; 2) do current remote sensing products provide advances in TWSC and discharge derived from the water balance?; 3) how does scale effect influence in the water balance closure accuracy?

Our methodology included an evaluation of each remote sensing dataset against observed measurements. We then used the remote sensing estimations to calculate the TWSC as a residual of the simplified water balance equation from small to large basins in South America, including yet unevaluated basins (most of the previous studies cover well-monitored basins in the Northern Hemisphere or only large basins in South America). Finally, to understand the potential of remote sensing for evaluating the terrestrial water

cycle, we assessed the uncertainties in the water balance using estimated errors for each independent hydrological variable.

3.2 Dataset descriptions and methodological analysis

3.2.1 Study area

The water balance was evaluated in South America on a monthly time scale in 50 wide basins, under a range of climatic regimes, for 2003 through 2014. The discharge stations of Brazilian Water Agency (ANA) and Argentina Hydrological network (BDHI), the basin areas, measurements sites used in the study and land-cover type for South America are presented in **Figure 3.1**. Further information about the size, location, biome, and climatic conditions of the basins are presented in **Supplementary Information Table SI3.1**.

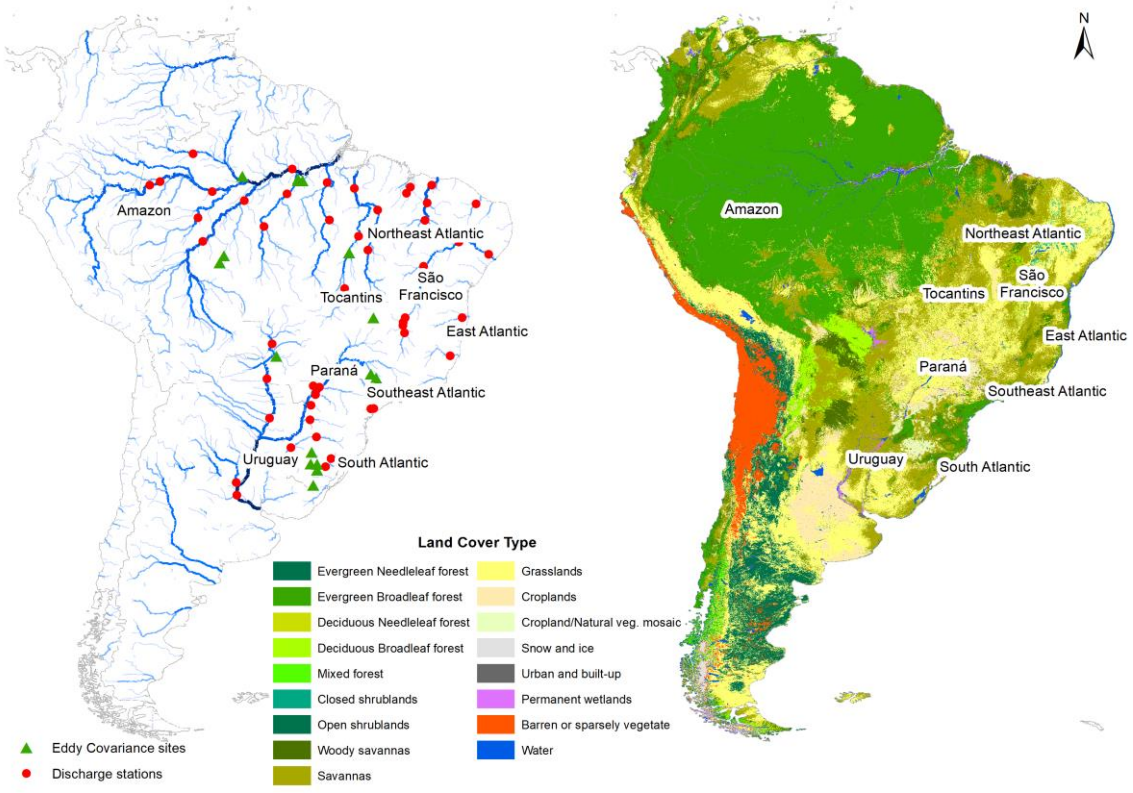

Figure 3.1 Location of the measurement sites and the discharge stations used to evaluate the water balance over different LULC conditions in South America.

The largest basins are concentrated in the Amazon region, the largest tropical rainforest in the world, at around 7 million km², and covering about 40% of South America.

Recently, the Amazon basin was affected by extreme droughts in 2005 and 2010 (Lewis et al. 2011; Marengo et al. 2008) and floods in 2009, 2012 and 2014, which caused enormous social and economic losses (Azarderakhsh et al. 2011; Marengo 2014; Marengo et al. 2012; Sena et al. 2012).

Some of the basins are in the heart of South America, in the Cerrado biome. The Cerrado is the second largest biome in South America, covering about 22% of Brazil, and is extremely important for water resources availability, because it is the source area of several large basins in Brazil (i.e., the São Francisco, which carries water to the semi-arid region of northeastern Brazil). Cerrado also has great relevance regarding groundwater, with a large area of the Guarani Aquifer system located in this biome (Oliveira et al. 2014). Furthermore, it is a hotspot for biodiversity, with many endemic species of fauna and flora (Hunke et al. 2015; Oliveira et al. 2014; Sano et al. 2010).

Tropical and subtropical basins are in the La Plata basin, the second largest basin in South America (after the Amazon), which covers Brazil, Argentina, Paraguay, Bolivia, and Uruguay. This basin is highly populated and has great economic importance due to the intensive agriculture and hydropower generation that occurs there; however, it has recurrent problems with droughts, floods, and intensive water use (Chen et al. 2010). The drought and flood events have caused severe economic and social losses here (Cavalcanti et al. 2015; Pasquini and Depetris 2007), such as the droughts that occurred in 1999/2000, 2006 (Chen et al. 2010), and 2009 (Abelen et al. 2015) and the flood in 1982/1983, 1992, 1997/1998, 2002/2003, 2007 (Cavalcanti et al. 2015; Chen et al. 2010), and 2009/2010 (Abelen et al. 2015). One of the largest hydropower plants in the world (the Itaipu plant), in terms of power generation, is located in this basin having a capacity of 14,000 MW, being responsible for 20% of the hydropower energy consumed in Brazil and supplying 80% of the electricity consumed in Paraguay (Nóbrega et al. 2011; Sperling 2012).

In southern, southeastern, and eastern Brazil, the available water resources are essential for irrigation, urban water supply and for hydropower generation. Extensive crops of irrigated rice are in the Uruguay and South Atlantic basins, representing around 70% of Brazil's production (12.4% of Brazil's total area lies in the South Atlantic and 7.9% in the Uruguay basins. These have a high demand for water (ANA 2015; CONAB 2015), thus the largest consumption in these basins is for irrigation (66% in the South Atlantic and 82% in the Uruguay basin).

3.2.2 Remote sensing dataset descriptions

Precipitation and ET datasets that were based on remote sensing estimations that were, commonly used, well validated and available at the global scale were selected to assess water balance in this study. For precipitation, we used the Tropical Rainfall Measuring Mission (TRMM) and The Multi-Source Weighted-Ensemble Precipitation (MSWEP) datasets, and for ET, we used MOD16 and GLEAM. We also used terrestrial water storage changes from GRACE, available from 2002 to present. A basin average for each remote sensing dataset was used to evaluate the terrestrial water balance in South America.

3.2.2.1 Precipitation

We used two different satellite-based precipitation products: TRMM3B43 version 7 (Huffman et al. 2007) and MSWEP version 2.1 (Beck et al. 2017a). The first precipitation dataset evaluated was that of the TRMM multi satellite precipitation analysis (TMPA), used to estimate tropical and subtropical rainfall. The TMPA datasets combines multiple satellite precipitation estimates and rain gauge measurements with a spatial resolution of 0.25° and 3-hourly, daily, and monthly temporal resolutions. The TRMM 3B43 dataset extended from 50° N to 50° S and covered the period from January 1998 to the present (Huffman et al. 2007, 2010). MSWEP, a global dataset with a spatial resolution of 0.1° and 3-hourly, daily, and monthly temporal resolution, was specifically designed for hydrological modeling (Beck et al. 2017a).The time-series extends from January 1979 to present. MSWEP dataset merges several high-quality precipitation datasets, including rain-gauge measurements, satellite observations, and reanalysis data, as a function of timescale and location (Beck et al. 2017a, 2019).

3.2.2.2 Evapotranspiration

Two global terrestrial ET datasets were used: MOD16 version 5 (Mu et al. 2011) and GLEAM version 3.2 (Martens et al. 2017; Miralles et al. 2011a). Both ET estimations were based on 8-day averages for computing uncertainties, and on monthly timescale for computing the water balance. It was used MOD16 at 0.05°, and GLEAM at 0.25° of

spatial resolution. Models approaches, main remote sensing data inputs, advantages, and limitations of these models it was presented in the **chapter 2**.

3.2.2.3 Terrestrial water storage

The GRACE mission was launched in 2002, with the main purpose of mapping variations in the Earth's gravitational field by measuring the distance between two orbiting satellites (Landerer and Swenson 2012; Swenson and Wahr 2006; Tapley et al. 2004). The available GRACE data are anomalies relative to a time-mean baseline, and so TWSC can be obtained as the time derivative of the anomalies (Long et al. 2014). Three different research centers process GRACE data: the GeoForschungsZentrum (GFZ), the Center of Space Research (CSR), University of Texas, and NASA Jet Propulsion Laboratory (JPL). We used a simple average of the three different solutions (GFZ, CSR, and JPL) to reduce the noise in the gravity field GRACE solutions (Sakumura et al. 2014). A summary of the remote sensing dataset used to assess the terrestrial water balance in South America is presented in **Table 3.1**.

Table 3.1. Summary of the remote sensing datasets used in this study for evaluating the water balance in South America.

Dataset	Version	Data availability	Spatial resolution	Temporal resolution	Data source	Reference
			Precipitation			
TRMM 3B43	7	1998 – 2019	0.25°	monthly	Mirador	(Huffman et al. 2007)
MSWEP	2.1	1979 – present	0.1°	monthly	GLOH2O	(Beck et al. 2017a, 2019)
			Evapotranspiration			
MOD16	5	2001 – present	500 m 0.05°	8-day monthly	Numerical Terradynamic Simulation Group	(Mu et al. 2011)
GLEAM	3.2	2003 –2020	0.25°	daily	GLEAM.eu	(Martens et al. 2017; Miralles et al. 2011a)
			Terrestrial water storage			
GRACE	5	2002 – 2017	1°	monthly	GRACE Tellus	(Tapley et al. 2004)
			Land use and land cover			
MCD12	6	2000 – 2016	500 m	yearly	NASA Earth Data	(Friedl et al. 2010)

3.2.3 Surface observations

3.2.3.1 River discharge measurements

To evaluate the water balance across 50 wide basins located in South America, we used daily measurements discharge from the ANA and BDHI networks from 2003 to 2014. We selected discharge stations with minimal failures during the period of study since we did not gap-fill the data. The respective datasets are available at http://hidroweb.ana.gov.br/ and at http://bdhi.hidricosargentina.gob.ar/.

3.2.3.2 Precipitation measurements

We also used 265 and 42 rain gauges monthly precipitation measurements from the Brazilian National Institute of Meteorology and BDHI network, respectively, to evaluate accuracy of the remote sensing precipitation estimations (TRMM and MSWEP). As in gauge measurements, we did not gap-fill in rain gauges, since we used a monthly temporal data, provided by agencies, with minimal failure, from 2003 to 2014.
The respective datasets are available at http://www.inmet.gov.br/projetos/rede/pesquisa/ and at http://bdhi.hidricosargentina.gob.ar/.

3.2.3.3 Evapotranspiration measurements

ET uncertainties of MOD16 and GLEAM models were evaluated using 16 measurements sites of the twenty-three presented in the **chapter 2** (**Table 2.2**), covering a wide range of LULC and climatic conditions in Brazil (**Table 3.2**).
The measurements sites are from LBA (Davidson and Artaxo 2004; Gonçalves de Gonçalves et al. 2013; Keller et al. 2004; Restrepo-Coupe et al. 2021b; Saleska et al. 2013) and the Sulflux network (Roberti and Acevedo 2012).
The LBA is an international program that was created in 1993 and is a pioneer in studies of interactions between terrestrial ecosystems and the atmosphere in a region of great human and natural complexity important results from the program have been summarized by Davidson et al. (2012) and Keller et al. (2009).The Sulflux network is a scientific and interinstitutional cooperation, created in 2008 with the goal of establishing a network for the continuous and extended-period measurement of water, energy and CO_2 flux involved

with interactions between the surface and atmosphere in the ecosystems of southern Brazil, based on several experimental sites, located in different LULC conditions (Roberti and Acevedo 2012). The measurements sites have been extensively described (see references in **Table 3.2**), in terms of their environmental characteristics, the equipment used, the measurement procedures, gap-filling methods, and data validation. We used 30-minutes and daily measured LE to evaluate ET estimates. All datasets were evaluated in terms of quality control, in order to remove spurious values, following methodology described in Souza et al. (2019), Rubert et al. (2018), and in Diaz et al. (2019). In addition, we excluded data for global radiation <10 and LE >100 W/m^2 at night and during the occurrence of precipitation. To convert measured LE (W/m^2) to ET (mm), we used **Equation 3.1** (Shuttleworth 2012). We did not gap-fill the data and to compute average ET, we used a maximum gap of 25%, following Fisher et al. (2009).

$$ET = \frac{LE}{\lambda} \tag{3.1}$$

Table 3.2 Measurements sites used to evaluate ET uncertainties.

Site	Name	Biome	Lat. (°)	Lon. (°)	Land cover	Data availability	Reference
FNS	Fazenda Nossa Senhora	Amazon	-10.76	-62.35	Pasture	Jun 2000–Mar 2004	(von Randow et al. 2004)
K34	Manaus – K34	Amazon	-2.60	-60.20	Tropical humid forest	Jan 2000–Sep 2006	(de Araújo et al. 2002)
K67	Santarém – K67	Amazon	-2.85	-54.95	Tropical humid forest	Jun 2002–Jan 2006	(Saleska et al. 2003)
K77	Santarém – K77	Amazon	-3.01	-54.53	Pasture and rainfed cropland (soybeans and rice)	Aug 2000–Nov 2005	(Sakai et al. 2004)
K83	Santarém – K83	Amazon	-3.01	-54.97	Tropical humid forest	Jun 2000–Mar 2004	(Goulden et al. 2004)
RJA	Reserva Jaru	Amazon	-10.08	-61.93	Tropical semideciduous forest	Jan 2000–Nov 2002	(von Randow et al. 2004)
PAN	Fazenda São Bento	Pantanal	-19.56	-57.01	Grassland	Sep 2000–Dec 2002	(de Oliveira et al. 2006)
BAN	Javaés/ Tocantins	Cerrado	-9.82	-50.15	Woodland savanna (seasonally flooded)	Oct 2003–Dec 2006	(Borma et al. 2009)
BRA	Brasília	Cerrado	-15.93	-47.87	Savanna (*campo sujo*)	Jan 2011–Dec 2011	(Santos et al. 2003)

PDG	Reserva Pé de Gigante	Cerrado	-21.61	-47.64	Woodland savanna	Jan 2001–Dec 2006	(da Rocha et al. 2002)
USE	Usina Santa Elisa	Cerrado	-21.72	-48.11	Cropland (rainfed sugarcane)	Jan 2001–Dec 2002	(Cabral et al. 2003)
CAS	Cachoeira do Sul	Pampa	-30.27	-53.14	Cropland (irrigated rice)	Oct 2009–Mar 2015	(Souza et al. 2019)
CRA	Cruz Alta	Pampa	-28.60	-53.66	Cropland (rainfed soybean and wheat)	Jan 2009–Sep 2014	(Aguiar 2011)
PAS	Pedras Altas	Pampa	-31.71	-53.53	Natural grassland	Sep 2013–Sep 2016	(Rubert et al. 2018)
PRS	Paraíso do Sul	Pampa	-29.74	-53.14	Cropland (irrigated rice)	Oct 2003–Mar 2004	(Timm et al. 2014; Zimmer et al. 2016)
SMA	Santa Maria	Pampa	-29.72	-53.76	Natural grassland	Jan 2013–Dec 2016	(Rubert et al. 2018)

3.2.4 Assessment of accuracy of the precipitation and evapotranspiration estimations

To assess the accuracy of the precipitation and *ET* estimations, we computed the scalar non-probabilistic metrics, such as the coefficient of correlation (*r*) (**Equation 3.2**), bias (**Equation 3.3**), the root mean squared error (RMSE) (**Equation 3.4**) and relative RMSE (**Equation 3.5**), between the observed (*Obs*) and estimated (*Est*) data in time *i*.

$$r = \frac{\sum_{i=1}^{n}(Obs_i - \overline{Obs})(Est_i - \overline{Est})}{\sqrt{\left[\sum_{i=1}^{n}(Obs_i - \overline{Obs})^2\right]\left[\sum_{i=1}^{n}(Est_i - \overline{Est})^2\right]}} \quad (3.2)$$

$$bias = \frac{1}{n}\sum_{i=1}^{n}(Est_i - Obs_i) \quad (3.3)$$

$$RMSE = \sqrt{\sum_{i=1}^{n}\frac{(Est_i - Obs_i)^2}{n}} \quad (3.4)$$

$$Relative\ RMSE\ (\%) = \frac{RMSE}{\overline{Obs_i}} \times 100 \quad (3.5)$$

where *n* is the sample number.

3.2.5 Water balance and uncertainty analysis

To evaluate the water balance (**Equation 3.6**) from 2003 to 2014 in South America, we used monthly average observations between two periods (Getirana et al. 2014; Oliveira et al. 2014; Rodell et al. 2004, 2011; Sheffield et al. 2009).

$$\frac{dS}{dt} = \frac{P_{(t+1)} + P_t}{2} - \frac{ET_{(t+1)} + ET_t}{2} - \frac{Q_{(t+1)} + Q_t}{2} \quad (3.6)$$

where S is the terrestrial water storage, P is precipitation, and Q is the basin discharge, with all variables in mm/month. Each variable was cumulated at time t. As remote sensing inputs, for precipitation, we used the TRMM and MSWEP datasets, whilst for ET we used MOD16 and GLEAM. Considering that GRACE terrestrial water storage (TWS) anomalies are given at irregularly-timed intervals, we computed these changes as the difference between two GRACE points, representing the average change in terrestrial water storage (Long et al. 2014; Oliveira et al. 2014) (**Equation 3.7**):

$$\frac{dS}{dt} \approx \frac{TWS}{dt} \approx \frac{TWS_{t+1} - TWS_t}{\Delta t} \quad (3.7)$$

Uncertainties in the monthly estimates of the water balance were assessed by combining the individual uncertainties for precipitation, ET, and discharge.

Assuming that the errors in these variables are independent and normally distributed, the relative uncertainty was given by the quadrature sum of errors of each variable (**Equation 3.8**) (Long et al. 2014; Rodell et al. 2004, 2011; Senay et al. 2011; Sheffield et al. 2009).

$$\upsilon_{dsdt} = \frac{\sqrt{\upsilon_P^2 P^2 + \upsilon_{ET}^2 ET^2 + \upsilon_Q^2 Q^2}}{|P - ET - Q|} \quad (3.8)$$

where υ is the relative uncertainty for each component of the water balance. The water balance uncertainty was computed at the 95% confidence interval as $\pm\upsilon_{dsdt}$.

The uncertainties in each component of the precipitation and ET estimations were assessed as the standard deviation of the differences between observed and estimated data at the 307 rain gauges and 16 measurements sites, respectively.

At the basin level, the precipitation uncertainties were averaged using rain gauge stations that were in each basin, whilst for ET, we computed the uncertainties for each LULC and then averaged for each basin according to the percentage of area occupied by the land cover class. We used MCD12Q1 of the 2008 as the reference for assessing LULC. For discharge, we considered an uncertainty of 10%, as used by Rodell et al. (2011), and double of the uncertainty, as used by Rodell et al. (2004). Some studies have considered a 10–15% uncertainty approximation for discharge measurements to be reasonable (Bjerklie et al. 2003; Coe et al. 2002).

We also computed the GRACE uncertainties for each basin. The GRACE anomalies data have measurement and leakage errors. Measurement errors are associated with instrument and loss signal retrieval errors, whilst leakage errors are related to the filtering process (Landerer and Swenson 2012; Rodell et al. 2011) (**Equation 3.9**):

$$Total\ error = \sqrt{Leakage\ error^2 + \ Measurement\ error^2} \tag{3.9}$$

Since GRACE errors are correlated in nearby pixels, we computed the covariance as specified at https://grace.jpl.nasa.gov/data/get-data/monthly-mass-grids-land/ (Maeda et al. 2017; Rodell et al. 2011). Then, to compute errors in the TWSC we multiplied the errors by √2 (Rodell et al. 2004, 2011).

To evaluate the water balance under distinct climatic conditions, we computed the runoff coefficient (*Qcoeff*) for each basin. This is a dimensionless coefficient that relates the amount of runoff to the amount of precipitation received (Guimberteau et al. 2013) (**Equation 3.10**):

$$Q_{coeff} = \frac{\bar{Q}}{\bar{P}} \tag{3.10}$$

where $\bar{Q}$and $\bar{P}$are average discharge and precipitation for 2003–2014.

3.3 Results and discussion

3.3.1 Uncertainties in precipitation and ET estimations

We assessed the individual uncertainties of the precipitation and ET remote sensing estimations to compute the water balance uncertainties, but, due to the spatial distribution of the rain gauges and measurements sites, we only evaluated the water balance uncertainties for 24 basins.

3.3.1.1 Uncertainties in Precipitation

Figure 3.2 shows the statistical metrics between the rain gauges and MSWEP and TRMM. MSWEP precipitation yielded a slightly higher accuracy (71% of rain gauges presented $r > 0.90$) than the TRMM estimations (around 60% of rain gauges presented $r > 0.90$). For the RMSE, both precipitation dataset, generally presented more errors in the Brazilian northeast (40 to 60%).

For TRMM, errors between 20 to 40% were verified in most rain gauges, whilst for MSWEP, fewer errors (0 to 20%) were shown for the Amazon and southern Brazil.

MSWEP presented underestimations for 74% of the rain gauges, mainly in southern and northeastern-coastal Brazil. In contrast, about 66% of rain the gauges assessed against TRMM presented overestimations, southern, southeastern, and northeastern Brazil, whilst on the northeastern coast of Brazil, TRMM underestimated the precipitation. These results agree with Oliveira et al. (2014), who assessed the water balance in the Brazilian Cerrado using precipitation from TRMM 3B42 (versions 6 and 7) and found overestimations, mainly in the Southern and underestimations in the northeastern, Brazilian Cerrado, with a lower bias for TRMM version 7. Rozante et al. (2010) also verified underestimates on the east coast of the northeastern region of Brazil, attributing this to the occurrence of warm clouds, and overestimates at the borders between Argentina, Paraguay, and Brazil due cold top clouds.

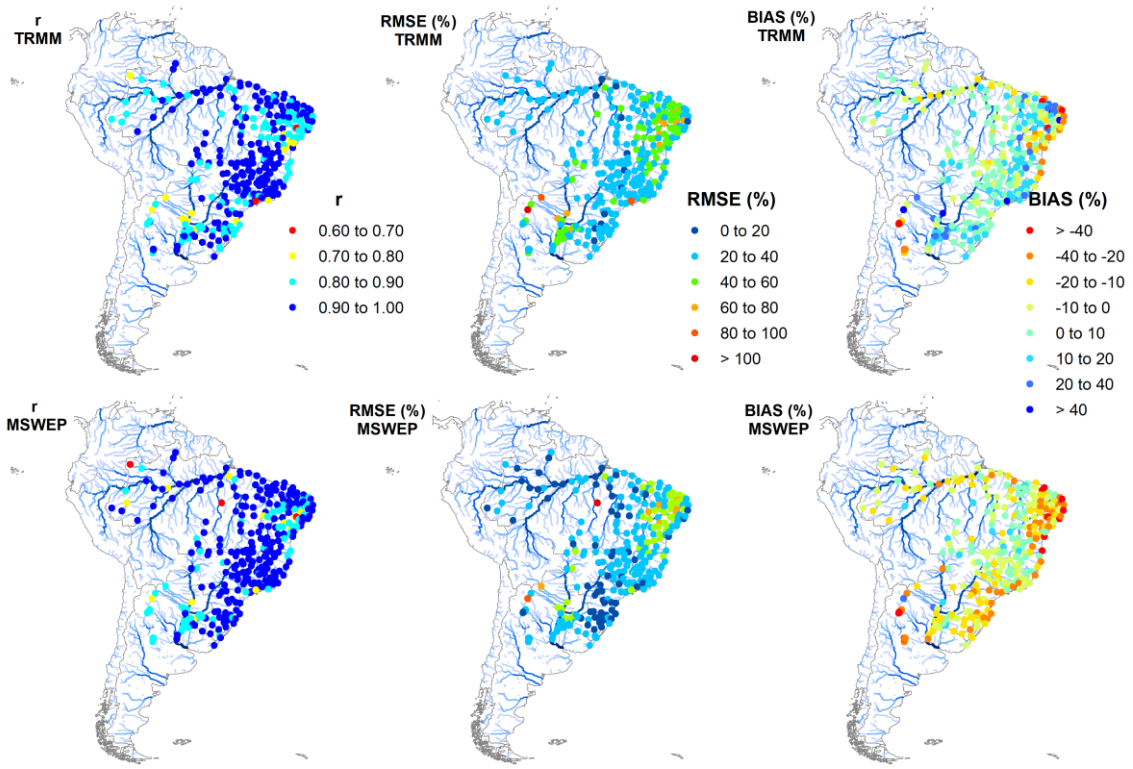

Figure 3.2 Statistical metrics between rain gauges and precipitation estimates (TRMM and MSWEP) over South America for 2003-2014 period.

The precipitation uncertainties in MSWEP and TRMM presented similar results (**Figure 3.3**), with more than half of the rain gauges showing uncertainties of between 0 to 40%. Overall, MSWEP yielded a mean uncertainty of about 37%, whilst for TRMM this value was 39%.

More uncertainties were observed, mainly in northeastern Brazil Northeast, downstream of the Paraná River and in all rain gauges in Argentina, for both precipitation datasets. These results demonstrated a relationship with the statistical metrics, indicating a satisfactory performance for both the MSWEP and TRMM precipitation datasets. Our results agree with those of Salio et al. (2015), who reported that rainfall estimates that included microwave and infrared information that gave remarkable results, improved by the incorporation of measured rainfall data into their calibration algorithms and, also with those of Beck et al. (2017b), who assessed 22 precipitation datasets for the entire world and verified that MSWEP version 2.0 demonstrated higher accuracy for all climate conditions, when compared to other datasets with a higher performance, mainly attributed to the incorporation of a daily rain-gauge correction scheme, whilst the other datasets incorporated monthly rain-gauge presented inferior performance.

A full statistical validation of MSWEP and TRMM are presented in **Supplementary Information Tables SI3.2** and **SI3.3**.

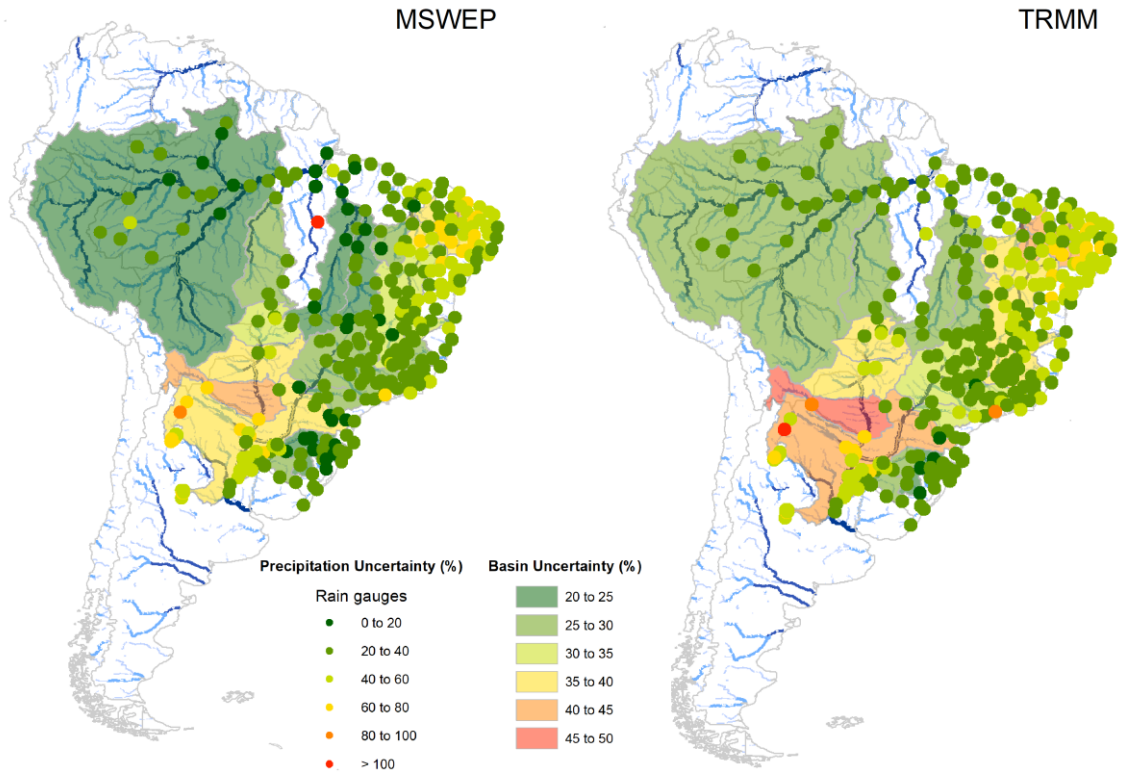

Figure 3.3 Precipitation uncertainty for MSWEP and TRMM estimations in South America based on rain gauge measurements.

3.3.1.2 Uncertainties in Evapotranspiration

In contrast to other studies that have evaluated *ET* uncertainty using theoretical values or *ET* model estimations (Azarderakhsh et al. 2011; Oliveira et al. 2014), we used 16 measurements sites from different LULC conditions. For each land cover type, we computed the standard deviation of the difference between *ET* remote sensing estimations and the sites, allowing the association of these uncertainties in 37 basins. **Table 3.3** and **Figure 3.4** show the *ET* uncertainties at all sites and in selected basins. Overall, the GLEAM *ET* presented lower uncertainties for mostly sites than MOD16 (**Figure 3.4**). For GLEAM *ET*, a range of between ~16 and 33% was observed, yielding higher accuracy for sites located in grassland (15.61%), followed by savanna and forest (18.54 and 18.67%, respectively),

whilst lower accuracy was found in the sites covered by cropland/pasture, located in Amazon and Pampa biomes (32.72 and 23.48%, respectively). For the MOD16 ET, higher performance was verified over forest and savanna (22.14 and 24.78%, respectively), and with lower accuracy for sites located on cropland/pasture and grassland for all evaluated biomes, ranging from 30.22 to 55.93%. Our results are comparable to those of Michel et al. (2016) and Khan et al. (2018) who evaluated ET estimations, including MOD16 and GLEAM, based on measurements sites, and of (Liu et al. 2016) who compared different ET products against the annual water balance ET estimates, verifying a superior performance of GLEAM ET estimates, although they did not find a significant discrepancy between the ET models evaluated.

Overall, these studies have emphasized that MOD16 underestimates ET, and GLEAM performs relatively better than the other models (including MOD16), mainly due to the detailed parameterization of interception losses (in tall and short vegetation) and the use of microwave information, as presented by Miralles et al. (2011a; b) and Martens et al. (2017).

Table 3.3. ET uncertainties calculated for the MOD16 and GLEAM estimations, according to land-cover classification.

Biome	Land cover	Measurements Sites	Uncertainties (%)	
			MOD16	GLEAM
Amazon	Tropical forest	K34, K67, K83, RJA	22.14	18.67
	Cropland/Pasture	FNS, K77	55.93	32.72
Cerrado	Savanna	BAN, BRA, PDG	24.78	18.54
	Cropland/Pasture	USE	35.82	-
	Grassland	PAN	50.04	-
Pampa	Cropland	CAS, CRA, PRS	30.22	23.48
	Grassland	PAS, SMA	36.77	15.61

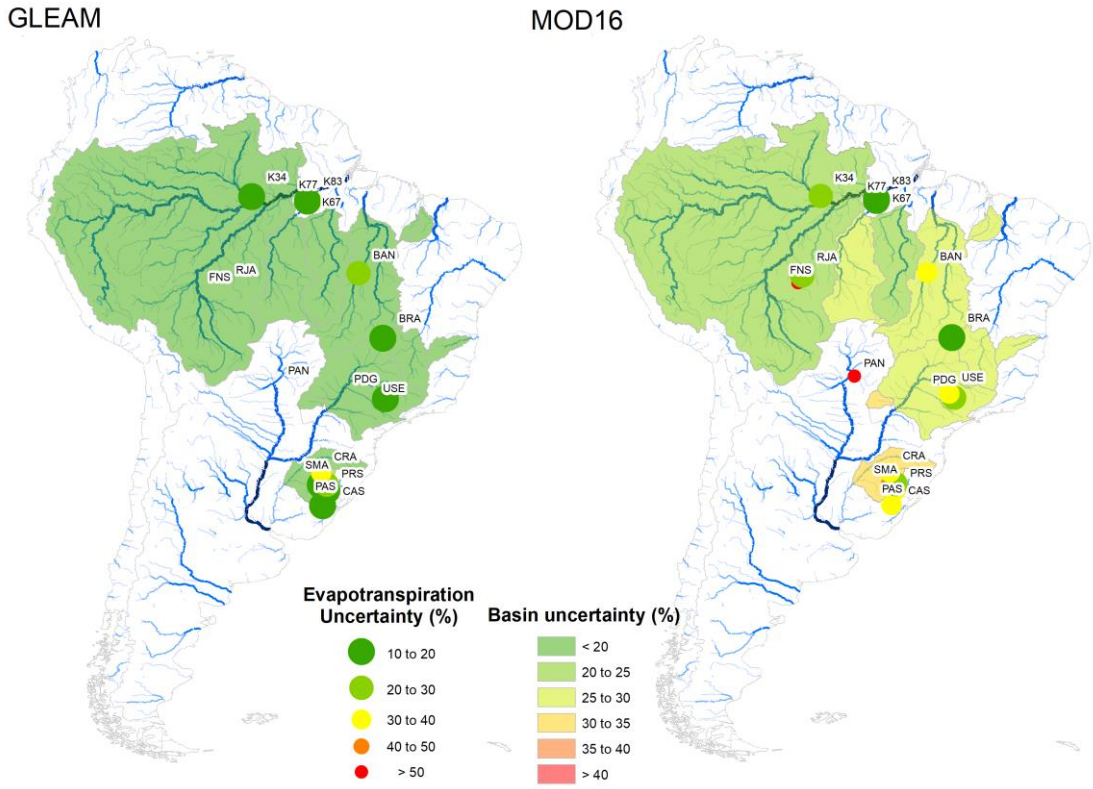

Figure 3.4 Evapotranspiration uncertainty for MOD16 and GLEAM models for selected basins in South America based on flux measurement sites.

3.3.1.3 Uncertainties in the terrestrial water balance

The uncertainties in the TWSC and discharge for all combinations of the precipitation and *ET* remote sensing datasets are presented in **Figure 3.5**.

For the TWSC, our results indicate uncertainties ranging between -44 and 96 mm/month and medians of between -43 and 22 mm/month for the combinations of MSWEP precipitation and GLEAM *ET* for most basins. On the other hand, the combination of TRMM precipitation and MOD16 *ET* presented higher medians, ranging between -44 to 50 mm/month and uncertainties of between -38 to 112 mm/month. Overall, for MSWEP precipitation and GLEAM *ET*, the median of the uncertainties ranged from -9 to 22 mm/month in the Tocantins, São Francisco, Paraná, northeastern and eastern Atlantic basins. In the Amazon, Uruguay, and South Atlantic basins, the median of uncertainties ranged between -60 to -21 mm/month.

The results also showed that the lowest discharge uncertainties were observed for the combination of MSWEP precipitation and GLEAM *ET*, where we observed a lower

median and amplitude, followed by the combinations TRMM/GLEAM, MSWEP/MOD16, and TRMM/MOD16.

For instance, at the Óbidos station (Amazon basin), the median uncertainty was ~55 mm/month, ranging between ~39 and ~72 mm/month, using the combination of MSWEP/GLEAM combination, whilst for TRMM/MOD16, the median uncertainty was 65 mm/month, ranging between 49 and 86 mm/month. These results demonstrate close agreement with the results found for the MSWEP and GLEAM accuracy assessment, when compared to the measured rainfall and *ET*, respectively, in different LULC and climatic conditions.

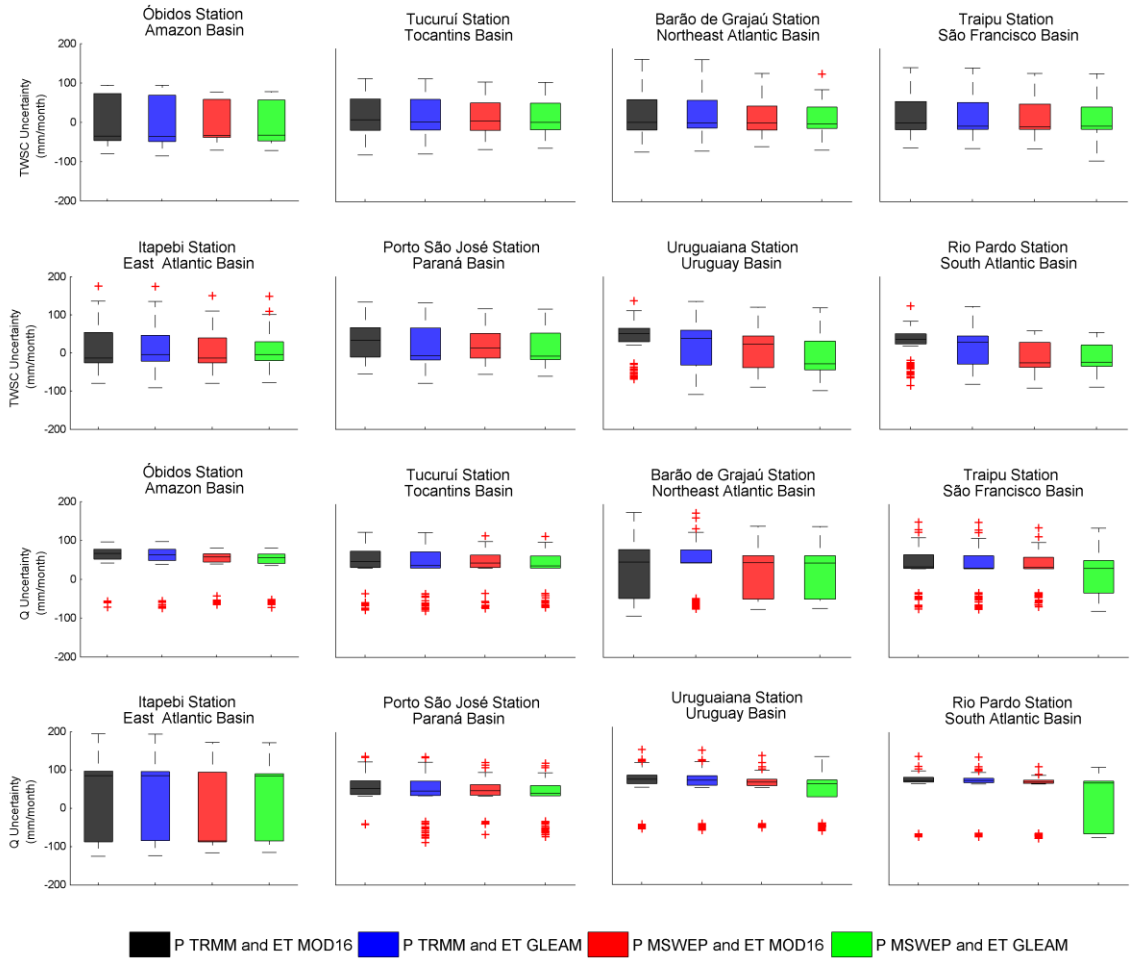

Figure 3.5 Uncertainties in terrestrial water storage changes and discharge inferred from remote sensing. The inbox lines represent the median, the boxes represent the inter-quartile range (IQR), the whiskers indicate variability outside the upper and lower quartiles (1.5IQR) and the red crosses represent the outliers.

Several studies have evaluated the uncertainties of discharge and ET estimates from the water balance perspective and the results are summarized in Table 3.4 (Azarderakhsh et al. 2011; Long et al. 2014; Oliveira et al. 2014; Rodell et al. 2011; Sheffield et al. 2009). Those references adopted discharge uncertainties ranging between 5 and 10% and estimated the TWSC uncertainties in a similar way that we estimated ours. However, due to precipitation and ET uncertainties, different methodologies were adopted. Some studies computed the uncertainties in precipitation and ET through the difference between remote sensing estimations and modeled data (Rodell et al. 2011; Sheffield et al. 2009) or adopted uncertainties based on the literature (Azarderakhsh et al. 2011; Long et al. 2014; Maeda et al. 2017). We adopted the standard deviation of the difference between the remote sensing estimations and the measured data. For ET, the uncertainty assessments were mostly based on literature references (Azarderakhsh et al. 2011; Oliveira et al. 2014) or were calculated using multiple ET datasets (Long et al., 2014). There is still no agreement on the methodology for determining ET uncertainties because it is still a challenge to obtain measured ET data at a consistent spatial and temporal scale. In this study, for the first time, measurements sites were used to assess MOD16 and GLEAM ET estimates, with a focus on water balance uncertainties.

Table 3.4 Uncertainties in terrestrial water storage changes, and precipitation and *ET* estimations based on remote sensing, and uncertainties in discharge based on water balance.

Study	Local	TWSC	Q	Precipitation	*ET*	Q Uncertainty	*ET* Uncertainty
(Sheffield et al. 2009)	Mississippi basin - EUA	25 mm for a 750km kernel half width	-	difference between precipitation data	difference in the upper and lower bounds of the RS-PM ensemble	0.4 to 2.9 mm/day	-
(Azarderakhsh et al. 2011)	Óbidos station - Amazon basin	0.47 to 0.70 mm/day (GRACE)	10% or 0.15 to 0.30 mm/day	1 to 1.19 mm/day (GPCP)	0.33 to 0.85 mm/day (MOD16)	1.17 mm/day	-
(Rodell et al. 2011)	Tocantins basin	estimated as in this present study (GRACE)	10%	~5% (TMPA and CMAP)	-	-	~2 mm/day
(Long et al. 2014)	South central United States - EUA	20 to 34 mm/month (GRACE)	5%	15% (PRISM)	5 mm/month (LSM); 10–15 mm/month (MODIS or AVHRR)	-	20–30 mm/month
(Oliveira et al. 2014)	Tocantins, Paraná, and São Francisco basins	25 to 174 mm/year (GRACE)	-	90 to 162 mm/year (TRMM)	6 to 262 mm/year (MOD16)	~600 mm/year ~600 mm/year ~450 mm/year	-
This study	Óbidos station – Amazon basin	25.83 mm/month (GRACE)	10% or 9.85 mm/month	27.86% or 54.23 mm/month (TRMM)	22.36% or 24.27 mm/month (MOD16)	61.18 mm/month	61.79 mm/month
				24.44% or 43.69 mm/month (MSWEP)	18.76% or 22.07 mm/month (GLEAM)	45.45 mm/month	52.72 mm/month
	Tucuruí station – Tocantins basin	32.45 mm/month (GRACE)	10% or 3.36 mm/month	28.46% or 39.97 mm/month (TRMM)	24.78% or 18.20 mm/month (MOD16)	51.12 mm/month	53.55 mm/month

			23.62% or 32.35 mm/month (MSWEP)	18.54% or 16.04 mm/month (GLEAM)	36.91 mm /month	49.31 mm/month
Barra station - São Francisco basin	36.92 mm/month (GRACE)	10% or 1.38 mm/month	36.01% or 34.74 mm/month (TRMM)	24.78% 14.77 or mm/month (MOD16)	41.36 mm/month	52.07 mm/month
			31.54% or 28.78 mm/month (MSWEP)	18.54% or 13.22 mm/month (GLEAM)	26.54 mm/month	47.81 mm/month
Porto São José station - Paraná basin	32.50 mm/month (GRACE)	10% or 3.19 mm/month	31.94% or 41.15 mm/month (TRMM)	24.78% or 15.46 mm/month (MOD16)	57.24 mm/month	55.91 mm/month
			28.74% or 32.34 mm/month (MSWEP)	18.54% or 15.75 mm/month (GLEAM)	29.40 mm/month	51.24 mm/month

The results found in this study for the basins located in the Cerrado (Tocantins, Paraná, and São Francisco) are similar to the results presented by Oliveira et al. (2014) and Rodell et al. (2011). For the combination MSWEP/GLEAM, we found lower discharge uncertainties (36.91, 29.40, and 26.54 mm/month) than in Oliveira et al. (2014) (with the use of TRMM/MOD16, they found 600, 600, and 450 mm/year), in the Tocantins, Paraná and São Francisco basins, respectively. Similar results were also observed the for ET uncertainty in the Tocantins basin, where the combination TRMM/MOD16 and MSWEP/GLEAM resulted in lower uncertainties (53.55 and 49.31 mm/month, respectively) than those found by Rodell et al. (2011) (about 2 mm/day).

Azarderakhsh et al. (2011) evaluated different combinations of water balance by remote sensing in 14 sub-basins located in the Amazon and found lower discharge uncertainties for the combinations TRMM/MOD16 (uncertainties of 23%) and Global Precipitation Climatology Project (GPCP)/MOD16 (uncertainties of 15%). In the Amazon basin from Óbidos station, for the combination of GPCP/MOD16, Azarderakhsh et al. (2011) found discharge uncertainties of 1.17 mm/day (or 35.1 mm/month), whilst we found uncertainties of 45.45mm/month, using the combination MSWEP/GLEAM.

Compared to other studies, our results demonstrate that the evaluation of water balance uncertainties derives a strong influence from estimations of the individual uncertainties of the inputs used. In in this context, the establishment of methods for estimating uncertainties is of the utmost importance for improving our understanding of the terrestrial water cycle.

As reported in other studies (Gao et al. 2010; Maeda et al. 2017; Oliveira et al. 2014; Rodell et al. 2011; Sahoo et al. 2011; Sheffield et al. 2009; Zhang et al. 2018), we verified that precipitation and TWSC are the main contributors to water balance total errors, but overall, the highest errors are from the precipitation datasets. Higher uncertainties were observed in precipitation than in ET. For instance, the average uncertainty in precipitation ranged between 23 to 46% for TRMM and 20 to 45% for MSWEP, while the uncertainties calculated against the measurement sites for the two ET models were between 22 and 33% for the MOD16, and lesser for GLEAM, with values ranging between 19 and 22%. For the TWSC based on GRACE, the uncertainties are also lower than for precipitation, ranging from 23 to 89 mm/month, for all evaluated basins. In addition, higher uncertainties in precipitation were observed during the wet season, in agreement with Maeda et al. (2017) and Zhang et al. (2018), who verified that the highest precipitation

uncertainties are mainly due to the lack of *in situ* gauges in the region, such as in the Amazon basin, and to an increase in precipitation measurement errors by remote sensing products during the rainy season.

We calculated the imbalance as the difference between the TWSC from the water balance and the TWSC from GRACE, as presented in **Figure 3.6**. A higher mean negative imbalance was found in the Amazon basins, where there are high ET and discharge rates, which are equivalent to, or greater than, the precipitation when summed. In the Tocantins and São Francisco basins, similar imbalance values were verified, with the median being close to 10 mm/month. Although the water balance closure has yet to be achieved using the current remote sensing datasets, we verified a close agreement with previous studies that merged multiple sources to close the water balance. For example, Sahoo et al. (2011) merged precipitation and ET from multiple remote sensing datasets and found an imbalance of between -70 a 50 mm/month in the Amazon basin. Using a similar methodology, Pan et al. (2012) found mean imbalances close to zero, with values ranging seasonally in the Amazon basin, whilst Zhang et al. (2018), using data assimilation techniques, found a non-closure of -46 mm/year for the Amazon and 47 mm/year for the Paraná basins.

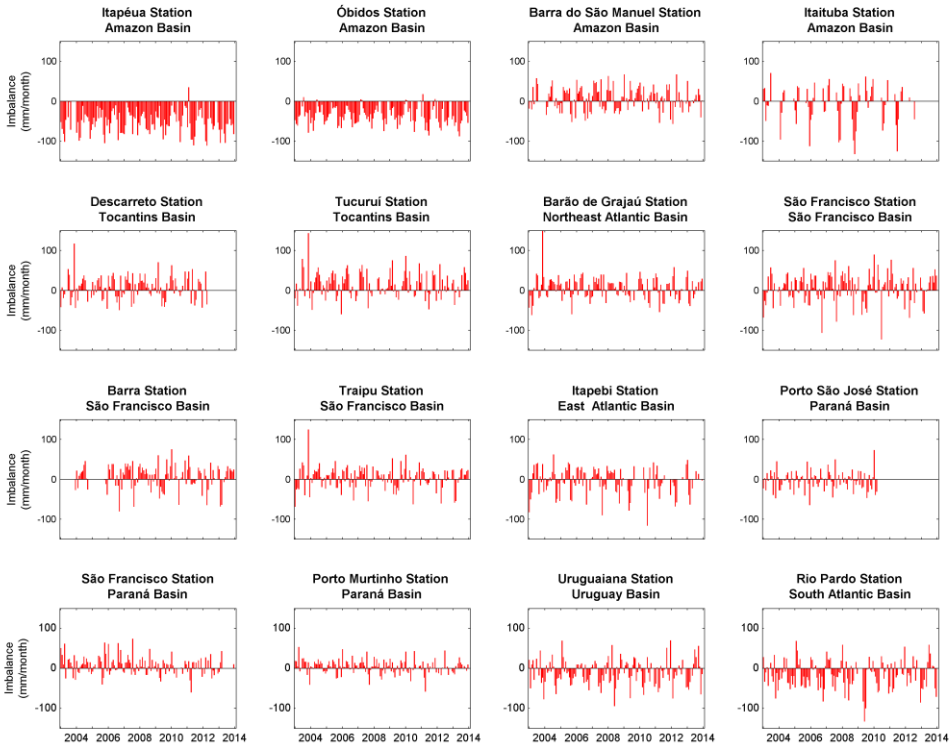

Figure 3.6 Imbalance in terrestrial water storage change ($TWSC_{water\ balance}$ - $TWSC_{GRACE}$) at selected basins in South America.

3.3.2 Assessment of water balance dynamics

Considering the multiple basins in South America, in different climate conditions and at different spatial scales, we determined whether the water balance accuracy and dynamics would change as a result of basin-scale effect. **Figure 3.7** shows a scatterplot of the TWSC from GRACE and the remote-sensing-based water balance, grouped into small (<100,000 km²), medium-sized (100,000 to 500,000 km²), and large (> 500,000 km²) basins.

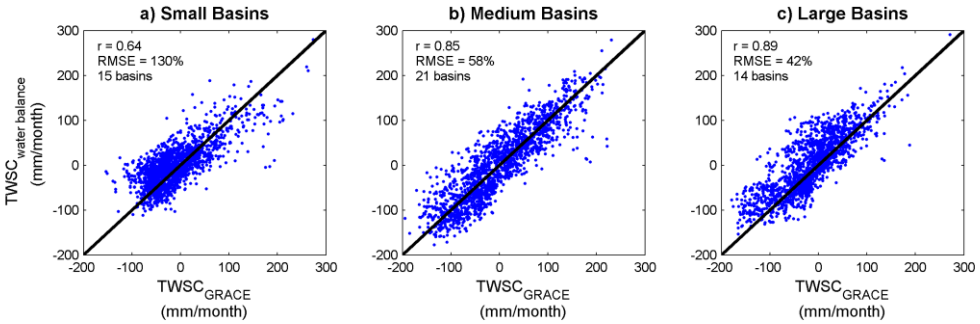

Figure 3.7 Scatterplot between monthly GRACE terrestrial water storage changes and remote sensing-based water balance over small basins (<100,000 km²) (a), medium basins (from 100,000 to 500,000 km²) (b) and large basins (area > 500,000 km²) (c).

In the largest basins, we found the highest correlation coefficients (r = ~0.85 and ~0.89), and RMSEs of around 58 and 42% for the medium-sized and large basins, respectively. On the other hand, basins with areas of less than 100,000 km² presented a correlation coefficient of about 0.64 and a RMSE of 130%.

The results for small basins can be explained by the growth GRACE errors inversely proportional to area size, and this way, higher errors will be more pronounced in small basins (Landerer and Swenson 2012; Scanlon et al. 2016). Our results agree with Rodell et al. (2011) that evaluated *ET* from water balance in some global basins, verified higher errors in water balance estimates over smaller basins and suggested that this fact can be primarily explained by the growth of GRACE errors in small area. However, we also found a good performance in the small basins, located predominantly under tropical wet-dry and tropical monsoon climates (Bacabal – 25,500 km², downstream - Mearim River, Cantanhede – 49,900 km², downstream - Itapecuru River and Peixe Gordo – 47,800 km², downstream - Jaguaribe River). These basins presented more accurate results for water balance, showing a correlation coefficient of about 0.88 and RMSE of 62%, close to those verified for medium-sized basins. In addition, medium-sized basins located in regions with moist climates in southern of Brazil, (Garruchos – 116,000 km², upstream – Uruguay River; Uruguaiana – 190,000 km², downstream – Uruguay River) yielded correlation coefficient of 0.56 and RMSE of 168%, with results similar to those found for the small basins.

Although the results shown better performance in larger basins, they also show that a basin's climatic conditions can influence the water balance accuracy, because medium-sized under subtropical climates with weak seasonal precipitation had higher errors than small basins in tropical climate.

In this context, we also evaluated which hydrological conditions yielded the more accurate results between measured discharge and that derived from the water balance. **Figure 3.8** presents scatterplots of the runoff coefficient, RMSE, and correlation coefficient for discharge from the water balance.

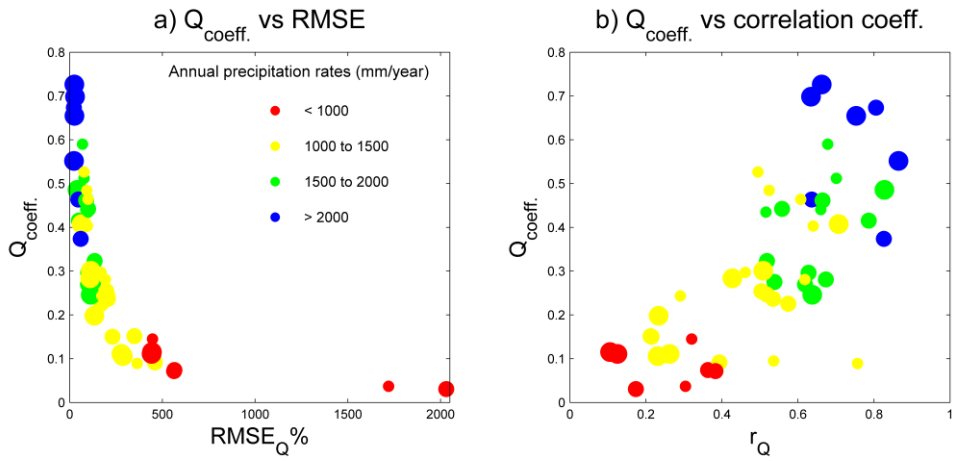

Figure 3.8 Scatterplot between runoff coefficient and RMSE in discharge (a) and between runoff coefficient and correlation coefficient in discharge (b). Marker sizes represent basins' size (small, medium, and large).

In the Amazon basins, we found higher *Qcoeff*, ranging from 0.55 to 0.72, mainly in the western, northwestern, and mainstream regions, with a RMSE in the discharge of ~39%, except for some basins located in the southeastern region, where the RMSE was ~99%. In the Tocantins and High São Francisco basins, we found *Qcoeff* of 0.27 and 0.25, and RMSE of 132 and 194%, respectively, whilst for the Medium and Low São Francisco basins, characterized by semi-arid climate, *Qcoeff* lowered to 0.15 and the RMSE increased to ~420%. For the other basins influenced by in semi-arid and arid climates, such as the northeastern Atlantic basin in Brazil and the Salado River basin in Argentina, with a *Qcoef* -0.06, we found a RMSE of more than 364%.

These results indicate that for semi-arid basins, discharge derived from the remote sensing water balance presented lower accuracy, whilst in the other basins, influenced mainly by tropical and subtropical climates, such as the Amazon, Paraná, and Uruguay, higher accuracy between the water balance and measured discharge were observed.

Overall, satisfactory water balance results were obtained for most of the evaluated basins (76%) where both the GRACE TWSC and remote-sensing-based water balance showed the same seasonal pattern of TWSC (**Figure 3.9**). Basins with large areas, located in

predominantly tropical climate regions, with seasonal precipitation, yielded correlation coefficients of around 0.89 and a RMSE around 48%. On the other hand, smaller basins, mainly located in subtropical climatic regions, showed results with an average correlation coefficient of around 0.52 and a RMSE of 164%.

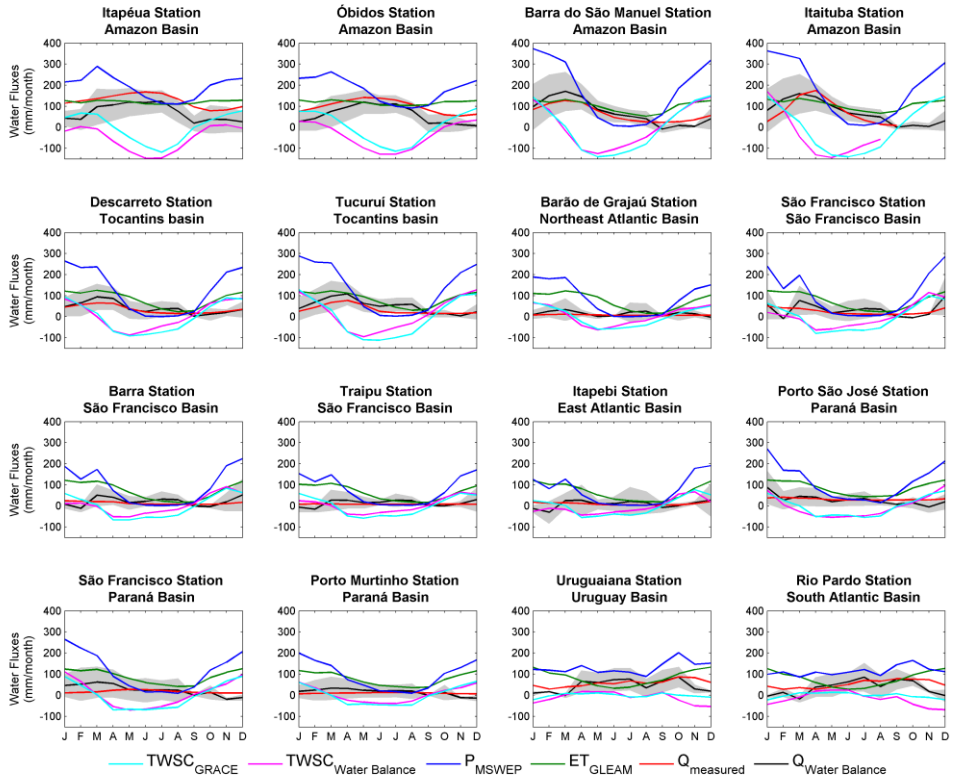

Figure 3.9. Seasonal water fluxes for South America basins. The shadow area represents uncertainties in discharge water balance based on remote sensing datasets.

High accuracy between the remote-sensing-based water balance and the GRACE TWSCs was found in the Amazon basins, which had predominantly tropical humid climates and high water and energy availability throughout the year. The average precipitation was around 123 to 249 mm/month, with pronounced seasonal cycles, related to the occurrence of the monsoon system, and a water discharge of around 45 to 168 mm/month. Regarding ET, the remote sensing estimations showed weak seasonal cycles, with values around 95 to 139 mm/month. Recently, (Maeda et al. 2017) assessed ET patterns across the Amazon basin and observed variations in average ET values among several evaluated sub-basins. In the Solimões basin, the highest ET values were determined in the drier months (September and October), whilst in the southern basins (Purus, Madeira and Tapajós), the highest ET rates were found in the months with higher precipitation rates. According to

these studies, the maximum ET rates did not correspond to the maximum precipitation rates, nor to the maximum radiation, thus supporting the assumption that ET in the Amazon is regulated by a balance of radiation, precipitation, and vegetation physiological controls rather than exclusively limited by one of these factors (Restrepo-Coupe et al. 2013).

Tocantins, São Francisco, and Paraná basins are mainly in the Cerrado biome, with a coverage of semi-decidual and decidual forests, seasonal precipitation, and ET rates, with precipitation presenting maximum values in the summer and minimum values in the winter (Reboita et al. 2010). da Rocha et al. (2009) found higher values over the wet season and lower values over the dry season in transitional forests, floodplains, and in the Cerrado woodlands. The authors attribute these values to the decline of photosynthesis and to strong LAI seasonality, which consequently affect ET patterns that are probably driven by soil moisture availability. In these basins, a moderate accuracy between the remote-sensing-based and GRACE TWSC was found (average values for basins: Tocantins r = 0.92, RMSE = 41%; São Francisco r = 0.87, RMSE = 50%; Paraná r = 0.73, RMSE = 120%), agreeing with (Oliveira et al. 2014) (Tocantins r = 0.93, São Francisco r = 0.91, Paraná r = 0.87), indicating that GRACE estimations are capable to representing water storage changes in the Cerrado basins, providing information about the seasonality dynamics of the water balance.

Sun et al. (2016) evaluated drought events in the São Francisco basin and found that the use of information on the TWS might be a good indicator of extreme water conditions, such as droughts and flood occurrences. In this context, our results supports those of previous studies (Oliveira et al. 2014; Sheffield et al. 2009; Sun et al. 2016), which demonstrated the good GRACE TWSC agreement with the remote-sensing-based water balance, our results to Cerrado basins demonstrate a precipitation decrease in the São Francisco basin, at Traipu station, around 21% and 20%, in 2007 and 2012–2014, respectively, when droughts were been recorded in the region (Paredes-Trejo et al. 2016; Sun et al. 2016).

In the Uruguay basin at the Uruguaiana station (and other basins located in humid subtropical climates), we found the smallest correlation coefficients, around 0.50, between the TWSC from GRACE and the remote-sensing-based water balance, with a RMSE of around 160%. In this region, precipitation was less seasonal (well distributed during the year), with the highest values associated with cold frontal systems (Do Nascimento et al. 2016; Reboita et al. 2010). As observed by Do Nascimento et al. (2016),

in these basins, the highest ET values are not related to higher water availability, as in Cerrado; here, precipitation is well distributed throughout the year, and ET rates are high due to energy availability over the summer months (December to March). The GRACE TWSC presented a less significant relationship with the remote-sensing-based water balance in these basins, compared to those located in the Amazon, Tocantins, and the northern/northeastern Atlantic that were evaluated previously. One explanation for this may be basin size, these being generally small (~56,000 km², on average) compared to those in other regions with higher correlation coefficients (areas of ~664,000 km² and even ~5 million km² basins), since GRACE errors are inversely proportional to area, and the highest uncertainties are more pronounced in small basins (Landerer and Swenson 2012; Scanlon et al. 2016).

3.4 Conclusions

The results of this research demonstrate that TRMM and MSWEP precipitation present a similar seasonal pattern in South American basins, with MSWEP yielding higher accuracy and lower uncertainty values than TRMM. For ET uncertainty, we verified higher correlation coefficients and lower RMSE for GLEAM for most sites. Then, we found the lowest uncertainties for water balance for combination of MSWEP precipitation and GLEAM ET estimations.

We found imbalances in the water balance for all these basins evaluated, which resulted from individual errors in the remote sensing datasets. Even though we verified that the water balance closure has not yet to be achieved. Our results demonstrate agreement with previous studies that used merging techniques for multiple variable sources (*in situ* observation, satellite remote sensing, land surface model, and reanalysis).

Better agreements between the TWSC from GRACE and the remote sensing water balance were found for medium (100,000 to 500,000 km²) and large basins (> 500,000 km²). However, the climatic conditions are also important, since we found good results in small basins, mainly influenced by tropical climates and worse results in medium-sizes basins that experienced subtropical humid climates.

basins located in semi-arid regions presented the lowest runoff coefficient and the highest discharge RMSE, indicating that high errors can be found for discharge calculated from the water balance in basins under semi-arid conditions in South America.

Finally, the water balance performance demonstrated satisfactory results for more than half of the basins, where nearly 76% presented correlation coefficients of ~ 0.89 and RMSE of ~48% between the TWSC from GRACE and the water balance. Lower agreements were found in the southern Brazil basins, under a predominantly humid subtropical climate. This region presents high precipitation rates all through the year, with no defined dry or wet seasons. The results demonstrated that is still necessary to advance the understanding of water balance dynamics under humid subtropical climate to understand limitations on GRACE data use and water balance using on remote sensing in these regions.

Although water balance closure using current remote sensing data, has not yet been achieved, this study underscores some important information about water balance cycle dynamics, related to the basin scale and climatic conditions, for multiple basins in South America. These results reinforce the great potential of remote sensing data in hydrological studies.

CHAPTER 4

What controls evapotranspiration in South America? An assessment of multiple climate and land cover conditions[4]

4.1 Introduction

LULC changes, including deforestation and cropland expansion, have historically modified the landscape in South America (Gatti et al. 2021). In the Amazon, deforestation rates decreased substantially until 2012, but since 2013, increases in deforestation in this region have been recorded (Aguiar et al. 2016; Silva Junior et al. 2021). This is especially true in recent years, when increases in deforestation have been observed, such as in the year 2020, in which the deforestation area was the highest in a decade (Silva Junior et al. 2021).

In South America, not only the Amazon Forest is under anthropogenic pressure but also are other biomes (savannas, grasslands, tropical dry forests, and others that make up the landscape of South America), which have lost 58% of their natural vegetation (Salazar et al. 2015). For instance, it is estimated that the Cerrado biome has already lost more than half of its native vegetation because of cropland expansion (Polizel et al. 2021; Sano et al. 2019), while in subtropical grasslands, in the Pampa biome, only 46% of the area is still covered by native vegetation (MapBiomas 2021). In arid areas, such as the Caatinga biome, more than 10% has experienced some environmental degradation (Mariano et al. 2018).

Deforestation, cropland expansion, and vegetation degradation can change surface–atmosphere interactions, modifying how H and LE heat fluxes are partitioned and changing the sensitivity to water stress (Borges et al. 2020; Duman et al. 2021; Khand et al. 2017; Laipelt et al. 2020; de Oliveira et al. 2019, 2021; von Randow et al. 2004, 2012, 2020; Restrepo-Coupe et al. 2013, 2021a). The degree of surface–atmosphere interaction can be assessed using the Jarvis and McNaughton decoupling factor (Ω) (Jarvis and McNaughton 1986), which reflects the relative importance of biotic and abiotic control over ET, depending on the degrees of aerodynamic (g_a) and surface (g_s) conductance

[4] Submitted to Global Change Biology.

(Jarvis and McNaughton 1986; Peng et al. 2019; Pereira 2004). These two important factors, g_a and g_s, control the exchange of water vapor from stomata and leaf surfaces to the atmosphere (Jarvis and McNaughton 1986; Monteith 1995). Tall vegetation canopies are aerodynamically rough in comparison to short canopies. Consequently, tall canopies are more efficient in shedding the energy they absorb, resulting in high g_a, with higher turbulence, and more efficient transfer of H and LE to the atmosphere (Monteith 1995). The surface conductance g_s reflects the control that vegetation exerts on the exchange of water vapor with the atmosphere through stomatal openings and is affected mainly by water vapor deficits, water availability in soil, photosynthetic capacity, CO_2 concentration, and temperature (Jarvis 1976; Leuning 1995).

The degree of surface–atmosphere decoupling also reflects how different vegetation types controls turbulent fluxes (De Kauwe et al. 2017). For instance, changes in vegetation cover (e.g., deforestation, cropland expansion, or irrigation) can affect g_a and g_s, consequently affecting turbulent fluxes (Chen et al. 2020; Jarvis and McNaughton 1986). Changes in the LAI also affect g_a and consequently turbulent heat transfer between the surface and the atmosphere, especially LE (Chen et al. 2020). In addition, changes in the biophysical properties of vegetation as a result of LULC changes are related to increases in surface temperature (Duman et al. 2021).

In the Amazon, reported differences between ET rates for forested and pasture areas have been attributed mainly to lower LAI and significant vegetation control in pastureland (von Randow et al. 2012), while in Caatinga, deforestation has contributed to increased water losses to the atmosphere and decreased vegetation potential to assimilate CO_2 (Borges et al. 2020; de Oliveira et al. 2021). Furthermore, conversion from grassland to cropland in the Pampa biome has reduced vegetation water use efficiency and CO_2 assimilation (Diaz et al. 2019).

To improve our understanding of the main drivers and ET controls across different biomes and to understand the potential impacts of LULC changes in South America, it is essential to use integrated and standardized assessments. Most recent studies on the subject have been conducted using a single site or just few ones. No analysis has yet been conducted based on multiple sites across South America, using the same method to evaluate the main biotic and abiotic ET controls and environmental drivers, to assess implications related to LULC change.

To understand how ET patterns can be impacted by LULC change across multiple biomes, we sought to answer two specific questions: *i*) what are the energy flux patterns across multiple biomes and LULC conditions?; and *ii*) how do ET controls range across different biomes and LULC conditions? To answer these questions, we evaluated the energy fluxes, g_a, g_s, and Ω over different biome and LULC conditions (as described in Section 4.3.1–4.3.4). We then assessed the main implications for energy fluxes and ET controls by comparing natural vegetation and changes in LULC (as described in Sections 4.4.1–4.4.2). Finally, we present the conclusions of the main findings of the study (Section 4.5).

4.2 Datasets and analysis method

4.2.1 Evapotranspiration measurement sites

We combined measurements from 20 flux measurement sites from the following research programs: *i*) LBA (Davidson and Artaxo 2004; Gonçalves de Gonçalves et al. 2013; Keller et al. 2004; Restrepo-Coupe et al. 2021b; Saleska et al. 2013), *ii*) Sulflux (Roberti and Acevedo 2012), *iii*) AmeriFlux (Baldocchi et al. 2001), *iv*) Fluxnet (Pastorello et al. 2020), *v*) ONDACBC (Borges et al. 2020; de Oliveira et al. 2021), and *vi*) PELD Pantanal (Biudes et al. 2015). Details of the sites were described in the **chapter 2**, and in **Table 4.1** and in **Figure 4.1** are provide details about the measurement sites and their locations.

Table 4.1. Flux sites measurements used to assess evapotranspiration seasonal controls and drivers in South America.

Site	Name	Biome	Lat. (°)	Lon. (°)	Land cover	Data availability	Reference
FNS	Fazenda Nossa Senhora	Amazon	-10.76	-62.35	Pasture	Jun 2000–Mar 2004	(von Randow et al. 2004)
FSN	Fazenda São Nicolau	Amazon	-9.85	-58.26	Pasture	Mar 2002–Oct 2003	(Priante-Filho et al. 2004)
K34	Manaus – K34	Amazon	-2.60	-60.20	Tropical humid forest	Jan 2000–Sep 2006	(de Araújo et al. 2002)
K67	Santarém – K67	Amazon	-2.85	-54.95	Tropical humid forest	Jun 2002–Jan 2006	(Saleska et al. 2003)
K77	Santarém – K77	Amazon	-3.01	-54.53	Pasture and rainfed cropland	Aug 2000–Nov 2005	(Sakai et al. 2004)

					(soybean and rice)		
K83	Santarém – K83	Amazon	-3.01	-54.97	Tropical humid forest	Jun 2000–Mar 2004	(Goulden et al. 2004)
QFR	Quistococha Forest Reserve	Amazon	-3.83	-73.31	Tropical peatland	Jan 2018–Dec 2019	(Griffis et al. 2020)
RJA	Reserva Jaru	Amazon	-10.08	-61.93	Tropical semideciduous forest	Jan 2000–Nov 2002	(von Randow et al. 2004)
NPW	Pantanal	Pantanal	-16.49	-56.41	Woodland savanna (seasonally flooded)	Dec 2013–Jun 2017	(Dalmagro et al. 2018)
BAN	Javaés/ Tocantins	Cerrado	-9.82	-50.15	Woodland savanna (seasonally flooded)	Oct 2003–Dec 2006	(Borma et al. 2009)
BRA	Brasília	Cerrado	-15.93	-47.87	Savanna (*campo sujo*)	Jan 2011–Dec 2011	(Santos et al. 2003)
PDG	Reserva Pé de Gigante	Cerrado	-21.61	-47.64	Woodland savanna	Jan 2001–Dec 2006	(da Rocha et al. 2002)
USE	Usina Santa Elisa	Cerrado	-21.72	-48.11	Cropland (rainfed sugarcane)	Jan 2001–Dec 2002	(Cabral et al. 2003)
CCG1	Campina Grande 1	Caatinga	-7.27	-35.97	Dense Caatinga	Jan 2013–Sep 2017	(Borges et al. 2020)
CCG2	Campina Grande 2	Caatinga	-7.25	-35.95	Sparse Caatinga	Mar 2013–Feb 2017	(Borges et al. 2020)
CAS	Cachoeira do Sul	Pampa	-30.27	-53.14	Cropland (irrigated rice)	Oct 2009–Mar 2015	(Souza et al. 2019)
CRA	Cruz Alta	Pampa	-28.60	-53.66	Cropland (rainfed soybean and wheat)	Jan 2009–Sep 2014	(Aguiar 2011)
PAS	Pedras Altas	Pampa	-31.71	-53.53	Natural grassland	Sep 2013–Sep 2016	(Rubert et al. 2018)
PRS	Paraíso do Sul	Pampa	-29.74	-53.14	Cropland (irrigated rice)	Oct 2003–Mar 2004	(Timm et al. 2014; Zimmer et al. 2016)
SMA	Santa Maria	Pampa	-29.72	-53.76	Natural grassland	Jan 2013–Dec 2016	(Rubert et al. 2018)

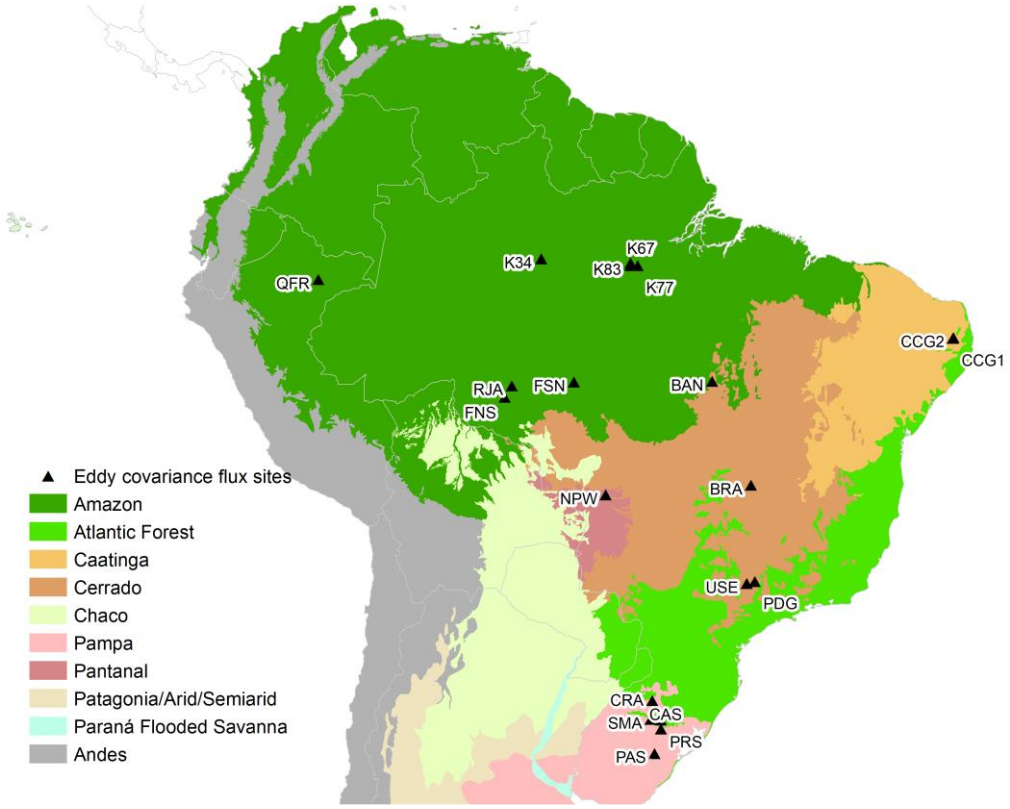

Figure 4.1. Location of the flux sites measurements in South America. South American biomes were adapted from Terrestrial Ecoregions of the World (Olson et al. 2001) and modified based on Turchetto-Zolet et al. (2013).

4.2.2 Data filtering and quality control

We used data from the LBA project with quality and analysis control (Gonçalves de Gonçalves et al. 2013). However, all datasets were filtered to remove spurious values of H and LE, applying the same method used by Souza et al. (2019) and Rubert et al. (2018). This study was limited to the daytime period to avoid extreme conductance values and dewfall conditions (Peng et al. 2019; Yebra et al. 2013; Zha et al. 2013). Thus, we excluded data for which the following conditions applied: shortwave incident radiation (Rg) <10 W/m^2 (when Rg measurements were missing, we used sunrise and sunset times for data filtering), relative humidity (RH) ≥ 95%, $Rn-G$ < 0 W/m², LE < 0 W/m², H < 0 W/m², and data collected during or within two days after precipitation events, to minimize inclusion of evaporation of water intercepted (E_I) by the canopy, following Peng et al. (2019), Zha et al. (2013), and Wever et al. (2002). We used 30-minutes or hourly data (depending on data availability) to compute daily fluxes. We did not gap-fill the data, and

to compute daily fluxes, we used a maximum gap of 25%, following Fisher et al. (2009), excluding a dataset when missing data exceeded this threshold.

4.2.3 Energy balance closure

The energy balance closure requires that the sum of turbulent fluxes ($LE + H$) be equivalent to the available energy (Wilson et al. 2002) (**Equation 4.1**).

$$LE + H = Rn - G - S \tag{4.1}$$

where S is the canopy storage heat flux, an important term for forest areas (Hasler and Avissar 2007; Wilson et al. 2002). Non-closure of the energy balance has implications for flux measurement analysis, especially when measured fluxes are compared with estimated fluxes (Wilson et al. 2002). Therefore, we closed the energy balance using the Bowen ratio (β). This method has been widely used to force energy balance closure, assuming that the eddy covariance system accurately measures β (**Equation 4.2**) and distributing the residual of the available energy for both H and LE, preserving β and conserving energy (**Equations4. 3-4.4**) (Hasler and Avissar 2007; Kustas et al. 1996; Shi et al. 2008; Twine et al. 2000).

$$\beta = \frac{H}{LE} \tag{4.2}$$

$$H = \frac{\beta}{1+\beta}\,(Rn - G - S) \tag{4.3}$$

$$LE = \frac{Rn-G-S}{1+\beta} \tag{4.4}$$

G is a fundamental part of the surface energy budget, typically representing 5–10% of Rn for dense vegetation (van Huissteden 2020; Kustas and Norman 2000; Ogée et al. 2001). However, under partial vegetation cover, G can account for more than 10% of Rn (Hasler and Avissar 2007; Kustas and Norman 2000). Therefore, when G was missing, we used 5% of Rn for forest and woodland savanna sites and 10% for pasture, grassland, cropland, and sites with partial vegetation cover (Hasler and Avissar 2007; van Huissteden 2020; Kustas and Norman 2000; Ogée et al. 2001). As the canopy storage heat flux (S) can reach approximately 5% (occasionally exceeding 10%) of Rn in the Amazon biome (Moore

and Fisch 1986), we considered 5% of Rn for this term for the Amazon humid forest sites. We neglected this term for pasture, cropland, and natural vegetation in other biomes.

4.2.4 Evapotranspiration control analysis

We assessed the influence of four environmental variables on the ET patterns: (i) Rn, (ii) VPD, (ii) g_a, and (iv) g_s. Whereas Rn, VPD, and g_a are related to abiotic factors and control of ET, and g_s provides information about the biophysical response of vegetation to water stress (Costa et al. 2010).

ET was calculated as the ratio of LE with a closed energy balance and the λ, at a daytime scale, according to Shuttleworth (2012).

To evaluate the controls and drivers on the ET seasonal patterns, we used Rn and VPD data measured at each site and computed g_a and g_s based on filtered data (using LE corrected with energy balance closure) at a daytime scale.

Values of g_s were computed by inverting the Penman–Monteith equation (**Equation 4.5**):

$$g_s = \frac{LE g_a}{\frac{\Delta}{\gamma} A - \left(\frac{\Delta}{\gamma}+1\right) LE + \rho C_p g a \frac{VPD}{\gamma}} \quad (4.5)$$

where A is the available energy ($Rn - G - S$).

Values of g_a were computed based on measurements of u and u_*, according to da Rocha et al. (2004), Peng et al. (2019), and Tan et al. (2019) (**Equation 4.6**). g_a represents the main control of the gas exchange, limiting the water transfer from the surface to the atmosphere (Katsoulas and Kittas 2011; Roberts et al. 2005).

$$\frac{1}{g_a} = \frac{u}{u_*^2} + \frac{1}{k u_*}\left[ln\left(\frac{z_0}{z_h}\right) + \Psi_m - \Psi_h\right] \quad (4.6)$$

Ψ_m and Ψ_h account for the effects of atmospheric stability on momentum and heat transfer computed according to da Rocha et al. (2004), Peng et al. (2019), Tan et al. (2019), and Verma (1989). z_0 and z_h represent the aerodynamic and water vapor roughness length, respectively, and k is the von Karman constant (0.41).

We also computed Ω (**Equation 4.7**), which reflects the degree to which the atmosphere near the surface canopy is decoupled from surrounding air conditions (Jarvis and

McNaughton 1986). Ω ranges between 0 and 1, depending on g_a and g_s. When g_s is much greater than g_a, the ratio ($\frac{g_a}{g_s}$) tends toward zero and Ω approaches 1, indicating that canopy atmosphere conditions are fully decoupled from the surrounding air. On the other hand, when g_a is high and g_s is low, the ratio ($\frac{g_a}{g_s}$) tends toward 1 and Ω approaches 0, indicating full coupling between the canopy surface and the atmospheric conditions (Jarvis and McNaughton 1986).

$$\Omega = \frac{1+\frac{\Delta}{\gamma}}{1+\frac{\Delta}{\gamma}+\frac{g_a}{g_s}} \quad (4.7)$$

4.3. Results

4.3.1 Patterns of energy fluxes

Our results demonstrate that the energy fluxes patterns differ markedly between the biomes and LULC in terms of the seasonal averages of Rn, H and LE and the ratios of β, LE/Rn, and H/Rn (**Figure 4.2** and **Table 4.2**). For instance, two well-defined seasonal patterns emerge from tropical humid forests in Amazon. At wetter sites (QRF, K34, K67, and K83), LE peaks during the dry season and reaches its lowest levels in the wet season, following Rn. The average LE/Rn yield rates higher than 0.6, with lower values of β (< 0.40) since most of the available energy is used to control ET. In the southern Amazon (RJA), LE reaches its minimum at the beginning of the dry season and peaks during the wet season. Another seasonal pattern was observed for cropland and pasture sites. At these sites, LE decreases markedly during the dry season, while H increases, especially at FSN and K77.

Seasonally flooded sites (BAN and NPW) also exhibit lower β values (0.32 and 0.38, respectively), similar to those observed in the Amazon tropical humid forest. However, LE at NPW decreases as the dry season progresses, while at BAN, LE reaches maximum rates at the beginning of the dry season (June) and then decreases until the end of this period (September), when the minimum LE is observed.

In Cerrado (at BRA), LE is not in phase with Rn. Whereas Rn reached minimum rates in June, LE decreases from May to September, reaching minimum rates at the end of the dry season. In contrast, at southern sites (PDG and USE), LE is positively correlated with Rn,

indicating that the available energy drives LE. However, during the dry season β>1 was observed, indicating that most of the available energy is used to heat the atmosphere in this period.

In the semiarid Caatinga (CCG1, and CCG2), H/Rn is higher than LE/Rn even during the wet season, in contrast to other biomes. Furthermore, β averages reach values higher than 6 in both wet and dry seasons. The main reason for these high β values is the limited water supply, which limits ET, while Rn is mainly used to heat the atmosphere. In contrast, in the subtropical humid Pampa (CAS, CRA, PAS, PRS, and SMA), throughout most of the year, the available energy is partitioned to evaporate water ($\beta < 1$). LE rates are lower during the autumn and winter and higher during the spring and summer, because Rn is an important ET driver at these sites.

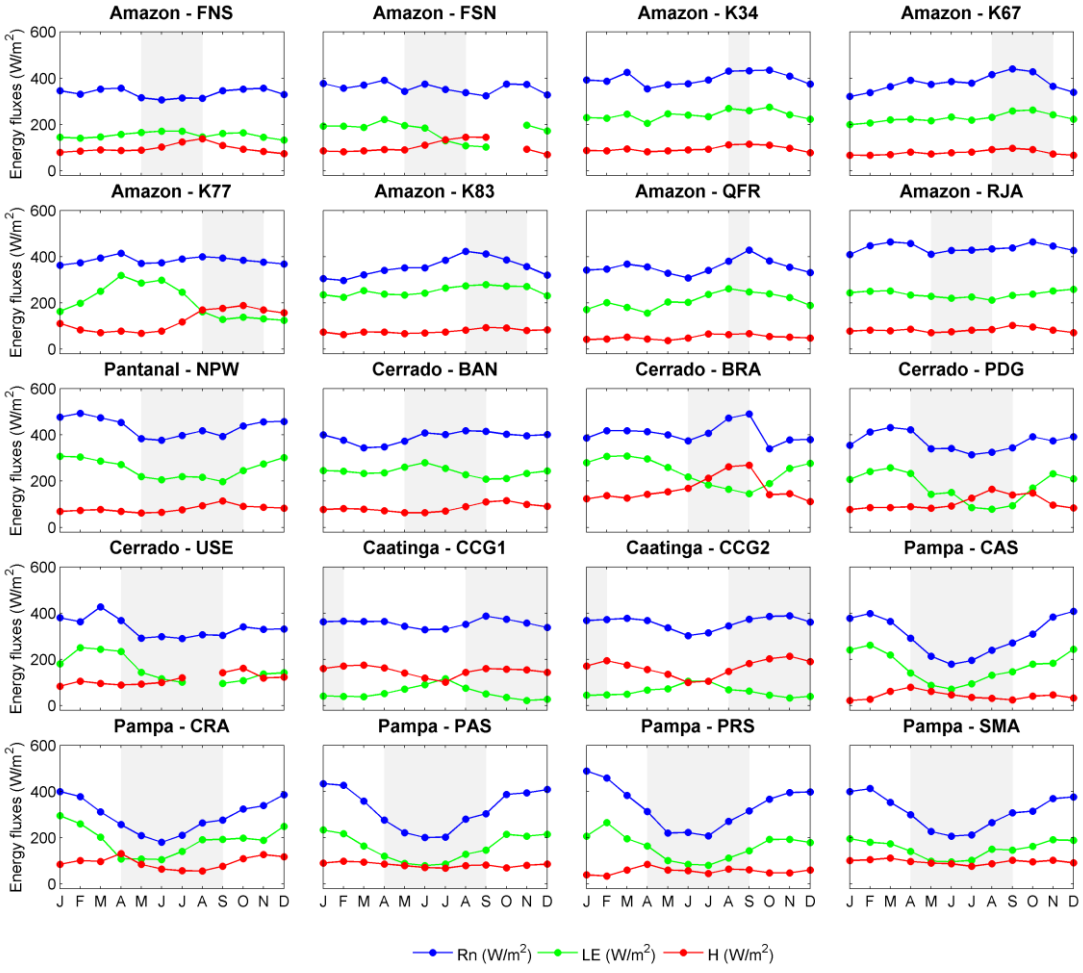

Figure 4.2: Patterns of daytime average monthly energy fluxes, net radiation (Rn) and sensible (H) and latent (LE) heat fluxes for sites listed in **Table 4.1**. Shaded areas indicate the dry season (autumn/winter for sites located in the Pampa biome).

Table 4.2. Annual and seasonal averages of Bowen ratio (β) and LE/Rn and H/Rn ratios.

Site	β			LE/Rn			H/Rn		
	Year	Dry/ Winter	Wet/ Summer	Year	Dry/ Winter	Wet/ Summer	Year	Dry/ Winter	Wet/ Summer
Amazon									
FNS	0.66	0.74	0.61	0.44	0.23	0.41	0.28	0.36	0.24
FSN	0.68	0.99	0.43	0.48	0.25	0.53	0.28	0.35	0.23
K34	0.40	0.45	0.40	0.59	0.26	0.59	0.23	0.24	0.23
K67	0.34	0.37	0.33	0.60	0.32	0.61	0.21	0.22	0.20
K77	1.02	1.56	0.81	0.53	0.23	0.59	0.31	0.44	0.26
K83	0.31	0.32	0.30	0.70	0.35	0.71	0.21	0.21	0.21
QFR	0.24	0.26	0.23	0.67	0.23	0.68	0.16	0.16	0.16
RJA	0.35	0.38	0.34	0.53	0.25	0.55	0.18	0.18	0.18
Pantanal									
NPW	0.32	0.38	0.27	0.59	0.33	0.63	0.18	0.20	0.16
Cerrado									
BAN	0.38	0.35	0.40	0.63	0.61	0.65	0.22	0.19	0.23
BRA	0.83	1.19	0.52	0.60	0.53	0.71	0.40	0.48	0.34
PDG	0.90	1.22	0.49	0.45	0.21	0.55	0.32	0.39	0.25
USE	0.92	1.00	0.85	0.43	0.23	0.45	0.33	0.34	0.31
Caatinga									
CCG1	6.06	7.72	4.16	0.16	0.13	0.22	0.42	0.43	0.40
CCG2	6.21	9.06	3.95	0.21	0.15	0.26	0.43	0.49	0.39
Pampa									
CAS	0.41	0.53	0.38	0.69	0.47	0.78	0.20	0.12	0.21
CRA	0.51	0.44	0.56	0.91	1.06	0.79	0.37	0.40	0.34
PAS	0.61	0.77	0.44	0.47	0.29	0.51	0.26	0.31	0.22
PRS	0.46	0.60	0.21	0.46	0.25	0.50	0.18	0.22	0.10
SMA	0.80	1.01	0.59	0.51	0.31	0.50	0.32	0.35	0.28

4.3.2 Patterns of aerodynamic conductance

Different g_a patterns were observed across South America because of differences in the climates, biomes, and LULC conditions (**Figure 4.3** and **Table 4.3**). At tropical sites located in the equatorial region of the Amazon, our results exhibited two patterns depending on the LULC: *i*) higher g_a (44.54–63.21 mm/s) in tropical forests (K34, K67, K67, K83, and QFR) and *ii*) lower g_a (16 mm/s) where natural vegetation was replaced by pasture/cropland (K77). Similar patterns were observed in the southern Amazon, where g_a for tropical semideciduous forest (RJA) was higher (42 mm/s) than for pasture areas (FNS and FSN) (~20 mm/s). For seasonally flooded areas (BAN and NPW), we obtained similar g_a values (39.79-41.40 mm/s), while for the Cerrado biome, we verified that in cropland (USE), g_a was lower (29.85 mm/s) than in natural savanna vegetation (BRA and PDG) (45.78 and 34.67 mm/s, respectively). Arid sites in the Caatinga biome (CCG1 and CCG2) also exhibited similar g_a values (39.41 and 42.78 mm/s, respectively).

Lower g_a values (from 19.83 to 29.50 mm/s) were obtained for the Pampa biome (CAS, CRA, PAS, PRS, and SMA), mainly because of the grassland and cropland predominance which present lower canopies.

g_a slightly varies from one season to another at most Amazon sites. However, at FNS, a pasture site in the southern Amazon, during the dry season, g_a was approximately 70% higher than in other seasons. In contrast at FSN, also a pasture site, g_a decreased by approximately 2% during the dry season. At both sites, changes in canopy height are related to cattle grazing, and canopy height changes affect surface roughness, which is a key factor in g_a. The only period during which g_a was significantly higher during the entire period for which data were available for the FNS site (1999–2002) was between June and September 2001, the same period during which a greater canopy height due to anthropogenic management was observed (Zanchi et al. 2009).

g_a did not change significantly in the seasonally flooded Pantanal area (NPW), whereas for natural LULC in Cerrado (BAN, BRA, and PDG), g_a increased by approximately 14–16% during the dry season, and at the cropland site (USE) g_a was approximately 37% higher during the dry season. For pasture in the Amazon (K77) and for cropland in the Cerrado (USE) biome, the pronounced g_a increase is also related to the crop cycle, i.e., with the harvest occurring at the end of the dry season (Juárez 2004).

At CCG1 (dense Caatinga), a pronounced decrease (-12%) in g_a was observed when the dry season started (August), which could be related to leaf loss— even when wind speed tends to increase, a decrease in the canopy could influence the g_a pattern. However, at CCG2 (sparse Caatinga), which has less leaf biomass throughout the year, the increase in g_a during the dry season (17%) could be related to less significant leaf loss in this period since the variation in the canopy height is not as significant as at CCG1.

Changes in g_a of approximately 1–8% were observed for most Pampa sites (CAS, PAS, PRS, and SMA); only at CRA (rainfed cropland) was g_a lower (16%) lower during the autumn/winter season. Furthermore, g_a pattern at the cropland sites is coincident with the crop cycle, since g_a reaches maximum values in March/April and in October/November, coincident with summer and winter cropland cycles at CRA, whereas at CAS and PRS (irrigated cropland), higher g_a values occur at the end of the growing season.

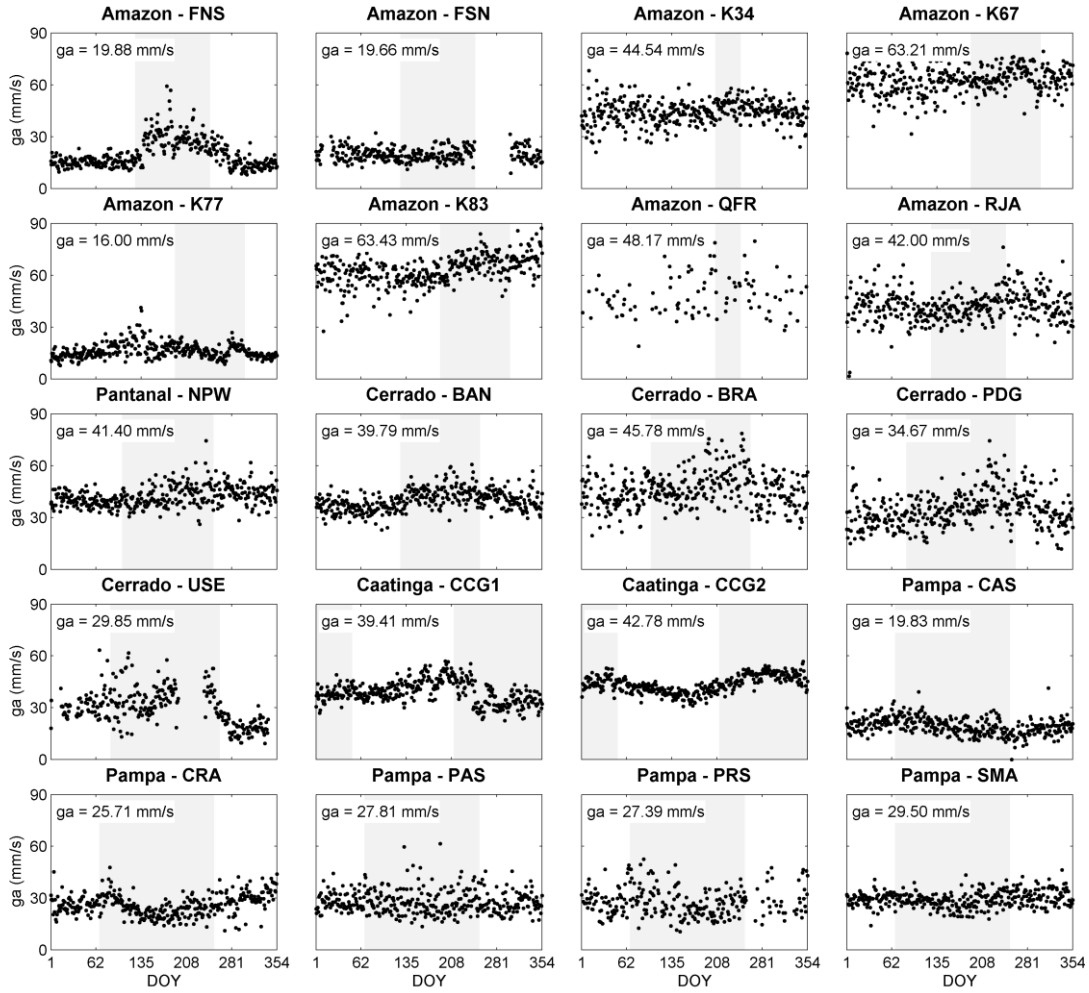

Figure 4.3. Patterns of aerodynamic conductance (g_a) at 20 South American measurement sites. Shaded areas indicate the dry season or autumn/winter season for sites located in the Pampa biome (CAS, CRA, PAS, PRS, and SMA).

4.3.3 Patterns of surface conductance

As with g_a, g_s exhibited different patterns across South America (**Figure 4.4**). For instance, higher g_s values occurred in the Amazon (K34, K67, K83, QFR, and RJA) and in croplands sites in the Pampa biome (CAS, CRA, PAS, PRS, and SMA), regions where water availability is not a limiting *ET* factor (except in the southern Amazon region). Hence, the surface resistance (defined as the inverse of the surface conductance) is lower. In contrast, at sites located in regions that experience longer dry season, such as Cerrado (BAN, BRA, PDG, and USE) and Caatinga (CCG1 and CCG2), g_s is lower, since at these locales, the canopy resistance to water exchange from the vegetation to the atmosphere is higher, especially during the dry season.

Furthermore, g_s varies not only across sites in the South America but also with the seasons and according to the LULC. Comparing the equatorial Amazon sites with forests (K34, K67, K83, and QFR) and with cropland/pasture (K77), we verified that at forested sites g_s varies slightly over the year, decreasing by approximately 14–27% during the dry season, while at K77, g_s decreases by approximately 77% during the same period. This illustrates that LULC changes can alter water vapor exchange. When we evaluated sites in the southern Amazon, we found differences in g_s for different LULC conditions. Despite all sites in this region (FNS, FSN and RJA) exhibiting pronounced changes in g_s over the year (decreasing by approximately 26–59% during the dry season), higher canopy conductance over forest than over pasture sites is significant. At seasonally flooded sites (NPW and BAN), a similar g_s reduction of approximately 28–38% was observed during the dry season. According to (Asbjornsen et al. 2011), vegetation from humid ecosystems, such as the vegetation in seasonally flooded regions, close their stomata even in high-humidity conditions, in contrast to vegetation in arid environments that supports extreme conditions of water stress.

The Cerrado sites with natural LULC (BRA and PDG) also demonstrated this increase in vegetation control over the dry season (42–48%). At the cropland site in this biome (USE), g_s decreases by approximately 15% during the dry season. This pattern is probably associated with the crop cycle: harvesting occurs mainly at the end of this period (Juárez 2004).

While higher g_s values were obtained for tropical and semideciduous forests, the lowest g_s values were obtained for Caatinga sites (CCG1 and CCG2), where we observed a marked decrease in g_s during the dry season (> 60%), demonstrating pronounced changes from season to season. In contrast, when we evaluated humid subtropics sites, we noticed that g_s varied according to the crop cycle at CAS, CRA, and PRS, whereas at grassland sites (PAS, and SMA), g_s did not exhibit significant seasonal variability.

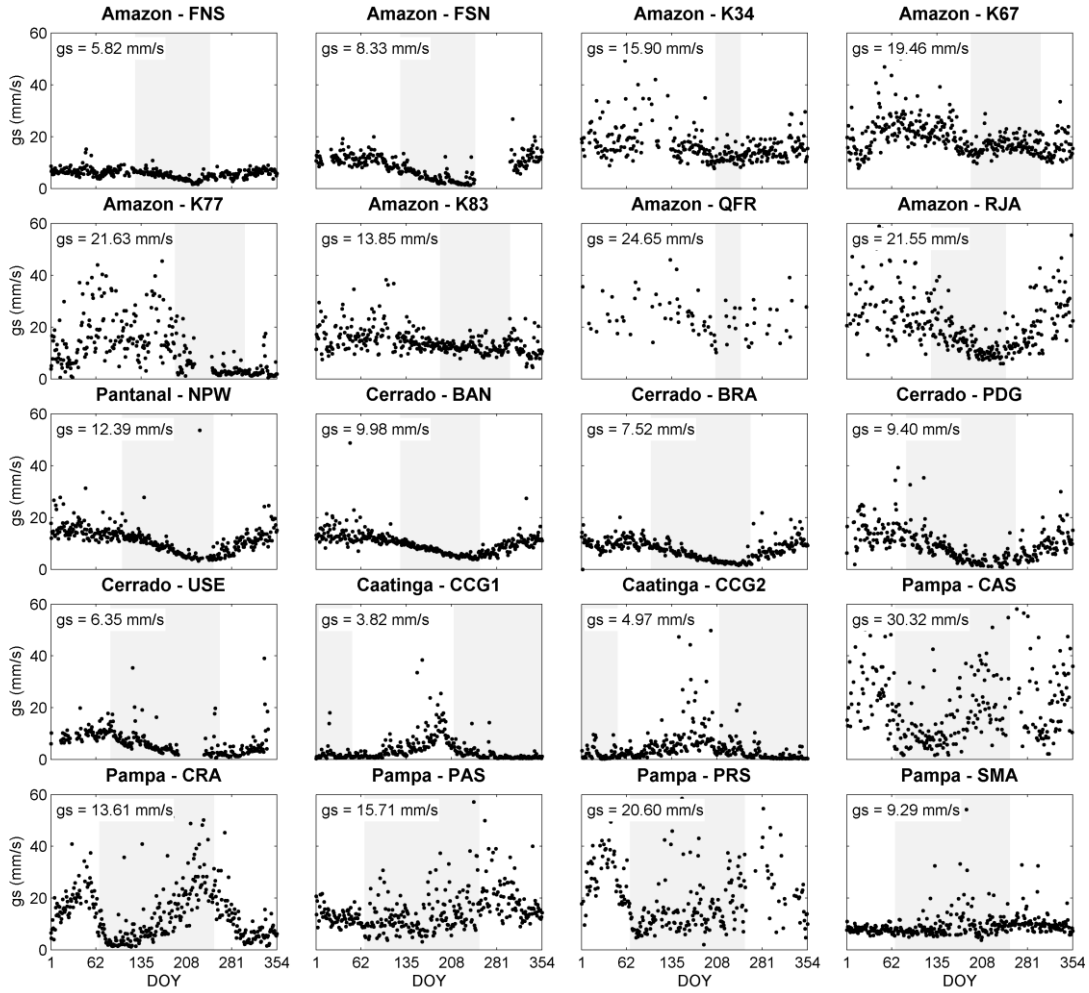

Figure 4.4. Patterns of surface conductance (g_s) at 20 South American measurement sites. Shaded areas indicate the dry season or autumn/winter season for sites located in the Pampa biome (CAS, CRA, PAS, PRS, and SMA).

4.3.4 Patterns of the Jarvis and McNaughton decoupling factor

Based on g_a and g_s, we assessed the vegetation–atmosphere interactions using the Jarvis and McNaughton factor, which reflects the importance of atmosphere and vegetation controls on ET. For sites in the Amazon (K34, K67, K83, QFR, and RJA), the Pampa (CAS, CRA, PAS, PRS, and SMA), and seasonally flooded areas (NPW and BAN), we obtained the highest **Ω** values, ranging from 0.47 to 0.65 (**Table 4.3**). This implies that in these ecosystem types, g_a is of greater importance than g_s in controlling water vapor exchange. When we evaluated the relationship between ET and the main controls and drivers (Rn, VPD, g_a, and g_s) presented in **Figure 4.5**, we observed that at these sites, under normal conditions of adequate water availability, ET is mainly driven by Rn, and

VPD, and controlled by g_a, suggesting the greater importance of abiotic factors in controlling ET.

As water availability decreases, the importance of g_s control on ET increases. This pattern is well represented mainly by arid sites in the Caatinga biome (CCG1 and CCG2), for which we obtained the lowest **Ω** values. For Cerrado sites (BRA and PDG) where there is a longer dry season (lasting 6 months) (da Rocha et al., 2009), we obtained lower **Ω** values than those observed in humid areas. For these biomes (Caatinga and Cerrado), we found a strong relationship between ET and g_s. For the Caatinga biome, the relationship between ET and g_s was significantly stronger than the relationships between ET and climate factors (Rn and VPD), suggesting a high degree of vegetation control over water vapor exchange in this region.

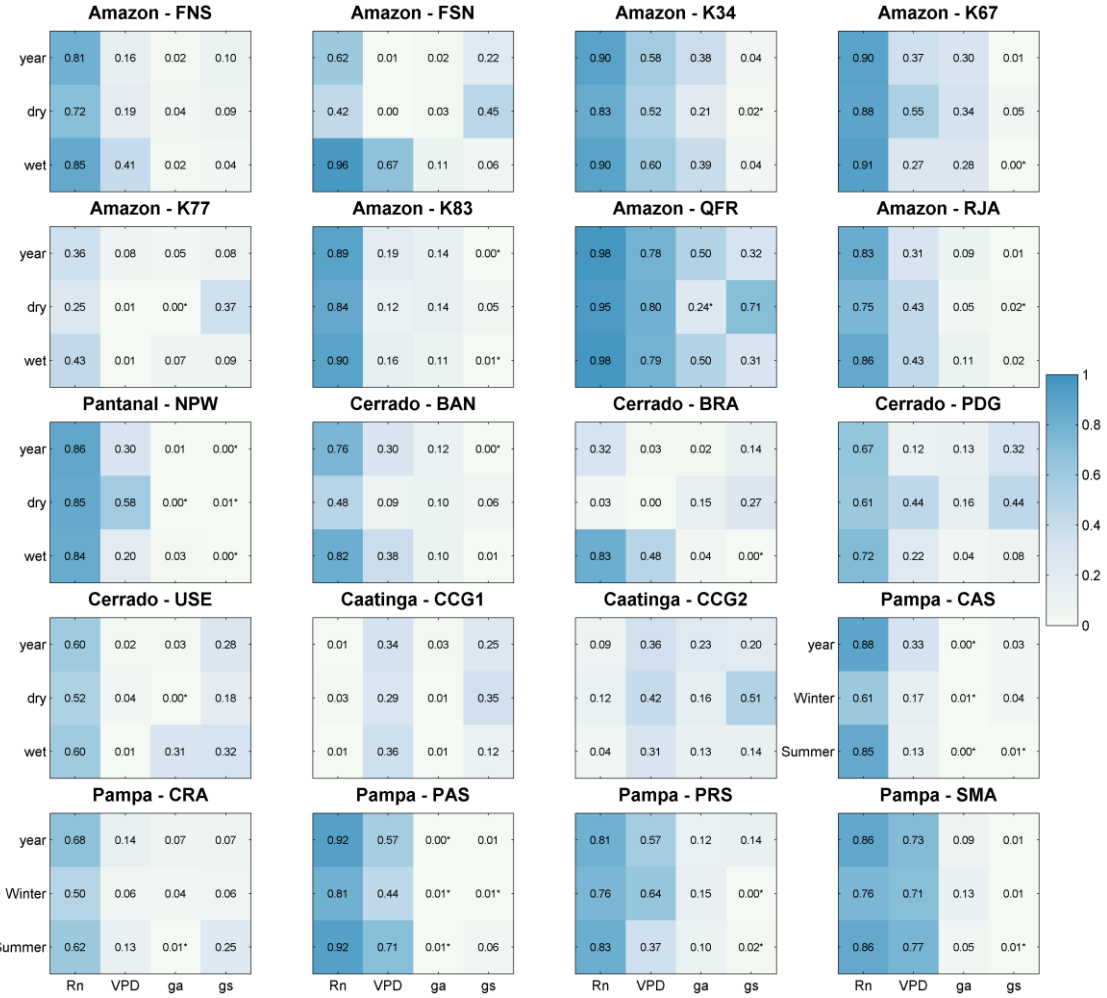

Figure 4.5. Coefficients of determination (R^2) for linear relationships between evapotranspiration (ET) and net radiation (Rn), vapor pressure deficit (VPD), and aerodynamic (g_a) and surface (g_s) conductance throughout the year and during dry and

wet seasons (for sites located in the Pampa biome, we used autumn/winter and spring/summer seasons). *Correlation is not significant at the 5% level.

Our results also demonstrated that Ω varies not only among biomes but also over the seasons, with these variations being more significant for sites with LULC changes (**Figure 4.6**). For instance, forested sites (K34, K67, K83, QFR, and RJA) in the Amazon slightly varies over the seasons, in contrast to cropland and pasture sites (FNS, FSN, and K77), where Ω exhibited pronounced seasonality, with values ranging from 0.62 to 0.69 during the wet season, being 26–33% lower in the dry season. Furthermore, at these sites, the relationship between ET and g_s was significant for the dry season (R^2 = 0.37–0.45), contrasting to forested sites in the equatorial and southern Amazon regions, where ET is mainly driven by abiotic factors (R^2 ranging between 0.83–0.98 and 0.19–0.78 for Rn and VPD, respectively).

Important results were also obtained by comparing Cerrado sites in natural vegetation (BRA and PDG) with a cropland site (USE). At the sites in natural vegetation, g_s exhibited a pronounced decrease over the dry season (25–41%), corroborating the increase effect of vegetation on ET, due to decline in water availability during this period. However, at USE (a cropland site), even during the wet season, the vegetation exerts important control on water vapor exchange (R^2 = 0.18 at dry season and R^2 = 0.32 at wet season), while at the natural vegetated sites the relationship between ET and g_s is significant only during the dry season (R^2 = 0.27–044 during the dry season and R^2 = 0–0.08 during the wet season).

When we assessed arid conditions at Caatinga biome sites, we verified that Ω is lower during both, the dry and wet seasons, with VPD and g_s being the two factors that are more related to ET. As mentioned previously, these sites also have different vegetation density conditions, dense (CCG1) and sparse (CCG2). Despite ET being controlled mainly by vegetation, our results demonstrated a higher relationship between ET and g_s (R^2 = 0.51) at sparse Caatinga than in dense vegetation (R^2 = 0.35), suggesting that vegetation conservation can influence ET vegetation controls in this region.

Pampa sites are characterized by cropland (CAS, CRA, and PRS) (irrigated and rainfed systems) or grassland LULC conditions (PAS and SMA). For these sites, we obtained higher Ω values (0.51–0.70) over the seasons and a significant relationship between ET and climate factors (R^2 = 0.68–0.92 for Rn and R^2 = 0.14–0.73 for VPD). However, for

rainfed cropland (CRA), over the spring/summer season, we detected an increase in the strength of the relationship between ET and g_s (R^2 = 0.25), which suggests that during this period, the vegetation exerts some control on ET, while at irrigated and natural land cover (grassland) sites, the relationship between ET and g_s is not significant.

A summary of the seasonal averages of g_a, g_s, and Ω is presented in **Table 4.3**, in addition to the seasonal differences (%) in these factors.

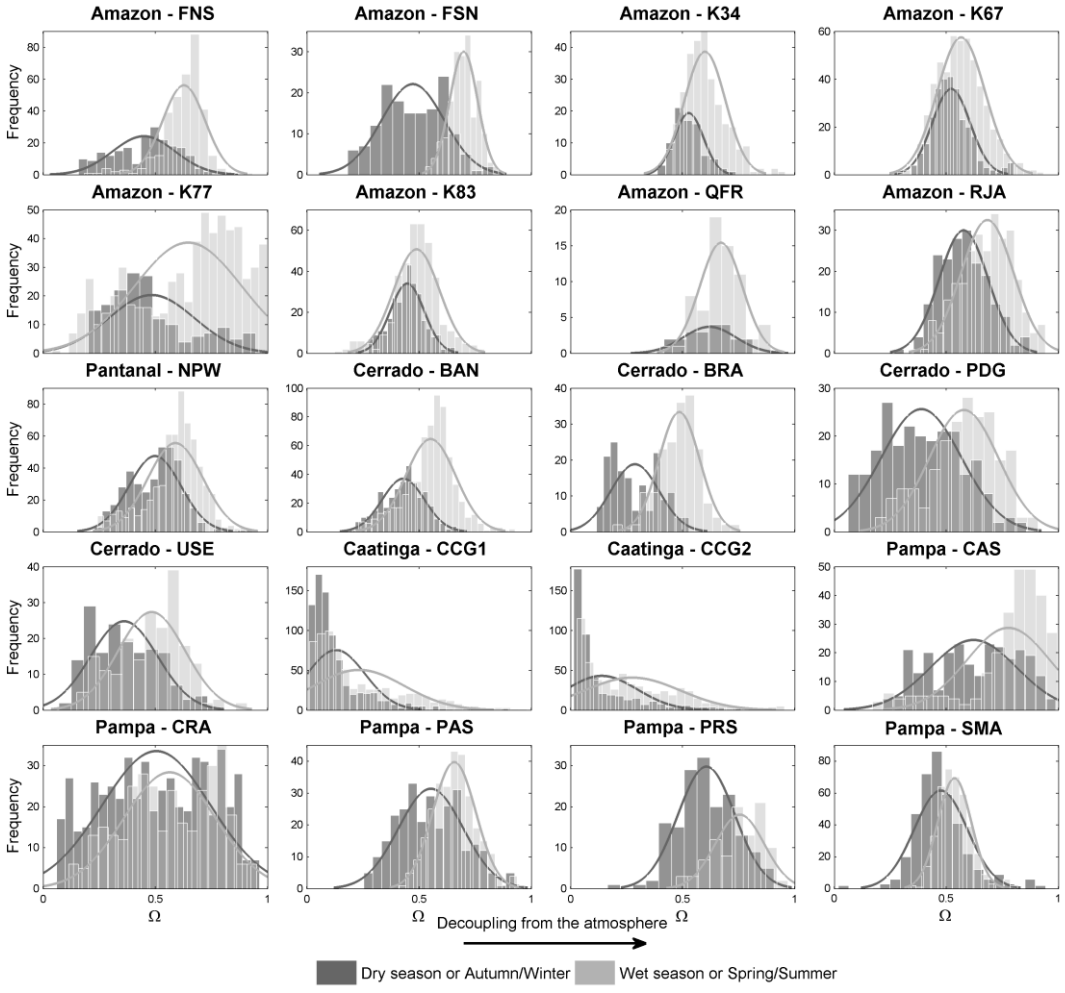

Figure 4.6. Distribution of Jarvis and McNaughton decoupling factor (Ω) for 20 sites located in South America. Tropical site climates were divided into dry and wet seasons, while those at subtropical humid sites (CAS, CRA, PAS, PRS, and SMA) were divided into autumn/winter and spring/summer seasons.

Table 4.3. Annual and interannual averages and dry season change (%) of aerodynamic conductance (g_a), surface conductance (g_s), and Jarvis and McNaughton decoupling factor (Ω).

Site	g_a (mm/s)				g_s (mm/s)				Ω			
	Annual	Dry/ Winter	Wet/ Summer	Dry season change (%)	Annual	Dry/ Winter	Wet/ Summer	Dry season change (%)	Annual	Dry/ Winter	Wet/ Summer	Dry season change (%)
Amazon												
FNS	19.88	27.05	15.91	70	5.82	4.79	6.47	-26	0.56	0.45	0.63	-28
FSN	19.66	19.42	19.84	-2	8.33	4.62	11.36	-59	0.60	0.47	0.70	-32
K34	44.54	47.94	43.96	9	15.90	12.28	16.94	-27	0.58	0.53	0.60	-12
K67	63.21	64.76	62.40	4	19.46	16.47	21.10	-22	0.55	0.52	0.57	-8
K77	16.00	16.75	15.74	6	21.63	5.88	25.87	-77	0.61	0.48	0.65	-25
K83	63.43	65.77	61.84	6	13.85	12.44	14.95	-17	0.47	0.45	0.49	-9
QFR	48.17	49.43	47.96	3	24.65	21.57	25.16	-14	0.66	0.62	0.67	-8
RJA	42.00	41.16	42.51	-3	21.55	14.81	26.25	-44	0.64	0.58	0.68	-15
Pantanal												
NPW	41.40	41.67	41.21	1	12.39	10.01	13.89	-28	0.55	0.50	059	-15
Cerrado												
BAN	39.79	43.37	37.94	14	9.98	7.10	11.53	-38	0.51	0.43	0.55	-22
BRA	45.78	49.57	42.65	16	7.52	5.02	9.64	-48	0.39	0.29	0.48	-41
PDG	34.67	37.07	32.02	16	9.40	7.02	12.11	-42	0.48	0.39	0.58	-33
USE	29.85	35.01	25.50	37	6.35	5.81	6.80	-15	0.43	0.36	0.48	-25
Caatinga												
CCG1	39.41	36.91	42.19	-12	3.82	1.94	5.92	-67	0.18	0.13	0.23	-44
CCG2	42.78	46.62	39.81	17	4.97	2.68	6.75	-60	0.22	0.14	0.28	-49
Pampa												
CAS	19.83	19.93	19.74	1	30.32	19.62	40.43	-51	0.70	0.62	0.78	-20
CRA	25.71	23.97	28.53	-16	13.61	13.96	13.02	7	0.53	0.50	0.56	-11
PAS	27.81	27.91	27.71	1	15.71	14.52	16.88	-14	0.60	0.55	0.66	-16
PRS	27.39	26.57	28.77	-8	20.60	16.09	28.17	-43	0.66	0.61	0.75	-20
SMA	29.50	28.65	30.36	-6	9.29	9.46	9.12	4	0.51	0.47	0.54	-11

4.4. Discussion

4.4.1 How do energy fluxes range over multiple biomes and LULC conditions across South America?

For the Amazon, our results demonstrated three different seasonal patterns of the energy fluxes. In tropical humid forests in the equatorial region (2–3°S) (at K34, K67, K83, and QFR), LE tends to follow Rn, whereas in the southwest Amazon (10°S) (at RJA), Rn increases after the mid-dry season, and LE does not follow this seasonal pattern (Restrepo-Coupe et al. 2021a), suggesting that ET is also controlled by biophysical processes (Costa et al. 2010; da Rocha et al. 2009). A third pattern in the Amazon emerges at sites where the LULC was changed due to deforestation or cropland/pasture expansion (K77, FNS, and FSN). Because LULC changes can modify energy partitioning, a significant increase in β from the wet to the dry season is observed. For instance, at K77, β = 0.81 was observed during the wet season, reflecting pasture growing phenology. However, β reached 1.56 over the dry season, indicating that during this season, H is the dominant component of turbulent fluxes. In contrast to tropical humid forest sites, LE decreases at cropland and pasture sites as the dry season progresses. This pattern is more evident at some sites, where during (K77) or at the end (FNS) of the dry season, H is higher than LE, since the highest LE rates occur during the wetter months, when the canopy is present or when the bare soil is wet (Sakai et al. 2004).

Increases in H at the end of the dry season also occur at seasonally flooded sites (NPW and BAN). At BAN, according to Borma et al. (2009), this pattern is due to decreasing rates in precipitation and soil moisture and an increase in Rn. However, they observed different seasonal patterns of LE: while LE is driven by Rn at NPW (16°S), decreasing rates of LE at BAN (10°S) are not totally explained by Rn, where a decrease in free surface water and soil moisture depletion could also drive LE (Borma et al. 2009).

Cerrado biome also exhibits different seasonal energy flux patterns depending on the latitude. For instance, at PDG and USE (21°S), LE tends to follow Rn. This pattern was also observed in previous research, illustrating the high relationship between available energy exerts and ET (da Rocha et al. 2009). In contrast, at BRA (15°S), LE is not in phase with Rn. At this site, LE decreases during the dry season despite the increase in

insolation, and as the wet season begins, the available energy is dissipated as LE and H decreases concurrently (Santos et al. 2003).

LE is also not in phase with Rn at CCG1 and CCG2 in Caatinga. LE follows the seasonal precipitation pattern closely, and the only time when LE exceed H is at the end of the wet season (Borges et al. 2020; Campos et al. 2019). In contrast, at Pampa sites (CAS, CRA, PAS, PRS and SMA), a strong relationship exists between Rn and LE, with lower fluxes during the autumn/winter and higher fluxes during the spring/summer. During most of the year, the available energy is partitioned to evaporate water from the surface to the atmosphere ($\beta < 1$). At these sites, the primary use of available energy is for LE, especially during the growing season (Diaz et al. 2019; Rubert et al. 2018; Souza et al. 2019). In addition, H does not vary substantially throughout the year, exhibiting maximum values soon after the harvest, demonstrated by values of $\beta > 1$ in our results.

4.4.2 How different are ET drivers over multiple biomes and LULC conditions?

g_a is an important abiotic ET factor that controls the transfer of water vapor from the surface to the atmosphere, while g_s is the main control that vegetation exerts on water exchange from inside the leaf to the atmosphere (Jarvis and McNaughton 1986; Monteith 1965). g_a is related to wind speed and canopy roughness, and g_s is related to VPD, water availability, and photosynthetic capacity. Thus, changes in LULC, air humidity, and soil proprieties can affect these factors, consequently affecting the magnitude of ET and impacting the energy, water, and carbon cycles.

Our results demonstrate that g_a, g_s, and Ω exhibit different patterns and magnitudes across multiple biomes and LULC conditions in South America. Several studies have emphasized that in the Amazon, the conversion from forest to cropland or pasture reduces ET rates and changes the energy partitioning into H and LE (Khand et al. 2017; Laipelt et al. 2020; de Oliveira et al. 2019; von Randow et al. 2004, 2012, 2020). These consequences result from tall forest being aerodynamically rougher than cropland or pasture, and this conversion affects turbulent fluxes, which are higher for rough surfaces than smooth surfaces (Bonan 2015). The replacement of the long root systems of forests by the shorter root systems of crops and pasture also influences the water vapor exchange since the shorter roots of agriculture/pasture may not reach the wetter layers of the soil

during the dry season. Thus decreasing g_s, which decreases LE and increases H (Bonan 2008; von Randow et al. 2004).

Our analysis results confirm earlier findings for two regions in the Amazon (the central and southern parts). The pattern of g_a is high and without clear seasonality in humid tropical forests, suggesting that turbulent activity and canopy roughness do not change substantially over the seasons at forested central Amazon sites (K34, K67, K83, and QFR). In contrast, in pasture and cropland sites (K77, FNS, and FNS), g_a exhibits different patterns throughout the year. Furthermore, g_s slightly decreases during the dry season at humid tropical forest sites (K34, K67, K83, and QFR), corroborating the findings of (Restrepo-Coupe et al. 2021a), who observed that minimum values of g_s occurred mainly during the dry season in the east to central part and in the southern part of the Amazon. They suggested that g_s decreases while LE increases during the dry season at equatorial forest sites, indicating a significant role of evaporation in this season. However, pasture sites (FNS and FNS), cropland (K77), and semideciduous tropical forest (RJA) exhibit pronounced g_s decreases, suggesting a greater importance of biophysical control on ET. This pattern occurs even in the central Amazon (K77), mainly due to shallow root depth and water stress, leading vegetation to close its stomata to avoid water loss to the environment (Costa et al. 2010; von Randow et al. 2012). Thus, for similar climatic conditions within the same biome but under different LULC conditions, g_a and g_s are significantly lower at converted (K77) than at forested sites (K34, K67, and K83), especially during the dry season, altering the decoupling between the surface and the atmosphere.

At sites in natural vegetation in Pantanal (NPW), Cerrado (BAN, BRA, and PDG), and Caatinga (CCG1 and CCG2), g_a increases during the dry season because of the increased frequency of cold front passages in central Brazil in this period (Borma et al. 2009; da Rocha et al. 2002; Sanches et al. 2011), or because of the influence of the Intertropical Convergence Zone (ITCZ) (dos Santos and Santos e Silva 2013). The variability in g_s is consistent with the seasonal decline in the soil water content and vegetation phenology and increase in VPD, since during the dry season, the leaf senescence mechanism responds to water stress, avoiding excessive loss of water by plants and hence reducing ET rates (Cabral et al. 2015; Marques et al. 2020). However, for cropland (USE), the importance of vegetation control on ET increases not only during the dry season, as in natural vegetation in Cerrado, but also during the wet season. This suggests that while

sites under natural LULC exhibit increases in water exchange's biophysical control mainly during drier months, this control occurs during both seasons for the cropland.

Under arid conditions, at the sparse Caatinga site (CCG2), the relationship between ET and g_s is stronger than at the dense Caatinga site (CCG1), suggesting that vegetation conservation can influence energy fluxes. Our results are consistent with those of de Oliveira et al. (2021), who showed that for sparse cover conditions, the average surface temperature is 3°C higher than in the dense Caatinga, probably due to the higher percentage of bare soil absorbing more energy, increasing the surface temperature. In addition, according to those researchers, deforestation contributes to the intensification of soil water loss, since ET under sparse cover conditions accounts for an average of 90% of the total annual precipitation, while under dense conditions this percentage is lower (74%).

Our comparison of the main ET controls for the Pampa biome revealed pronounced variability in g_s throughout the year at cropland sites (CAS, CRA, and PRS), while at grassland (PAS and SMA), g_s slightly varies. Findings for the cropland site in this biome suggest that biophysical conditions might have a more significant influence over ET interannual variability, since the atmospheric conditions do not entirely explain interannual variability observed over five years (Diaz et al. 2019). For grassland sites in the same biome, Rubert et al. (2018) suggested that strong ET pattern is mainly due to Rn and VPD variability. Furthermore, those researchers found differences in ET magnitudes for grasslands sites and suggested that these differences are likely to be associated with vegetation biophysical control, corroborating our finding that demonstrates differences in g_s patterns and magnitudes for the grassland sites.

4.5 Conclusions

In answer to the two key questions posed earlier, our results demonstrate that there are different energy flux patterns across South America. In wetter environments, where ET is strongly related to the available energy, such as in tall forests in the Amazon, g_a and g_s are higher, and the decoupling factor is greater than 0.5 throughout the year. In subtropical regions, the decoupling factor is also high, as in the Amazon, but because of the surface roughness and vegetation canopy height, g_a is not very high. In places where precipitation is significantly seasonal, such as Cerrado and Pantanal, ET is significantly

lower in the drier months, when the influence of vegetation control on ET processes increase, whereas in arid regions, such as the Caatinga biome, the available energy is not the main driver of ET, and the vegetation exerts an important control on water vapor exchange between the surface and the atmosphere.

Our study results also underscore the fact that these patterns can be impacted by LULC change. In the central Amazon region, at cropland sites, LE and H do not exhibit the same available energy partitioning pattern as at forest sites. In addition, reductions in the canopy height and roughness directly influence aerodynamic conductance and consequently turbulent exchange fluxes. Changes in the patterns of energy fluxes and aerodynamic and surface conductance were clear for humid sites in the Amazon and in all biomes assessed here, whether at pasture, agricultural, or natural vegetation degradation sites, as shown for the Caatinga biome.

Changes in LULC directly impact the main abiotic (such as aerodynamic conductance) and biotic (surface conductance) controls, consequently affecting water vapor exchange between the surface and the atmosphere. These impacts become especially important in the face of current deforestation and cropland expansion scenarios in South America. Given that we can observe direct impacts of LULC changes on the moisture exchange between the surface and the atmosphere, how will these impacts be amplified over large areas that experience LULC changes? It is crucial to answer this question in the future to improve our understanding of how LULC changes can affect large areas in South America.

CHAPTER 5

How the remote sensing models represent evapotranspiration at different land use and land cover conditions in the Amazon?[5]

5.1 Introduction

The Amazon rainforest is the largest tropical forest in the world and has a significant influence on regional and global climate due to forest-atmosphere fluxes exchanges (Cohen et al. 2007). Through the so-called "flying rivers" Amazon Forest recycle about 70% of the precipitation (Van Der Ent et al. 2010; Pearce 2020), being an important source of moisture during the dry season in the La Plata basin, in South America (Martinez and Dominguez 2014).

Despite the ecosystem importance of maintenance of forest vegetation, the Amazon Forest has been subject of increased deforestation for half a century (Nobre et al. 2016), especially in the south and eastern region, when the natural vegetation has been replaced by pasture and farming uses. For instance, recent data from *MapBiomas* project (Souza et al. 2020) inform that forest coverage decreased of around 445 thousand of km² (reduction around 12%), between 1985 and 2020, while pasture areas increased about 300%, and soybean areas, presented an increase of 7,500, during these 36 years.

These LULC transformation is especially significant to the so-called "arc deforestation" region, in the southern and eastern Amazon. For example, only in Tapajós basin the forest loss between 1985-2020 was around 89 thousand of km², while the pasture areas increased 433% and soybean areas reached 786 km² in 2020, an increase about 6,293%.

Several studies have been showed how the environmental changes in the Amazon are impacting the hydrology and atmospheric circulation of the basin. These changes are associated with significant energy fluxes partitioning modifications (Baker and Spracklen 2019; Dias et al. 2015; Khand et al. 2017; Laipelt et al. 2020; de Oliveira et al. 2020; Panday et al. 2015; von Randow et al. 2004; Wongchuig et al. 2021), precipitation (Wongchuig et al. 2021), in addition to an increase in river discharge (Costa et al. 2003;

[5] Under internal review.

Dias et al. 2015), dry season length (Costa and Pires 2010), and fire incidence and carbon emissions (Aragão et al. 2018).

However, these impacts are not fully understood in the Amazon, since is not trivial the representation of the physical processes related in the surface and atmosphere interactions. A great effort has been made to measure energy and water fluxes through distinct approaches, mainly based on Bowen ratio (Biudes et al. 2015), and eddy covariance sites (Baldocchi et al. 2001; Borges et al. 2020; Gonçalves de Gonçalves et al. 2013; Keller et al. 2004; de Oliveira et al. 2021; Pastorello et al. 2020; Restrepo-Coupe et al. 2021b; Roberti and Acevedo 2012; Saleska et al. 2013). ET obtained through these approaches is crucial to improve our knowledge of how environmental and biological control and drive ET in several LULC and climate conditions worldwide (da Rocha et al. 2009). However, ET measurements do not have sufficient density to represent all climate and vegetation cover heterogeneity in large scales. In the Amazon, we have only eight public measurements towers, from the LBA project (Davidson and Artaxo 2004; Gonçalves de Gonçalves et al. 2013; Keller et al. 2004; Restrepo-Coupe et al. 2021b; Saleska et al. 2013), that cover mainly forested locals in the central region, while only two of these towers cover pasture and agriculture sites.

To overcome this scale challenge, ET estimations based on remote sensing data have become a dominant means to derive water and energy fluxes from local to global scale. Using it with meteorological data, several models estimate ET in different spatial and temporal resolutions.

Through remote sensing advent, many ET models have been proposed, mainly based on MODIS sensor data (starting in 2000). One of the models widely used by the scientific community is MOD16 (Mu et al. 2007, 2011), based on the *Penman-Monteith* approach and on information from the vegetation index and meteorological data. The GLEAM model (Martens et al. 2017; Miralles et al. 2011a), based on the *Priestley and Taylor* equation, has also been extensively used, and has the proposal to use as much sensing information as possible. Recently, PML (Gan et al. 2018; Zhang et al. 2016b, 2019) also based on the *Penman-Monteith* approach, and SSEBOP based on simplified surface energy balance (Senay et al. 2013, 2020) have become available to the scientific community, further expanding the range of opportunities in remote sensing ET science.

These models have been freely available for use, covering the entire globe, for a long-term period, offering a crucial source of information about large scale ET. Specifically, regarding the Amazon basin-forest, these models have been allowed to characterize

spatial and temporal ET patterns, to improve the knowledge about the drivers and limiting factors on ET processes, showing that ET present different behaviors depending on latitude and energy and water limitation (Fisher et al. 2017; Mao et al. 2015; Talsma et al. 2018). A full and comprehensive revision of ET Amazon can be found in Fassoni-Andrade et al. (2021).

Despite the valuable contribution of remote sensing models to characterize and to understanding ET processes, several studies have been showing that ET estimations from the models can substantially differ between them (Maeda et al. 2017; Melo et al. 2021; Michel et al. 2016; Sörensson and Ruscica 2018; Talsma et al. 2018).

Recently, Fassoni-Andrade et al. (2021) emphasized that while most remote sensing models agree with the ET measurements showing an increase in rates, during the dry season (at northeastern Amazon), and in the central region, where equatorial wet areas prevail, the models diverge to demonstrate the seasonal ET cycle. Melo et al. (2021) showed that remote sensing can reasonably estimate ET despite the models informed different tendency of overestimation and underestimation when compared to measurements. Maeda et al. (2017) demonstrated that ET patterns in the Amazon differ in time and magnitude, driven by a combination of energy and water availability, since neither radiation nor precipitation alone could explain ET patterns.

Accurate and finer spatial and temporal ET estimates from remote sensing have been a challenge and a great opportunity to overcome open scientific questions and applications that heavy depended on fully ET understanding (Fisher et al. 2017). This is especially true for the Amazon basin-forest system, where in face of climate change scenarios, large-scale ET estimations are essential to provide high quality information about water use and water stress among different land cover types and drought long-term monitoring, in addition to improving how the LULC can impact water, energy and carbon cycles.

To improve models' estimates is critical to understanding the ET process in a wide range of LULC and climate, based on measurements, seeking to understand how the models are representing these processes and what their potentials and limitations. Several studies were conducted to evaluate the ET models' performance, mainly at sites in the North Hemisphere (Chen et al. 2016; Ershadi et al. 2015; McCabe et al. 2016; Michel et al. 2016; Mu et al. 2011; Xu et al. 2019), assessing, especially MOD16 and GLEAM, while other models, mainly PML and SSEBOP, are not still extensively evaluated. In addition, most studies have focused on the impact of these changes on total ET estimates, and

analyses involving individual ET components remain unknown, largely because most models do not provide this information. Assessing how transpiration, soil evaporation, and loss interception are impacted due to LULC changes is important because environmental changes conditions and/or vegetation conditions, can affect plant phenology, water-use efficiency, the atmospheric demand vapor, and soil moisture, impacting differently the ET components (Zhang et al. 2016b).

Given the importance of delving into the ET processes in the Amazon, a multi-model analysis at tropical system is fundamental to understand how the models represent the water fluxes exchange between the surface and the atmosphere at multiple LULC condition, as well as providing an understanding of the accuracy of these models. In this context, we proposed to extend the accuracy and ET pattern analyses in the Amazon region, by incorporating data from wetter regions, fewer evaluated, such as the western and northern regions, conducting an evaluation focusing on model performance according to LULC. Furthermore, we also assessed the performance of ET models and its components, over Tapajós basin, at forest, pasture, and soybeans areas.

To address these main purposes, we seek to answer two scientific questions: *i*) what is the accuracy of the main freely available ET models to represent the ET patterns in a tropical system?, and *ii*) can the remote sensing models represent the differences in LULC in the total ET flux and in its components?

5.2 Data

5.2.1 Basin-Forest Amazon system

The Amazon basin was selected to evaluate the ET models' accuracy and patterns. And, due to anthropogenic pressure, with agricultural areas expansion, the Tapajós basin was selected to assess the model's performance to represent the LULC in the total ET flux and its components. **Figure 5.1** presents the localization of Amazon and Tapajós basins, in South America, in addition to presenting the localization of the measurement sites used to evaluate the accuracy and pattern representation from the remote sensing models.

The Amazon basin was evaluated, since this region is the place of the major tropical forest in the world, and the largest hydrological basin covering about 6 million km², spending over seven countries, and hosting four of the ten largest Rivers in the world (Fassoni-

Andrade et al. 2021; Marengo et al. 2012; Salati et al. 1979). The Amazon basin drains about one-third of the land surface of South America, constituting around 15-20% of the total freshwater flux on the globe (Salati et al. 1979; Salati and Vose 1984). Precipitation varies spatially in the Amazon. Northern is the most humid region, where the annual precipitation account 3,000 mm, without define dry season (Heerspink et al. 2020; Maeda et al. 2017). On the other hand, in central region, the rainfall is about 2,000 mm/year with a short dry season (~3 months, from August to October) (Maeda et al. 2017; da Rocha et al. 2009). And, in the east and southern regions there is a longer dry period (4-5 months, from August to November), with the lowest precipitation rates (1,500 mm/year) (Maeda et al. 2017; da Rocha et al. 2009). As to precipitation, the ET also varies from the west to east and north to south gradient, where based on water balance approach it was verified that in the northeastern ET reaches the highest rates (~ 1497 mm/year), while in the southeastern, there are the lowest rates (~ 986 mm/year), recycling through the forest from 49 to 65% of the precipitation in the basin (Maeda et al. 2017).

The second part of this study was conducted at Tapajós basin, since this basin is an important sub-basin in the Amazon, which has been suffering with anthropogenic pressure, where significant part of forest has been replaced by pasture and soybeans areas (Arias et al. 2018). The Tapajos basin is in the southeastern part of the Amazon basin, covering 492,263 km² (around 12.8% of the Amazon basin) and four Brazilian states (Amazonas, Rondônia, Pará, and Mato Grosso). The Tapajós River is the fifth largest Amazon River tributary (1,880 km of length), contributing to 10.9% of Amazon discharge (ANA 2011; MMA 2011; Mohor et al. 2015). The basin has a tropical climate, with annual precipitation ranging from 1,600-1,800 in the southern, and 2,200-2,400 mm/year in the central west. It presents longer rainy season extending from December to May, and three months of dry season from June to August (ANA 2011; Arias et al. 2018). Cerrado and tropical evergreen rainforest (Amazon biome) cover the basin from the south to the north, respectively. The natural vegetation has been under anthropogenic pressure in the last decade (~50 last years; Nobre et al. (2016)) due to the expansion of pasture and crop areas.

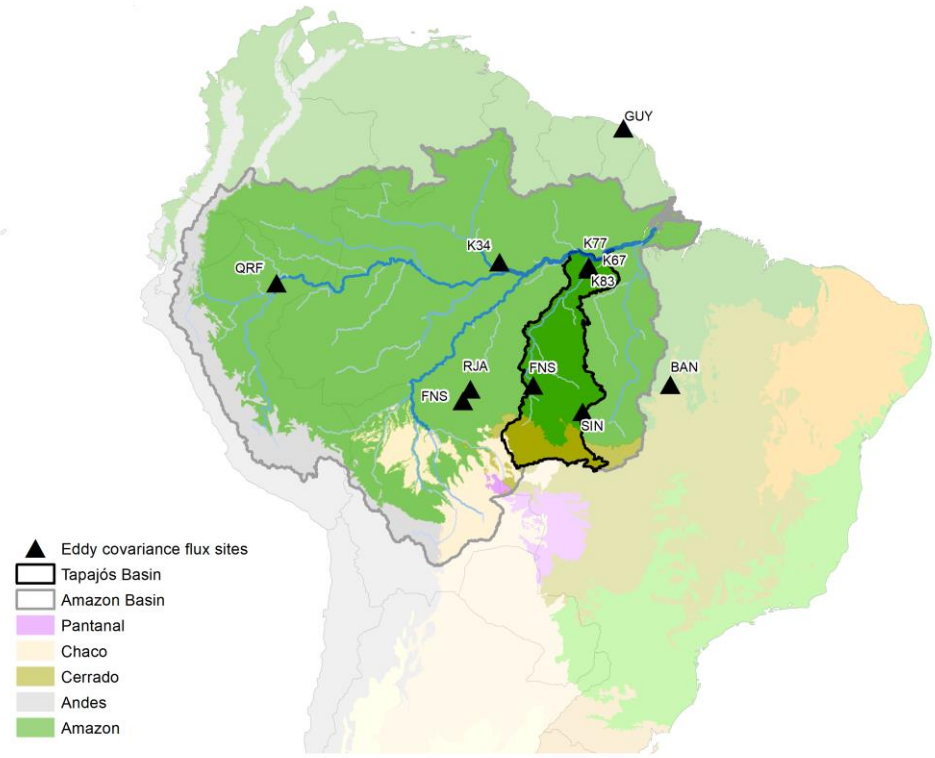

Figure 5.1. Location of the Amazon and Tapajós basins and part of measurement sites in South America. South America biomes were adapted from the Terrestrial Ecoregions of the World (Olson et al. 2001) and modified based on Turchetto-Zolet et al. (2013).

5.2.2 Evapotranspiration models

Four global and available *ET* models were used in this study. One of them is based on simplified surface energy balance equation: SSEBOP (Senay et al. 2013, 2020); two are based in the *Penman-Monteith* approach: MOD16 (Mu et al. 2007, 2011) and PML (Gan et al. 2018; Zhang et al. 2016b, 2019); and the last one is based on the *Priestley and Taylor* equation: GLEAM model (Martens et al. 2017; Miralles et al. 2011a). Detailed information about models' formulation and inputs source can be found in the models' references presented in **Table 5.1**, and in **chapter 2** is presented a comprehensive review of these models.

Table 5.1 summarizes the characteristics of the models used and present the main references of each model where the reader can find detailed information about the models' formulation.

Table 5.1: Summary of evapotranspiration models evaluated in this study

Model	Methods	Spatial	Spatial	Remote sensing source	References
GLEAM (v. 3.3b)	Priestley-Taylor approach	0.25 degree	daily	AIRS, CERES, MODIS, ESA-CCI, SMOS	(Martens et al. 2017; Miralles et al. 2011a)
MOD16 (v. 6)	Penman-Monteith approach	500 meters	8 days	MODIS	(Mu et al. 2007, 2011)
PML (v. 2)	Penman-Monteith approach	500 meters	8 days	MODIS	(Gan et al. 2018; Zhang et al. 2019)
SSEBOP (v. 4)	Surface energy balance	1 km	10 days	MODIS	(Senay et al. 2013, 2020)

5.2.3 Amazon evapotranspiration measurement sites

A network of eleven measurement sites was used in this study, covering forest, pasture, and cropland locals in the Amazon biome. The measurements sites are from: *i*) LBA program (Davidson and Artaxo 2004; Gonçalves de Gonçalves et al. 2013; Keller et al. 2004; Restrepo-Coupe et al. 2021b; Saleska et al. 2013) *ii*) AmeriFlux (Baldocchi et al. 2001), *iii*) Fluxnet (Pastorello et al. 2020), and *iv*) PELD Pantanal (Biudes et al. 2015). **Figure 5.1** and **Table 5.2** present the localization and summarized some information about the measurement sites in the Amazon.

Table 5.2. The measurement sites.

Site	Name	Biome	Lat. (°)	Lon. (°)	Land cover	Data availability	Reference
FNS	Fazenda Nossa Senhora	Amazon	-10.76	-62.35	Pasture	Jun 2000–Mar 2004	(von Randow et al. 2004)
FSN	Fazenda São Nicolau	Amazon	-9.85	-58.26	Pasture	Mar 2002–Oct 2003	(Priante-Filho et al. 2004)
K34	Manaus – K34	Amazon	-2.60	-60.20	Tropical humid forest	Jan 2000–Sep 2006	(de Araújo et al. 2002)
K67	Santarém – K67	Amazon	-2.85	-54.95	Tropical humid forest	Jun 2002–Jan 2006	(Saleska et al. 2003)
K77	Santarém – K77	Amazon	-3.01	-54.53	Pasture and rainfed cropland (soybean and rice)	Aug 2000–Nov 2005	(Sakai et al. 2004)
K83	Santarém – K83	Amazon	-3.01	-54.97	Tropical humid forest	Jun 2000–Mar 2004	

							(da Rocha et al. 2004)
QFR	Quistococha Forest Reserve	Amazon	-3.83	-73.31	Tropical peatland	Jan 2018–Dec 2019	(Griffis et al. 2020)
RJA	Reserva Jaru	Amazon	-10.08	-61.93	Tropical semideciduous forest	Jan 2000–Nov 2002	(von Randow et al. 2004)
BAN	Javaés/ Tocantins	Cerrado	-9.82	-50.15	Woodland savanna (seasonally flooded)	Oct 2003–Dec 2006	(Borma et al. 2009)

5.2.4 Land use and land cover data

In this study, we based our analysis on the LULC classes from MapBiomas project (Souza et al. 2020). This project aims to provide high-quality and high resolution (30 meters) information about the LULC in the Brazilian territory for each year since 1985, based on Landsat imagery collection and the Random Forest algorithm. We used information from collection 6, the latest one, covering the 2003-2017 period (available at https://mapbiomas.org/).

5.3 Methods

5.3.1 Data filtering and quality control of evapotranspiration measurements

To assess the accuracy of remote sensing we used 30-minutes and/or hourly measured LE data based on measurement sites. These data were filtered to remove spurious values, following methodology describe in Souza et al. (2019), Rubert et al. (2018), and in (Diaz et al. 2019). In addition, we did not gap-fill the measurement data and we used the latent heat of evaporation to compute ET using LE data. In addition, we compute daily average ET using a maximum gap of 25% Fisher et al. (2009).

5.3.2 Assessing remote sensing evapotranspiration models

As each of the remote sensing evapotranspiration models used in this study present a different temporal scale, we standardized this temporal scale in order to provide the same magnitude of temporal information. For the MOD16 and SSEBOP models that provide ET data as an 8 and 10-day cumulative, respectively, the daily average ET was computed.

In the GLEAM model ET data is already provided at a daily scale and PML provides the data as an 8-day daily average, thus for these models no time scale adjustment was required.

5.3.3 Evapotranspiration at different land use and land cover conditions

To evaluate how the models represent ET and its components, at different LULC, in a region with several transformations in the last years, we assessed the Tapajós basin, in order to understand if the ET models are influenced by these changes. Thus, we used maps from the MapBiomas (Souza et al. 2020), to generate one-hundred points randomly in each class (forest, pasture, and soybean), for each evaluated year, from 2003 until 2017. To avoid great discrepancies between ET processes depending on biome (Cerrado and Amazon), we restrict the analysis only to Amazon biome, in the Tapajos basin. Thus, we evaluated the individual ET components under forest, pasture, and soybean areas, to assess how the ET components (transpiration, soil evaporation, loss interception) are influenced by different LULC. This analysis was only possibly to GLEAM and PML models that make available the ET components separately.

5.3.4 Statistical analysis

To evaluate the accuracy and patterns of the models, compared to the ET measurements we computed the correlation coefficient, RMSE and BIAS, considering all models at average daily basis. In addition, was applied a mean test (*t test*), for three different temporal conditions, annual, dry, and wet seasons.

5.4 Results

5.4.1 Patterns and accuracy of the remote sensing ET models over measurements sites in the Amazon

ET patterns vary over a range of climatic and LULC conditions in the Amazon and among the remote sensing models. **Figure 5.2** presents ET patterns over Amazon measurements sites and the **Figure 5.3** presents the correlation coefficient, BIAS and RMSE, between

the *ET* models and the measurements sites in whole Amazon. Detailed *ET* patterns are also available at **Supplementary Information** (**Figures SI5.1-5.4**).

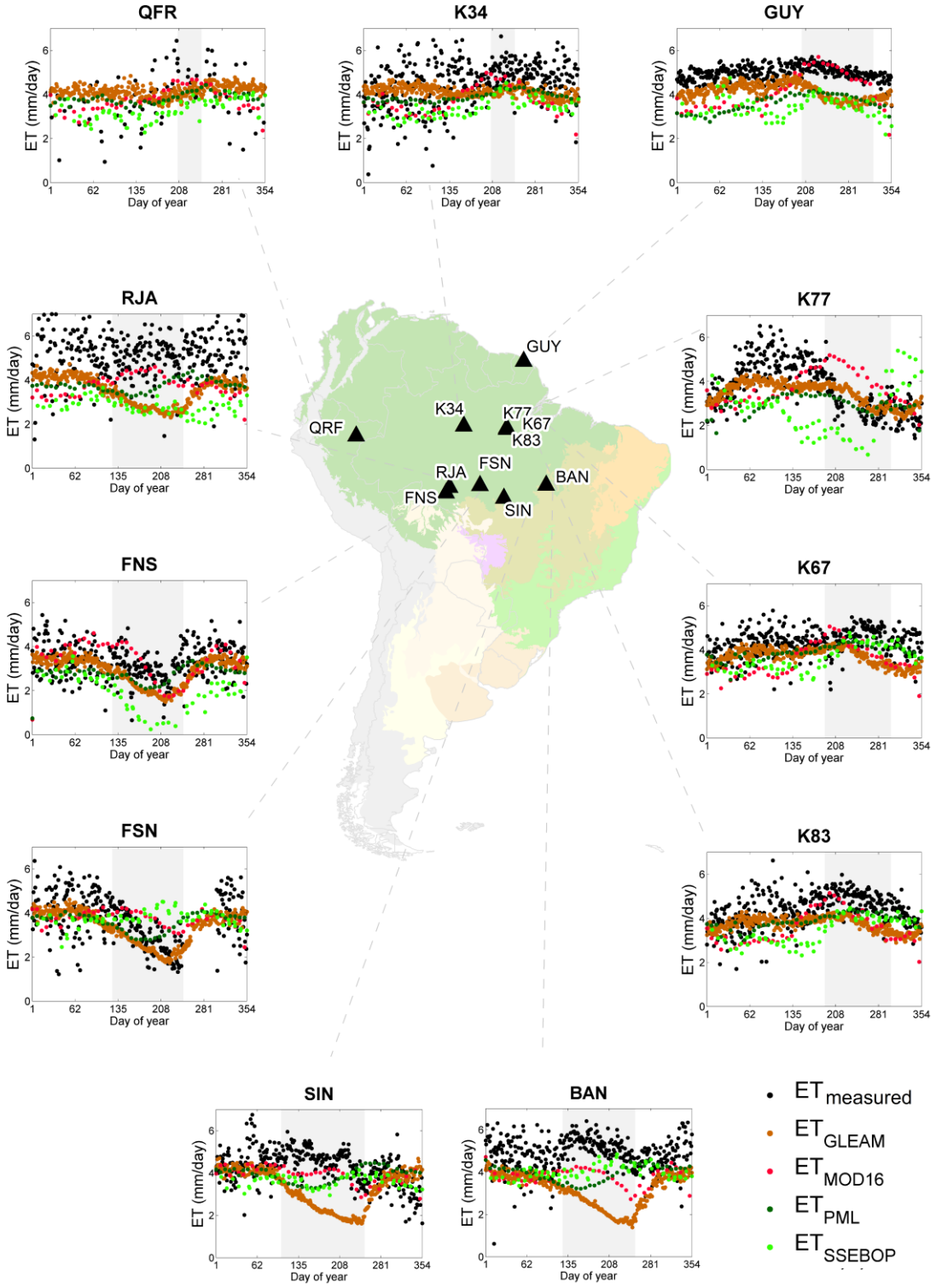

Figure 5.2: *ET* patterns at eleven measurement sites in the Amazon, through remote sensing models (GLEAM, MOD16, PML, and SSEBOP), and measurement data (ET measured). Shaded areas indicate the dry season. South American biomes were adapted from the Terrestrial Ecoregions of the World (Olson et al. 2001), and modified based on Turchetto-Zolet et al. (2013).

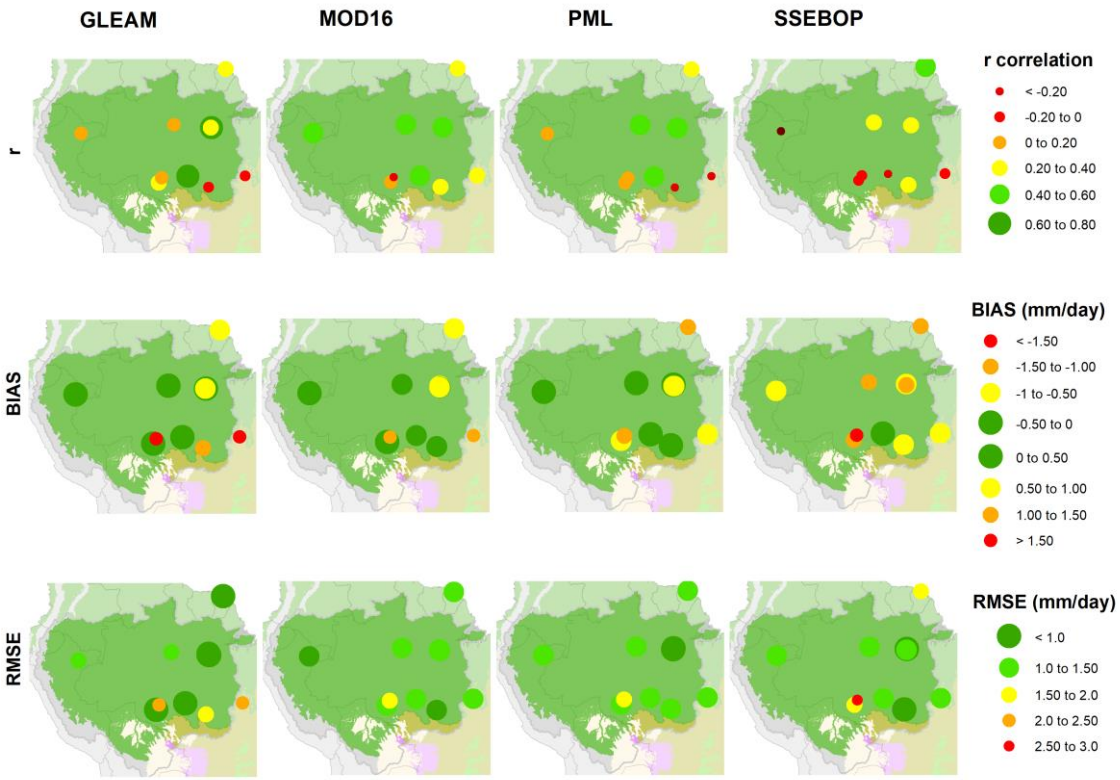

Figure 5.3: Statistical metrics (correlation, BIAS, and RMSE) between the *ET* measurements and estimations from the remote-sensing models (GLEAM, MOD16, PML, and SSEBOP), in the Amazon. South American biomes were adapted from the Terrestrial Ecoregions of the World (Olson et al. 2001) and modified based on Turchetto-Zolet et al. (2013).

5.4.1.1 Forested sites in equatorial region

Forested sites at equatorial Amazon, mainly limited by energy (da Rocha et al., 2009), was a challenge to the models to represent *ET* patterns, besides that, most of them showed significant agreement with the measurements. For instance, GLEAM model showed weak to moderate correlation coefficient (*r* from 0 to 0.35) with the measurements. The model does not represent well *ET* patterns in most equatorial sites. At GUY, K67 and K83,

GLEAM model shows a pronounced decrease in ET rates during dry season (August–November), while the measurements show a non-significant reduction (GUY and K83), or even an increase in this period (K67). In the most humid sites (K34 and QFR), GLEAM does not capture the ET patterns (r = 0 at K34 and r = 0.16 at QFR). In addition, to all these sites, the model underestimate ET rates (BIAS from -0.84 to -0.31 mm/day), except at QFR (BIAS = 0.28 mm/day), and present RMSE higher than 0.87 mm/day.

Better agreement between the estimations and the measurements at equatorial Amazon was found using MOD16 (r from 0.34 to 0.52). However, as was observed to the GLEAM, MOD16 also underestimate the measurements, informing BIAS from -0.94 to -0.46 mm/day to all sites, expect to QFR, where the model performed well (r = 0.52, BIAS = 0.19 mm/day, and RMSE = 1.00 mm/day).

In addition, MOD16 demonstrates an increase in ET at the end of the rainy and at the beginning of the dry season, even to those sites where the measurements inform a slight variation between the seasons (GUY, K34, K67, and K83). However, for the wettest region in the Amazon (QFR), MOD16 was the model that came closest to the ET pattern.

The performance of PML and SSEBOP at equatorial forested sites was also better than GLEAM, showing moderate correlation coefficient with the measurements at all sites, except to K67 and QFR, where both models presented poor statistical metrics (r from -0.62 to 0.18, BIAS from -0.72 to 0.17 mm/day, and RMSE from 0.82 to 1.40 mm/day). Following the other models, PML and SSEBOP underestimate ET rates in most central Amazon, especially at GUY site. Furthermore, we verified that is still a challenge to these models to capture ET patterns in this region. Despite these models capture the maintenance or ET increase during dry season, it seems that they exaggerate to inform the increase in ET rates (SSEBOP) or inform this increase even to locals where a slight decrease occurs in this period (GUY).

5.4.1.2 Cropland/Pasture site in equatorial region

In contrast to the results found at equatorial forested sites, at cropland/pasture (K77) in the same region, GLEAM showed the best performance to capture the ET pattern (r = 0.77). However, it is important highlighted that the GLEAM model has a lower spatial resolution (0.25°), being a challenge to represent ET fluxes at tower scale and considering LULC changes. Thus, it is possible that the model is representing the same pattern

modeled for the forest sites in this region, shown by GUY, K67 and K83, with a decline in ET flux during the less rainy months.

For MOD16, PML and SSEBOP models the representation of ET pattern in this cropland/pasture site in this region was clearly a challenge (r from -0.31 to 0.44). MOD16 shows a pronounced increase in ET rates during the dry season – same behavior captured to forested sites in the same region – while the measurements inform a consistently decrease over this period. The PML captured the ET decrease during the dry season, however, underestimate the ET rates (BIAS = -0.95 mm/day), especially over the rainy season. And the SSEBOP showed an opposite pattern from the measurements, showing a pronounced decrease over the rainy season, and a consistent increase in the end of the dry season (r = -0.31, RMSE = 2.24 mm/day and BIAS = -1.18 mm/day).

5.4.1.3 Tropical semideciduous forest sites in southern region

Divergent patterns were observed between the models to represent the ET at forested sites in the southwestern Amazon region (RJA and SIN). GLEAM showed the worst performance (r = 0.11 at RJA and r = -0.09) comparing to the other models. The model shows a pronounced ET decreasing during the dry season, while the measurements showed non-decreasing (RJA site), or a decreasing in the end of the dry and the in beginning of the rainy (August–October) season (SIN). MOD16 also presented a poor performance, especially to RJA, where the model seems to reproduce the pattern from the tropical forest in the central Amazon, showing an increase in ET rates during the dry season, in contrast to the measurements (r = -0.21). PML also present a poor statistical metrics to these sites (r = 0.12 at RJA and r = -0.31 to SIN). In addition, the model represents ET pattern similarly at both sites, with a decrease in ET from the beginning to the middle of dry season, while increase rates are observed to end of this period. However, in none of these sites, the measurements inform this pattern. When we evaluate SSEBOP model, we verified a high underestimation at RJA (BIAS = -2.49 mm/day), and a poor agreement with the measurements (r = -0.01 at RJA and r = 0.27 at SIN). The model also does not capture well ET pattern in these locals, showing a decreasing in the ET rates in the middle of the dry season, while at RJA the ET do not demonstrate a clearly decline, and at SIN, ET decrease as dry season progress.

5.4.1.4 Pasture in southwestern Amazon

At pasture sites (FNS and FSN), in the southwestern Amazon, the measurements inform higher ET rates over the rainy season (January - March), while lower ET is observed as dry season progress (May–August). When we evaluate the models' performance, we verified that GLEAM captured well this pattern, demonstrating a pronounced decrease in ET rates over the dry season, corroborating with the measurements. In addition, a moderate relationship with the measurements (r = 0.33 at FNS and r = 0.60 at FSN), and lower BIAS (-0.41 at FNS and 0.35 mm/day at FSN) was found to GLEAM model.
MOD16 and PML also performed better in these sites, capturing the ET patterns and presented a lower BIAS when compared to GLEAM, especially to MOD16 (BIAS = 0.07 mm/day at FNS and BIAS = -0.05 mm/day at FNS). In contrast to these results, SSEBOP did not represent the ET pattern. The model showed a negative correlation coefficient with the measurements, and a higher RMSE (1.26 – 1.79 mm/day, at FNS and FSN, respectively). Additionally, SSEBOP showed divergences in representing the ET pattern. While at FNS, the model showed an overestimation in reduction of ET during the dry period (BIAS = -1.40 mm/day), at FSN the model informed a maximum ET peak over the dry season, contrasting to the measurements which inform minimal rates in this period.

5.4.1.5 Seasonally flooded site

The last land cover condition evaluated is the seasonally flooded site located in a transitional region between Amazon and Cerrado biomes. This site presents an ET pattern with lower values over the rainy season and higher ET rates during the drier months. This occurs since the water availability is not a limiting factor for ET, as in the central Amazon region, because the seasonally flooded vegetation has access to the water in the soil during the less rainy months (May - September) (Borma et al. 2009). Furthermore, ET reaches the highest rates during the dry period as there is less cloud cover and consequently more solar radiation.
Most models were unable to represent this pattern, showing negative correlation coefficient with the measurements (r from -0.24 to -0.08), except to MOD16, the only model that capture the ET pattern at BAN (r = 0.34). For example, GLEAM and PML

showed a pronounced decreasing in ET over the dry season while the measurements showed an increase over this period, and for SSEBOP, the ET in BAN almost do not varies, presenting a slight increase in the end of the dry season.

5.4.2 Patterns of evapotranspiration at forest, pasture, and soybean areas in the Tapajós basin

The distribution of ET values at forest, pasture, and soybean areas are presented in **Figure 5.4** for each model evaluated in this study (GLEAM, MOD16, PML and SSEBOP). The results show that median values of ET are lower in pasture and soybean than forest region, for all models. ET is always higher in the forest followed by pasture and soybean. In addition, higher variability was observed to pasture using MOD16, and to soybeans when we evaluated PML and SSEBOP, while for GLEAM there is no great variability different between the land cover types.

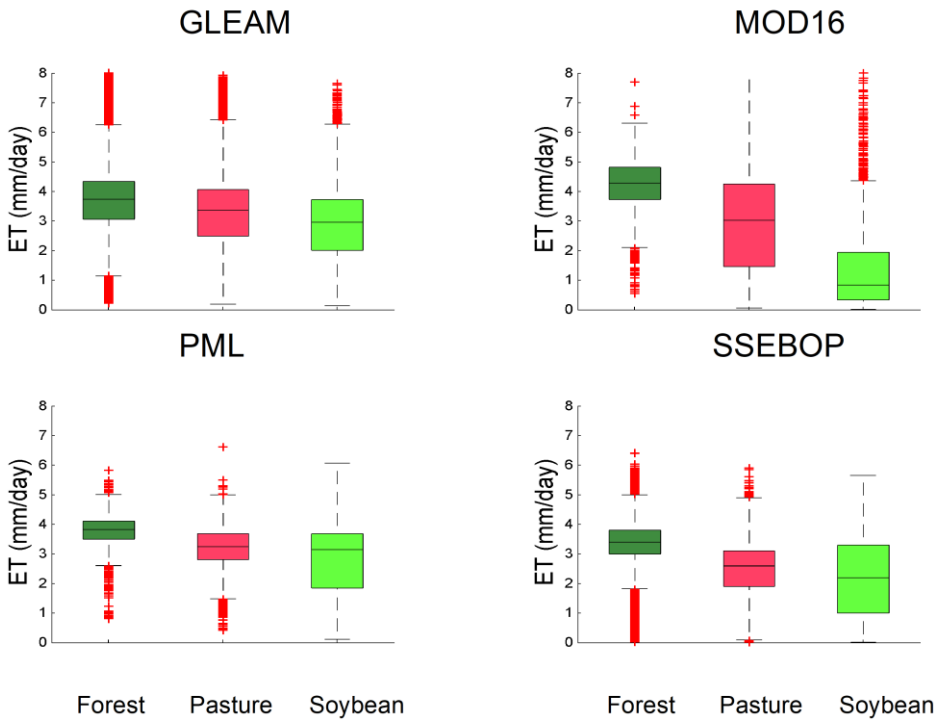

Figure 5.4: Box plot of evapotranspiration for the forest, pasture, and soybean areas, to the 2003-2017 period, and for the GLEAM, MOD16, PML and SSEBOP models. The horizontal inbox lines represent the median, the boxes represent the inter-quartile range

(IQR), the vertical lines indicate variability outside the upper and lower quartiles (1.5IQR), and the red crosses represent the outliers.

Previous studies demonstrated based on energy balance approach that the magnitudes of the energy balance components and ET are related to the density of land cover, being that at pasture and cropland areas, water limitation can affect more the ET processes than forest areas (Khand et al. 2017; de Oliveira et al. 2017, 2019). When we evaluated the ET variability, we verified that, except to GLEAM, the models suggesting that as lower cover density vegetation as greater the ET dispersion, while for forest there is almost no ET variability.

The results also showed that the annual average of ET values from pasture and soybeans are statistically different, according to *t test*, from forest areas, at annual and dry season basis (**Tables SI5.1 and SI5.2**). For GLEAM, MOD16 and PML models, at some years, the difference between forest and pasture and/or soybean are not significantly (**Table SI5.3**). Furthermore, for these models, the average wet season ET at pasture and soybean can be higher than forested areas, while for the SSEBOP, the ET at forested areas are always higher than in pasture and soybeans (**Table SI5.1**).

Is important to highlight that in this period (wet season), less radiation reach the surface due to the higher cloud coverage, directly affecting the ET processes. In addition, during the wet season, is when occur the growing crop season to soybean in this region (October-January) (CONAB 2019), when the highest ET rates are expected for these land cover type.

Our results also demonstrated that all models capture the reduce in ET rates during the dry season, at pasture and soybean areas (**Figure 5.5**), demonstrating a more significant ET decline in the end of dry season (August-September), and to a more pronounced ET reduction to the soybean than to pasture areas. However, when we assessed ET in forested areas, the models show significant disagreement between them. As dry season progress, the GLEAM model informs a reduction in ET over forested areas that is not observed by the other models (MOD16, PML, and SSEBOP). Despite the other models show an increase in ET rates during the dry season, they diverge to inform the ET maximum peak. Whilst MOD16 shows that ET reach the maximum rates in the middle of the dry season,

PML and SSEBOP show higher *ET* values from the middle to the end of this period.

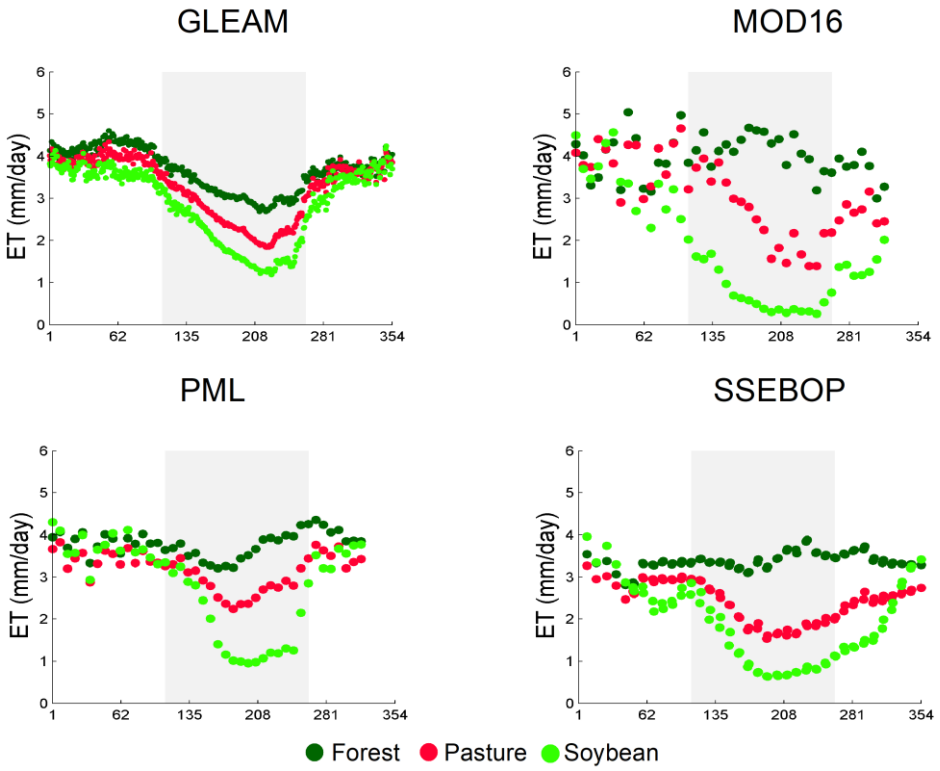

Figure 5.5: Average evapotranspiration patterns for the forest, pasture, and soybean areas, over 2003-2017 period, for the GLEAM, MOD16, PML and SSEBOP models. The dry season are represented by the shadowed areas.

5.4.3 Patterns of evapotranspiration components (transpiration, soil evaporation and loss interception) at forest, pasture, and soybean areas in the Tapajós basin

ET components were evaluated only on the GLEAM and PML models, in which the individual components are available separately. **Figure 5.6** presents the *ET* component distribution in terms of percentage, in forest, pasture, and soybean areas. A significant disagreement between these models to estimate the *ET* individual components is observed. For instance, while for GLEAM, model the transpiration is higher for soybean areas (78%), followed by pasture (72%) and forest (71%), respectively. To PML, a opposite scenario is observed, with higher transpiration to forested areas (81%) than to pasture and soybeans (79 and 70%, respectively). However, both models agree with a decrease in loss interception as decrease the canopy density, showing that pasture and soybean areas present lower loss interception (from 9 to 14%) than forest (18-20%).

Whilst, when we evaluated the soil evaporation component, the models presented significant divergencies. While for GLEAM, the soil evaporation is almost similar in pasture and soybean (14 and 13%), and lower to forested areas (9%), for PML for forested areas this component is almost nonexistent in the total ET flux (1%) and is an import component to soybean (21%) than to pasture areas (8%).

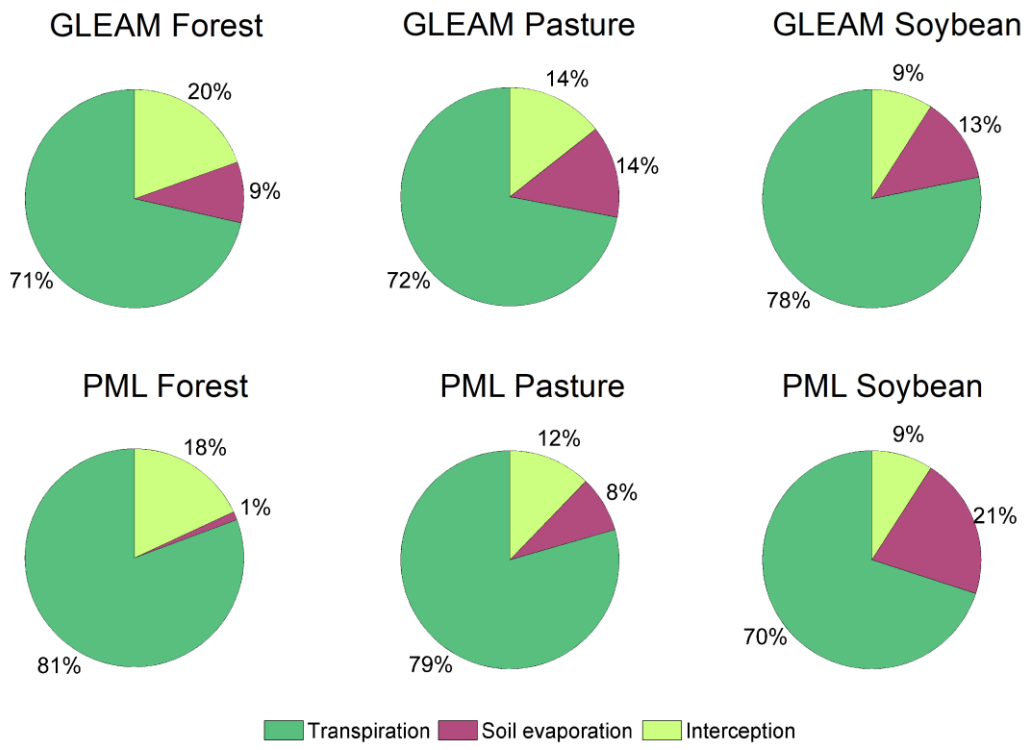

Figure 5.6: Evapotranspiration components (transpiration, soil evaporation, and interception) for the GLEAM and PML models (average over 2003-2017 period), in the Tapajós basin.

When we evaluated ET components patterns, we verified that GLEAM model shows an increase in the transpiration during the dry season at forest areas (**Figure 5.7**). At pasture and soybean, the transpiration declines in the same period.

Furthermore, to forested areas, the soil evaporation component is higher over the wet season, and declines during the dry season, as well as observed to other vegetation types. However, when we evaluate the PML model, the soil evaporation is not significantly to the total ET flux, and almost do not vary over the year. Thus, the model's difference between the ET increase or decreasing representation, over the dry season, is linked with the model's soil evaporation component estimation.

Corroborating to our findings it was related that errors in soil evaporation estimate based on GLEAM, is highly correlated with the MOD44B product, showing a clearly underestimate the field measurements, mainly in areas under higher fraction of vegetation and lower bare soil, attributing uncertainties to this component (Talsma et al. 2018).

On the other hand, the PML model showed significant variations between the soil evaporation in function of the land cover types, showing a significant contribution to total *ET*, mainly to soybean areas. Furthermore, to both land cover types (pasture and soybean), the soil evaporation presents a seasonal behavior, decreasing the rates over the dry season. For both models, the loss interception demonstrates a clear seasonality, with a pronounced decrease during the dry season since there are lesser precipitation events in this period. In addition, this *ET* component also demonstrate changes according to land cover type, being lower as vegetation canopy density decrease.

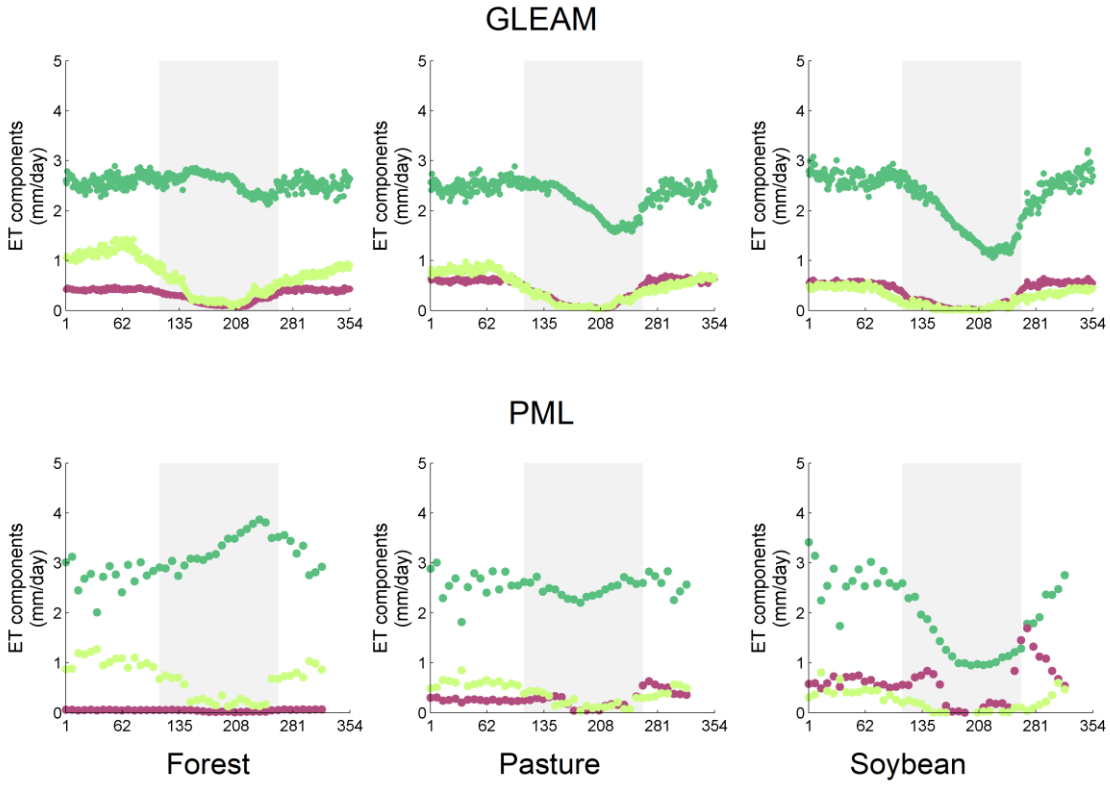

Figure 5.7: Average evapotranspiration components patterns for the forest, pasture, and soybean areas, over 2003-2017 period, for the GLEAM, and PML models. The dry season are represented by the shadowed areas.

5.5 Discussion

5.5.1 How accuracy the remote sensing models estimate and ET pattern in the Amazon basin?

Our results show divergencies between the models to represent the seasonal ET patterns in Amazon, as demonstrated by other studies world-wide (Maeda et al. 2017; Mao et al. 2015; McCabe et al. 2016; Michel et al. 2016; Miralles et al. 2016). These disagreements are even more significant when the individual ET components are evaluated (Miralles et al. 2016; Talsma et al. 2018).

Some main reasons to the disagreement between the models have been discussed, mainly related to input data and model structure (de Andrade et al. 2021; Chao et al. 2021; Chen et al. 2016; Elnashar et al. 2021; Mao et al. 2015; McCabe et al. 2016; Michel et al. 2016; Miralles et al. 2016; Senay et al. 2020; Talsma et al. 2018; Yin et al. 2020; Zhang et al. 2019). However, specifically over the Amazon basin, physical processes of the water exchange between the surface and the atmosphere are not fully understood (Baker et al. 2021; Maeda et al. 2017). Covering the whole Amazon region, we have only few flux measurements sites (only eight public flux towers are available), and the most of them do not cover long-term period. The knowledge provides by these measurements' sites are essential to improve our knowledge about the patterns, drivers and ET controls in the Amazon. Thus, the improvement of the models' performance in the Amazon is also dependent of how much we know about the ET processes, in each LULC, and climatic conditions.

Specifically, about each model, some characteristics of input and assumption is worthy to highlighted about their performance in the Amazon. When we evaluated GLEAM model, three main patterns were observed: *i*) difficult to represent the maintenance and/or increase in ET, at forested sites in the equatorial region, *ii*) overestimation in ET decreasing at tropical semideciduous forest sites in the southwestern part, and *iii*) an opposite pattern of measurements, to represent ET at seasonally flooded site in the transitional region between the Amazon and Cerrado biomes. Except to QFR, the GLEAM model underestimates the ET rates, especially during the dry season, probably relate to overestimate water stress over the drier months (May–September).

Based on *Priestley and Taylor* approach, the GLEAM model computes both, transpiration and soil evaporation constraining them by a multiplicative stress factor (Martens et al.

2016; Miralles et al. 2011a). The stress factor to constrain soil evaporation is based on multilayer soil model driven by observations of precipitation and updated through assimilation of microwave surface soil moisture (Martens et al. 2016). As emphasized by Liu et al. (2011) and Michel et al. (2016), microwave surface soil moisture presents higher uncertainties at densely vegetated regions, such as Amazon tropical forest, due to the attenuation of the microwave signal from the ground by the vegetation. Therefore, the soil moisture can contribute to uncertainty to the GLEAM model in the equatorial region. Additionally, even the model captures the increase in ET or maintenance over the dry season, in equatorial sites, the decreasing in soil evaporation estimated to the model is overestimated, contributing to the pronounced reduction of total ET in this period. Is also important to highlight the low spatial resolution of the GLEAM (0.25º) that also contribute to the discrepancies with the measurements, where daytime fluxes are typically representative of a 2–3 km^2 (de Araújo et al. 2002).

MOD16 model, do not exaggerate in the ET decreasing over the dry season at pasture and (FNS and FSN) and tropical semideciduous forest sites (RJA and SIN), capturing well the pattern in the seasonally flooded site (BAN), and agreeing to the measurements, to represent the increase or maintenance of ET rates during the dry season, at equatorial sites (GUY, K34, K67, K83 and QFR). However, as was verified to GLEAM, MOD16 also underestimates the ET flux in most sites, mainly over the rainy season. In addition, the model shows an increase in ET over the drier months, even in those sites when the ET does not increase or in sites under pasture/cropland where the measurements show a pronounced decrease in this period. According to Miralles et al. (2016) there is tendency of the MOD16 to underestimate the ET flux in the tropics and subtropics may be due to an overestimation of evaporative stress. Talsma et al. (2018) in agreement with the mentioned study, emphasize that MOD16 strongly underestimates transpiration flux when compared to the measurements. According to the authors, this behavior is mainly due the use of fraction of absorbed photosynthetically active radiation (*fAPAR*) from MODIS to driving the transpiration, since the underestimation is consistent across all land cover types, and *fAPAR* is used to partition radiation, consequently, the accuracy of the model might vary seasonally as phenology changes. Furthermore, the MOD16 relies heavily on land cover type to calibration and parametrization, using a static LULC product (MCD12Q1) as input (Mu et al. 2011), that have an overall accuracy of 73.6% in the current collection (Sulla-Menashe et al. 2019). Thus, ET measurements can also be affected if the LULC is not correctly mapped.

PML model, corroborating with the GLEAM and MOD16, showed a tendency to underestimate ET flux, especially over the dry season, and did not was able to capture ET patterns at tropical semideciduous forest sites (RJA and SIN) and at seasonally flooded sites (BAN). However, the model demonstrated a good performance at forested sites, in the central Amazon (GUY, K34, K67, K83 and QFR), and in pasture sites, in the southwestern region (FNS and FSN). Elnashar et al. (2021) evaluated multiple global ET products and verified PML model showed the best agreement with the measurements, informing a great performance over croplands, grasslands, forests, and humid areas. In addition to that, Chao et al. (2021) evaluated PML over several basins in the United States and verified that the model tends to overestimate ET under basins with lower ET rates (< 400 mm/year), and underestimates in basins with higher ET rates (> 800 mm/year), corroborating to our findings.

Some uncertainties in the PML model were highlighted by Chao et al. (2021) and Zhang et al. (2019), such as: *i*) the model simplifies the soil evaporation physical process; *ii*) the uncertainty in LULC type from the MCD12Q1 product also influences parameterization and accuracy of the model; and *iii*) specifically about the Amazon region, the model uses only two measurements sites to calibrate the model.

The last model evaluated here is the SSEBOP, the only one that is based on a simplified energy balance approach. The SSEBOP performs well at most forested sites in the central Amazon, however, under cropland (K77), pasture (FNS and FSN), tropical semideciduous forest (RJA and SIN), and at seasonally flooded site (BAN), the model demonstrated a significant disagreement with the measurements. Overall, the model showed a difficult to represent ET fluxes when water availability is an important factor in ET processes. For example, at pasture sites, the model exaggerated in the ET decrease during the dry season in FNS, and in FSN, showing an increase in ET in this same period, in opposite to the measurements. At K77, a pasture/cropland site in the central Amazon, the model also did not capture the ET pattern, as well as in RJA and SIN (forests) and BAN (seasonally flooded) sites.

The model can be subject to biases because of various factors from the structure to input sources. Most important forcing variable of the SSEBOP model is the land surface temperature (Senay et al. 2020). The land surface temperature version used in this study is from the MODIS (collection 6), with an accuracy better than 1°K (Duan et al. 2019). However, it was demonstrated that errors around 0.35% in land surface temperature can

lead to an ET SSEBOP error approximately of 20% (Chen et al. 2016). de Andrade et al. (2021) evaluated the SSEBOP model at Urucuia Aquifer System in Brazil, and Chen et al. (2016) assessed this model at multiple measurement sites in the United States. These studies emphasized that a predefined differential temperature for cold and hot conditions is a great advantage for this model, working well at a wide range of LULC, climate conditions, and through time. However, minimization of uncertainties in ET reference, equivalent dry-bulb temperature, and in the k factor, can significantly improve the ET SSEBOP estimations.

Overall, after individually evaluating the performance of the main freely available remote sensing-based models for estimating ET, it was found that it is still a challenge for these models to accurately represent the magnitude of ET at different LULC conditions in the Amazon, with all models consistently underestimating the measurements. Furthermore, representing a system not constrained by water availability also proved to be one of the reasons for capturing the ET pattern in the equatorial Amazon region. Especially for the GLEAM, which showed pronounced reduction of ET rates in the dry season, or for the MOD16 and SSEBOP which seem to exaggerate in representing the ET driven by radiation, showing significant increase of ET rate in this period, even in sites, where ET hardly varies or even slight decreases. Representing ET at agricultural/pasture locations also proved to be a challenge for the models. The only one that was able to capture the pattern at K77 was GLEAM, which could very well be representing the same pattern observed at other nearby forested sites, and not in fact representing differently the LULC type at this site. The ET pattern in the seasonal rainforest was also a reason for divergence between the models and measurements. While GLEAM overestimated water stress at these sites during the dry period, other models showed poor statistical metrics and a tendency to significantly reduce ET rates. When seasonally flooded site was evaluated, all models performed poorly, except for MOD16, which was the only one that was able to capture the ET pattern at BAN. Finally, most models, seem to better represent pasture locals, in water limited regions, probably due to the calibration of the water stress factor, except for SSEBOP which showed negative correlation coefficients at these sites.

5.5.2 How is the evapotranspiration flux and its components patterns at different LULC in Tapajós basin?

When we evaluated these three vegetation types in the Tapajós basin (forest, pasture, and soybean), we verified that all models indicate different ET magnitude dependent of the land cover type, where ET at forested areas are always higher than in pasture and soybean ones. As related by de Oliveira et al. (2017, 2019), and von Randow et al. (2004), the lower ET at pasture or agricultural areas is mainly due to some reasons: *i*) the reduction of root system, since pasture and cropland cannot reach deep layers in the soil as tall trees in the Amazon Forest do during the dry period, *ii*) the decrease in the soil water storage capacity, due to the animal and machinery trapping, reducing its porosity consequently compacting the soil, *iii*) the decrease of roughness length, hence reducing the atmospheric turbulence, and *iv*) the increase in albedo, mainly related to higher reflection and lesser absorption of solar radiation from the pasture and cropland leaves, consequently, decrease in Rn.

Nevertheless, the models disagree to represent the ET pattern at these different LULC types. These findings it was observed when evaluate these models compared to the measurement's sites. GLEAM consistently indicate a decrease in ET over the dry season at forested areas, emphasizing the water stress factor is might not calibrate to Amazon, being difficult to this model an adequately represent the ET pattern in this region.

As we find to MOD16, PML and SSEBOP, it was demonstrated that at site scale, while forested sites in the central Amazon do not present clear seasonality and tend to maintain or increase ET during the dry season, at pasture and crops areas, ET presents a seasonal behavior, decreasing during the dry season mainly in the southwestern Amazon sites (Hasler and Avissar 2007; von Randow et al. 2004, 2012). The studies not only showed large discrepancies in ET according to land cover type in the Amazon, but also showed differences in the radiation balance and energy partition, over pasture/cropland and forest areas. For example, based on measurement sites, it was observed that Rn in pasture is lower than in forest due combination of the increase in reflected short-wave radiation and the increase in long wave radiation loss. Consequently H is higher contributing the decreasing in ET in pasture sites (von Randow et al. 2004). In addition, Restrepo-Coupe et al. (2013) demonstrated that in contrast to common idea that water-limitation constrains photosynthesis in the Amazon Forest, during the dry season at equatorial Amazon Forest,

the levels of photosynthetic activity increase, in opposite to observed in the southern region or in pasture and agricultural sites in the Amazon.

Reinforcing these findings, studies based on vegetation index models, demonstrated that deforestation leads to ET and LAI decline, while warming and potential ET increases in the Amazon (Baker and Spracklen 2019; Wongchuig et al. 2021; Wu et al. 2020).

The disagreement between the models to represent ET patterns is even more significant when we evaluate the individual ET components. Theoretically, in adequate water and climatic conditions, the greater vegetation covered the greater the number of stomata, and consequently more water flux is transferred from the surface to the atmosphere through plant transpiration. In dense canopy, more precipitation is intercepted by vegetation, consequently, the water evaporation intercepted by the canopy increases. And finally, as soil is covered by vegetation, less radiation reaches it, being soil evaporation lower. As cover density decreases, decrease the quantity of leaf stomata, and consequently transpiration, also the evaporation of water intercepted by the canopy, while increase the land–atmosphere connection, increasing the soil evaporation. We verified that it is still a challenge for the GLEAM to represent adequately this previously mentioned theoretical behavior, especially for soil evaporation. While the was the model that most closely captured the behavior mentioned, indicating a reduction in transpiration and loss interception, combined with the increase in soil evaporation, as vegetation canopy density decreases.

Many efforts have been made to evaluate the quality of the total ET flux of different global models based on remote sensing, such as: *i*) MOD16, *ii*) GLEAM, *iii*) JPL, *iv*) PML, *v*) SSEBOP, and others (Chao et al. 2021; Elnashar et al. 2021; García et al. 2013; Kim et al. 2012; Michel et al. 2016; Miralles et al. 2016; Ruhoff et al. 2013; Talsma et al. 2018). These studies have shown that models are able to estimate ET reasonably well, agreeing to show a similar total evaporative flux. However, some studies have shown that the individual components of ET diverge considerably between models (Melo et al. 2021; Miralles et al. 2016; Talsma et al. 2018), as we verified here to forest, pasture, and soybean areas in the Tapajós basin.

While Miralles et al. (2016) and Talsma et al. (2018) conducted an analysis of total ET fluxes and its components worldwide, Melo et al. (2021) evaluated some remote-sensing models over South America.

As reinforced by Melo et al. (2021), the inconsistencies in the ET components, depending on the approach, do not necessarily affect the total ET flux. For instance, in the GLEAM case, as all components (transpiration, soil evaporation, and loss interception) are independently estimated, the uncertainties in the estimations can contribute to uncertainty in the total ET flux. However, the partitioning components estimations is unlikely to influence the ET total flux, for models in which ET components are derived from the estimates of a proxy value of the total ET flux, such as MOD16 and PML (Zhang et al. 2019).

The different models approach implies in divergencies between them to estimate total ET flux, but mainly the ET components. Although these ET components divergencies do not affect considerably the total ET flux in some models, accurate estimations of these components are essential to improve our knowledge of the water and carbon cycles, and their processes over multiple LULC and climate conditions, improving our ability to manage and monitor carbon and water resources, mainly in future climatic change scenarios.

5.6 Conclusions

The information provided by the measurements are essential to improve our knowledge about the ET patterns, drivers, and controls. Thus, the improvement of the model's performance in the Amazon region is also dependent of how much we know about the ET process, in each LULC, and climatic conditions.

Overall, the models evaluated here showed discrepancies between them and between the measurements to represent the ET patterns in the Amazon and at different land cover types in the Tapajós basin. However, they present together, a great opportunity to hydrologic studies. For instance, while most models do not represent well the pattern in the seasonal flooded site (BAN), the MOD16 captured the ET pattern in this site. At pasture sites (FNS and FSN), GLEAM, MOD16 and PML were the best models to represent the ET pattern. In addition, GLEAM came closer to the pattern for cropland (K77), and SSEBOP represented well the ET at humid locals (GUY and K34).

At Tapajós basin, MOD16, PML and SSEBOP models demonstrated that the ET pattern varies according to the vegetation type (forest, pasture, and soybean). And, while ET components (transpiration, soil evaporation and loss interception) for GLEAM are unable

to represent the differences at LULC condition, the PML model seems to reflect previous finding based on ET measurements in the Amazon.

Additionally, the refinement of the spatial scale and more accurate information of LULC also prove to be significant for improving ET patterns representation, since the models do not seem to represent the ET at cropland/pasture site in the central Amazon. When we evaluated each model at different LULC conditions, we observed that ET patterns represented at seasonally flooded, cropland, and in a system where the water is not a limiting factor, is still a challenge to the most global models.

Thus, is worthy to highlight the caution to assess ET in the Amazon, since the models presenting divergencies in most LULC conditions, and the choice by the only one model to assess the ET process can attribute uncertainties in the analysis. Despite the challenge that still exist, remote sensing has been a crucial way to improve our understanding of the water flux exchange between the surface and the atmosphere in the Amazon (Fassoni-Andrade et al. 2021). Future remote sensing missions (McCabe et al. 2017; Sheffield et al. 2018) and expansion of the sites network, in addition to continuous measurement over the South America (Biudes et al. 2015; Borges et al. 2020; Gonçalves de Gonçalves et al. 2013; de Oliveira et al. 2021; Restrepo-Coupe et al. 2021b; Roberti and Acevedo 2012; Saleska et al. 2013), are a unique opportunity to validation, calibration and consequently the improve the ET estimations, providing high quality information that allowing us to advance to ET-based science.

CHAPTER 6

6.1 Final conclusions

The water and energy fluxes were assessed over South America through remote sensing models and measurements, in order to investigate the performance of the main remote sensing products to provide accurate information of the water fluxes dynamic. Additionally, we focused on the ET measurements aiming to improve our understanding about the patterns, drivers, and controls over multiple vegetation types and climate conditions. Finally, we investigated the remote sensing model's performance in representing accurately the patterns of the total ET and its components.

Based on the first study we verified that the current remote sensing products were not able to achieve the water balance closure in South America due to the uncertainties of the individual components. Evaluating the water balance uncertainties, we observed that the lowest uncertainties were found for combination of MSWEP precipitation and GLEAM ET estimations. Furthermore, these uncertainties are influenced by basin scales and by climatic conditions, since our results demonstrated better results for large basins and for basins under tropical climate conditions.

Through the second study we verified that abiotic and biotic factors present different importance in controlling ET according to land cover type and over the seasons of the year. For instance, while in wetter environments the abiotic factors are the exerts main control on ET, in arid regions and/or longer dry season, the importance of biotic factor on ET processes increase. In addition, our results demonstrated that changes in LULC can directly impact the main abiotic (such as aerodynamic conductance) and biotic (surface conductance) controls, consequently affecting water vapor exchange between the surface and the atmosphere.

Finally, the last study demonstrated that the models present lower accuracy at humid regions, especially at seasonal flooded site, while in regions where the water availability limiting ET the models performed better. When we evaluate the individual ET components (transpiration, soil evaporation and loss interception), we verified higher discrepancies between the models in representing the differences in the fluxes according to the LULC condition. However, this study also demonstrated that despite the discrepancies between the measurement sites and between the models, they are together a great opportunity to achieve accurate ET estimations.

6.2 Future perspectives

Lessons in this study point to future opportunities and open questions in ET-based science to address. For instance, to advance on the understanding of ET processes and their implications, it is crucial to ensure the maintenance and worldwide expansion of the energy and water flux measurements network and the establishment of collaborative networks. In addition, it is essential to focus on the development of uncertainty analysis methods, as they provide valuable information about the reasons of the models' uncertainty at different vegetation and climate conditions. Finally, we are facing a great opportunity to develop a regional, or even global, model based on the estimates of the current ET models, weighted by their uncertainties, that can provide robust water and energy information.

Furthermore, remote sensing missions focusing on ET and photosynthetic activity, such as ECOSTRESS and the Fluorescence Explorer mission, additionally with the continuation of the Landsat temporal series, the visible infrared imaging radiometer suite instrument (VIIRS) (MODIS successor), and GRACE-FO, are together with the increase of cloud computation, a valuable opportunity to achieve two important open gaps in the ET-based science, obtaining information for long-term periods, and for finer spatial scales.

All the efforts that have been made in modeling and measuring water and energy fluxes have been essential to improve our understanding about the ET processes and how they may be impacted due to climate change and LULC changes. Since these impacts are observed at a local scale, it is opportune to investigate how they can be amplified considering large, modified areas, for long-term periods. Despite the limitations of the models and remote sensing products assessed in this study, the information they have been providing and will still provide to us, is a unique opportunity to advances in hydrological science studies.

References

Abelen, S., F. Seitz, R. Abarca-del-rio, and A. Güntner. 2015. “Droughts and Floods in the La Plata Basin in Soil Moisture Data and GRACE.” *Remote Sens.*, 7324–7349. https://doi.org/10.3390/rs70607324.

Aguiar, A. P. D., I. C. G. Vieira, T. O. Assis, E. L. Dalla-Nora, P. M. Toledo, R. A. Oliveira Santos-Junior, M. Batistella, A. S. Coelho, E. K. Savaget, L. E. O. C. Aragão, C. A. Nobre, and J. P. H. Ometto. 2016. “Land use change emission scenarios: Anticipating a forest transition process in the Brazilian Amazon.” *Glob. Chang. Biol.*, 22 (5): 1821–1840. Blackwell Publishing Ltd. https://doi.org/10.1111/gcb.13134.

Aguiar, L. J. G. 2011. “Fluxos de massa e energia para a cultura de milho (mays L.) no Rio Grande do Sul.” Universidade Federal de Viçosa.

Allen, R. G., A. Irmak, R. Trezza, J. M. H. Hendrickx, W. G. M. Bastiaanssen, and J. Kjaersgaard. 2011. “Satellite-based ET estimation in agriculture using SEBAL and METRIC.” *Hydrol. Process.*, 25 (26): 4011–4027. https://doi.org/10.1002/hyp.8408.

Allen, R. G., M. Tasumi, and R. Trezza. 2007. “Satellite-Based Energy Balance for Mapping Evapotranspiration with Internalized Calibration (METRIC)—Model.” *J. Irrig. Drain. Eng.*, 133 (4): 380–394. American Society of Civil Engineers (ASCE). https://doi.org/10.1061/(asce)0733-9437(2007)133:4(380).

Almagro, A., P. T. S. Oliveira, A. A. Meira Neto, T. Roy, and P. Troch. 2021. “CABra: A novel large-sample dataset for Brazilian catchments.” *Hydrol. Earth Syst. Sci.*, 25 (6): 3105–3135. https://doi.org/10.5194/hess-25-3105-2021.

ANA. 2011. “Plano Estratégico de Recursos Hídricos da Bacia Amazônica – Afluentes da Margem Direita.” Brasília, Brazil: Federal Water Agency.

ANA. 2015. “Conjuntura dos Recursos Hídricos.” Brasília, Brazil: Federal Water Agency.

ANA. 2020. “Evapotranspiração Real Sensoriamento Remoto no Brasil.” Brasília, Brazil: Federal Water Agency.

Anderson, M. C., W. P. Kustas, J. M. Norman, C. R. Hain, J. R. Mecikalski, L. Schultz,

M. P. González-Dugo, C. Cammalleri, G. D'Urso, A. Pimstein, and F. Gao. 2011. "Mapping daily evapotranspiration at field to continental scales using geostationary and polar orbiting satellite imagery." *Hydrol. Earth Syst. Sci.*, 15 (1): 223–239. https://doi.org/10.5194/hess-15-223-2011.

Anderson, M. C., C. A. Zolin, P. C. Sentelhas, C. R. Hain, K. Semmens, M. Tugrul Yilmaz, F. Gao, J. A. Otkin, and R. Tetrault. 2016. "The Evaporative Stress Index as an indicator of agricultural drought in Brazil: An assessment based on crop yield impacts." *Remote Sens. Environ.*, 174: 82–99. Elsevier Inc. https://doi.org/10.1016/j.rse.2015.11.034.

de Andrade, B. C. C., E. J. de Andrade Pinto, A. L. Ruhoff, and G. B. Senay. 2021. "Remote sensing-based actual evapotranspiration assessment in a data-scarce area of Brazil: A case study of the Urucuia Aquifer System." *Int. J. Appl. Earth Obs. Geoinf.*, 98. https://doi.org/10.1016/j.jag.2021.102298.

Aragão, L. E. O. C., L. O. Anderson, M. G. Fonseca, T. M. Rosan, L. B. Vedovato, F. H. Wagner, C. V. J. Silva, C. H. L. Silva Junior, E. Arai, A. P. Aguiar, J. Barlow, E. Berenguer, M. N. Deeter, L. G. Domingues, L. Gatti, M. Gloor, Y. Malhi, J. A. Marengo, J. B. Miller, O. L. Phillips, and S. Saatchi. 2018. "21st Century drought-related fires counteract the decline of Amazon deforestation carbon emissions." *Nat. Commun.*, 9 (1). Nature Publishing Group. https://doi.org/10.1038/s41467-017-02771-y.

de Araújo, A. C., A. D. Nobre, B. Kruijt, J. A. Elbers, R. Dallarosa, P. Stefani, C. von Randow, A. O. Manzi, A. D. Culf, J. H. C. Gash, R. Valentini, and P. Kabat. 2002. "Comparative measurements of carbon dioxide fluxes from two nearby towers in a central Amazonian rainforest : The Manaus LBA site." *J. Geophys. Res.*, 107 (20): 1–20. https://doi.org/10.1029/2001JD000676.

Arias, M. E., E. Lee, F. Farinosi, F. F. Pereira, and P. R. Moorcroft. 2018. "Decoupling the effects of deforestation and climate variability in the Tapajós river basin in the Brazilian Amazon." *Hydrol. Process.*, 32 (11): 1648–1663. John Wiley and Sons Ltd. https://doi.org/10.1002/hyp.11517.

Arias, P. A., J. A. Martínez, J. D. Mejía, M. J. Pazos, J. C. Espinoza, and S. Wongchuig-Correa. 2020. "Changes in Normalized Difference Vegetation Index in

the Orinoco and Amazon River Basins: Links to Tropical Atlantic Surface Temperatures." *J. Clim.*, 33 (19): 8537–8559. https://doi.org/10.1175/JCLI-D-19-0696.1.

Asbjornsen, H., G. R. Goldsmith, M. S. Alvarado-Barrientos, K. Rebel, F. P. Van Osch, M. Rietkerk, J. Chen, S. Gotsch, C. Tobón, D. R. Geissert, A. Gómez-Tagle, K. Vache, and T. E. Dawson. 2011. "Ecohydrological advances and applications in plant-water relations research: A review." *J. Plant Ecol.* Oxford University Press.

Azarderakhsh, M., W. B. Rossow, F. Papa, H. Norouzi, and R. Khanbilvardi. 2011. "Diagnosing water variations within the Amazon basin using satellite data." *J. Geophys. Res. Atmos.*, 116 (24): 1–18. https://doi.org/10.1029/2011JD015997.

Baker, J. C. A., D. C. de Souza, P. Kubota, W. Buermann, C. A. S. Coelho, M. B. Andrews, M. Gloor, L. Garcia-Carreras, S. N. Figueroa, and D. V. Spracklen. 2021. "An assessment of land-atmosphere interactions over South America using satellites, reanalysis and two global climate models." *J. Hydrometeorol.*, 22 (4): 905–922.

Baker, J. C. A., and D. V. Spracklen. 2019. "Climate Benefits of Intact Amazon Forests and the Biophysical Consequences of Disturbance." *Front. For. Glob. Chang.*, 2. Frontiers Media SA. https://doi.org/10.3389/ffgc.2019.00047.

Baldocchi, D., E. Falge, L. Gu, R. Olson, D. Hollinger, S. Running, P. Anthoni, C. Bernhofer, K. J. Davis, R. Evans, J. Fuentes, A. Goldstein, G. Katul, B. Law, X. Lee, Y. Malhi, T. Meyers, W. Munger, W. Oechel, K. T. Paw, K. Pilegaard, H. P. Schmid, R. Valentini, S. Verma, T. Vesala, K. Wilson, S. Wofsy, R. Hall, and H. Hall. 2001. *FLUXNET: A New Tool to Study the Temporal and Spatial Variability of Ecosystem-Scale Carbon Dioxide, Water Vapor, and Energy Flux Densities*.

Barbosa, H. A., T. V. Lakshmi Kumar, F. Paredes, S. Elliott, and J. G. Ayuga. 2019. "Assessment of Caatinga response to drought using Meteosat-SEVIRI Normalized Difference Vegetation Index (2008–2016)." *ISPRS J. Photogramm. Remote Sens.*, 148: 235–252. Elsevier B.V. https://doi.org/10.1016/j.isprsjprs.2018.12.014.

Bastiaanssen, W. G. M. 1995. "Regionalization of surface flux densities and moisture indicators in composite terrain." Wageningen,The Netherlands : Agricultural University.

Bastiaanssen, W. G. M., J. Wang, M. Menenti, R. A. Feddes, and A. A. M. Holtslag. 1998. “A remote sensing surface energy balance algorithm for land (SEBAL) New IACS Vision in Action (NIVA) View project Optical Properties of Aerosols over Tibetan Plateau View project A remote sensing surface energy balance algorithm for land (SEBAL) 1. Formula.” *J. Hydrol.*

Beck, H. E., A. I. J. M. Van Dijk, V. Levizzani, J. Schellekens, D. G. Miralles, B. Martens, and A. De Roo. 2017a. “MSWEP: 3-hourly 0.25° global gridded precipitation (1979-2015) by merging gauge, satellite, and reanalysis data.” *Hydrol. Earth Syst. Sci.*, 21 (1): 589–615. https://doi.org/10.5194/hess-21-589-2017.

Beck, H. E., N. Vergopolan, M. Pan, V. Levizzani, A. I. J. M. Van Dijk, G. P. Weedon, L. Brocca, F. Pappenberger, G. J. Huffman, and E. F. Wood. 2017b. “Global-scale evaluation of 22 precipitation datasets using gauge observations and hydrological modeling.” *Hydrol. Earth Syst. Sci.*, 21: 6201–6217.

Beck, H. E., E. F. Wood, M. Pan, C. K. Fisher, D. G. Miralles, A. I. J. M. Van Dijk, T. R. McVicar, and R. F. Adler. 2019. “MSWep v2 Global 3-hourly 0.1° precipitation: Methodology and quantitative assessment.” *Bull. Am. Meteorol. Soc.*, 100 (3): 473–500. American Meteorological Society. https://doi.org/10.1175/BAMS-D-17-0138.1.

Berbery, E. H., and V. R. Barros. 2002. “The hydrologic cycle of the La Plata basin in South America.” *J. Hydrometeorol.*, 3 (6): 630–645. https://doi.org/10.1175/1525-7541(2002)003<0630:THCOTL>2.0.CO;2.

Biudes, M. S., G. L. Vourlitis, N. G. Machado, P. H. Z. de Arruda, G. A. R. Neves, F. de Almeida Lobo, C. M. U. Neale, and J. de Souza Nogueira. 2015. “Patterns of energy exchange for tropical ecosystems across a climate gradient in Mato Grosso, Brazil.” *Agric. For. Meteorol.*, 202: 112–124. Elsevier. https://doi.org/10.1016/j.agrformet.2014.12.008.

Bjerklie, D. M., S. L. Dingman, C. J. Vorosmarty, C. H. Bolster, and R. G. Congalton. 2003. “Evaluating the potential for measuring river discharge from space.” *J. Hydrol.*, 278: 17–38. https://doi.org/10.1016/S0022-1694(03)00129-X.

Bonal, D., A. Bosc, S. Ponton, J. Y. Goret, B. Burban, P. Gross, J. M. Bonnefond, J.

Elbers, B. Longdoz, D. Epron, J. M. Guehl, and A. Granier. 2008. “Impact of severe dry season on net ecosystem exchange in the Neotropical rainforest of French Guiana.” *Glob. Chang. Biol.*, 1: 1917–1933. https://doi.org/10.1111/j.1365-2486.2008.01610.x.

Bonan, G. B. 2008. “Forests and Climate Change: Forcings, Feedbacks, and the Climate Benefits of Forests.” *Science (80-.).*, 320: 1444–1449.

Bonan, G. B. 2015. “Plant Canopies.” *Ecol. Climatol.*, 264–288. Cambridge University Press.

Borges, C. K., C. A. C. dos Santos, R. G. Carneiro, L. L. da Silva, G. de Oliveira, D. Mariano, M. T. Silva, B. B. da Silva, B. G. Bezerra, A. M. Perez-Marin, and S. de S. Medeiros. 2020. “Seasonal variation of surface radiation and energy balances over two contrasting areas of the seasonally dry tropical forest (Caatinga) in the Brazilian semi-arid.” *Environ. Monit. Assess.* Springer.

Borma, L. S., H. R. da Rocha, O. M. R. Cabral, C. von Randow, E. Collicchio, D. Kurzatkowski, P. J. Brugger, H. Freitas, R. Tannus, L. Oliveira, C. D. Rennó, and P. Artaxo. 2009. “Atmosphere and hydrological controls of the evapotranspiration over a floodplain forest in the Bananal Island region, Amazonia.” *J. Geophys. Res. Biogeosciences*, 114 (1). Blackwell Publishing Ltd. https://doi.org/10.1029/2007JG000641.

Brêda, J. P. L. F., R. C. D. de Paiva, W. Collischonn, J. M. Bravo, V. A. Siqueira, and E. B. Steinke. 2020. “Climate change impacts on South American water balance from a continental-scale hydrological model driven by CMIP5 projections.” *Clim. Change*, 159 (4): 503–522. Climatic Change. https://doi.org/10.1007/s10584-020-02667-9.

Cabral, O. M. R., H. R. D. A. Rocha, M. A. V Ligo, O. Brunini, and M. A. S. Dias. 2003. “Fluxos Turbulentos de calor sensível, vapor de água e CO2 sobre plantação de cana-de-açúcar (Saccharum sp.) em Sertãozinho-SP.” *Rev. Bras. Meteorol.*, 18 (1): 61–70.

Cabral, O. M. R., H. R. da Rocha, J. H. C. Gash, H. C. de Freitas, and M. A. V Ligo. 2015. “Water and energy fluxes from a woodland savanna (Cerrado) in southeast Brazil.” *J. Hydrol. Reg. Stud.*, 4: 22–40. Elsevier B.V.

Camilloni, I. A., R. I. Saurral, and N. B. Montroull. 2013. “Hydrological projections of fluvial floods in the Uruguay and Paraná basins under different climate change scenarios.” *Int. J. River Basin Manag.*, 11 (4): 389–399. https://doi.org/10.1080/15715124.2013.819006.

Campos, S., K. R. Mendes, L. L. da Silva, P. R. Mutti, S. S. Medeiros, L. B. Amorim, C. A. C. dos Santos, A. M. Perez-Marin, T. M. Ramos, T. V. Marques, P. S. Lucio, G. B. Costa, C. M. Santos e Silva, and B. G. Bezerra. 2019. “Closure and partitioning of the energy balance in a preserved area of a Brazilian seasonally dry tropical forest.” *Agric. For. Meteorol.*, 271: 398–412. Elsevier B.V. https://doi.org/10.1016/j.agrformet.2019.03.018.

Cavalcanti, I. F. A., A. F. Carril, O. C. Penalba, A. M. Grimm, C. G. Menéndez, and E. Sanchez. 2015. “Precipitation extremes over La Plata Basin – Review and new results from observations and climate simulations.” *J. Hydrol.*, 523: 211–230.

Chao, L., K. Zhang, J. Wang, J. Feng, and M. Zhang. 2021. “A comprehensive evaluation of five evapotranspiration datasets based on ground and grace satellite observations: Implications for improvement of evapotranspiration retrieval algorithm.” *Remote Sens.*, 13 (12). MDPI AG. https://doi.org/10.3390/rs13122414.

Chen, C., D. Li, Y. Li, S. Piao, X. Wang, M. Huang, P. Gentine, R. R. Nemani, and R. B. Myneni. 2020. “Biophysical impacts of Earth greening largely controlled by aerodynamic resistance.” *Science (80-.).*, 6: 1-9*. https://doi.org/10.1126/sciadv.abb1981.

Chen, J. L., C. R. Wilson, B. D. Tapley, L. Longuevergne, Z. L. Yang, and B. R. Scanlon. 2010. “Recent la Plata basin drought conditions observed by satellite gravimetry.” *J. Geophys. Res. Atmos.*, 115 (22): 1–12. https://doi.org/10.1029/2010JD014689.

Chen, M., G. B. Senay, R. K. Singh, and J. P. Verdin. 2016. “Uncertainty analysis of the Operational Simplified Surface Energy Balance (SSEBop) model at multiple flux tower sites.” *J. Hydrol.*, 536: 384–399. Elsevier B.V. https://doi.org/10.1016/j.jhydrol.2016.02.026.

Ciemer, C., N. Boers, H. M. J. Barbosa, J. Kurths, and A. Rammig. 2018. “Temporal evolution of the spatial covariability of rainfall in South America.” *Clim. Dyn.*, 51

(1–2): 371–382. Springer Berlin Heidelberg. https://doi.org/10.1007/s00382-017-3929-x.

Cleugh, H. A., R. Leuning, Q. Mu, and S. W. Running. 2007. “Regional evaporation estimates from flux tower and MODIS satellite data.” *Remote Sens. Environ.*, 106 (3): 285–304. https://doi.org/10.1016/j.rse.2006.07.007.

Coe, M. T., M. H. Costa, A. Botta, and C. Birkett. 2002. “Long-term simulations of discharge and floods in the Amazon Basin.” *J. Geophys. Res. Atmos.*, 107 (20): 1–17. https://doi.org/10.1029/2001JD000740.

Cohen, J. C. P., J. da C. Beltrão, A. W. Gandu, and R. R. da Silva. 2007. “Influência do desmatamento sobre o ciclo hidrológico na Amazônia.” *Cienc. Cult.*, 2 (13): 2–5.

CONAB. 2015. “A cultura do arroz.” Brasília, Brazil: Companhia Nacional de Abastecimento.

CONAB. 2019. “Calendário de Plantio e Colheita de Grãos no Brasil 2019.” Brasília, Brazil: Companhia Nacional de Abastecimento.

Costa, M. H., M. C. Biajoli, L. Sanches, A. C. M. Malhado, L. R. Hutyra, H. R. da Rocha, R. G. Aguiar, and A. C. de Araújo. 2010. “Atmospheric versus vegetation controls of Amazonian tropical rain forest evapotranspiration: Are the wet and seasonally dry rain forests any different?” *J. Geophys. Res. Biogeosciences*, 115 (4). Blackwell Publishing Ltd. https://doi.org/10.1029/2009JG001179.

Costa, M. H., A. Botta, and J. A. Cardille. 2003. “Effects of large-scale changes in land cover on the discharge of the Tocantins River, Southeastern Amazonia.” *J. Hydrol.*, 283 (1–4): 206–217. Elsevier. https://doi.org/10.1016/S0022-1694(03)00267-1.

Costa, M. H., and G. F. Pires. 2010. “Effects of Amazon and Central Brazil deforestation scenarios on the duration of the dry season in the arc of deforestation.” *Int. J. Climatol.*, 30 (13): 1970–1979. https://doi.org/10.1002/joc.2048.

Dalmagro, H. J., M. J. Lathuillière, I. Hawthorne, D. D. Morais, O. B. Pinto, E. G. Couto, and M. S. Johnson. 2018. “Carbon biogeochemistry of a flooded Pantanal forest over three annual flood cycles.” *Biogeochemistry*, 139 (1): 1–18. Springer

International Publishing. https://doi.org/10.1007/s10533-018-0450-1.

Dalmagro, H. J., P. H. Zanella de Arruda, G. L. Vourlitis, M. J. Lathuillière, J. de S. Nogueira, E. G. Couto, and M. S. Johnson. 2019. "Radiative forcing of methane fluxes offsets net carbon dioxide uptake for a tropical flooded forest." *Glob. Chang. Biol.*, 25 (6): 1967–1981. Blackwell Publishing Ltd. https://doi.org/10.1111/gcb.14615.

Davidson, E. A., A. C. de Araújo, P. Artaxo, J. K. Balch, I. F. Brown, M. M. C. Bustamante, E. A. Davidson, A. C. De Arau, M. T. Coe, R. S. Defries, M. Keller, M. Longo, J. W. Munger, and W. Schroeder. 2012. "The Amazon basin in transition." *Nature*, 481: 321–329. https://doi.org/10.1038/nature10717.

Davidson, E. A., and P. Artaxo. 2004. "Globally significant changes in biological processes of the Amazon Basin : results of the Large-scale Biosphere – Atmosphere Experiment." *Glob. Chang. Biol.*, 519–529. https://doi.org/10.1111/j.1529-8817.2003.00779.x.

Dias, L. C. P., M. N. Macedo, M. H. Costa, M. T. Coe, and C. Neill. 2015. "Effects of land cover change on evapotranspiration and streamflow of small catchments in the Upper Xingu River Basin, Central Brazil." *J. Hydrol. Reg. Stud.*, 4 (PB): 108–122. Elsevier. https://doi.org/10.1016/j.ejrh.2015.05.010.

Diaz, M. B., D. R. Roberti, J. V. Carneiro, V. de A. Souza, and O. L. L. de Moraes. 2019. "Dynamics of the superficial fluxes over a flooded rice paddy in southern Brazil." *Agric. For. Meteorol.*, 276–277. Elsevier B.V. https://doi.org/10.1016/j.agrformet.2019.107650.

Duan, S. B., Z. L. Li, H. Li, F. M. Göttsche, H. Wu, W. Zhao, P. Leng, X. Zhang, and C. Coll. 2019. "Validation of Collection 6 MODIS land surface temperature product using in situ measurements." *Remote Sens. Environ.*, 225: 16–29. Elsevier Inc. https://doi.org/10.1016/j.rse.2019.02.020.

Duman, T., C. W. Huang, and M. E. Litvak. 2021. "Recent land cover changes in the Southwestern US lead to an increase in surface temperature." *Agric. For. Meteorol.*, 297. Elsevier B.V. https://doi.org/10.1016/j.agrformet.2020.108246.

Elnashar, A., L. Wang, B. Wu, W. Zhu, and H. Zeng. 2021. "Synthesis of global actual evapotranspiration from 1982 to 2019." *Earth Syst. Sci. Data*, 13 (2): 447–480.

Copernicus GmbH. https://doi.org/10.5194/essd-13-447-2021.

Van Der Ent, R. J., H. H. G. Savenije, B. Schaefli, and S. C. Steele-Dunne. 2010. "Origin and fate of atmospheric moisture over continents." *Water Resour. Res.*, 46 (9). https://doi.org/10.1029/2010WR009127.

Ershadi, A., M. F. McCabe, J. P. Evans, and E. F. Wood. 2015. "Impact of model structure and parameterization on Penman-Monteith type evaporation models." *J. Hydrol.*, 525: 521–535. Elsevier. https://doi.org/10.1016/j.jhydrol.2015.04.008.

Fassoni-Andrade, A. C., A. S. Fleischmann, F. Papa, R. C. D. de Paiva, S. Wongchuig, J. M. Melack, A. A. Moreira, A. Paris, A. L. Ruhoff, C. Barbosa, D. A. Maciel, E. Novo, F. Durand, F. Frappart, F. Aires, G. M. Abrahão, J. Ferreira-Ferreira, J. C. Espinoza, L. Laipelt, M. H. Costa, R. Espinoza-Villar, S. Calmant, and V. Pellet. 2021. "Amazon Hydrology From Space: Scientific Advances and Future Challenges." *Rev. Geophys.* John Wiley and Sons Inc.

Filho, T. K., E. Delgado, P. Roberto, and S. De Rezende. 2005. "Regiões pluviometricamente homogêneas no Brasil." *Pesqui. Agropecu. Bras.*, 40 (1): 311–322.

Fisher, J. B., Y. S. Malhi, D. Bonal, H. R. da Rocha, A. C. de Araújo, M. Gamo, M. L. Goulden, T. Hirano, A. R. Huete, H. Kondo, T. Kumagai, H. W. Loescher, S. D. Miller, A. D. Nobre, Y. Nouvellon, S. F. Oberbauer, S. Panuthai, O. Roupsard, S. R. Saleska, K. Tanaka, N. Tanaka, K. P. Tu, and C. von Randow. 2009. "The land – atmosphere water flux in the tropics." *Glob. Chang. Biol.*, 15 (October 2008): 2694–2714. https://doi.org/10.1111/j.1365-2486.2008.01813.x.

Fisher, J. B., F. S. Melton, E. M. Middleton, C. R. Hain, M. C. Anderson, R. G. Allen, K. P. Tu, D. G. Miralles, J. Perret, J. P. Lagouarde, D. E. Waliser, A. J. Purdy, A. French, D. Schimel, J. S. Famiglietti, G. Stephens, and E. F. Wood. 2017. "The future of evapotranspiration: Global requirements for ecosystem functioning, carbon and climate feedbacks, agricultural management, and water resources." *Water Resour. Res.*, 2618–2626. https://doi.org/10.1002/ 2016WR020175.

Fisher, J. B., K. P. Tu, and D. Baldocchi. 2008. "Global estimates of the land – atmosphere water flux based on monthly AVHRR and ISLSCP-II data , validated at 16 FLUXNET sites." *Remote Sens. Environ.*, 112: 901–919.

https://doi.org/10.1016/j.rse.2007.06.025.

Frappart, F., F. Papa, Y. Malbeteau, J. G. León, G. Ramillien, C. Prigent, L. Seoane, F. Seyler, and S. Calmant. 2015. “Surface Freshwater Storage Variations in the Orinoco Floodplains Using Multi-Satellite Observations.” *Remote Sens.*, 7 (December 2014): 89–110. https://doi.org/10.3390/rs70100089.

Fredlund, D. G., H. Rahardjo, and M. D. Fredlund. 2012. *Unsaturated soil mechanics in engineering practice*. Hoboken, New Jersey, USA: John Willey & Sons.

Friedl, M. A., D. Sulla-menashe, B. Tan, A. Schneider, N. Ramankutty, A. Sibley, and X. Huang. 2010. “Remote Sensing of Environment MODIS Collection 5 global land cover : Algorithm re fi nements and characterization of new datasets.” *Remote Sens. Environ.*, 114 (1): 168–182. Elsevier Inc. https://doi.org/10.1016/j.rse.2009.08.016.

Funk, C., P. Peterson, M. Landsfeld, D. Pedreros, J. Verdin, S. Shukla, G. Husak, J. Rowland, L. Harrison, A. Hoell, and J. Michaelsen. 2015. “The climate hazards infrared precipitation with stations - A new environmental record for monitoring extremes.” *Sci. Data*, 2: 1–21. https://doi.org/10.1038/sdata.2015.66.

Gallay, M., J. M. Martinez, A. Mora, B. Castellano, S. Yépez, G. Cochonneau, J. A. Alfonso, J. M. Carrera, J. L. López, and A. Laraque. 2019. “Assessing Orinoco river sediment discharge trend using MODIS satellite images.” *J. South Am. Earth Sci.*, 91 (December 2018): 320–331. Elsevier. https://doi.org/10.1016/j.jsames.2019.01.010.

Gan, M. A., V. E. Kousky, and C. F. Ropelewski. 2004. “The South America Monsoon circulation and its relationship to rainfall over west-central Brazil.” *J. Clim.*, 17 (1): 47–66. https://doi.org/10.1175/1520-0442(2004)017<0047:TSAMCA>2.0.CO;2.

Gan, R., Y. Zhang, H. Shi, Y. Yang, D. Eamus, L. Cheng, F. H. S. Chiew, and Q. Yu. 2018. “Use of satellite leaf area index estimating evapotranspiration and gross assimilation for Australian ecosystems.” *Ecohydrology*, 11 (5). John Wiley and Sons Ltd. https://doi.org/10.1002/eco.1974.

Gao, H., Q. Tang, C. R. Ferguson, E. F. Wood, and D. P. Lettenmaier. 2010. “Estimating the water budget of major US river basins via remote sensing.” *Int. J.*

Remote Sens., (August 2013): 37–41. https://doi.org/10.1080/01431161.2010.483488.

García, M., I. Sandholt, P. Ceccato, M. Ridler, E. Mougin, L. Kergoat, L. Morillas, F. Timouk, R. Fensholt, and F. Domingo. 2013. "Remote Sensing of Environment Actual evapotranspiration in drylands derived from in-situ and satellite data : Assessing biophysical constraints." *Remote Sens. Environ.*, 131: 103–118. Elsevier Inc. https://doi.org/10.1016/j.rse.2012.12.016.

Gatti, L. V., L. S. Basso, J. B. Miller, M. Gloor, L. Gatti Domingues, H. L. G. Cassol, G. Tejada, L. E. O. C. Aragão, C. Nobre, W. Peters, L. Marani, E. Arai, A. H. Sanches, S. M. Corrêa, L. Anderson, C. Von Randow, C. S. C. Correia, S. P. Crispim, and R. A. L. Neves. 2021. "Amazonia as a carbon source linked to deforestation and climate change." *Nature*, 595 (7867): 388–393. Springer US. https://doi.org/10.1038/s41586-021-03629-6.

Getirana, A. C. V., E. Dutra, M. Guimberteau, J. Kam, H.-Y. Li, B. Decharme, Z. Zhang, A. Ducharne, A. Boone, G. Balsamo, M. Rodell, A. M. Toure, Y. Xue, C. D. Peters-Lidard, S. V. Kumar, K. R. Arsenault, G. Drapeau, L. Ruby Leung, J. Ronchail, and J. Sheffield. 2014. "Water Balance in the Amazon Basin from a Land Surface Model Ensemble." *J. Hydrometeorol.*, 2586–2615. https://doi.org/10.1175/JHM-D-14-0068.1.

Gomis-Cebolla, J., J. C. Jimenez, J. A. Sobrino, C. Corbari, and M. Mancini. 2019. "Intercomparison of remote-sensing based evapotranspiration algorithms over amazonian forests." *Int. J. Appl. Earth Obs. Geoinf.*, 80: 280–294. Elsevier B.V. https://doi.org/10.1016/j.jag.2019.04.009.

Gonçalves de Gonçalves, L. G., S. R. Saleska, I. Baker, N. Restrepo-coupe, M. Nobre, B. Poulter, H. Verbeeck, J. B. Fisher, M. A. Arain, P. Arkin, B. P. Cestaro, B. O. D. Christoffersen, D. Galbraith, X. Guan, B. J. J. M. Van Den Hurk, K. Ichii, H. M. Acioli, A. K. Jain, N. Levine, C. Lu, G. Miguez-macho, D. R. Roberti, A. Sahoo, K. Sakaguchi, K. Schaefer, M. Shi, W. J. Shuttleworth, H. Tian, Z. Yang, and X. Zeng. 2013. "Overview of the Large-Scale Biosphere – Atmosphere Experiment in Amazonia Data Model Intercomparison Project (LBA-DMIP)." *Agric. For. Meteorol.*, 183: 111–127. https://doi.org/10.1016/j.agrformet.2013.04.030.

Goulden, M. L., S. D. Miller, H. R. da Rocha, M. C. Menton, H. C. de Freitas, A. M. E Silva Figueira, and C. A. D. De Sousa. 2004. “Diel and Seasonal Patterns of Tropical Forest CO2 Exchange.” *Ecol. Appl.*, 14 (4): 42–54.

Griffis, T., D. Roman, J. Wood, J. Deventer, L. Fachin, J. Rengifo, D. Del Castillo, R. Kolka, R. Chimner, J. del Aguila, C. Wayson, K. Hergoualc, J. M. Baker, and D. Ricciuto. 2020. “Hydrometeorological sensitivities of net ecosystem carbon dioxide 1 and methane exchange of an Amazonian palm swamp peatland.” *Agric. For. Meteorol.*

Guimberteau, M., J. Ronchail, J. C. Espinoza, M. Lengaigne, B. Sultan, J. Polcher, G. Drapeau, J.-L. Guyot, A. Ducharne, and P. Ciais. 2013. “Future changes in precipitation and impacts on extreme streamflow over Amazonian sub-basins.” *Environ. Res. Lett.*, 8. https://doi.org/10.1088/1748-9326/8/1/014035.

Hamilton, S. K., S. J. Sippel, and J. M. Melack. 1996. “Inundation patterns in the Pantanal wetland of South America determined from passive microwave remote sensing.” *Arch. Hydrobiol.*, 1 (137): 1–23.

Hasler, N., and R. Avissar. 2007. “What Controls Evapotranspiration in the Amazon Basin ?” *J. Hydrometeorol.*, 380–395. https://doi.org/10.1175/JHM587.1.

Heerspink, B. P., A. D. Kendall, M. T. Coe, and D. W. Hyndman. 2020. “Trends in streamflow, evapotranspiration, and groundwater storage across the Amazon Basin linked to changing precipitation and land cover.” *J. Hydrol. Reg. Stud.*, 32. Elsevier B.V. https://doi.org/10.1016/j.ejrh.2020.100755.

Ho, J. T., J. R. Thompson, and C. Brierley. 2015. “Projections of hydrology in the Tocantins-Araguaia Basin, Brazil: uncertainty assessment using the CMIP5 ensemble.” *Hydrol. Sci. J.*, 61 (3): 551–567. https://doi.org/10.1080/02626667.2015.1057513.

Huffman, G. J., R. F. Adler, D. T. Bolvin, G. Gu, E. J. Nelkin, K. P. Bowman, Y. Hong, E. F. Stocker, and D. B. Wolff. 2007. “The TRMM Multisatellite Precipitation Analysis (TMPA): Quasi-Global , Multiyear , Combined-Sensor Precipitation Estimates at Fine Scales.” *J. Hydrometeorol.*, 8: 38–56. https://doi.org/10.1175/JHM560.1.

Huffman, G. J., R. F. Adler, D. T. Bolvin, and E. J. Nelkin. 2010. “The TRMM Multi-

satellite Precipitation Analysis (TMPA).” *Satell. Rainfall Appl. Surf. Hydrol.*, M. Gebremichael and F. Hossain, eds., 3–22. Springer Netherlands.

van Huissteden, J. 2020. *Thawing Permafrost: Permafrost Carbon in a Warming Arctic*.

Hunke, P., E. N. Mueller, B. Schröder, and P. Zeilhofer. 2015. “The Brazilian Cerrado: Assessment of water and soil degradation in catchments under intensive agricultural use.” *Ecohydrology*, 8 (6): 1154–1180. John Wiley and Sons Ltd. https://doi.org/10.1002/eco.1573.

Hutyra, L. R., J. W. Munger, S. R. Saleska, E. Gottlieb, B. C. Daube, A. L. Dunn, D. F. Amaral, P. B. De Camargo, and S. C. Wofsy. 2007. “Seasonal controls on the exchange of carbon and water in an Amazonian rain forest.” *J. Geophys. Res.*, 112: 1–16. https://doi.org/10.1029/2006JG000365.

IBGE. 2004. “Mapa de Biomas do Brasil, primeira aproximação.” Rio de Janeiro, Brazil: Instituto Brasileiro de Geografia e Estatística.

Jarvis, P. G. 1976. “The interpretation of the variations in leaf water potential and stomatal conductance found in canopies in the field.” *Philos. Trans. R. Soc. London. B, Biol. Sci.*, 273 (927): 593–610. The Royal Society. https://doi.org/10.1098/rstb.1976.0035.

Jarvis, P. G., and K. G. McNaughton. 1986. “Stomatal Control of Transpiration: Scaling Up from Leaf to Region.” *Adv. Ecol. Res.*, 15.

Juárez, R. I. N. 2004. “Variabilidade climática regional e controle da vegetação no sudeste: um estudo de observações sobre cerrado e cana-de-açúcar e modelagem numérica da atmosfera.” Universidade de São Paulo.

Jung, M., M. Reichstein, P. Ciais, S. I. Seneviratne, J. Sheffield, M. L. Goulden, G. B. Bonan, A. Cescatti, J. Chen, R. De Jeu, A. J. Dolman, W. Eugster, D. Gerten, D. Gianelle, N. Gobron, J. Heinke, J. Kimball, B. E. Law, L. Montagnani, Q. Mu, and B. Mueller. 2010. “Recent decline in the global land evapotranspiration trend due to limited moisture supply.” *Nature*, 467: 951–954. https://doi.org/10.1038/nature09396.

Katsoulas, N., and C. Kittas. 2011. “Greenhouse Crop Transpiration Modelling.” *Evapotranspiration - From Meas. to Agric. andEnvironmental Appl.*, 1–410.

Rijeka, Croatia : InTech Europe.

De Kauwe, M. G., B. E. Medlyn, J. Knauer, and C. A. Williams. 2017. “Ideas and perspectives: How coupled is the vegetation to the boundary layer?” *Biogeosciences*, 14 (19): 4435–4453. Copernicus GmbH. https://doi.org/10.5194/bg-14-4435-2017.

Keller, M., M. M. C. Bustamante, J. Gash, and P. Silva Dias. 2009. *Amazonia and Global Change*. Washington, DC: American Geophysical Union (AGU).

Keller, M., A. Lencar, G. R. P. A. Sner, B. O. B. Raswell, M. E. B. Ustamante, S. C. M. Iller, D. A. M. Arkewitz, and A. N. D. N. Obre. 2004. “Ecologinal Research in the Large-Scale Biosphere-Atmosphere Experiment in Amazonia: Early Results.” *Ecol. Appl.*, 14 (May 2003): 3–16.

Khan, M. S., U. W. Liaqat, J. Baik, and M. Choi. 2018. “Stand-alone uncertainty characterization of GLEAM , GLDAS and MOD16 evapotranspiration products using an extended triple collocation approach.” *Agric. For. Meteorol.*, 252 (December 2017): 256–268.

Khand, K., I. Numata, J. Kjaersgaard, and G. L. Vourlitis. 2017. “Dry season evapotranspiration dynamics over human-impacted landscapes in the southern Amazon using the landsat-based METRIC model.” *Remote Sens.*, 9 (7). MDPI AG. https://doi.org/10.3390/rs9070706.

Kim, H. W., K. Hwang, Q. Mu, S. O. Lee, and M. Choi. 2012. “Validation of MODIS 16 Global Terrestrial Evapotranspiration Products in Various Climates and Land Cover Types in Asia.” *KSCE J. Civ. Eng.*, 16: 229–238. https://doi.org/10.1007/s12205-012-0006-1.

Kustas, W. P., and J. M. Norman. 2000. “A Two-Source Energy Balance Approach Using Directional Radiometric Temperature Observations for Sparse Canopy Covered Surfaces.” *Agron. J.*, 92: 847–854.

Kustas, W. P., D. I. Stannard, and K. J. Allwine ’. 1996. “Variability in surface energy flux partitioning during Washita ’92: Resulting effects on Penman-Monteith and Priestley-Taylor parameters.” *Agric. For. Meteorol.*, 82: 171–193.

Laipelt, L., A. L. Ruhoff, A. S. Fleischmann, R. H. Bloedow Kayser, E. de M. Kich, H.

R. da Rocha, and C. M. Usher Neale. 2020. “Assessment of an automated calibration of the SEBAL Algorithm to estimate dry-season surface-energy partitioning in a Forest-Savanna Transition in Brazil.” *Remote Sens.*, 12 (7). MDPI AG. https://doi.org/10.3390/rs12071108.

Landerer, F. W., and S. C. Swenson. 2012. “Accuracy of scaled GRACE terrestrial water storage estimates.” *Water Resour. Res.*, 48 (September 2011): 1–11. https://doi.org/10.1029/2011WR011453.

Leuning, R. 1995. “A critical appraisal of a combined stomatal-photosynthesis model for C3 plants.” *Plant, Cell Environ.*, 18: 339–355.

Leuning, R., Y. Zhang, A. Rajaud, H. A. Cleugh, and K. Tu. 2008. “A simple surface conductance model to estimate regional evaporation using MODIS leaf area index and the Penman-Monteith equation.” *Water Resour. Res.*, 44 (10). American Geophysical Union. https://doi.org/10.1029/2007WR006562.

Lewis, S. L., P. M. Brando, O. L. Phillips, G. M. F. van der Heijden, and D. Nepstad. 2011. “The 2010 Amazon Drought.” *Science (80-.).*, 331: 554–554. https://doi.org/10.1126/science.1146961.

Liu, W., L. Wang, J. Zhou, Y. Li, F. Sun, G. Fu, and X. Li. 2016. “A worldwide evaluation of basin-scale evapotranspiration estimates against the water balance method.” *J. Hydrol.*, 538: 82–95. Elsevier B.V. https://doi.org/10.1016/j.jhydrol.2016.04.006.

Liu, Y. Y., R. A. M. de Jeu, M. F. McCabe, J. P. Evans, and A. I. J. M. van Dijk. 2011. “Global long-term passive microwave satellite-based retrievals of vegetation optical depth.” *Geophys. Res. Lett.*, 38. https://doi.org/10.1029/2011GL048684.

Loarie, S. R., D. B. Lobell, G. P. Asner, Q. Mu, and C. B. Field. 2011. “Direct impacts on local climate of sugar-cane expansion in Brazil.” *Nat. Clim. Chang.*, 1 (2): 105–109. https://doi.org/10.1038/nclimate1067.

Long, D., L. Longuevergne, and B. R. Scanlon. 2014. “Uncertainty in evapotranspiration from land surface modeling, remote sensing, and GRACE satellites.” *Water Resour. Res.*, 50 (7): 5510–5531. https://doi.org/10.1002/2013WR014910.Received.

Maeda, E. E., X. Ma, F. H. Wagner, H. Kim, T. Oki, D. Eamus, and A. Huete. 2017. "Evapotranspiration seasonality across the Amazon Basin." *Earth Syst. Dyn.*, 8 (2): 439–454. Copernicus GmbH. https://doi.org/10.5194/esd-8-439-2017.

Mao, J., W. Fu, X. Shi, D. M. Ricciuto, J. B. Fisher, R. E. Dickinson, Y. Wei, W. Shem, S. Piao, K. Wang, C. R. Schwalm, H. Tian, M. Mu, A. Arain, P. Ciais, R. Cook, Y. Dai, D. Hayes, F. M. Hoffman, M. Huang, S. Huang, D. N. Huntzinger, A. Ito, A. Jain, A. W. King, H. Lei, C. Lu, A. M. Michalak, N. Parazoo, C. Peng, S. Peng, B. Poulter, K. Schaefer, E. Jafarov, P. E. Thornton, W. Wang, N. Zeng, Z. Zeng, F. Zhao, Q. Zhu, and Z. Zhu. 2015. "Disentangling climatic and anthropogenic controls on global terrestrial evapotranspiration trends." *Environ. Res. Lett.*, 10 (9). Institute of Physics Publishing. https://doi.org/10.1088/1748-9326/10/9/094008.

MapBiomas. 2021. "Mapbiomas Brasil." *Collect. 6*. https://mapbiomas.org/.

Marengo, J. A. 2014. "O futuro clima do Brasil." *Rev. USP*, 8. São Paulo.

Marengo, J. A., C. A. Nobre, J. Tomasella, M. D. Oyama, G. S. de Oliveira, R. de Oliveira, H. Camargo, L. M. Alves, and I. F. Brown. 2008. "The Drought of Amazonia in 2005." *Am. Meteorol. Soc.*, 495–516. https://doi.org/10.1175/2007JCLI1600.1.

Marengo, J. A., J. Tomasella, W. R. Soares, L. M. Alves, and C. A. Nobre. 2012. "Extreme climatic events in the Amazon basin Climatological and hydrological context of recent floods." *Theor. Appl. Climatol.*, 73–85. https://doi.org/10.1007/s00704-011-0465-1.

Marengo, J. A., R. R. Torres, and L. M. Alves. 2016. "Drought in Northeast Brazil—past, present, and future." *Theor. Appl. Climatol.*, 129 (3–4): 1189–1200. Springer-Verlag Wien. https://doi.org/10.1007/s00704-016-1840-8.

Mariano, D. A., C. A. C. do. Santos, B. D. Wardlow, M. C. Anderson, A. V. Schiltmeyer, T. Tadesse, and M. D. Svoboda. 2018. "Use of remote sensing indicators to assess effects of drought and human-induced land degradation on ecosystem health in Northeastern Brazil." *Remote Sens. Environ.*, 213: 129–143. Elsevier Inc. https://doi.org/10.1016/j.rse.2018.04.048.

Marques, T. V., K. Mendes, P. Mutti, S. Medeiros, L. Silva, A. M. Perez-Marin, S. Campos, P. S. Lúcio, K. Lima, J. dos Reis, T. M. Ramos, D. F. da Silva, C. P.

Oliveira, G. B. Costa, A. C. D. Antonino, R. S. C. Menezes, C. M. Santos e Silva, and B. G. Bezerra. 2020. “Environmental and biophysical controls of evapotranspiration from Seasonally Dry Tropical Forests (Caatinga) in the Brazilian Semiarid.” *Agric. For. Meteorol.*, 287. Elsevier B.V. https://doi.org/10.1016/j.agrformet.2020.107957.

Martens, B., D. G. Miralles, H. Lievens, R. Van Der Schalie, R. A. M. de Jeu, D. Fernández-Prieto, H. E. Beck, W. A. Dorigo, and N. E. C. Verhoest. 2017. “GLEAM v3: Satellite-based land evaporation and root-zone soil moisture.” *Geosci. Model Dev.*, 10 (5): 1903–1925. Copernicus GmbH. https://doi.org/10.5194/gmd-10-1903-2017.

Martens, B., D. Miralles, H. Lievens, D. Fernández-prieto, and N. E. C. Verhoest. 2016. “Improving terrestrial evaporation estimates over continental Australia through assimilation of SMOS soil moisture.” *Int. J. Appl. Earth Obs. Geoinf.*, 48: 146–162. Elsevier B.V. https://doi.org/10.1016/j.jag.2015.09.012.

Martinez, J. A., and F. Dominguez. 2014. “Sources of Atmospheric Moisture for the La Plata River Basin.” *Am. Meteorol. Soc.*, 6737–6753. https://doi.org/10.1175/JCLI-D-14-00022.s1.

McCabe, M. F., A. Ershadi, C. Jimenez, D. G. Miralles, D. Michel, and E. F. Wood. 2016. “The GEWEX LandFlux project: Evaluation of model evaporation using tower-based and globally gridded forcing data.” *Geosci. Model Dev.*, 9 (1): 283–305. Copernicus GmbH. https://doi.org/10.5194/gmd-9-283-2016.

McCabe, M. F., M. Rodell, D. E. Alsdorf, D. G. Miralles, R. Uijlenhoet, W. Wagner, A. Lucieer, R. Houborg, N. E. C. Verhoest, T. E. Franz, J. Shi, H. Gao, and E. F. Wood. 2017. “The future of Earth observation in hydrology.” *Hydrol. Earth Syst. Sci.*, 21 (7): 3879–3914. Copernicus GmbH. https://doi.org/10.5194/hess-21-3879-2017.

Melo, D. C. D., J. A. A. Anache, V. P. Borges, D. G. Miralles, B. Martens, J. B. Fisher, R. L. B. Nóbrega, A. Moreno, O. M. R. Cabral, T. R. Rodrigues, B. G. Bezerra, C. M. S. Silva, A. A. M. Neto, M. S. B. Moura, T. V. Marques, S. Campos, J. S. Nogueira, R. Rosolem, R. M. S. Souza, A. C. D. Antonino, D. Holl, M. Galleguillos, J. F. Perez-Quezada, A. Verhoef, L. Kutzbach, J. R. S. Lima, E. S.

Souza, M. I. Gassman, C. F. Perez, N. Tonti, G. Posse, D. Rains, P. T. S. Oliveira, and E. Wendland. 2021. “Are Remote Sensing Evapotranspiration Models Reliable Across South American Ecoregions?” *Water Resour. Res.*, 57 (11). John Wiley and Sons Inc. https://doi.org/10.1029/2020WR028752.

Melton, F. S., J. Huntington, R. Grimm, J. Herring, M. Hall, D. Rollison, T. Erickson, R. G. Allen, M. C. Anderson, J. B. Fisher, A. Kilic, G. B. Senay, J. Volk, C. Hain, L. Johnson, A. L. Ruhoff, P. Blankenau, M. Bromley, W. Carrara, B. Daudert, C. Doherty, C. Dunkerly, M. Friedrichs, A. Guzman, G. Halverson, J. Hansen, J. Harding, Y. Kang, D. Ketchum, B. Minor, C. Morton, S. Ortega-Salazar, T. Ott, M. Ozdogan, P. M. ReVelle, M. Schull, C. Wang, Y. Yang, and R. G. Anderson. 2021. “OpenET: Filling a Critical Data Gap in Water Management for the Western United States.” *J. Am. Water Resour. Assoc.*, 1–24.

Menezes, R., V. Sampaio, and Pérez-Marin. 2012. “Biogeochemical cycling in terrestrial ecosystems of the Caatinga Biome.” *Braz. J. Biol*, 72 (3): 643–653.

Michel, D., C. Jiménez, D. G. Miralles, M. Jung, M. Hirschi, A. Ershadi, B. Martens, M. F. Mccabe, and C. D. Michel. 2016. “The WACMOS-ET project – Part 1 : Tower-scale evaluation of four remote-sensing-based evapotranspiration algorithms.” *Hydrol. Earth Syst. Sci.*, 803–822. https://doi.org/10.5194/hess-20-803-2016.

Miralles, D. G., M. J. Van Den Berg, J. H. Gash, R. M. Parinussa, R. A. M. De Jeu, H. E. Beck, T. R. H. Holmes, C. Jiménez, N. E. C. Verhoest, W. A. Dorigo, A. J. Teuling, and A. J. Dolman. 2014. “El Niño – La Niña cycle and recent trends in continental evaporation.” *Nat. Clim. Chang.*, 4 (1): 1–5. Nature Publishing Group. https://doi.org/10.1038/nclimate2068.

Miralles, D. G., T. R. H. Holmes, R. A. M. de Jeu, J. H. Gash, A. G. C. A. Meesters, and A. J. Dolman. 2011a. “Global land-surface evaporation estimated from satellite-based observations.” *Hydrol. Earth Syst. Sci.*, 15 (2): 453–469. https://doi.org/10.5194/hess-15-453-2011.

Miralles, D. G., R. A. M. De Jeu, J. H. Gash, T. R. H. Holmes, and A. J. Dolman. 2011b. “Magnitude and variability of land evaporation and its components at the global scale.” *Hydrol. Earth Syst. Sci*, 15: 967–981. https://doi.org/10.5194/hess-

15-967-2011.

Miralles, D. G., C. Jiménez, M. Jung, D. Michel, A. Ershadi, M. F. Mccabe, M. Hirschi, and B. Martens. 2016. “The WACMOS-ET project – Part 2 : Evaluation of.” *Hydrol. Earth Syst. Sci.*, 20: 823–842. https://doi.org/10.5194/hess-20-823-2016.

MMA. 2011. “Levantamento da ictiofauna, caracterização genética e da fauna parasitária da bacia hidrográfica do Rio Tapajós.” Brasília, Brazil: Ministério do Meio Ambiente - Instituto Chico Mendes de Conservação e Biodiversidade.

Modernel, P., W. A. H. Rossing, M. Corbeels, S. Dogliotti, V. Picasso, and P. Tittonell. 2016. “Land use change and ecosystem service provision in Pampas and Campos grasslands of southern South America.” *Environ. Res. Lett.*, 11 (11). Institute of Physics Publishing. https://doi.org/10.1088/1748-9326/11/11/113002.

Mohor, G. S., D. A. Rodriguez, J. Tomasella, and J. L. Siqueira Júnior. 2015. “Exploratory analyses for the assessment of climate change impacts on the energy production in an Amazon run-of-river hydropower plant.” *J. Hydrol. Reg. Stud.*, 4 (PB): 41–59. Elsevier. https://doi.org/10.1016/j.ejrh.2015.04.003.

Monteith, J. L. 1965. *Evaporation and environment. In Symposia of the society for experimental biology*. Cambridge: Cambridge University Press (CUP).

Monteith, J. L. 1995. *Accommodation between transpiring vegetation and the convective boundary layer*. *J. Hydrol. ELSEVIER*.

Monteith, J. L., and M. H. Unsworth. 1990. *Principles of Environmental Physics*. London: Edward Arnold.

Moore, C., and G. Fisch. 1986. “Estimating Heat Storage in Amazonian Tropical Forest.” *Agric. For. Meteorol.*, 38: 147–169.

Moreira, A. A., A. L. Ruhoff, D. R. Roberti, V. de A. Souza, H. R. da Rocha, and R. C. D. de Paiva. 2019. “Assessment of terrestrial water balance using remote sensing data in South America.” *J. Hydrol.*, 575 (April): 131–147. https://doi.org/10.1016/j.jhydrol.2019.05.021.

Mu, Q., F. A. Heinsch, M. Zhao, and S. W. Running. 2007. “Development of a global evapotranspiration algorithm based on MODIS and global meteorology data.” *Remote Sens. Environ.*, 111 (4): 519–536.

https://doi.org/10.1016/j.rse.2007.04.015.

Mu, Q., M. Zhao, and S. W. Running. 2011. “Improvements to a MODIS global terrestrial evapotranspiration algorithm.” *Remote Sens. Environ.*, 115 (8): 1781–1800. https://doi.org/10.1016/j.rse.2011.02.019.

Do Nascimento, M. G., D. L. Herdies, and D. O. De Souza. 2016. “The South American Water Balance : The Influence of Low-Level Jets.” *Am. Meteorol. Soc.*, (2014): 1429–1450. https://doi.org/10.1175/JCLI-D-15-0065.1.

Nobre, C. A., G. Sampaio, L. S. Borma, J. C. Castilla-rubio, J. S. Silva, and M. Cardoso. 2016. “Land-use and climate change risks in the Amazon and the need of a novel sustainable development paradigm.” *Proc. Natl. Acad. Sci. U. S. A.*, 113 (39): 10759–10768. https://doi.org/10.1073/pnas.1605516113.

Nóbrega, M. T., W. Collischonn, C. E. M. Tucci, and A. R. Paz. 2011. “Uncertainty in climate change impacts on water resources in the Rio Grande Basin, Brazil.” *Hydrol. Earth Syst. Sci.*, 15 (2): 585–595. https://doi.org/10.5194/hess-15-585-2011.

Ogée, J., E. Lamaud, Y. Brunet, P. Berbigier, and J. M. Bonnefond. 2001. “A long-term study of soil heat flux under a forest canopy.” *Agric. For. Meteorol.*, 106: 173–186.

de Oliveira, G., M. B. Araújo, T. F. Rangel, D. Alagador, and J. A. F. Diniz-Filho. 2012. “Conserving the Brazilian semiarid (Caatinga) biome under climate change.” *Biodivers. Conserv.*, 21 (11): 2913–2926. https://doi.org/10.1007/s10531-012-0346-7.

de Oliveira, G., N. A. Brunsell, E. C. Moraes, Y. E. Shimabukuro, T. V. dos Santos, C. von Randow, R. G. de Aguiar, and L. E. O. C. Aragao. 2019. “Effects of land-cover changes on the partitioning of surface energy and water fluxes in Amazonia using high-resolution satellite imagery.” *Ecohydrology*, 12 (6). John Wiley and Sons Ltd. https://doi.org/10.1002/eco.2126.

de Oliveira, G., N. A. Brunsell, E. C. Moraes, E. Yosio, G. Bertani, T. V Santos, L. E. O. C. Aragao, G. De Oliveira, N. A. Brunsell, E. C. Moraes, and E. Yosio. 2017. “Evaluation of MODIS-based estimates of water-use efficiency in Amazonia.” *Int. J. Remote Sens.*, 38 (19): 5291–5309. Taylor & Francis.

https://doi.org/10.1080/01431161.2017.1339924.

de Oliveira, G., J. M. Chen, G. A. V. Mataveli, M. E. D. Chaves, J. Rao, M. Sternberg, T. V. Dos Santos, and C. A. C. Dos Santos. 2020. "Evapotranspiration and precipitation over pasture and soybean areas in the Xingu River basin, an expanding amazonian agricultural frontier." *Agronomy*, 10 (8). MDPI AG. https://doi.org/10.3390/agronomy10081112.

de Oliveira, M. B. L., C. von Randow, A. O. Manzi, R. C. dos S. Alvalá, L. D. de A. Sá, M. de M. V. B. R. Leitão, and A. de Souza. 2006. "Fluxos Turbulentos de energia sobre o Pantanal Sul Mato-Grossense." *Rev. Bras. Meteorol.*, 21 (3b): 159–165.

de Oliveira, M. L., C. A. C. dos Santos, G. de Oliveira, A. M. Perez-Marin, and C. A. G. Santos. 2021. "Effects of human-induced land degradation on water and carbon fluxes in two different Brazilian dryland soil covers." *Sci. Total Environ.*, 792: 148458. Elsevier BV. https://doi.org/10.1016/j.scitotenv.2021.148458.

Oliveira, P. T. S., M. A. Nearing, M. S. Moran, D. C. Goodrich, E. Wendland, and H. V. Gupta. 2014. "Trends in water balance components across the Brazilian Cerrado." *Water Resour. Res.*, 50 (9): 7100–7114. Blackwell Publishing Ltd. https://doi.org/10.1002/2013WR015202.

de Oliveira Serrão, E. A., M. T. Silva, T. R. Ferreira, L. C. P. de Ataide, R. T. S. Wanzeler, V. de P. R. da Silva, A. M. M. de Lima, and F. de A. S. de Sousa. 2021. "Large-Scale hydrological modelling of flow and hydropower production, in a Brazilian watershed." *Ecohydrol. Hydrobiol.*, 21 (1): 23–35. https://doi.org/10.1016/j.ecohyd.2020.09.002.

Oliveira, T. E. de, D. S. de Freitas, M. Gianezini, C. F. Ruviaro, D. Zago, T. Z. Mércio, E. A. Dias, V. do N. Lampert, and J. O. J. Barcellos. 2017. "Agricultural land use change in the Brazilian Pampa Biome: The reduction of natural grasslands." *Land use policy*, 63: 394–400. Elsevier Ltd. https://doi.org/10.1016/j.landusepol.2017.02.010.

Olson, D. M., E. Dinerstein, E. Wikramanayake, N. D. Burgess, G. V. N. Powell, E. C. Underwood, J. A. D'Amico, I. Itoua, H. E. Strand, J. C. Morrison, C. J. Loucks, T. F. Allnutt, T. H. Ricketts, Y. Kura, J. F. Lamoreux, W. W. Wettengel, P. Hedao, and K. R. Kassem. 2001. "Terrestrial Ecoregions of the World: A new Map of Life

and Earth.” *Bioscience*, 51 (11): 933–938.

Overbeck, G. E., S. C. Müller, A. Fidelis, J. Pfadenhauer, V. D. Pillar, C. C. Blanco, I. I. Boldrini, R. Both, and E. D. Forneck. 2007. “Brazil’s neglected biome: The South Brazilian Campos.” *Perspect. Plant Ecol. Evol. Syst.*, 9 (2): 101–116. Elsevier GmbH. https://doi.org/10.1016/j.ppees.2007.07.005.

Pan, M., A. K. Sahoo, T. J. Troy, R. K. Vinukollu, J. Sheffield, and wood. 2012. “Multisource Estimation of Long-Term Terrestrial Water Budget for Major Global River Basins.” *Am. Meteorol. Soc.*, 3191–3207. https://doi.org/10.1175/JCLI-D-11-00300.1.

Panday, P. K., M. T. Coe, M. N. Macedo, P. Lefebvre, and A. D. de A. Castanho. 2015. “Deforestation offsets water balance changes due to climate variability in the Xingu River in eastern Amazonia.” *J. Hydrol.*, 523 (February 2015): 822–829. https://doi.org/10.1016/j.jhydrol.2015.02.018.

Paredes-Trejo, F., H. A. Barbosa, J. Giovannettone, T. V. Lakshmi Kumar, M. K. Thakur, C. de O. Buriti, and C. Uzcátegui-Briceño. 2021. “Drought assessment in the São Francisco River Basin using satellite-based and ground-based indices.” *Remote Sens.*, 13 (19). https://doi.org/10.3390/rs13193921.

Paredes-Trejo, F., L. Brito-Castillo, H. Barbosa Alves, and E. Guevara. 2016. “Main features of large-scale oceanic-atmospheric circulation related to strongest droughts during rainy season in Brazilian São Francisco River Basin.” *Int. J. Climatol.*, 36 (12): 4102–4117. https://doi.org/10.1002/joc.4620.

Pasquini, A. I., and P. J. Depetris. 2007. “Discharge trends and flow dynamics of South American rivers draining the southern Atlantic seaboard : An overview.” *J. Hydrol.*, 333: 385–399. https://doi.org/10.1016/j.jhydrol.2006.09.005.

Pastorello, G., C. Trotta, E. Canfora, H. Chu, D. Christianson, Y. W. Cheah, C. Poindexter, J. Chen, A. Elbashandy, M. Humphrey, P. Isaac, D. Polidori, A. Ribeca, C. van Ingen, L. Zhang, B. Amiro, C. Ammann, M. A. Arain, J. Ardö, T. Arkebauer, S. K. Arndt, N. Arriga, M. Aubinet, M. Aurela, D. Baldocchi, A. Barr, E. Beamesderfer, L. B. Marchesini, O. Bergeron, J. Beringer, C. Bernhofer, D. Berveiller, D. Billesbach, T. A. Black, P. D. Blanken, G. Bohrer, J. Boike, P. V. Bolstad, D. Bonal, J. M. Bonnefond, D. R. Bowling, R. Bracho, J. Brodeur, C.

Brümmer, N. Buchmann, B. Burban, S. P. Burns, P. Buysse, P. Cale, M. Cavagna, P. Cellier, S. Chen, I. Chini, T. R. Christensen, J. Cleverly, A. Collalti, C. Consalvo, B. D. Cook, D. Cook, C. Coursolle, E. Cremonese, P. S. Curtis, E. D'Andrea, H. R. da Rocha, X. Dai, K. J. Davis, B. De Cinti, A. de Grandcourt, A. De Ligne, R. C. De Oliveira, N. Delpierre, A. R. Desai, C. M. Di Bella, P. di Tommasi, H. Dolman, F. Domingo, G. Dong, S. Dore, P. Duce, E. Dufrêne, A. Dunn, J. Dušek, D. Eamus, U. Eichelmann, H. A. M. ElKhidir, W. Eugster, C. M. Ewenz, B. Ewers, D. Famulari, S. Fares, I. Feigenwinter, A. Feitz, R. Fensholt, G. Filippa, M. Fischer, J. Frank, M. Galvagno, M. Gharun, D. Gianelle, B. Gielen, B. Gioli, A. Gitelson, I. Goded, M. Goeckede, A. H. Goldstein, C. M. Gough, M. L. Goulden, A. Graf, A. Griebel, C. Gruening, T. Grünwald, A. Hammerle, S. Han, X. Han, B. U. Hansen, C. Hanson, J. Hatakka, Y. He, M. Hehn, B. Heinesch, N. Hinko-Najera, L. Hörtnagl, L. Hutley, A. Ibrom, H. Ikawa, M. Jackowicz-Korczynski, D. Janouš, W. Jans, R. Jassal, S. Jiang, T. Kato, M. Khomik, J. Klatt, A. Knohl, S. Knox, H. Kobayashi, G. Koerber, O. Kolle, Y. Kosugi, A. Kotani, A. Kowalski, B. Kruijt, J. Kurbatova, W. L. Kutsch, H. Kwon, S. Launiainen, T. Laurila, B. Law, R. Leuning, Y. Li, M. Liddell, J. M. Limousin, M. Lion, A. J. Liska, A. Lohila, A. López-Ballesteros, E. López-Blanco, B. Loubet, D. Loustau, A. Lucas-Moffat, J. Lüers, S. Ma, C. Macfarlane, V. Magliulo, R. Maier, I. Mammarella, G. Manca, B. Marcolla, H. A. Margolis, S. Marras, W. Massman, M. Mastepanov, R. Matamala, J. H. Matthes, F. Mazzenga, H. McCaughey, I. McHugh, A. M. S. McMillan, L. Merbold, W. Meyer, T. Meyers, S. D. Miller, S. Minerbi, U. Moderow, R. K. Monson, L. Montagnani, C. E. Moore, E. Moors, V. Moreaux, C. Moureaux, J. W. Munger, T. Nakai, J. Neirynck, Z. Nesic, G. Nicolini, A. Noormets, M. Northwood, M. Nosetto, Y. Nouvellon, K. Novick, W. Oechel, J. E. Olesen, J. M. Ourcival, S. A. Papuga, F. J. Parmentier, E. Paul-Limoges, M. Pavelka, M. Peichl, E. Pendall, R. P. Phillips, K. Pilegaard, N. Pirk, G. Posse, T. Powell, H. Prasse, S. M. Prober, S. Rambal, Ü. Rannik, N. Raz-Yaseef, D. Reed, V. R. de Dios, N. Restrepo-Coupe, B. R. Reverter, M. Roland, S. Sabbatini, T. Sachs, S. R. Saleska, E. P. Sánchez-Cañete, Z. M. Sanchez-Mejia, H. P. Schmid, M. Schmidt, K. Schneider, F. Schrader, I. Schroder, R. L. Scott, P. Sedlák, P. Serrano-Ortíz, C. Shao, P. Shi, I. Shironya, L. Siebicke, L. Šigut, R. Silberstein, C. Sirca, D. Spano, R. Steinbrecher, R. M. Stevens, C. Sturtevant, A. Suyker, T. Tagesson, S. Takanashi, Y. Tang, N. Tapper, J. Thom, F. Tiedemann,

M. Tomassucci, J. P. Tuovinen, S. Urbanski, R. Valentini, M. van der Molen, E. van Gorsel, K. van Huissteden, A. Varlagin, J. Verfaillie, T. Vesala, C. Vincke, D. Vitale, N. Vygodskaya, J. P. Walker, E. Walter-Shea, H. Wang, R. Weber, S. Westermann, C. Wille, S. Wofsy, G. Wohlfahrt, S. Wolf, W. Woodgate, Y. Li, R. Zampedri, J. Zhang, G. Zhou, D. Zona, D. Agarwal, S. Biraud, M. Torn, and D. Papale. 2020. "The FLUXNET2015 dataset and the ONEFlux processing pipeline for eddy covariance data." *Sci. data*, 7 (1): 225. NLM (Medline). https://doi.org/10.1038/s41597-020-0534-3.

Pearce, F. 2020. "Weather Makers: Forests supply the world with rain. A controversial Russian theory claims they also make wind." New York: American Association for the Advancement of Science.

Pelicice, F. M., A. A. Agostinho, A. Akama, J. D. Andrade Filho, V. M. Azevedo-Santos, M. V. M. Barbosa, L. M. Bini, M. F. G. Brito, C. R. dos Anjos Candeiro, É. P. Caramaschi, P. Carvalho, R. A. de Carvalho, L. Castello, D. B. das Chagas, C. C. Chamon, G. R. Colli, V. S. Daga, M. S. Dias, J. A. F. Diniz Filho, P. Fearnside, W. de Melo Ferreira, D. A. Z. Garcia, T. K. Krolow, R. F. Kruger, E. M. Latrubesse, D. P. Lima Junior, S. de Fátima Lolis, F. A. C. Lopes, R. D. Loyola, A. L. B. Magalhães, A. Malvasio, P. De Marco, P. R. Martins, R. Mazzoni, J. C. Nabout, M. L. Orsi, A. A. Padial, H. R. Pereira, T. N. A. Pereira, P. B. Perônico, M. Petrere, R. T. Pinheiro, E. F. Pires, P. S. Pompeu, T. C. G. Portelinha, E. E. Sano, V. L. M. dos Santos, P. H. F. Shimabukuro, I. G. da Silva, L. B. e. Souza, F. L. Tejerina-Garro, M. P. de Campos Telles, F. B. Teresa, S. M. Thomaz, L. H. Tonella, L. C. G. Vieira, J. R. S. Vitule, and J. Zuanon. 2021. "Large-scale Degradation of the Tocantins-Araguaia River Basin." *Environ. Manage.*, 68 (4): 445–452. Springer US. https://doi.org/10.1007/s00267-021-01513-7.

Penatti, N. C., T. I. R. de Almeida, L. G. Ferreira, A. E. Arantes, and M. T. Coe. 2015. "Satellite-based hydrological dynamics of the world's largest continuous wetland." *Remote Sens. Environ.*, 170: 1–13. Elsevier Inc. https://doi.org/10.1016/j.rse.2015.08.031.

Peng, L., Z. Zeng, Z. Wei, A. Chen, E. F. Wood, and J. Sheffield. 2019. "Determinants of the ratio of actual to potential evapotranspiration." *Glob. Chang. Biol.*, 25 (4):

1326–1343. Blackwell Publishing Ltd. https://doi.org/10.1111/gcb.14577.

Penman, H. L. 1948. *Natural Evaporation from Open Water, Bare Soil and Grass*. *Proc. R. Soc. Lond. A. Math. Phys. Sci.*

Pereira, A. R. 2004. "The Priestley-Taylor parameter and the decoupling factor for estimating reference evapotranspiration." *Agric. For. Meteorol.*, 125 (3–4): 305–313. https://doi.org/10.1016/j.agrformet.2004.04.002.

Polizel, S. P., R. M. da S. P. Vieira, J. Pompeu, Y. da C. Ferreira, E. R. de Sousa-Neto, A. A. Barbosa, and J. P. H. B. Ometto. 2021. "Analysing the dynamics of land use in the context of current conservation policies and land tenure in the Cerrado – MATOPIBA region (Brazil)." *Land use policy*, 109 (August). https://doi.org/10.1016/j.landusepol.2021.105713.

Popescu, I., L. Brandimarte, M. S. U. Perera, and M. Peviani. 2012. "Assessing residual hydropower potential of the la Plata Basin accounting for future user demands." *Hydrol. Earth Syst. Sci.*, 16 (8): 2813–2823. https://doi.org/10.5194/hess-16-2813-2012.

Priante-Filho, N., G. L. Vourlitis, M. M. S. Hayashi, J. D. S. Nogueira, J. H. Campelo, P. C. Nunes, L. S. E. Souza, E. G. Couto, W. Hoeger, F. Raiter, J. L. Trienweiler, E. J. Miranda, P. C. Priante, C. L. Fritzen, M. Lacerda, L. C. Pereira, M. S. Biudes, G. S. Suli, S. Shiraiwa, S. R. Do Paulo, and M. Silveira. 2004. "Comparison of the mass and energy exchange of a pasture and a mature transitional tropical forest of the southern Amazon Basin during a seasonal transition." *Glob. Chang. Biol.*, 10 (5): 863–876. https://doi.org/10.1111/j.1529-8817.2003.00775.x.

Priestley, C. H. B., and R. J. Taylor. 1972. "On the Assessment of Surface Heat Flux and Evaporation Using Large-Scale Parameters." *Mon. Weather Rev.*, 100 (2): 81–92. https://doi.org/10.1175/1520-0493(1972)100<0081:otaosh>2.3.co;2.

Progênio, M. F., and C. J. C. Blanco. 2020. "Cumulative distribution function of daily rainfall in the Tocantins–Araguaia hydrographic region, Amazon, Brazil." *Nat. Resour. Model.*, 33 (2). John Wiley & Sons, Ltd. https://doi.org/10.1111/nrm.12264.

von Randow, C., A. O. Manzi, B. Kruijt, P. J. De Oliveira, and F. B. Zanchi. 2004. "Comparative measurements and seasonal variations in energy and carbon

exchange over forest and pasture in South West Amazonia." *Theor. Appl. Climatol.*, 26: 5–26. https://doi.org/10.1007/s00704-004-0041-z.

von Randow, R. de C. S., C. von Randow, R. W. A. Hutjes, J. Tomasella, and B. Kruijt. 2012. "Evapotranspiration of deforested areas in central and southwestern Amazonia." *Theor. Appl. Climatol.*, 109 (1–2): 205–220. Springer-Verlag Wien. https://doi.org/10.1007/s00704-011-0570-1.

von Randow, R. de C. S., J. Tomasella, C. von Randow, A. C. de Araújo, A. O. Manzi, R. Hutjes, and B. Kruijt. 2020. "Evapotranspiration and gross primary productivity of secondary vegetation in Amazonia inferred by eddy covariance." *Agric. For. Meteorol.*, 294. Elsevier B.V. https://doi.org/10.1016/j.agrformet.2020.108141.

Reboita, M. S., M. A. Gan, R. Porfírio, D. A. Rocha, and T. Ambrizzi. 2010. "Regimes de Precipitação na América do Sul: Uma Revisão Bibliográfica." *Rev. Bras. Meteorol.*, 185–204.

Reichert, J. M., M. F. Rodrigues, J. J. Z. Peláez, R. Lanza, J. P. G. Minella, J. G. Arnold, and R. B. L. Cavalcante. 2017. "Water balance in paired watersheds with eucalyptus and degraded grassland in Pampa biome." *Agric. For. Meteorol.*, 238: 282–295.

Restrepo-Coupe, N., L. P. Albert, M. Longo, I. Baker, N. M. Levine, L. M. Mercado, A. C. de Araújo, B. O. D. Christoffersen, M. H. Costa, D. R. Fitzjarrald, D. Galbraith, H. Imbuzeiro, Y. Malhi, C. von Randow, X. Zeng, P. Moorcroft, and S. R. Saleska. 2021a. "Understanding water and energy fluxes in the Amazonia: Lessons from an observation-model intercomparison." *Glob. Chang. Biol.*, 27 (9): 1802–1819. Blackwell Publishing Ltd. https://doi.org/10.1111/gcb.15555.

Restrepo-Coupe, N., N. M. Levine, B. O. D. Christoffersen, L. P. Albert, J. Wu, M. H. Costa, D. Galbraith, H. Imbuzeiro, G. Martins, A. C. de Araújo, Y. S. Malhi, X. Zeng, P. Moorcroft, and S. R. Saleska. 2017. "Do dynamic global vegetation models capture the seasonality of carbon fluxes in the Amazon basin? A data-model intercomparison." *Glob. Chang. Biol.*, 23 (1): 191–208. Blackwell Publishing Ltd. https://doi.org/10.1111/gcb.13442.

Restrepo-Coupe, N., H. R. da Rocha, L. R. Hutyra, A. C. de Araújo, L. S. Borma, and B. O. D. Christoffersen. 2021b. *LBA-ECO CD-32 Flux Tower Network Data*

Compilation, Brazilian Amazon: 1999-2006, V2. Oak Ridge, Tennessee, USA.

Restrepo-Coupe, N., H. R. da Rocha, L. R. Hutyra, A. C. de Araújo, L. S. Borma, B. O. D. Christoffersen, O. M. R. Cabral, P. B. de Camargo, F. L. Cardoso, A. C. L. da Costa, D. R. Fitzjarrald, M. L. Goulden, B. Kruijt, J. M. F. Maia, Y. S. Malhi, A. O. Manzi, S. D. Miller, A. D. Nobre, C. von Randow, L. D. A. Sá, R. K. Sakai, J. Tota, S. C. Wofsy, F. B. Zanchi, and S. R. Saleska. 2013. "What drives the seasonality of photosynthesis across the Amazon basin? A cross-site analysis of eddy flux tower measurements from the Brasil flux network." *Agric. For. Meteorol.*, 182–183: 128–144. https://doi.org/10.1016/j.agrformet.2013.04.031.

Roberti, D. R., and O. C. Acevedo. 2012. "A Brazilian Network of Carbon Flux Stations." *Am. Geophys. Union*, 93 (21): 203–203.

Roberts, J. M., J. H. C. Gash, M. Tani, and L. A. Bruijnzeel. 2005. *Forests, water and people in the humid tropics*. (M. Bonell and L. A. Bruijnzeel, eds.). Cambridge University Press.

da Rocha, H. R., H. C. Freitas, R. Rosolem, R. I. N. Juárez, R. N. Tannus, M. A. V Ligo, O. M. R. Cabral, and M. A. F. S. Dias. 2002. "Measurements of CO2 exchange over a woodland savanna (Cerrado Sensu stricto) in southeast Brasil." *Biota Neotrop.*, 2 (1).

da Rocha, H. R., M. L. Goulden, S. D. Miller, M. C. Menton, L. D. V O Pinto, H. C. de Freitas, and A. M. E. S. Figueira. 2004. "Seasonality of Water and Heat Fluxes over a Tropical Forest in Eastern Amazonia." *Ecol. Appl.*, 14 (June 2000): 22–32.

da Rocha, H. R., A. O. Manzi, O. M. R. Cabral, S. D. Miller, M. L. Goulden, S. R. Saleska, N. R. Coupe, S. C. Wofsy, L. S. Borma, P. Artaxo, G. Vourlitis, J. S. Nogueira, F. L. Cardoso, A. D. Nobre, B. Kruijt, H. C. Freitas, C. von Randow, R. G. Aguiar, and J. F. Maia. 2009. "Patterns of water and heat flux across a biome gradient from tropical forest to savanna in brazil." *J. Geophys. Res. Biogeosciences*, 114 (1): 1–8. Blackwell Publishing Ltd. https://doi.org/10.1029/2007JG000640.

Rodell, M., J. S. Famiglietti, J. Chen, S. I. Seneviratne, P. Viterbo, S. Holl, and C. R. Wilson. 2004. "Basin scale estimates of evapotranspiration using GRACE and other observations." *Geophys. Res. Lett.*, 31 (20): L20504.

https://doi.org/10.1029/2004GL020873.

Rodell, M., E. B. Mcwilliams, J. S. Famiglietti, H. K. Beaudoing, and J. Nigro. 2011. "Estimating evapotranspiration using an observation based terrestrial water budget." *Hydrol. Process.*, 4092 (December): 4082–4092. https://doi.org/10.1002/hyp.8369.

Rodrigues, T. R., G. L. Vourlitis, F. D. A. Lobo, R. G. De Oliveira, and J. D. S. Nogueira. 2014. "Seasonal variation in energy balance and canopy conductance for a tropical savanna ecosystem of south central Mato Grosso, Brazil." *J. Geophys. Res. Biogeosciences*, 119 (1): 1–13. Blackwell Publishing Ltd. https://doi.org/10.1002/2013JG002472.

Rozante, J. R., D. S. Moreira, L. G. G. de Goncalves, and D. A. Vila. 2010. "Combining TRMM and surface observations of precipitation: Technique and validation over South America." *Weather Forecast.*, 25 (3): 885–894. https://doi.org/10.1175/2010WAF2222325.1.

Rubert, G. C., D. R. Roberti, L. S. Pereira, F. L. F. Quadros, H. F. de C. Velho, and O. L. L. de Moraes. 2018. "Evapotranspiration of the Brazilian Pampa biome: Seasonality and influential factors." *Water (Switzerland)*, 10 (12). MDPI AG. https://doi.org/10.3390/w10121864.

Ruhoff, A. L., A. R. Paz, L. E. O. C. Aragão, Q. Mu, Y. Malhi, W. Collischonn, and S. W. Running. 2013. "Assessment of the MODIS global evapotranspiration algorithm using eddy covariance measurements and hydrological modelling in the Rio Grande basin." *Hydrol. Sci. J.*, 6667. https://doi.org/10.1080/02626667.2013.837578.

Sahoo, A. K., M. Pan, T. J. Troy, R. K. Vinukollu, J. Shef, and E. F. Wood. 2011. "Reconciling the global terrestrial water budget using satellite remote sensing." *Remote Sens. Environ.*, 115: 1850–1865. https://doi.org/10.1016/j.rse.2011.03.009.

Sakai, R. K., D. R. Fitzjarrald, O. L. L. Moraes, R. M. Staebler, O. C. Acevedo, M. J. Czikowsky, R. Da Silva, E. Brait, and V. Miranda. 2004. "Land-use change effects on local energy, water, and carbon balances in an Amazonian agricultural field." *Glob. Chang. Biol.*, 10 (5): 895–907. https://doi.org/10.1111/j.1529-8817.2003.00773.x.

Sakumura, C., S. Bettadpur, and S. Bruinsma. 2014. “Ensemble prediction and intercomparison analysis of GRACE time-variable gravity field models.” *Geophys. Res. Lett.*, 41 (5): 1389–1397. American Geophysical Union. https://doi.org/10.1002/2013GL058632.

Salati, E., A. Dall’Olio, E. Matsul, and J. R. Gat. 1979. “Recycling of Water in the Amazon Basin: An Isotopic Study.” *Water Resour. Res.*, 15 (5): 1250–1258.

Salati, E., and P. B. Vose. 1984. “Amazon Basin: A system in equilibrium.” *Science (80-.).*, 225 (4658): 129–138. https://doi.org/10.1126/science.225.4658.129.

Salazar, A., G. Baldi, M. Hirota, J. Syktus, and C. Mcalpine. 2015. “Land use and land cover change impacts on the regional climate of non-Amazonian South America : A review.” *Glob. Planet. Change*, 128: 103–119. Elsevier B.V. https://doi.org/10.1016/j.gloplacha.2015.02.009.

Saleska, S. R., J. P. Kennett, L. D. Stott, V. Kirchhoff, M. Menton, and J. W. Munger. 2003. “Carbon in Amazon Forests : Unexpected Seasonal Fluxes and Disturbance-Induced Losses.” *Science (80-.).*, 1554 (203). https://doi.org/10.1126/science.1091165.

Saleska, S. R., H. R. da Rocha, A. R. Huete, C. A. Nobre, P. Artaxo, and Y. E. Shimabukuro. 2013. “LBA-ECO CD-32 Flux Tower Network Data Compilation, Brazilian Amazon: 1999-2006. ORNL DAAC.”

Salio, P., M. P. Hobouchian, Y. García Skabar, and D. Vila. 2015. “Evaluation of high-resolution satellite precipitation estimates over southern South America using a dense rain gauge network.” *Atmos. Res.*, 163: 146–161. Elsevier B.V. https://doi.org/10.1016/j.atmosres.2014.11.017.

Sanches, L., G. L. Vourlitis, M. D. C. Alves, O. B. Pinto-Júnior, and J. D. S. Nogueira. 2011. “Seasonal patterns of evapotranspiration for a vochysia divergens forest in the brazilian pantanal.” *Wetlands*, 31 (6): 1215–1225. https://doi.org/10.1007/s13157-011-0233-0.

Sano, E. E., R. Rosa, J. L. S. Brito, and L. G. Ferreira. 2010. “Land cover mapping of the tropical savanna region in Brazil.” *Environ. Monit. Assess.*, 166 (1–4): 113–124. https://doi.org/10.1007/s10661-009-0988-4.

Sano, E. E., R. Rosa, C. A. de M. Scaramuzza, M. Adami, E. L. Bolfe, A. C. Coutinho, J. C. D. M. Esquerdo, L. E. P. Maurano, I. da S. Narvaes, F. J. B. de O. Filho, E. B. da Silva, D. de C. Victoria, L. G. Ferreira, J. L. S. Brito, A. P. Bayma, G. H. de Oliveira, and G. Bayma-Silva. 2019. "Land use dynamics in the Brazilian Cerrado in the period from 2002 to 2013." *Pesqui. Agropecu. Bras.*, 54. Embrapa. https://doi.org/10.1590/S1678-3921.pab2019.v54.00138.

Santos, A. J. B., G. T. D. A. Silva, H. S. Miranda, A. C. Miranda, and J. Lloyd. 2003. "Effects of fire on surface carbon, energy and water vapour fluxes over campo sujo savanna in central Brazil." *Funct. Ecol.*

dos Santos, A. T. S., and C. M. Santos e Silva. 2013. "Seasonality, interannual variability, and linear tendency of wind speeds in the Northeast Brazil from 1986 to 2011." *Sci. World J.*, 2013. Hindawi Publishing Corporation. https://doi.org/10.1155/2013/490857.

dos Santos, W. P., J. C. Avanzi, M. R. Viola, S. C. Chou, S. F. Acuña-Guzman, L. M. Pontes, and N. Curi. 2022. "Projections of rainfall erosivity in climate change scenarios for the largest watershed within Brazilian territory." *Catena*, 213 (February). https://doi.org/10.1016/j.catena.2022.106225.

Satyamurty, P., C. P. W. da Costa, and A. O. Manzi. 2013. "Moisture source for the Amazon Basin: A study of contrasting years." *Theor. Appl. Climatol.*, 111 (1–2): 195–209. Springer-Verlag Wien. https://doi.org/10.1007/s00704-012-0637-7.

Scanlon, B. R., Z. Zhang, H. Save, D. N. Wiese, F. W. Landerer, D. Long, L. Longuevergne, and J. Chen. 2016. "Global evaluation of new GRACE mascon products for hydrologic applications." *Water Resour. Res.*, 9412–9429. https://doi.org/10.1002/2016WR019494.Received.

Sena, J. A., L. A. B. de Deus, M. A. V. Freitas, and L. Costa. 2012. "Extreme Events of Droughts and Floods in Amazonia: 2005 and 2009." *Water Resour. Manag.*, 26 (6): 1665–1676. https://doi.org/10.1007/s11269-012-9978-3.

Senay, G. B. 2018. "Satellite psychrometric formulation of the operational simplified surface energy balance (SSEBop) model for." *Appl. Eng. Agric.*, 34 (3): 555–566. American Society of Agricultural and Biological Engineers. https://doi.org/https://doi.org/10.13031/aea.12614.

Senay, G. B., S. Bohms, R. K. Singh, P. H. Gowda, N. M. Velpuri, H. Alemu, and J. P. Verdin. 2013. “Operational Evapotranspiration Mapping Using Remote Sensing and Weather Datasets: A New Parameterization for the SSEB Approach.” *J. Am. Water Resour. Assoc.*, 49 (3): 577–591. https://doi.org/10.1111/jawr.12057.

Senay, G. B., S. Kagone, and N. M. Velpuri. 2020. “Operational global actual evapotranspiration: Development, evaluation, and dissemination.” *Sensors (Switzerland)*, 20 (7). MDPI AG. https://doi.org/10.3390/s20071915.

Senay, G. B., S. Leake, P. L. Nagler, G. Artan, J. Dickinson, J. T. Cordova, and E. P. Glenn. 2011. “Estimating basin scale evapotranspiration (ET) by water balance and remote sensing methods.” *Hydrol. Process.*, 4049 (December): 4037–4049. https://doi.org/10.1002/hyp.8379.

Sheffield, J., C. R. Ferguson, T. J. Troy, E. F. Wood, and M. F. McCabe. 2009. “Closing the terrestrial water budget from satellite remote sensing.” *Geophys. Res. Lett.*, 36 (7). https://doi.org/10.1029/2009GL037338.

Sheffield, J., E. F. Wood, M. Pan, H. E. Beck, A. Serrat-capdevila, and K. Verbist. 2018. “Satellite Remote Sensing for Water Resources Management : Potential for Supporting Sustainable Development in Data-Poor Regions.” *Water Resour. Res.*, 9724–9758. https://doi.org/10.1029/2017WR022437.

Shi, T. T., D. X. Guan, J. B. Wu, A. Z. Wang, C. J. Jin, and S. J. Han. 2008. “Comparison of methods for estimating evapotranspiration rate of dry forest canopy: Eddy covariance, Bowen ratio energy balance, and Penman-Monteith equation.” *J. Geophys. Res. Atmos.*, 113 (19). Blackwell Publishing Ltd. https://doi.org/10.1029/2008JD010174.

Shuttleworth, W. J. 2012. *Terrestrial hydrometeorology*. John Wiley & Sons.

Silva Junior, C. H. L., A. C. M. Pessôa, N. S. Carvalho, J. B. C. Reis, L. O. Anderson, and L. E. O. C. Aragão. 2021. “The Brazilian Amazon deforestation rate in 2020 is the greatest of the decade.” *Nat. Ecol. Evol.* Nature Research.

Siqueira, V. A., R. C. D. de Paiva, A. S. Fleischmann, F. M. Fan, A. L. Ruhoff, P. R. M. Pontes, A. Paris, S. Calmant, and W. Collischonn. 2018. “Toward continental hydrologic – hydrodynamic modeling in South America.” *Hydrol. Earth Syst. Sci.*, (May): 1–50.

Sörensson, A. A., and R. C. Ruscica. 2018. “Intercomparison and Uncertainty Assessment of Nine Evapotranspiration Estimates Over South America Water Resources Research.” *Water Resour. Res.*, 1–18. https://doi.org/10.1002/2017WR021682.

Sorribas, M. V., R. C. D. de Paiva, J. M. Melack, J. M. Bravo, C. Jones, L. Carvalho, E. Beighley, B. Forsberg, and M. H. Costa. 2016. “Projections of climate change effects on discharge and inundation in the Amazon basin.” *Clim. Change*, 136 (3–4): 555–570. https://doi.org/10.1007/s10584-016-1640-2.

Souza, C. M., J. Z. Shimbo, M. R. Rosa, L. L. Parente, A. A. Alencar, B. F. T. Rudorff, H. Hasenack, M. Matsumoto, L. G. Ferreira, P. W. M. Souza-Filho, S. W. de Oliveira, W. F. Rocha, A. V. Fonseca, C. B. Marques, C. G. Diniz, D. Costa, D. Monteiro, E. R. Rosa, E. Vélez-Martin, E. J. Weber, F. E. B. Lenti, F. F. Paternost, F. G. C. Pareyn, J. V. Siqueira, J. L. Viera, L. C. F. Neto, M. M. Saraiva, M. H. Sales, M. P. G. Salgado, R. Vasconcelos, S. Galano, V. V. Mesquita, and T. Azevedo. 2020. “Reconstructing three decades of land use and land cover changes in brazilian biomes with landsat archive and earth engine.” *Remote Sens.*, 12 (17). MDPI AG. https://doi.org/10.3390/RS12172735.

Souza, V. de A., D. R. Roberti, A. L. Ruhoff, T. Zimmer, D. S. Adamatti, L. G. G. de Gonçalves, M. B. Diaz, R. de C. M. Alves, and O. L. L. de Moraes. 2019. “Evaluation of MOD16 Algorithm over Irrigated Rice Paddy Using Flux Tower Measurements in Southern Brazil.” *Water*, 11 (9): 1911. https://doi.org/10.3390/w11091911.

Sperling, E. Von. 2012. “Hydropower in Brazil : overview of positive and negative environmental aspects.” *Energy Procedia*, 18: 110–118. Elsevier B.V. https://doi.org/10.1016/j.egypro.2012.05.023.

Stewart, J. B. 1989. “On the use of the Penrnan-Monteith equation for determining area! évapotranspiration.” *Estim. ofArealEvapotranspiroeio*, 3–12. Vancouver: IAHS Publ.

Stokes, M. F., S. L. Goldberg, and J. T. Perron. 2018. “Ongoing River Capture in the Amazon.” *Geophys. Res. Lett.*, 45 (11): 5545–5552. https://doi.org/10.1029/2018GL078129.

Sulla-Menashe, D., J. M. Gray, S. P. Abercrombie, and M. A. Friedl. 2019. "Hierarchical mapping of annual global land cover 2001 to present: The MODIS Collection 6 Land Cover product." *Remote Sens. Environ.*, 222: 183–194. Elsevier Inc. https://doi.org/10.1016/j.rse.2018.12.013.

Sun, T., V. G. Ferreira, X. He, and S. A. Andam-akorful. 2016. "Water Availability of São Francisco River Basin Based on a Space-Borne Geodetic Sensor." *Water*. https://doi.org/10.3390/w8050213.

Swann, A. L. S., and C. D. Koven. 2017. "A Direct Estimate of the Seasonal Cycle of Evapotranspiration over the Amazon Basin." *Am. Meteorol. Soc.*, 2173–2186. https://doi.org/10.1175/JHM-D-17-0004.1.

Swenson, S., and J. Wahr. 2006. "Post-processing removal of correlated errors in GRACE data." *Geophys. Res. Lett.*, 33 (8). https://doi.org/10.1029/2005GL025285.

Talsma, C. J., S. P. Good, C. Jimenez, B. Martens, J. B. Fisher, D. G. Miralles, M. F. McCabe, and A. J. Purdy. 2018. "Partitioning of evapotranspiration in remote sensing-based models." *Agric. For. Meteorol.*, 260–261: 131–143. Elsevier B.V. https://doi.org/10.1016/j.agrformet.2018.05.010.

Tan, Z. H., J. F. Zhao, G. Z. Wang, M. P. Chen, L. Y. Yang, C. S. He, N. Restrepo-Coupe, S. S. Peng, X. Y. Liu, H. R. da Rocha, Y. Kosugi, T. Hirano, S. R. Saleska, M. L. Goulden, J. Zeng, F. J. Ding, F. Gao, and L. Song. 2019. "Surface conductance for evapotranspiration of tropical forests: Calculations, variations, and controls." *Agric. For. Meteorol.*, 275: 317–328. Elsevier B.V. https://doi.org/10.1016/j.agrformet.2019.06.006.

Tapley, B. D., S. Bettadpur, M. Watkins, and C. Reigber. 2004. "The gravity recovery and climate experiment : Mission overview and early results." *Geophys. Res. Lett.*, 31 (November 2002): 1–4. https://doi.org/10.1029/2004GL019920.

Timm, A. U., D. R. Roberti, N. A. Streck, L. G. G. de Gonçalves, O. C. Acevedo, O. L. L. de Moraes, V. Silva Moreira, G. A. Degrazia, M. Ferlan, and D. L. Toll. 2014. "Energy Partitioning and Evapotranspiration over a Rice Paddy in Southern Brazil." *Am. Meteorol. Soc.*, 1975–1988. https://doi.org/10.1175/JHM-D-13-0156.1.

Tucci, C. E. M., and R. T. Clarke. 1998. “Environmental Issues in the la Plata Basin.” *Int. J. water*, (April 2013): 37–41.

Tundisi, J. G., O. Rocha, and B. Braga. 1998. “Reservoir Management in South America.” *Int. J. Water Resour. Dev.*, 0627 (1998). https://doi.org/10.1080/07900629849367.

Turchetto-Zolet, A. C., F. Pinheiro, F. Salgueiro, and C. Palma-Silva. 2013. “Phylogeographical patterns shed light on evolutionary process in South America.” *Mol. Ecol.*

Twine, T. E., W. P. Kustas, J. M. Norman, D. R. Cook, P. R. Houser, T. P. Meyers, J. H. Prueger, P. J. Starks, and M. L. Wesely. 2000. “Correcting eddy-covariance flux underestimates over a grassland.” *Agric. For. Meteorol.*, 103: 279–300.

Vergopolan, N., and J. B. Fisher. 2016. “The impact of deforestation on the hydrological cycle in Amazonia as observed from remote sensing.” *Int. J. Remote Sens.*, 37 (22): 5412–5430. Taylor and Francis Ltd. https://doi.org/10.1080/01431161.2016.1232874.

Verma, S. B. 1989. “Aerodynamic resistances to transfers of heat, mass and momentum.” *Estim. areal evapotranspiration*, D. L. Spittlehouse, M. D. Novak, and D. T. Price, eds., 13–20. British Columbia: IAHS Publication.

Villar, R. E., J. Ronchail, J.-L. Guyot, G. Cochonneau, N. Filizola, W. Lavado, E. De Oliveira, R. Pombosa, and P. Vauchel. 2009. “Spatio-temporal rainfall variability in the Amazon basin countries (Brazil, Peru, Bolivia, Colombia, and Ecuador).” *Int. J. Climatol.*, 2029 (March 2008): 2011–2029. https://doi.org/10.1002/joc.

Vourlitis, G. L., N. P. Filho, M. M. S. Hayashi, J. de S. Nogueira, F. T. Caseiro, and J. H. Campelo. 2002. “Seasonal variations in the evapotranspiration of a transitional tropical forest of Mato Grosso, Brazil.” *Water Resour. Res.*, 38 (6): 30-1-30–11. American Geophysical Union (AGU). https://doi.org/10.1029/2000wr000122.

Wang, K., and R. E. Dickinson. 2012. “A review of global terrestrial evapotranspiration: Observation, modeling, climatology, and climatic variability.” *Rev. Geophys.* Blackwell Publishing Ltd.

Wever, L. A., L. B. Flanagan, and P. J. Carlson. 2002. “Seasonal and interannual

variation in evapotranspiration, energy balance and surface conductance in a northern temperate grassland." *Agric. For. Meteorol.*, 112: 31–49.

Wilson, K., A. Goldstein, E. Falge, M. Aubinet, D. Baldocchi, P. Berbigier, C. Bernhofer, R. Ceulemans, H. Dolman, C. Field, A. Grelle, A. Ibrom, B. E. Law, A. Kowalski, T. Meyers, J. Moncrieff, R. Monson, W. Oechel, J. Tenhunen, R. Valentini, and S. Verma. 2002. *Energy balance closure at FLUXNET sites*. *Agric. For. Meteorol.*

Wongchuig, S., J. C. Espinoza, T. Condom, H. Segura, J. Ronchail, P. A. Arias, C. Junquas, A. Rabatel, and T. Lebel. 2021. "A regional view of the linkages between hydro-climatic changes and deforestation in the Southern Amazon." *Int. J. Climatol.* John Wiley and Sons Ltd. https://doi.org/10.1002/joc.7443.

Wu, J., V. Lakshmi, D. Wang, P. Lin, M. Pan, X. Cai, E. F. Wood, and Z. Zeng. 2020. "The reliability of global remote sensing evapotranspiration products over Amazon." *Remote Sens.*, 12 (14). MDPI AG. https://doi.org/10.3390/rs12142211.

Xu, T., Z. Guo, Y. Xia, V. G. Ferreira, S. Liu, K. Wang, Y. Yao, X. Zhang, and C. Zhao. 2019. "Evaluation of twelve evapotranspiration products from machine learning, remote sensing and land surface models over conterminous United States." *J. Hydrol.*, 578. Elsevier B.V. https://doi.org/10.1016/j.jhydrol.2019.124105.

Xu, X.-K., and J. K. Levy. 2011. "Analyzing Potential Evapotranspiration and Climate Drivers in China." *Chinese J. Geophys.*, 54 (2): 125–134.

Yebra, M., A. Van Dijk, R. Leuning, A. Huete, and J. P. Guerschman. 2013. "Evaluation of optical remote sensing to estimate actual evapotranspiration and canopy conductance." *Remote Sens. Environ.*, 129: 250–261. https://doi.org/10.1016/j.rse.2012.11.004.

Yin, L., X. Wang, X. Feng, B. Fu, and Y. Chen. 2020. "A comparison of SSEBop-model-based evapotranspiration with eight evapotranspiration products in the Yellow River Basin, China." *Remote Sens.*, 12 (16). MDPI AG. https://doi.org/10.3390/RS12162528.

Zanchi, F. B., M. J. Waterloo, L. J. G. Aguiar, C. von Randow, B. Kruijt, F. L. Cardoso, and A. O. Manzi. 2009. "Estimativa do Índice de Área Foliar (IAF) e Biomassa em

pastagem no estado de Rondônia, Brasil." *Acta Amaz.*, 39 (2): 335–348. https://doi.org/10.1590/s0044-59672009000200012.

Zha, T., C. Li, S. Kellomäki, H. Peltola, K. Y. Wang, and Y. Zhang. 2013. "Controls of Evapotranspiration and CO2 Fluxes from Scots Pine by Surface Conductance and Abiotic Factors." *PLoS One*, 8 (7). https://doi.org/10.1371/journal.pone.0069027.

Zhang, K., J. S. Kimball, and S. W. Running. 2016a. "A review of remote sensing based actual evapotranspiration estimation." *Wiley Interdiscip. Rev. Water*. John Wiley and Sons Inc.

Zhang, Y., D. Kong, R. Gan, F. H. S. Chiew, T. R. McVicar, Q. Zhang, and Y. Yang. 2019. "Coupled estimation of 500 m and 8-day resolution global evapotranspiration and gross primary production in 2002–2017." *Remote Sens. Environ.*, 222: 165–182. Elsevier Inc. https://doi.org/10.1016/j.rse.2018.12.031.

Zhang, Y., R. Leuning, L. B. Hutley, J. Beringer, I. McHugh, and J. P. Walker. 2010. "Using long-term water balances to parameterize surface conductances and calculate evaporation at 0.05° spatial resolution." *Water Resour. Res.*, 46 (5). https://doi.org/https://doi.org/10.1029/2009WR008716.

Zhang, Y., M. Pan, J. Sheffield, A. L. Siemann, C. K. Fisher, M. Liang, H. E. Beck, N. Wanders, R. F. MacCracken, P. R. Houser, T. Zhou, D. P. Lettenmaier, R. T. Pinker, J. Bytheway, C. D. Kummerow, and E. F. Wood. 2018. "A Climate Data Record (CDR) for the global terrestrial water budget: 1984-2010." *Hydrol. Earth Syst. Sci.*, 22 (1): 241–263. https://doi.org/10.5194/hess-22-241-2018.

Zhang, Y., J. L. Peña-arancibia, T. R. Mcvicar, F. H. S. Chiew, J. Vaze, C. Liu, X. Lu, H. Zheng, Y. Wang, Y. Y. Liu, D. G. Miralles, and M. Pan. 2016b. "Multi-decadal trends in global terrestrial evapotranspiration and its components." *Nat. Publ. Gr.*, (December 2015): 1–12. Nature Publishing Group. https://doi.org/10.1038/srep19124.

Zimmer, T., M. Baptistela Stefanello, V. Silva Moreira, M. Bortoluzzi Diaz, V. de Arruda Souza, and D. Regina Roberti. 2016. "Estimating the Soil Thermal Conductivity Using Experimental Soil Heat Flux in a Rice Paddy Area." *Am. J. Environ. Eng.*, 6 (4A): 103–108. https://doi.org/10.5923/s.ajee.201601.15.

Supplementary Information S3

Table SI3.1: Discharge stations and upstream basin areas used to assess the water balance.

Country	Basin	Name	Code	Lat (°)	Lon (°)	Upstream Area – (km^2)	River	Biome (IBGE/WWF)	Predominant climate (Koppen)
Brazil	Amazon	São Paulo de Olivença	11400000	-3.45	-68.91	1,010,000	Solimões/Amazonas	Amazon	Equatorial/ Tropical monsoon (Af/Am)
Brazil	Amazon	Santo Antônio do Iça	11500000	-3.10	-67.93	1,130,000	Solimões/Amazonas	Amazon	Equatorial/ Tropical moonson (Af/Am)
Brazil	Amazon	Itapéua	13150000	-4.05	-63.02	1,780,000	Solimões/Amazonas	Amazon	Equatorial/ Tropical moonson (Af/Am)
Brazil	Amazon	Canutama	13880000	-6.53	-64.38	236,000	Purus	Amazon	Equatorial/ Tropical monsoon (Af/Am)
Brazil	Amazon	Serrinha	14420000	-0.48	-64.82	293,000	Negro	Amazon	Equatorial (Af)
Brazil	Amazon	Porto Velho	15400000	-8.74	-63.91	976,000	Madeira	Amazon	Tropical wet-dry/ Tropical monsoon (Aw/Am)
Brazil	Amazon	Fazenda Vista Alegre	15860000	-4.89	-60.02	1,310,000	Madeira	Amazon	Tropical wet-dry/ Tropical monsoon (Aw/Am)
Brazil	Amazon	Óbidos	17050001	-1.91	-55.51	4,670,000	Solimões/Amazonas	Amazon	Equatorial/ Tropical mosoon (Af/Am)
Brazil	Amazon	Barra do São Manuel	17430000	-7.33	-58.15	333,000	Tapajós	Amazon/Cerrado	Tropical wet-dry/ Tropical monsoon (Aw/Am)
Brazil	Amazon	Itaituba	17730000	-4.27	-55.98	458,000	Tapajós	Amazon/Cerrado	Tropical wet-dry/ Tropical monsoon (Aw/Am)
Brazil	Amazon	Boa Sorte	18460000	-6.73	-51.99	210,000	Xingu	Amazon/Cerrado	Tropical wet-dry climate (Aw)
Brazil	Amazon	Altamira	18850000	-3.21	-52.21	448,000	Xingu	Amazon/Cerrado	Tropical wet-dry/ Tropical monsoon (Aw/Am)
Brazil	Tocantins	Miracema do Tocantins	22500000	-9.56	-48.38	185,000	Tocantins	Cerrado	Tropical wet-dry climate (Aw)
Brazil	Tocantins	Descarreto	23700000	-5.78	-47.46	297,000	Tocantins	Cerrado	Tropical wet-dry climate (Aw)
Brazil	Tocantins	Luiz Alves	25950000	-13.20	-50.58	117,000	Araguaia	Cerrado	Tropical wet-dry climate (Aw)
Brazil	Tocantins	Conceição do Araguaia	27500000	-8.26	-49.25	332,000	Araguaia	Cerrado	Tropical wet-dry climate (Aw)
Brazil	Tocantins	Tucuruí	29700000	-3.75	-49.65	764,000	Tocantins	Amazon/Cerrado	Tropical wet-dry climate (Aw)

Brazil	North/ Northeast Atlantic	Bacabal	33290000	-4.21	-44.76	25,500	Mearim	Cerrado	Tropical wet-dry climate Aw)
Brazil	North/ Northeast Atlantic	Cantanhede	33680000	-3.62	-44.37	49,900	Itapecuru	Cerrado	Tropical wet-dry climate (Aw)
Brazil	North/ Northeast Atlantic	Barão de Grajaú	34311000	-6.76	-43.02	140,000	Parnaíba	Cerrado	Tropical wet-dry climate (Aw)
Brazil	North/ Northeast Atlantic	Teresina - CHESF	34690000	-5.13	-42.81	237,000	Parnaíba	Cerrado/Caatinga	Tropical wet-dry/ Semi-arid climate (Aw/ BSh)
Brazil	North/ Northeast Atlantic	Luzilândia	34879500	-3.45	-42.37	298,000	Parnaíba	Cerrado/Caatinga	Tropical wet-dry/ Semi-arid climate (Aw/ BSh)
Brazil	North/ Northeast Atlantic	Peixe Gordo	36390000	-5.22	-38.19	47,800	Jaguaribe	Caatinga	Semi-arid climate (BSh)
Brazil	São Francisco	Pirapora Barreiro	41135000	-17.36	-44.94	62,200	São Francisco	Cerrado	Tropical wet-dry climate (Aw)
Brazil	São Francisco	Cachoeira da Manteiga	42210000	-16.65	-45.08	107,000	São Francisco	Cerrado	Tropical wet-dry climate (Aw)
Brazil	São Francisco	São Romão	43200000	-16.37	-45.07	154,000	São Francisco	Cerrado	Tropical wet-dry climate (Aw)
Brazil	São Francisco	São Francisco	44200000	-15.94	-44.86	184,000	São Francisco	Cerrado	Tropical wet-dry climate (Aw)
Brazil	São Francisco	Barra	46998000	-11.09	-43.14	425,000	São Francisco	Cerrado	Tropical wet-dry climate (Aw)
Brazil	São Francisco	Santa Maria da Boa Vista	48290000	-8.80	-39.82	535,000	São Francisco	Cerrado/Caatinga	Tropical wet-dry/ Semi-arid climate (Aw/ BSh)
Brazil	São Francisco	Traipu	49660000	-9.97	-37.00	630,000	São Francisco	Cerrado/Caatinga	Tropical wet-dry/ Semi-arid climate (Aw/ BSh)
Brazil	East Atlantic	Itapebi	54950000	-15.94	-39.52	68,100	Jequitinhonha	Cerrado/Atlantic Forest	Tropical wet-dry climate (Aw)
Brazil	East Atlantic	Colatina	56994500	-19.53	-40.62	76,400	Doce	Atlantic Forest	Tropical monsoon/ Tropical wet-dry climate (Am/Aw)
Brazil	Paraná	UHE Porto Primavera	63995080	-22.48	-52.95	572,000	Paraná	Cerrado/Atlantic Forest	Humid subtropical climate (Cwa/ Cwb)
Brazil	Paraná	Barramento Porto São José	64575003	-22.71	-53.18	676,000	Paraná	Cerrado/Atlantic Forest	Humid subtropical climate

									(Cwa/Cfa)
Brazil	Paraná	UHE Itaipu Ivinhema	64617000	-22.38	-53.52	31,900	Ivinhema	Cerrado/Atlantic Forest	Humid subtropical climate (Cfa)
Brazil	Paraná	Novo Porto Taquara	64693000	-23.19	-53.31	34,400	Ivaí	Atlantic Forest	Humid subtropical climate (Cfa)
Brazil	Paraná	Balsa Santa Maria	64830000	-24.18	-53.74	20,900	Piquiri	Atlantic Forest	Humid subtropical climate (Cfa)
Brazil	Paraná	Estreito do Iguaçu Novo	65986000	-25.55	-53.84	63,300	Iguaçu	Atlantic Forest	Humid subtropical climate (Cfa/Cfb)
Brazil	Paraná	São Francisco	66810000	-18.39	-57.39	243,000	Paraguay	Cerrado/Pantanal	Tropical wet-dry climate (Aw)
Brazil	Paraná	Porto Murtinho	67100000	-21.70	-57.89	576,000	Paraguay	Cerrado/Pantanal/Dry Chaco	Tropical wet-dry climate (Aw)
Brazil	Uruguay	Iraí	74100000	-27.17	-53.22	61,900	Uruguay	Atlantic Forest	Humid subtropical climate (Cfa)
Brazil	Uruguay	Garruchos	75550000	-28.18	-55.64	116,000	Uruguay	Atlantic Forest/ Pampa	Humid subtropical climate (Cfa)
Brazil	Uruguay	Uruguaiana	77150000	-29.74	-57.08	190,000	Uruguay	Atlantic Forest/ Pampa	Humid subtropical climate (Cfa)
Brazil	Southeast Atlantic	Eldorado	81380000	-24.51	-48.10	14,700	Ribeira do Iguape	Atlantic Forest	Humid subtropical climate (Cfa/Cfb)
Brazil	Southeast Atlantic	Registro	81683000	-24.48	-47.84	20,900	Ribeira do Iguape	Atlantic Forest	Humid subtropical climate (Cfa/Cfb)
Brazil	South Atlantic	Rio Pardo	85900000	-29.99	-52.37	38,700	Jacuí	Atlantic Forest/ Pampa	Humid subtropical climate (Cfa)
Brazil	South Atlantic	Encantado	86720000	-29.23	-51.85	19,100	Taquari	Atlantic Forest	Humid subtropical climate (Cfa)
Argentina	Paraná	Puerto Pilcomayo	2606	-25.42	-57.65	905,941	Paraguay	Cerrado/Pantanal/Dry Chaco	Tropical wet-dry climate (Aw)
Argentina	La Plata	Ruta Provincial	3216	-31.49	-60.78	210,003	Salado	Dry Chaco	Subtropical climate (Cfa/Cwa)
Argentina	Paraná	Timbues	3316	-32.65	-60.73	2,535,233	Paraná	Cerrado/Atlantic Forest/Pantanal/Dry and humid Chaco	Tropical wet-dry/ Subtropical climate (Aw/Cfa)

Table SI3.2: Statistical metrics between remote sensing and measured precipitation.

Name	Code	r		RMSE		BIAS		Number of rain gauges
		TRMM	MSWEP	TRMM	MSWEP	TRMM	MSWEP	
Puerto Pilcomayo	2606	0.87	0.88	47.44	40.96	14.53	-2.41	10
Ruta Provincial	3216	-	-	-	-	-	-	-
Timbues	3316	0.90	0.91	41.29	33.88	7.26	-12.68	76
São Paulo de Olivença	11400000	-	-	-	-	-	-	-
Santo Antônio do Içá	11500000	-	-	-	-	-	-	-
Itapéua	13150000	0.87	0.90	54.94	42.68	5.85	-14.64	7
Canutama	13880000	-	-	-	-	-	-	-
Serrinha	14420000	-	-	-	-	-	-	-
Porto Velho	15400000	-	-	-	-	-	-	-
Fazenda Vista Alegre	15860000	-	-	-	-	-	-	-
Óbidos	17050001	0.88	0.90	53.86	42.60	-3.08	-16.87	20
Barra do São Manuel	17430000	0.94	0.94	49.95	47.61	2.02	1.36	4
Itaituba	17730000	0.94	0.94	48.09	46.32	3.12	5.56	5
Boa Sorte	18460000	-	-	-	-	-	-	-
Altamira	18850000	-	-	-	-	-	-	-
Miracema do Tocantins	22500000	0.93	0.93	43.85	41.59	-6.54	-6.63	6
Descarreto	23700000	0.93	0.94	42.08	38.19	-5.58	-8.15	8
Luiz Alves	25950000	-	-	-	-	-	-	-
Conceição do Araguaia	27500000	-	-	-	-	-	-	-
Tucuruí	29700000	0.93	0.95	43.16	35.36	0.12	-4.93	15
Bacabal	33290000	-	-	-	-	-	-	-
Cantanhede	33680000	-	-	-	-	-	-	-
Barão de Grajaú	34311000	0.89	0.92	43.51	33.35	3.43	-0.72	5
Teresina - Chesf	34690000	0.90	0.91	38.53	34.69	6.56	-0.51	9
Luzilândia	34879500	0.91	0.92	37.02	32.68	7.55	-0.49	11
Peixe Gordo	36390000	0.92	0.93	32.81	32.26	-0.33	-13.01	4
Pirapora	41135000	0.94	0.95	41.40	36.96	6.04	0.23	7
Cachoeira da Manteiga	42210000	0.94	0.95	39.89	35.24	3.22	-1.82	10
São Romão	43200000	0.94	0.95	39.38	36.05	3.26	-2.67	14
São Francisco	44200000	0.95	0.96	39.03	35.29	4.03	-1.72	15
Barra	46998000	0.93	0.95	37.52	33.22	7.20	0.74	28
Santa Maria da Boa Vista	48290000	0.93	0.95	36.07	31.95	6.26	0.09	32
Traipu	49660000	0.91	0.92	35.80	31.68	5.11	-3.04	38
Itapebi	54950000	0.95	0.96	30.43	27.79	8.95	0.09	6
Colatina	56994500	0.95	0.97	37.65	29.63	8.95	-1.10	4
UHE Porto Primavera	63995080	0.93	0.95	40.83	34,14	7.35	-10.86	32
Barramento Porto São José	64575003	0.93	0.94	40.48	32.90	6.91	-12.74	37
Ivinhema	64617000	-	-	-	-	-	-	-
Novo Porto Taquara	64693000	-	-	-	-	-	-	-

Balsa Santa Maria	64830000	-	-	-	-	-	-	-
Estreito do Iguaçu Novo	65986000	-	-	-	-	-	-	-
São Francisco	66810000	0.90	0.92	48.34	42.51	12.41	-1.80	6
Porto Murtinho	67100000	0.89	0.90	46.74	40.99	11.81	-4.30	8
Iraí	74100000	0.91	0.94	35.94	25.29	13.77	-22.73	7
Garruchos	75550000	0.90	0.92	38.13	28.33	13.01	-21.36	10
Uruguaiana	77150000	0.90	0.91	39.25	31.52	14.03	-15.33	16
Eldorado	81380000	-	-	-	-	-	-	-
Registro	81683000	-	-	-	-	-	-	-
Rio Pardo	85900000	0.92	0.93	32.30	25.57	12.83	-25.29	4
Encantado	86720000	0.90	0.93	34.60	24.81	17.05	-18.13	4

Table SI3.3: Precipitation and Evapotranspiration uncertainties calculated for basins in South America.

Name	**Code**	**Precipitation Uncertainty (%)**		**Evapotranspiration Uncertainty (%)**		**Number of rain gauges**
		TRMM	MSWEP	MOD16	GLEAM	
Puerto Pilcomayo	2606	45.82	41.88	31.03	18.54	10
Ruta Provincial	3216	-	-	-	-	-
Timbues	3316	41.54	38.17	34.91	18.54	76
São Paulo de Olivença	11400000	-	-	22.34	18.76	-
Santo Antônio do Içá	11500000	-	-	22.32	18.74	-
Itapéua	13150000	28.61	24.94		18.72	7
Canutama	13880000	-	-	22.14	18.67	-
Serrinha	14420000	-	-	22.14	18.67	-
Porto Velho	15400000	-	-	23.34	19.17	-
Fazenda Vista Alegre	15860000	-	-	22.42	18.79	-
Óbidos	17050001	28.15	24.44	22.36	18.76	20
Barra do São Manuel	17430000	27.35	26.55	26.17	20.34	4
Itaituba	17730000	26.36	25.95	24.65	19.71	5
Boa Sorte	18460000	-	-	23.28	19.14	-
Altamira	18850000	-	-	22.59	18.86	-
Miracema do Tocantins	22500000	28.31	26.99	34.55	18.54	6
Descarreto	23700000	27.09	24.94	34.12	18.54	8
Luiz Alves	25950000	-	-	39.47	18.54	-
Conceição do Araguaia	27500000	-	-	34.86	18.54	-
Tucuruí	29700000	28.46	23.62	33.32	18.54	15
Bacabal	33290000	-	-	26.95	18.54	-
Cantanhede	33680000	-	-	26.12	18.54	-
Barão de Grajaú	34311000	38.36	29.40	29.09	18.54	5
Teresina - Chesf	34690000	41.73	39.98	-	-	9
Luzilândia	34879500	41.49	37.84	-	-	11
Peixe Gordo	36390000	43.68	44.70	-	-	4
Pirapora	41135000	34.87	30.67	40.61	18.54	7
Cachoeira da Manteiga	42210000	34.68	29.73	39.54	18.54	10
São Romão	43200000	32.90	29.25	40.86	18.54	14
São Francisco	44200000	32.54	28.60	41.28	18.54	15
Barra	46998000	36.01	31.54	38.31	18.54	28
Santa Maria da Boa Vista	48290000	37.90	32.95	38.83	18.54	32
Traipu	49660000	42.10	37.65	40.08	18.54	38
Itapebi	54950000	37.20	34.73	27.90	18.54	6

Colatina	56994500	36.98	29.81	-	-	4
UHE Porto Primavera	63995080	31.97	28.96	42.10	18.54	32
Barramento Porto São José	64575003	31.94	28.74	41.38	18.54	37
Ivinhema	64617000	-	-	39.55	18.54	-
Novo Porto Taquara	64693000	-	-	-	-	-
Balsa Santa Maria	64830000	-	-	-	-	-
Estreito do Iguaçu Novo	65986000	-	-	-	-	-
São Francisco	66810000	35.71	32.17	33.11	18.54	6
Porto Murtinho	67100000	38.17	35.46	31.11	18.54	8
Iraí	74100000	23.62	19.59	-	-	7
Garruchos	75550000	26.13	22.88	-	-	10
Uruguaiana	77150000	29.96	27.38	32.86	20.30	16
Eldorado	81380000	-	-	-	-	-
Registro	81683000	-	-	-	-	-
Rio Pardo	85900000	22.86	21.78	31.77	21.61	4
Encantado	86720000	24.42	19.91	-	-	4

Table SI3.4: Statistical metrics between remote sensing and measured evapotranspiration at eddy covariance sites.

Site	r		RMSE (mm.day^{-1})		Relative RMSE (%)		BIAS (mm.day^{-1})		Uncertainty (%)		Number of samples	
	MOD16	GLEAM	MOD16	GLEAM	MOD16	GLEAM	MOD16	GLEAM	MOD16	GLEAM	MOD16	GLEAM
BAN	0.58	0.49	1.24	0.79	35.62	22.81	-1.28	-0.24	36.50	23.65	84	82
BRA	0.88	0.93	0.53	0.45	15.92	13.54	-1.35	-0.98	17.18	18.44	39	39
CAS	0.79	0.93	0.71	0.39	18.94	11.49	-1.70	-0.81	30.72	17.06	14	13
CAX	0.55	-	0.28	-	8.07	-	0.55	-	27.42	-	5	-
CRA	0.74	0.80	0.82	0.81	26.03	26.04	-1.13	-0.31	32.33	29.12	68	65
FNS	-0.31	-	1.29	-	59.41	-	0.77	-	70.73	-	51	-
K34	0.30	0.42	0.66	0.33	22.35	11.63	0.92	1.21	27.47	18.89	108	75
K67	0.21	-0.06	0.46	0.52	14.68	16.72	0.72	0.89	18.97	24.31	111	82
K77	0.07	0.53	0.44	0.63	16.45	23.73	0.95	1.05	41.12	32.72	199	118
K83	0.32	0.20	0.33	0.39	8.51	10.11	-0.03	-0.19	10.51	12.82	46	14
PAN	0.19	-	0.74	-	31.68	-	-1.49	-	50.04	-	49	-
PAS	0.15	0.81	1.07	0.49	28.97	13.36	-1.63	0.10	32.52	13.64	27	26
PDG	0.83	0.95	0.47	0.29	17.72	11.44	0.24	-0.39	20.64	13.53	30	16
PRS	0.80	0.85	0.47	0.53	18.54	21.25	-0.87	-0.38	27.60	24.26	24	23
RJA	0.23	-	0.67	-	23.57	-	0.90	-	26.36	-	67	-
SMA	0.57	0.96	0.38	0.34	24.70	16.21	-0.46	0.58	41.02	17.58	33	32
USE	0.72	-	0.82	-	35.38	-	-0.38	-	35.82	-	43	-

Table SI3.5: Statistical metrics of remote sensing water balance.

Name	Code	P – ET – Q *vs* TWSC GRACE			ET + TWSC + Q *vs* P MSWEP			P -TWSC - Q *vs* ET GLEAM			P – ET -TWSC *vs* Q measured		
		r	RMSE	BIAS	r	RMSE	BIAS	r	RMSE	BIAS	r	RMSE	BIAS
Puerto Pilcomayo	2606	0.89	12.71	2.39	0.92	25.21	-3.10	0.73	24.89	3.10	0.23	25.03	3.10
Ruta Provincial	3216	0.50	14.09	-0.59	0.76	29.35	1.18	0.71	30.24	-1.18	0.17	30.15	-1.18
Timbues	3316	0.88	12.46	-1.86	0.92	23.94	1.46	0.76	23.85	-1.46	0.23	23.82	-1.46
São Paulo de Olivença	11400000	0.81	30.25	-59.79	0.86	36.19	59.65	0.05	35.32	-59.65	0.63	34.55	-59.65
Santo Antônio do Içá	11500000	0.80	33.33	-63.23	0.86	35.92	62.82	0.11	35.53	-62.82	0.66	33.20	-62.82
Itapéua	13150000	0.93	22.86	-54.22	0.86	31.80	54.74	0.27	32.35	-54.74	0.75	32.13	-54.74
Canutama	13880000	0.92	31.74	-26.09	0.95	34.50	25.41	0.37	34.15	-25.41	0.79	34.25	-25.41
Serrinha	14420000	0.84	26.28	-56.66	0.84	34.42	56.80	0.10	38.38	-56.80	0.81	37.59	-56.80
Porto Velho	15400000	0.91	23.55	-20.28	0.94	31.52	20.45	0.48	30.71	-20.45	0.71	31.71	-20.45
Fazenda Vista Alegre	15860000	0.96	21.94	-29.25	0.96	26.44	29.93	0.71	27.53	-29.93	0.83	27.66	-29.93
Óbidos	17050001	0.96	16.83	-37.96	0.93	24.15	38.25	0.22	23.67	-38.25	0.86	22.96	-38.25
Barra do São Manuel	17430000	0.97	25.04	5.63	0.95	41.49	-6.02	0.58	42.26	6.02	0.83	38.56	6.02
Itaituba	17730000	0.91	48.56	-8.66	0.94	49.76	-14.47	0.35	51.52	14.47	0.64	38.82	14.47
Boa Sorte	18460000	0.93	34.73	4.79	0.94	46.01	-6.38	0.44	46.13	6.38	0.63	46.65	6.38
Altamira	18850000	0.91	39.21	10.67	0.93	44.36	-10.63	0.34	44.79	10.63	0.62	44.42	10.63
Miracema do Tocantins	22500000	0.93	27.74	14.30	0.91	47.41	-15.54	0.62	49.66	15.54	0.57	47.56	15.54
Descarreto	23700000	0.93	25.52	6.55	0.93	40.81	-7.83	0.66	43.23	7.83	0.67	40.48	7.83
Luiz Alves	25950000	0.91	37.91	9.85	0.90	52.35	-19.55	0.49	61.40	19.55	0.52	60.65	19.55
Conceição do Araguaia	27500000	0.92	36.94	15.72	0.92	49.65	-15.73	0.47	49.79	15.73	0.54	50.57	15.73
Tucuruí	29700000	0.94	28.20	15.13	0.94	39.40	-14.02	0.58	39.43	14.02	0.64	39.12	14.02
Bacabal	33290000	0.90	32.09	17.95	0.89	41.19	-18.63	0.65	50.07	18.63	0.54	46.50	18.63
Cantanhede	33680000	0.91	30.81	21.94	0.92	35.03	-23.00	0.74	46.06	23.00	0.76	38.72	23.00
Barão de Grajaú	34311000	0.85	28.38	5.75	0.90	34.51	-6.95	0.69	40.29	6.95	0.39	38.15	6.95
Teresina - Chesf	34690000	0.84	26.13	4.07	0.91	32.73	-4.94	0.70	34.78	4.94	0.36	33.86	4.94
Luzilândia	34879500	0.85	25.77	5.62	0.91	32.39	-6.48	0.71	34.19	6.48	0.38	33.15	6.48
Peixe Gordo	36390000	0.83	27.22	1.43	0.88	35.02	-2.09	0.75	38.53	2.09	0.30	38.48	2.09
Pirapora	41135000	0.85	37.11	0.57	0.87	51.34	-1.84	0.57	58.20	1.84	0.46	58.15	1.84
Cachoeira da Manteiga	42210000	0.86	32.77	2.16	0.88	52.31	-3.54	0.54	55.64	3.54	0.50	54.05	3.54
São Romão	43200000	0.87	31.76	4.52	0.88	52.07	-5.92	0.55	55.81	5.92	0.52	54.21	5.92

São Francisco	44200000	0.88	30.93	5.95	0.88	51.62	-7.95	0.56	55.21	7.95	0.53	53.49	7.95
Barra	46998000	0.89	25.27	5.97	0.87	46.06	-7.20	0.62	49.25	7.20	0.21	49.27	7.20
Santa Maria da Boa Vista	48290000	0.89	23.43	5.66	0.88	39.44	-6.82	0.69	42.29	6.82	0.11	42.31	6.82
Traipu	49660000	0.87	22.30	3.64	0.88	36.01	-4.93	0.68	37.78	4.93	0.13	37.73	4.93
Itapebi	54950000	0.80	29.54	-6.07	0.85	45.36	2.87	0.56	48.77	-2.87	0.32	48.66	-2.87
Colatina	56994500	0.82	36.08	-5.16	0.87	49.63	2.95	0.55	58.51	-2.95	0.62	55.33	-2.95
UHE Porto Primavera Barramento	63995080	0.90	25.41	-4.14	0.90	38.36	3.41	0.67	42.19	-3.41	0.51	39.90	-3.41
Porto São José	64575003	0.91	22.00	-3.58	0.92	32.77	2.49	0.71	36.01	-2.49	0.43	35.26	-2.49
Ivinhema	64617000	0.66	30.66	-4.75	0.76	39.77	3.91	0.41	48.38	-3.91	0.29	49.29	-3.91
Novo Porto Taquara	64693000	0.49	30.16	-26.01	0.74	37.68	25.72	0.28	41.37	-25.72	0.64	44.98	-25.72
Balsa Santa Maria	64830000	0.43	35.07	-25.00	0.74	41.47	24.88	0.19	42.13	-24.88	0.66	48.44	-24.88
Estreito do Iguaçu Novo	65986000	0.61	35.31	-25.08	0.57	43.96	26.85	0.21	52.43	-26.85	0.52	56.65	-26.85
São Francisco	66810000	0.94	22.07	7.33	0.90	36.40	-7.42	0.72	38.89	7.42	0.21	39.46	7.42
Porto Murtinho	67100000	0.93	14.73	4.39	0.91	28.21	-4.86	0.74	28.89	4.86	0.26	28.56	4.86
Iraí	74100000	0.53	32.40	-22.01	0.63	39.26	22.71	0.30	49.32	-22.71	0.70	52.51	-22.71
Garruchos	75550000	0.53	33.46	-13.75	0.62	42.18	14.53	0.23	49.60	-14.53	0.66	54.70	-14.53
Uruguaiana	77150000	0.59	30.86	-10.56	0.58	43.46	12.26	0.25	51.67	-12.26	0.56	56.38	-12.26
Eldorado	81380000	0.41	29.29	-36.41	0.68	39.98	35.78	0.36	48.51	-35.78	0.52	49.81	-35.78
Registro	81683000	0.46	27.61	-41.83	0.68	36.44	42.32	0.43	45.85	-42.32	0.49	46.32	-42.32
Rio Pardo	85900000	0.54	34.73	-16.76	0.57	43.32	17.51	0.25	45.86	-17.51	0.61	51.76	-17.51
Encantado	86720000	0.44	31.67	-28.19	0.60	43.57	29.09	0.39	49.35	-29.09	0.68	52.13	-29.09

Supplementary Information S5

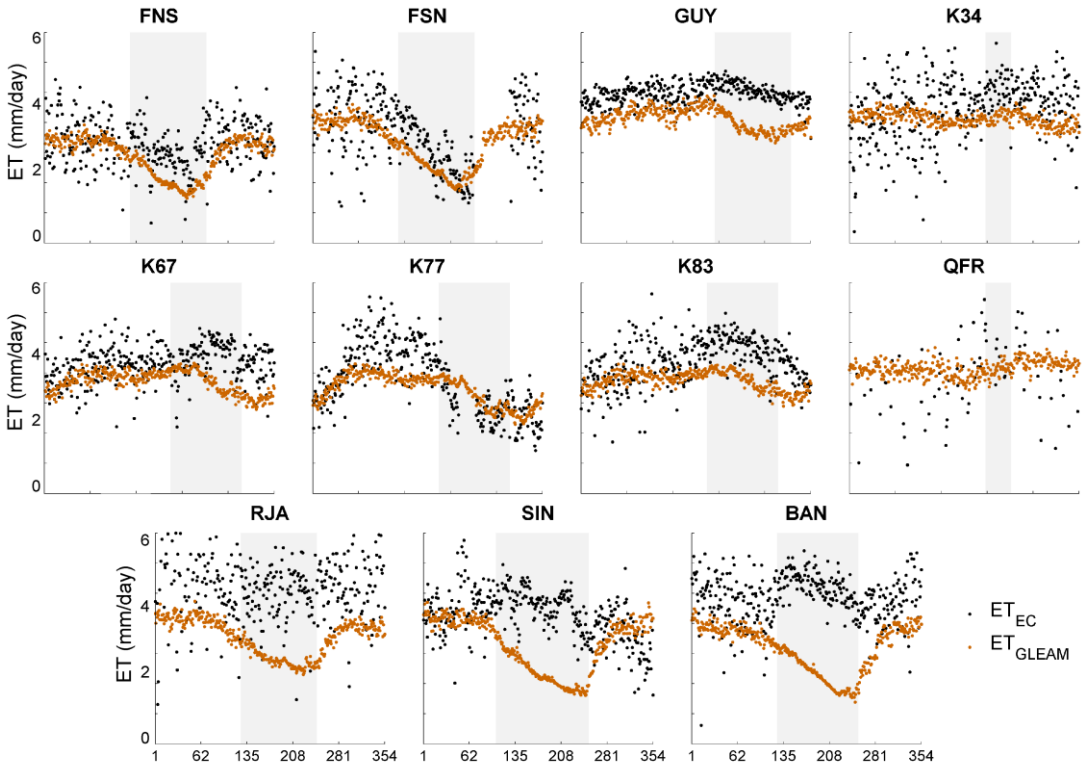

Figure SI5.1: GLEAM *ET* patterns at eleven measurements sites in the Amazon. Shaded areas indicate the dry season.

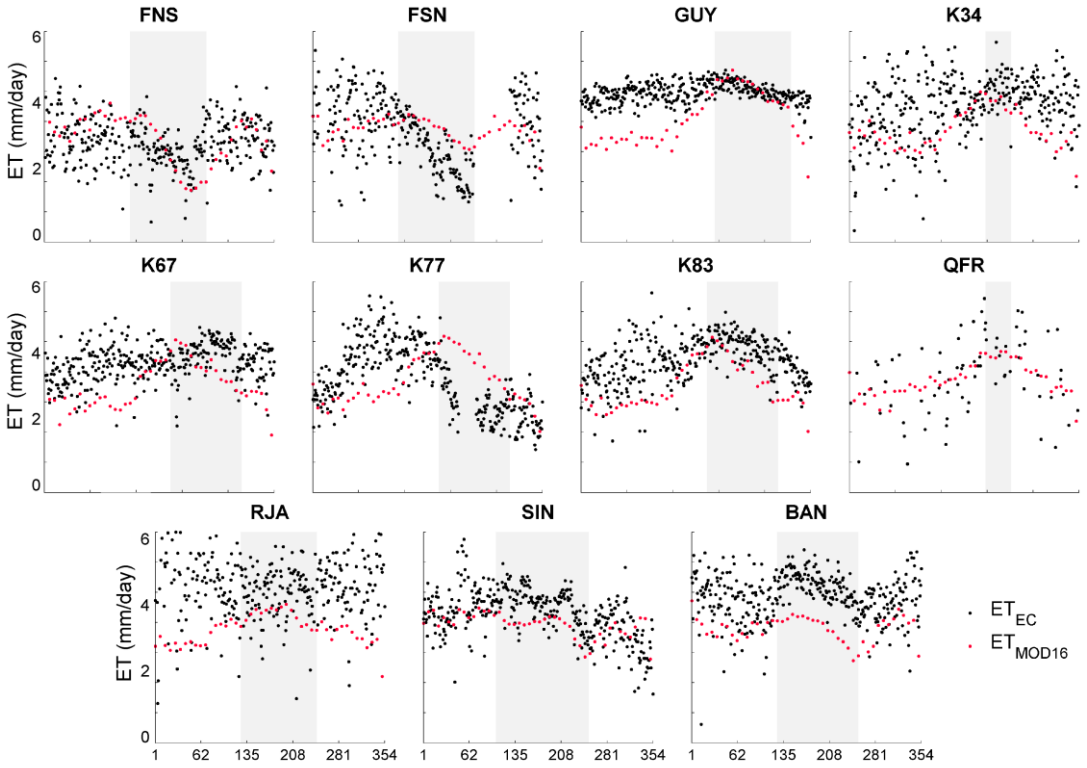

Figure SI5.2: MOD16 *ET* patterns at eleven measurements sites in the Amazon. Shaded areas indicate the dry season.

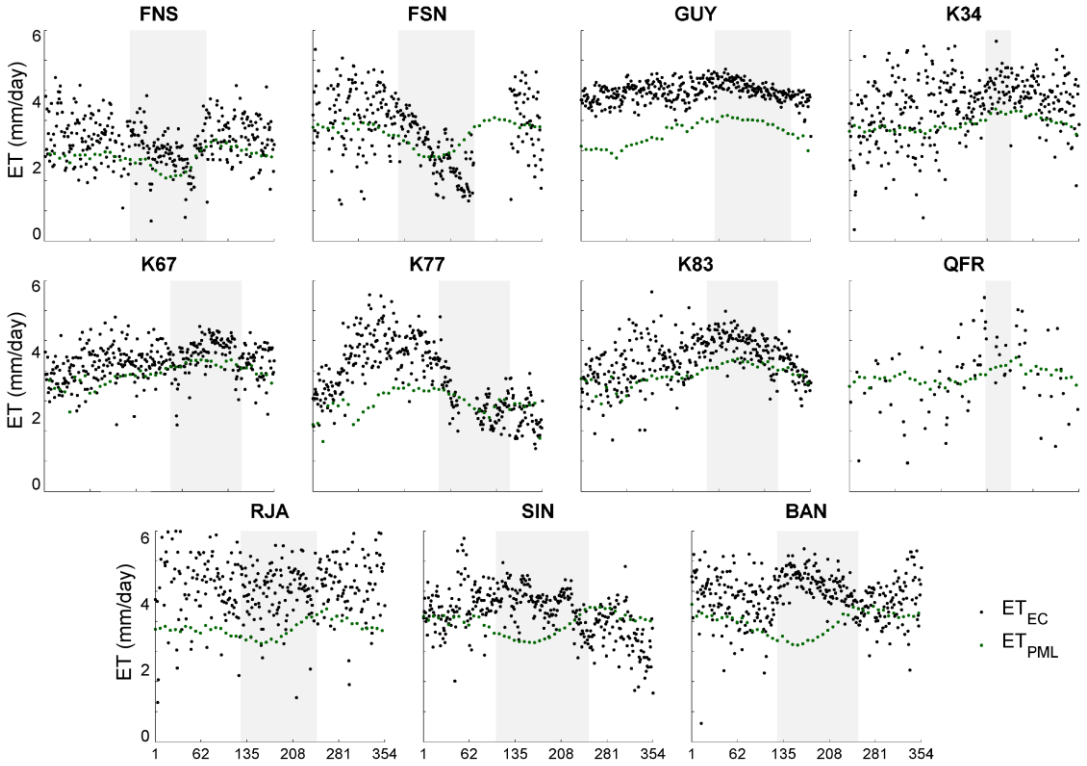

Figure SI5.3: PML *ET* patterns at eleven measurements sites in the Amazon. Shaded areas indicate the dry season.

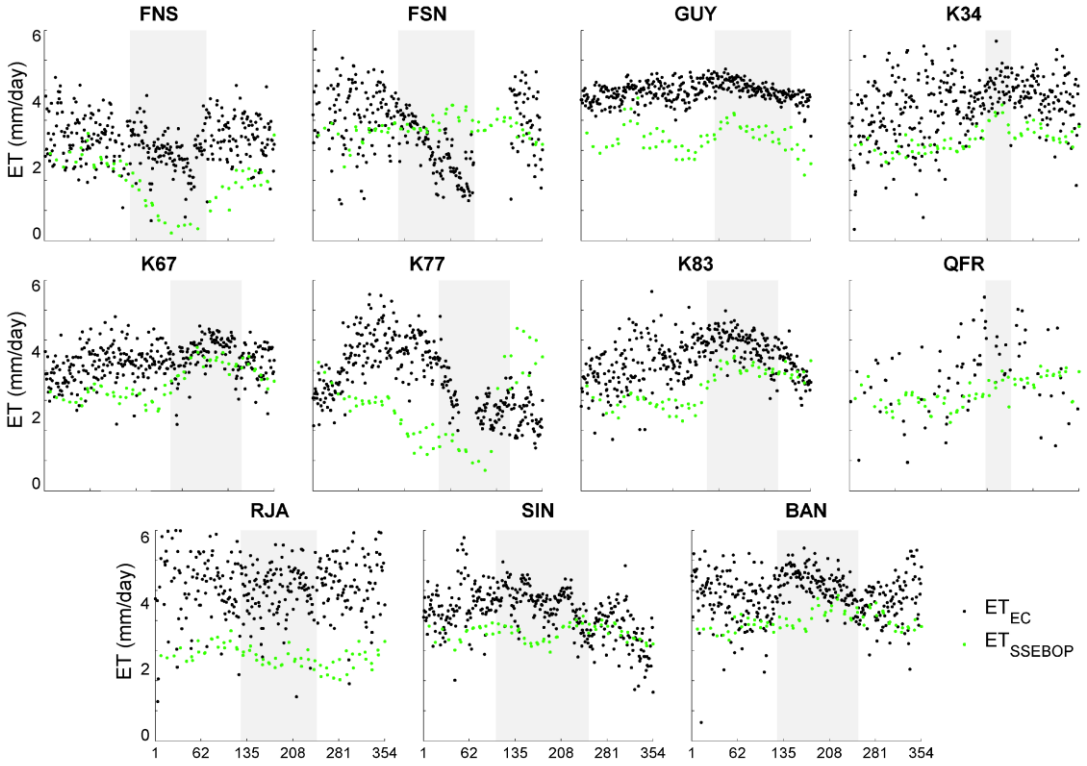

Figure SI5.4: SSEBOP *ET* patterns at eleven measurements sites in the Amazon. Shaded areas indicate the dry season.

Table SI5.1: Annual average ET under forest, pasture, and soybean areas, for 2003-2017 period.

	GLEAM			MOD16			PML			SSEBOP		
	ET Forest (mm/day)	ET Pasture (mm/day)	ET Soybean (mm/day)	ET Forest (mm/day)	ET Pasture (mm/day)	ET Soybean (mm/day)	ET Forest (mm/day)	ET Pasture (mm/day)	ET Soybean (mm/day)	ET Forest (mm/day)	ET Pasture (mm/day)	ET Soybean (mm/day)
2003	2.63	2.42	2.21	3.99	3.05	1.79	2.89	2.28	1.52	3.35	2.43	1.81
2004	2.66	2.35	2.16	3.97	3.23	1.83	2.89	2.29	1.44	3.44	2.51	1.92
2005	2.47	2.22	2.10	3.91	3.12	1.86	2.96	2.42	1.55	3.27	2.42	1.75
2006	2.53	2.31	2.30	4.06	3.46	1.99	2.93	2.44	1.59	3.42	2.44	1.90
2007	2.56	2.32	2.19	4.00	3.43	1.95	3.06	2.52	1.59	3.45	2.54	1.78
2008	2.45	2.20	2.22	3.90	3.34	2.17	3.12	2.63	1.81	3.40	2.48	2.00
2009	2.59	2.35	2.45	4.13	3.70	2.63	3.13	2.72	2.06	3.38	2.57	2.10
2010	2.51	2.23	2.06	3.96	3.47	2.47	3.17	2.60	1.69	3.31	2.40	1.83
2011	2.61	2.23	2.15	3.94	3.32	2.38	3.10	2.47	1.77	3.35	2.35	1.97
2012	2.59	2.30	2.30	3.91	3.40	2.44	3.11	2.48	1.87	3.43	2.44	2.17
2013	2.56	2.27	2.26	4.00	3.63	2.60	3.02	2.47	1.82	3.38	2.48	2.08
2014	2.60	2.34	2.22	4.06	3.73	2.58	3.11	2.56	1.84	3.34	2.42	2.05
2015	2.57	2.32	2.41	4.10	3.58	2.73	3.23	2.63	2.13	3.36	2.22	2.10
2016	2.62	2.41	2.30	4.11	3.74	2.62	3.12	2.63	2.02	3.25	2.45	1.94
2017	2.49	2.30	2.22	3.91	3.50	2.62	3.08	2.54	1.99	3.33	2.36	2.08

All annual pasture and soybean averages are significantly different from forest averages, at the 0.05 significance level, according to the t test.

Table SI5.2: Dry season average ET under forest, pasture, and soybean areas, for 2003-2017 period.

	GLEAM			MOD16			PML			SSEBOP		
	ET Forest (mm/day)	ET Pasture (mm/day)	ET Soybean (mm/day)	ET Forest (mm/day)	ET Pasture (mm/day)	ET Soybean (mm/day)	ET Forest (mm/day)	ET Pasture (mm/day)	ET Soybean (mm/day)	ET Forest (mm/day)	ET Pasture (mm/day)	ET Soybean (mm/day)
2003	2.60	2.17	1.69	4.13	2.54	0.77	3.14	2.19	0.96	3.41	2.03	0.89
2004	2.70	2.17	1.70	4.10	2.87	1.01	3.11	2.22	0.99	3.51	2.19	1.16
2005	2.42	1.98	1.50	4.00	2.73	0.88	3.19	2.34	0.96	3.30	2.00	0.72
2006	2.48	2.08	1.82	4.22	2.98	0.99	3.22	2.37	1.07	3.45	1.95	0.98
2007	2.48	2.05	1.55	4.05	2.80	0.90	3.34	2.44	1.05	3.57	2.16	0.96
2008	2.46	2.00	1.72	4.23	2.93	1.34	3.34	2.46	1.17	3.43	2.09	1.25
2009	2.69	2.25	2.10	4.40	3.64	2.01	3.22	2.52	1.35	3.47	2.28	1.30
2010	2.41	1.91	1.41	4.04	2.94	1.43	3.40	2.50	1.10	3.40	2.06	0.95
2011	2.63	1.96	1.61	4.38	3.06	1.65	3.38	2.42	1.21	3.37	1.78	0.99
2012	2.57	2.12	1.89	4.19	3.18	1.84	3.29	2.38	1.36	3.50	2.09	1.55
2013	2.61	2.17	1.91	4.27	3.31	1.97	3.22	2.39	1.27	3.37	2.00	1.26
2014	2.68	2.26	1.87	4.48	3.63	2.05	3.35	2.55	1.39	3.41	2.04	1.18
2015	2.70	2.15	1.98	4.45	3.34	2.22	3.38	2.49	1.62	3.47	1.86	1.41
2016	2.60	2.20	1.77	4.27	3.38	1.76	3.25	2.51	1.42	3.30	2.05	1.19
2017	2.50	2.15	1.77	4.19	3.17	1.92	3.31	2.48	1.41	3.37	1.98	1.28

All dry season pasture and soybean averages are significantly different from forest averages, at the 0.05 significance level, according to the t test.

Table SI5.3: Wet season average ET under forest, pasture, and soybean areas, for 2003-2017 period.

	GLEAM			MOD16			PML			SSEBOP		
	ET Forest (mm/day)	ET Pasture (mm/day)	ET Soybean (mm/day)	ET Forest (mm/day)	ET Pasture (mm/day)	ET Soybean (mm/day)	ET Forest (mm/day)	ET Pasture (mm/day)	ET Soybean (mm/day)	ET Forest (mm/day)	ET Pasture (mm/day)	ET Soybean (mm/day)
2003	2.65	2.60*	2.59*	3.87	3.51*	2.75	2.67	2.37	2.03	3.30	2.72	2.46
2004	2.63	2.48	2.48	3.85	3.57*	2.61	2.70	2.35	1.85	3.40	2.74	2.46
2005	2.51	2.40	2.53*	3.83	3.48*	2.74	2.75	2.48*	2.09	3.26	2.72	2.48
2006	2.57	2.48*	2.65*	3.93	3.89*	2.90	2.67	2.51*	2.06	3.40	2.78	2.56
2007	2.62	2.51	2.65*	3.95	4.00*	2.95	2.81	2.60*	2.08	3.37	2.80	2.37
2008	2.44	2.34	2.58	3.58	3.73*	3.00	2.92	2.79*	2.39	3.39	2.77	2.54
2009	2.53	2.42	2.70	3.88	3.75*	3.19	3.06	2.90*	2.72	3.31	2.78	2.67
2010	2.59	2.45	2.54*	3.88	3.96*	3.42*	2.97	2.70	2.22	3.24	2.65	2.45
2011	2.59	2.43	2.54*	3.53	3.57*	3.05	2.85	2.53	2.29	3.33	2.75	2.66
2012	2.60	2.44	2.60*	3.65	3.59*	2.98	2.94	2.57	2.33	3.38	2.69	2.62
2013	2.53	2.35	2.51*	3.76	3.92*	3.17	2.83	2.53	2.33	3.39	2.83	2.66
2014	2.54	2.40	2.47*	3.69	3.83*	3.10	2.90	2.56	2.25	3.30	2.70	2.68
2015	2.48	2.45*	2.72	3.78	3.79*	3.19	3.10	2.76	2.60	3.27	2.48	2.60
2016	2.64	2.56*	2.67*	3.97	4.06*	3.41	3.01	2.73	2.57	3.21	2.73	2.47
2017	2.48	2.42*	2.54*	3.67	3.81*	3.29*	2.87	2.60	2.53	3.30	2.63	2.64

* Wet season pasture and soybean averages that are not significantly different from forest averages, at the 0.05 significance level, according to the t test.